5-2012

# Computational modelling of cobalamin-dependent enzymatic reactions : activation of Co-C bond in adenosylcobalamin-dependent mutases and cob(II)alamin/cob(I)alamin redox process in methyltransferases.

Manoj Kumar
*University of Louisville*

# COMPUTATIONAL MODELLING OF COBALAMIN-DEPENDENT ENZYMATIC REACTIONS: ACTIVATION OF Co-C BOND IN ADENOSYLCOBALAMIN-DEPENDENT MUTASES AND COB(II)ALAMIN/COB(I)ALAMIN REDOX PROCESS IN METHYLTRANSFERASES

By

Manoj Kumar
B.A., Himachal Pradesh University, Shimla, India, 2004
M.S., Panjab University, Chandigarh, India, 2006

A Dissertation
Submitted to the Faculty of the
College of Arts and Sciences of the University of Louisville
in Partial Fulfillment of the Requirements
for the Degree of

Doctor of Philosophy

Department of Chemistry
University of Louisville
Louisville, Kentucky

May, 2012

# COMPUTATIONAL MODELLING OF COBALAMIN-DEPENDENT ENZYMATIC REACTIONS: ACTIVATION OF Co-C BOND IN ADENOSYLCOBALAMIN-DEPENDENT MUTASES AND COB(II)ALAMIN/COB(I)ALAMIN REDOX PROCESS IN METHYLTRANSFERASES

By

Manoj Kumar
B.A., Himachal Pradesh University, Shimla, India, 2004
M.S., Panjab University, Chandigarh, India, 2006

A Dissertation Approved on
April 6th, 2012

by the following Dissertation Committee:

Dissertation Director: Dr. Pawel M. Kozlowski

Dr. Craig A. Grapperhaus

Dr. Richard J. Wittebort

Dr. Frederick A. Luzzio

Dr. John C. Morrison

# DEDICATION

This dissertation is dedicated to my grandfather late Sh. Gurdas Ram,

and to my parents Sh. Rampal and Smt. Sunita Kumari.

# ACKNOWLEDGEMENTS

I would like to thank my advisor, Dr. Pawel M. Kozlowski, for being a mentor and friend to me over the course of my graduate studies. His guidance and experience have been invaluable tools in my progress.

I would also like to thank several of the faculty members of the University of Louisville. I sincerely offer my thanks to my committee members Dr. Grapperhaus, Dr. Wittebort, Dr. Luzzio and Dr. Morrison for their assistance with my progress towards my doctorate. Special thanks also are extended to Dr. Lamm and Dr. Rypkema, former faculty members at the University of Louisville for their valuable suggestions. I also have unending gratitude towards Prof. Harjinder Singh, IIIT, Heydrabad, India and Prof. Swapan K. Pati, JNCASR, Bangalore, India for motivating me to take up science as a career. My career as a graduate student would have been much more difficult without the faithful efforts of the staff of the Chemistry Department especially that of Sherry Nalley, Syble Bullock and Steve. Sincere regards are also extended to James Simrall, Cardinal Research Cluster for his help with the supercomputer related technical issues.

Several students in the Chemistry Department also deserve special mention for their friendship and assistance. Fellow lab mates Jadwiga Kuta, Neeraj Kumar, Karina Kornobis and Peiyu have been real assets. Special thanks to Ed, Rajat, Davinder and Manish for their counsel and assistance.

I would like to thank my parents for giving me invaluable educational opportunities. Special thanks to my close family that include my late grandfather, grandmother, uncles, aunts, brothers and sisters for their unconditional support and love and who were always there with encouraging words for me when I needed them.

# ABSTRACT

## COMPUTATIONAL MODELLING OF COBALAMIN-DEPENDENT ENZYMATIC REACTIONS: INITIAL STEP OF $B_{12}$ CATALYSIS IN ADENOSYLCOBALAMIN-DEPENDENT MUTASES AND COB(II)ALAMIN/COB(I)ALAMIN REDOX PROCESS IN METHYLTRANSFERASES

Manoj Kumar

April 6th, 2012

The role of the active site tyrosine residue in the Co-C5' bond activation in the context of adenosylcobalamin-dependent mutases has been computationally investigated. The density functional, complete active space self-consistent field and quantum mechanics/molecular mechanics calculations have predicted that the deprotonated tyrosine can serve as a redox center potentially causing the one-electron reduction of $B_{12}$ cofactor. As a result, the reduced form of adenosylcobalamin has been suggested to participate in $B_{12}$ catalysis and an alternate mechanism for explaining the origin of catalysis in adenosylcobalamin-dependent mutases has been proposed. The implications of the involvement of the reduced $B_{12}$ cofactor in the initial step of $B_{12}$ catalysis that involve Co-C5'

cleavage and subsequent hydrogen atom abstraction from the substrate has been computationally studied by means of density functional calculations. The energetic demands of the reaction have been found to be significantly lowered when the reaction is mediated by the one-electron reduced form of the cofactor.

During the second part of this dissertation, an unprecedented $Co^{1+}$ ion induced H-bonding interaction ($Co^{1+}$--H) has been computationally validated. The H-bond forming capacity of $Co^{1+}$ ion that is a dominant $d^8$ configuration has been suggested to be rooted in the availability of appropriately oriented filled d-orbitals which can serve as H-bond acceptors to interact with the acidic ends of the axial ligands. Because of a $Co^{1+}$--H interaction, cob(I)alamin, a $Co^{1+}$ ion-based ubiquitous $B_{12}$ intermediate, has been suggested to be a pentacoordinated square pyramidal or hexacoordinated octahedral complex in addition to its commonly accepted tetracoordinated square planar geometry. In specific, the QM/MM calculations on methionine synthase-bound cob(I)alamin (PDB-code: 3IVA @ 2.2 Å resolution; 1BMT @ 3.0 Å resolution) has provided the convincing evidence of an enzyme-induced $Co^{1+}$--H interaction. The $Co^{1+}$--H interaction exerts an anodic shift upon the reduction potential of the $Co^{2+}/Co^{1+}$ process which is a common chemical event in a large family of methyltransferases and ATP:corrinoid adenosyltransferases. Building upon these insights, an alternate mechanistic pathway for the enzyme-induced $Co^{2+}/Co^{1+}$ redox process has been suggested that is mediated by the square pyramidal cob(I)alamin rather than its square planar form.

# TABLE OF CONTENTS

# LIST OF TABLES

# LIST OF FIGURES

# LIST OF SCHEMES

# CHAPTER I

# INTRODUCTION

The $B_{12}$ cofactors belong to a class of $Co^{III}$ containing organocorrinoids, in which the $Co^{III}$ ion is equatorially coordinated by four tetrapyrrole nitrogens of the corrin macrocycle and in the $\alpha$ ("lower") axial coordination site by the 5,6-dimethylbenzimidazole (DBI) of the nucleotide loop connected to the corrin ring (Figure 1). The ligand X occupying the $\beta$ ("upper") axial site is different for different types of cobalamins (XCbl). Alkylcobalamins or, more generally, organocobalamins, where X is a C-bonded to Co ligand R, are generally denoted as RCbl. Particularly, R is a methyl group (Me) in the case of methylcobalamin (MeCbl), that serves as a cofactor in $B_{12}$-dependent methyltransferases, while it is 5'-deoxy-5'-adenosyl (Ado) group in the case of adenosylcobalamin (AdoCbl) cofactor in $B_{12}$-dependent mutases, isomerases and eliminases.[1-19] Cyanocobalamin (CNCbl), popularly known as vitamin $B_{12}$, has R= $CN^-$ and is a non-alkylcobalamin. The other known non-alkylcobalamins are azidocobalamin ($N_3$Cbl), aquocobalamin ($H_2OCbl^+$) and hydroxocobalamin (HOCbl), respectively. It should be noted that vitamin $B_{12}$ is not a biologically active species. However

another member of non-alkylcobalamin family, HOCbl has recently been shown to act as a photocatalytic source of hydroxyl radicals for the investigation of biological complexes such as DNA and RNA.[20,21]

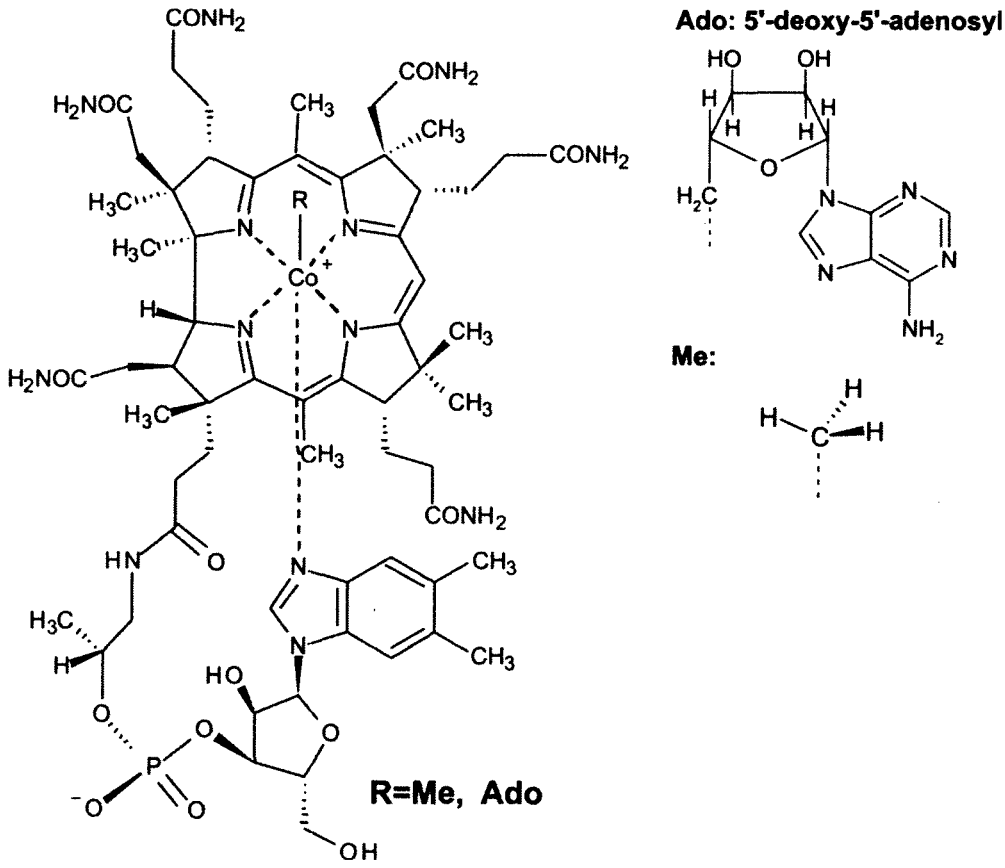


Figure 1. Molecular Structure of RCbl.

The relatively weak organometallic Co-C bond in derivatives of vitamin $B_{12}$ (i.e., MeCbl and AdoCbl) continues to provide fascinating avenues for experimental as well as computational research in the field of bioinorganic chemistry.[1-19] The inherent reactivity of the Co-C bond plays a pivotal role in a variety of

physiological events. In all these enzymes, the rapid cleavage of the organometallic Co-C bond constitutes one of the critical steps of their catalytic cycles. The Co-C bond is of moderate strength and its bond dissociation energy (BDE) lies in the range of 32-40 kcal/mol for MeCbl[22,23] and 26-34 kcal/mol for AdoCbl.[25-27] The most remarkable aspect of the enzymatic catalysis employing coenzyme $B_{12}$ is the observed rate enhancement,[22] which exceeds that of the uncatalyzed reaction taking place in solution by about 12 orders of magnitude for AdoCbl-dependent enzymes.

Taking into account that the cleavage of the Co-C bond is not a rate determining step,[28] its strength must be significantly reduced by ~50%, in order to achieve the observed rate enhancement.[29] However, the mechanism of the Co-C bond activation remains elusive, because the intermediates involved in the $B_{12}$-dependent enzymatic catalysis are short-lived and many of them are spectroscopically "silent". Because of this situation, computational modeling has become an indispensable guiding tool for understanding the mechanism of the Co-C bond activation in $B_{12}$ cofactors. Here, we have utilized a variety of computational tools to understand the mechanism of the initial step of catalysis in AdoCbl-dependent mutases namely methylmalonyl coenzyme A mutase (MCM) and glutamate mutase (GLM) respectively that consist of Co-C bond cleavage and subsequent hydrogen atom (H-atom) abstraction from the substrate.

Cob(II)alamin ($Co^{2+}Cbx^{30}$) to cob(I)alamin ($Co^{1+}Cbx$) reduction (i.e., $Co^{2+}$/ $Co^{1+}$) constitutes an important chemical event in many methyltransferases such as methionine synthase (MetH),[31] corrinoid/Fe-S protein (CFeSP),[32]

methanol:CoM (MtaBC),[33] monomethylamine:CoM (MtmBC),[34a] dimethylamine:CoM (MtbB1C),[34b] trimethylamine:CoM (MttB1C),[34c] dimethylsulfide:CoM (MtsAB)[34d].[16] This reduction process is not only implicated in the reaction cycles of methyltransferases, but also forms an essential chemical component in ATP:corrinoid adenosyltransferases (ACAs)[35] (e.g., CobA, PduO and EutT)[36-38] en route to the de novo synthesis of adenosylated derivative of vitamin $B_{12}$, AdoCbl. Despite being a ubiquitous chemical event, the precise molecular mechanism as to how this thermodynamically challenging $Co^{2+}/Co^{1+}$ reduction process is accomplished within enzymes remains to be fully elucidated. The study in the second part of this dissertation focuses on understanding the mechanistic details of the $Co^{2+}/Co^{1+}$ reduction process of the methyltransferases using modern computational tools.

The dissertation is composed of two parts. The first part is the investigation of the mechanism of the initial step of catalysis in AdoCbl-dependent MCM and GLM mutases that comprises Co-C bond breakage and subsequent H-atom abstraction from the substrate. In chapter II, the alternate role of the active site tyrosine (Y) residue as an electron transfer (ET) agent has been studied and an alternate Co-C bond activation mechanism for $B_{12}$-dependent mutases has been suggested. The energetic implications of the ET between the Y residue and the AdoCbl cofactor in the context of the initial step of catalysis i.e., Co-C bond cleavage and subsequent H-atom abstraction from the substrate has been discussed in Chapter III. The second part is the study of the $Co^{2+}/Co^{1+}$ reduction process in the models as well as MetH-bound complexes.

The unusual H-bond forming ability of $Co^{1+}$ ion (a dominant $d^8$ electronic configuration)[39,40] in $Co^{1+}$Cbx model complexes, and its structural as well as biological implications in the context of $Co^{2+}/Co^{1+}$ process have been investigated in chapter IV. The existence of an unprecedented MetH-bound $Co^{1+}$--H interaction induced by the axial ligand conformational change and its role in the $Co^{2+}/Co^{1+}$ redox process has been discussed in chapter V. The study of alternate coordination environments of $Co^{1+}$Cbx in the model as well as MetH-bound complexes have been developed in chapter VI. The possible involvement of the local enzyme scaffold especially that of the active site tyrosine residue of MetH enzyme in the $Co^{1+}$--H bond formation has been studied in chapter VII.

## 1.1 $B_{12}$ Catalysis in Adenosylcobalamin-Dependent Mutases

AdoCbl or coenzyme $B_{12}$ catalyzes a variety of chemically difficult transformations that involve intramolecular 1,2-type hydrogen exchange with a functional group (alkyl, hydroxyl or amino) on adjacent carbon atoms (Schemes 1 and 2).[1-19] It is generally accepted that the catalytic reaction is initiated by the homolytic cleavage of the Co-C bond of AdoCbl cofactor leading to the formation (at least formally) of 5'-deoxy-5'-adenosyl radical (Ado$^{\bullet}$) and $Co^{2+}$Cbx.[41] The Ado$^{\bullet}$ then abstracts H-atom from the substrate, which is followed by rearrangement of the substrate-derived radical into a product-related radical. The re-abstraction of H-atom closes the catalytic cycle.

There are several fundamental issues related to AdoCbl-dependent enzyme catalysis which remain elusive. The most fundamental is the question of the ~$10^{12}$–fold rate enhancement of the Co-C bond cleavage inside the enzyme

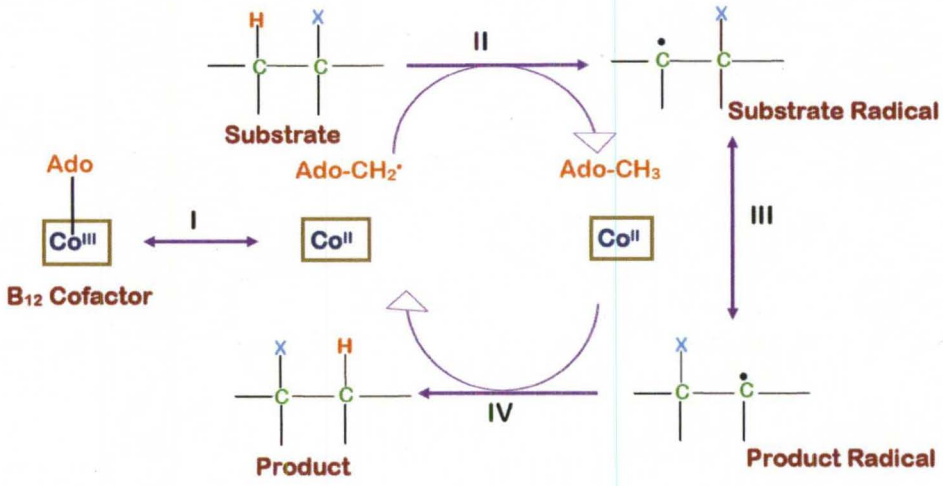


Scheme 1. General catalytic mechanism for AdoCbl-dependent enzymes.

environment[22] in comparison to thermal homolysis of the free cofactor in solution. The Co-C bond cleavage in isolated coenzyme $B_{12}$ is energetically unfavorable with the bond dissociation energy (BDE) estimated at ~31.0 kcal/mol.[25-27] In contrast, the homolysis of the Co-C bond inside enzyme is rapid and is not a rate determining step[28] implying that its strength must be significantly reduced by ~17.0 kcal/mol during catalytic turnover.[29] The enzyme also shifts the equilibrium towards the homolysis products giving equilibrium constant close to unity inside the enzyme.[28b,28d,41,42,43,44] In addition, the homolytic cleavage of the Co-C bond

is kinetically coupled to the H-atom abstraction from the substrate.[28b,28d,42,43,44,45,46] Although it is generally believed that AdoCbl cofactor is only required to initiate the radical reaction and resulting $Co^{2+}$Cbx behaves like a spectator (i.e. does not participate in subsequent steps), Buckel et al.,[47] challenged this traditional view and proposed that $Co^{2+}$Cbx in AdoCbl-dependent mutases such as MCM or GLM plays a more active role. It was suggested that the $Co^{2+}$Cbx acts as a conductor by stabilizing both Ado$^{\bullet}$ and the product-related radical intermediates. The $Co^{2+}$Cbx-mediated stabilization of radicals may occur via a concerted mechanism involving Co-C cleavage and H-atom abstraction from substrate. Thus, the concept of $Co^{2+}$Cbx being a spectator[48] can be applied to a subclass of AdoCbl-dependent enzymes known as eliminases that are exemplified by diol dehydratase[49] and glycerol dehydratase[50].

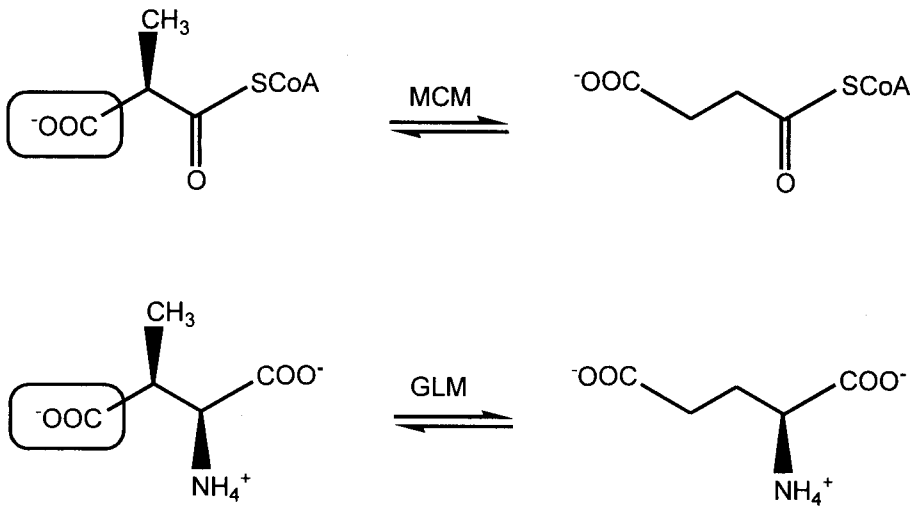


Scheme 2. 1,2-type reactions catalyzed by MCM and GLM mutases. The carboxylic group that can interact with the Y residue has been indicated by box.

Several mechanistic explanations have been suggested to account for the enhanced cleavage of Co-C bond inside the enzyme. Earlier proposals have been primarily of steric nature[3,22,41,51,52,53,54,55-60] and emphasized importance of factors such as deformation of corrin ring,[41,51,52] role of $\alpha$-axial ligand,[53,54] bending of $\beta$-axial ligand[55-60] and steric strain induced by the substrate binding[3,22,57]. However, recent crystallographic,[2,61,62,63-65] spectroscopic[54,67,68,69] as well as computational studies[70-72] reveal the invalidity of steric proposals to fully explain the observed catalytic effect. Taking into account that mechanism of AdoCbl-dependent enzyme catalysis has been difficult to probe experimentally; several groups have started using computational tools to acquire insight into the activation of the Co-C bond in AdoCbl-dependent mutases. Two AdoCbl-dependent mutases, MCM and GLM received particular attention because of their reliable crystal structures.[62,73] The calculations for the Co-C bond cleavage and subsequent H-atom transfer have been reported for model systems in gas phase[74-78] as well as inside the proteins[79,80]. Jensen and Ryde performed comprehensive QM/MM calculations focusing primary on the Co-C bond cleavage in the GLM-bound AdoCbl cofactor.[81] The mechanistic aspects of the subsequent H-atom abstraction step were also briefly discussed. The Co-C BDE for AdoCbl cofactor was significantly reduced from ~34.2 kcal/mol in vacuum to ~1.9 kcal/mol inside the GLM enzyme which was attributed to several factors. The entire catalytic effect was made up of four contributing components with the most significant coming from the geometrical distortion of the cofactor by the

protein which was larger in $Co^{III}$ state than in $Co^{II}$ state, and the stabilization of the dissociated state via electrostatic interactions of the cofactor with the protein residues. Our research group modeled the Co-C bond homolysis and subsequent H-atom abstraction using a truncated model of the GLM substrate in the gas phase.[82] The concerted pathway was predicted to be energetically more favorable than stepwise by ~7.0 kcal/mol thus confirming the conductor hypothesis of Buckel et al.[47] Radom and co-workers[83] also performed a similar analysis in the gas phase emphasizing the importance of the ribose orientation in the substrate activation. They obtained a stepwise pathway pointing out that the longer Co••C bond in TS for H-abstraction was due to use of the full GLM substrate in their calculations instead of a truncated propanol model applied previously. Their calculations also identified sizeable stabilization of TS by ~7.2 kcal/mol for one distinct orientation of the ribose part of AdoCbl as a result of favorable C-H••O3' hydrogen bond formation with corrin macrocycle. Thus, the conductor hypothesis[47] was also confirmed in this study with similar energetic effect but having a different origin.

Warshel et al.,[84] employed the empirical valence bond methodology along with the free energy perturbation approach to investigate the Co-C bond cleavage and subsequent H-atom abstraction in the case of MCM enzyme. They showed that the concerted mechanism in MCM was more favorable and it was concluded that the catalytic effect mainly originate from the electrostatic interaction between the ribose and the protein. Morokuma et al.,[85] also investigated the origin of the catalytic effect in MCM enzyme, but using the

ONIOM QM/MM methodology. These authors pointed out that the cobalt-carbon bond coordinate alone is not a sufficient reaction coordinate to study the catalytic event. The transition state for the Co-C bond cleavage that was studied as a function of the conformational change in the Ado moiety was predicted for the homolysis step. They also obtained significant reduction of the Co-C BDE confirming previously reported results of Jensen and Ryde[81] that the catalytic effect can be decomposed into several components such as cage effect or the effect of coenzyme geometrical distortion. When the formation of an Ado radical and subsequent H-atom transfer from the substrate was studied it was concluded that the initial Co-C bond cleavage and the subsequent H-atom transfer occur in a stepwise manner in the protein and that the concerted pathway in the gas phase is favored by 7.7 kcal/mol.

Although the consensus with regard to the origin of the enormous catalytic activity in $B_{12}$ dependent enzymes is still lacking, yet the one-electron reduction of the cofactor, that leads to weakened Co-C bond, has attracted considerable attention.[86-90] Almost three decades ago, electrochemical studies by Lexa and Savéant[86] demonstrated that the addition of an electron to the $B_{12}$ cofactor leads to significant reduction in the BDE of Co-C bond that could explain the catalytic effect observed inside the protein environment. Later on, other experimental studies confirmed and extended this finding.[87,88,89-90] Despite the potential relevance to $B_{12}$–dependent enzyme catalysis, the mechanism of reductive cleavage has not been deciphered until recently.[89] It has been hypothesized that the added electron directly goes to $\sigma^*_{Co\text{-}C}$ orbital and formation of 3-electron bond

is primarily responsible for the observed bond weakening. However recent reports[91-94] show that initial addition of an electron leads to the formation of a $\pi^*_{corrin}$ anion radical with electron delocalized over the equatorial ligand. Consequently, the cleavage of the Co-C bond must involve several distinctive steps, one of them being the transition of added electron between two electronic states $\pi^*_{corrin}$ and $\sigma^*_{Co\text{-}C}$. It was established that lowering in BDE arises due to involvement of two electronic states: intial $\pi^*_{corrin}$ state that is formed upon one-electron addition and final $\sigma^*_{Co\text{-}C}$ state. Upon stretching the Co-C bond, the added electron moves to the $\sigma^*_{Co\text{-}C}$ state and the final cleavage involves a three electron bond $(\sigma)^2$ $(\sigma^*)^1$. This finding has been demonstrated for one-electron-reduced (1e-Red) MeCbl[91,93-94] as well as alkyl-cobalt(III)phthalocyanin (Pc)[92] complexes. In case of 1e-Red MeCbl, the lowering in BDE was estimated to be ~45% while it was ~37% as far as 1e-Red Pc-based model compound was concerned. The reductive Co-C bond cleavage mechanism involving transfer of $Me^{\bullet}$ from MeCbl to the substrate radical ($CH_3S^{\bullet}$) has also been investigated by means of DFT, complete active space self-consistent field (CASSCF) followed by second order perturbation theory (CASPT2),[93] and hybrid quantum mechanics/molecular mechanics (QM/MM) calculations[94]. It has been shown that the deprotonated substrate ($CH_3\text{-}S^-$) can serve as a redox center causing one-electron reduction of the cofactor and thereby can induce the efficient Me group transfer. The QM/MM analysis of MetH catalyzed methyl transfer reaction suggested an energy barrier of $\leq$ 8.5 kcal/mol for the reductive reaction pathway[94] which is comparable to what has been estimated for an $S_N2$ reaction[95].

Although the BDE lowering caused by one-electron reduction is in line with what is required to achieve the observed ~$10^{12}$ orders of enzymatic rate enhancement, the reductive cleavage mechanism[91-94] has never been considered as a possible mode of activation largely due to the highly unfavorable redox chemistry of $B_{12}$ cofactors (-1.20 to -1.60 V vs standard calomel electrode (SCE)).[86,89] However it is well-documented in literature,[96-103] that the complex interactions operative within the protein framework can significantly alter the redox potential of a cofactor or the active site. For example, a single residue (Gln), in case of superoxide dismutase (SOD), has been found to induce a redox modulation of over 1V range owing to changes in its local environment.[96] Similarly, low dielectric constant of the protein active site and the H-bond network have been suggested to modulate the redox potential of the Y residue and $P_{680}^{+}$ motif in the case of photosystem-II (PS-II).[97] Even the hydrophobic residues in the binding pockets of myoglobin and cytochromes have been found to exert a redox tuning of ~500 mV.[98-100] Variations in the ligation and spin states of the heme framework also impart a significant amount of modulation upon the redox behavior of hemoproteins.[101-103] This growing body of evidence about the redox tuning of protein-encapsulated redox cofactors suggest that the electrochemical behavior of enzyme-bound $B_{12}$ cofactors may also be tunable, and the possibility of ET-based activation mechanism in the context of AdoCbl-dependent enzymes cannot be entirely ruled out.

In the first study in Chapter II, the role of the active site tyrosine residue as an ET agent in the case of AdoCbl-dependent GLM and MCM mutases has been

investigated by means of the DFT, CASSCF and QM/MM computational methods. For the model DFT calculations, the AdoCbl cofactor that was simplified with respect to the corrin amide side chains was used while PhOH was used to mimick the active site Y residue in the case of GLM and MCM enzymes respectively. The simplified $CH_3CH_2Cbl$ was used as the AdoCbl model for carrying out the CASSCF calculations that are aimed at gaining detailed information about the electronic structure of AdoCbl--$Y^-$ complex. The QM/MM calculations were performed to investigate the catalytic role of Y89 residue in the MCM enzyme (PDB-code: 4REQ @ 2.2 Å resolution)[56]. The computational Y89F mutation was also carried out to better understand the role of Y89 residue in the context of the Co-C bond cleavage and subsequent H-atom abstraction from the substrate. An alternate mechanism for the activation of Co-C bond cleavage in the AdoCbl-dependent mutases has been proposed.

Taking into account that the one-electron reduction of the cofactor exerts an appreciable amount of the catalytic effect upon the Co-C bond cleavage process,[86-90] the initial step of $B_{12}$ catalysis that consists of Co-C bond breakage and subsequent H-atom abstraction from the substrate in the context of GLM enzyme has been investigated considering the involvement of the reduced AdoCbl cofactor. The simplified ribosylcobalamin (RibCbl) and propionaldehyde has been used in the DFT calculations to mimick the AdoCbl and glutamate substrate respectively. The intrinsic reaction coordinate calculations have been performed to locate the transition state involved in the reaction.

## 1.2 Cob(II)alamin/Cob(I)alamin Redox Process in Methyltransferases

$Co^{1+}$Cbx supplies significant mechanistic assistance for the reactions catalyzed by a wide body of methyltransferases namely MetH,[31] CFeSP,[32] MtaBC,[33] MtmBC,[34a] MtbB1C,[34b] MttB1C,[34c] MtsAB[34d] and many more.[35] $Co^{1+}$Cbx is not only relevant for methyltransferase chemistry, but also forms an essential chemical component in ACAs[36] (e.g., CobA, PduO and EutT)[37-40] leading to the de novo synthesis of AdoCbl (Scheme 3). In addition to its impeccable biological profile, $Co^{1+}$Cbx also plays a deterministic role in the biofriendly detoxification reactions of halogenated organic compounds[104,105,106] that are major contaminants prevalent in the soil and groundwater of many

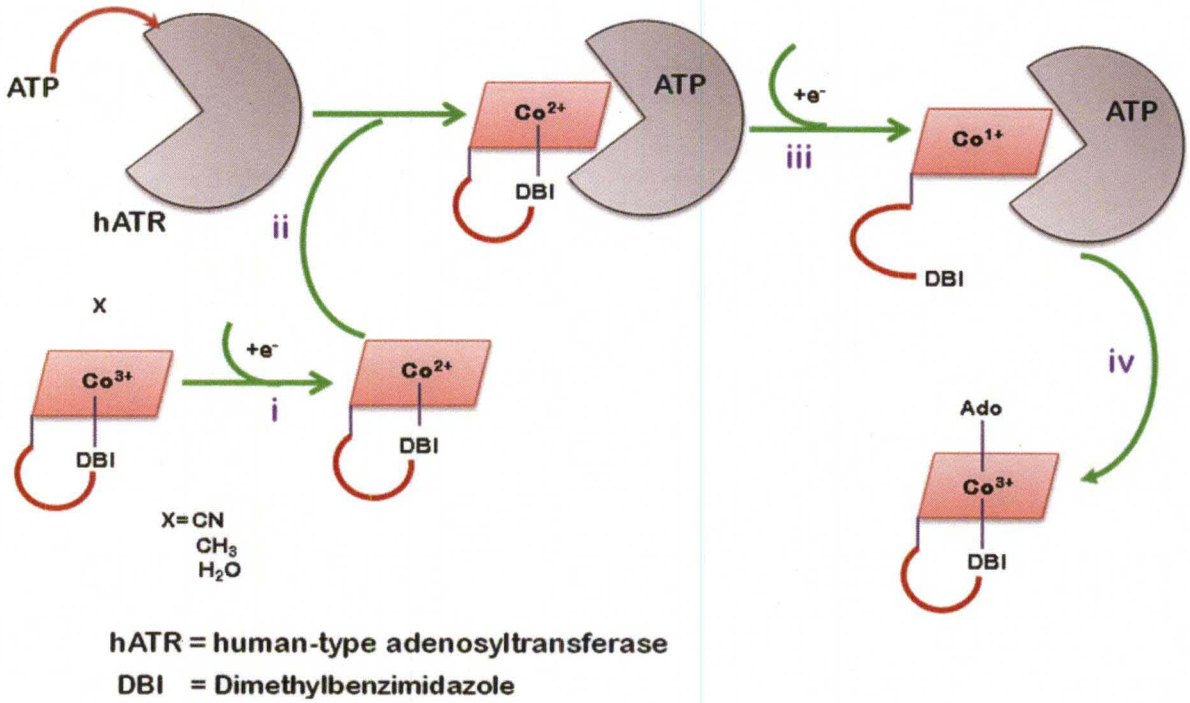


Scheme 3. Biochemical Pathway of ATP:corrinoid adenosyltransferases.

industrial sites[107]. Because of the large repertoire of functions $Co^{1+}$Cbx serve, understanding its structural and electronic properties is an important pursuit. Interestingly, methyltransferases and ACAs not only share the same intermediate platform, but also a common mechanistic feature i.e., $Co^{2+}/Co^{1+}$ reduction is executed at some stage of their respective reaction cycles.[16] For example, in the case of E. Coli cobalamin-dependent MetH enzyme (Scheme 4),[31] $Co^{2+}/Co^{1+}$ reduction is needed during the reactivation cycle when $Co^{1+}$Cbx is deactivated yielding $Co^{2+}$Cbx. This deactivation reaction is reported to occur once every ~2000 catalytic turnovers.[108] In another methyltransferase namely CFeSP enzyme,[32] the similar deactivation process occurs once every 100 catalytic cycles.[109] In order to maintain the proper catalytic functioning of the enzyme, $Co^{2+}$Cbx has to be converted back into the biologically active MeCbl form which

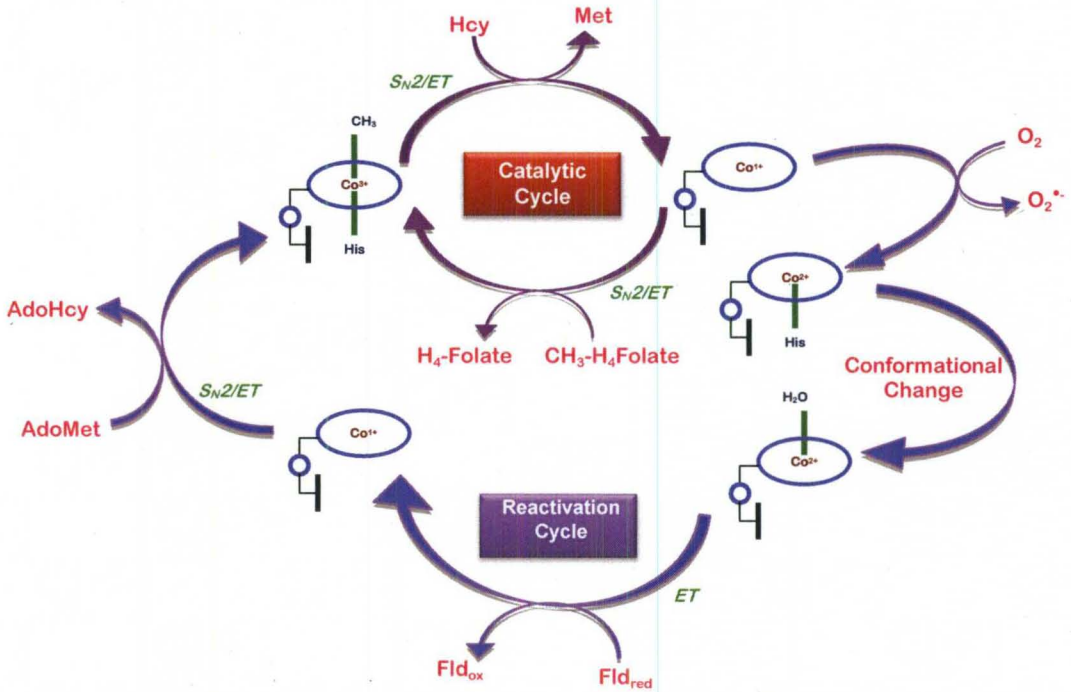


Scheme 4. Reaction cycle of MetH enzyme. The main catalytic cycle is shown in dark maroon whereas the reactivation cycle is shown in blue.

is a two-step process: (i) initially a conformational change is induced at the $Co^{2+}$Cbx where the $\alpha$-axial H759 ligand is displaced[110] and is substituted by the $\beta$-axial $H_2O$ ligand[111]. This is the rate determining step of the reactivation cycle and involves a significant amount of the conformational motion of the interacting domains.[110] (ii) The $Co^{2+}$Cbx is then reduced into $Co^{1+}$Cbx with the assistance of biological electron donor flavodoxin followed by the subsequent methylation by the adenosyl-L-methionine (AdoMet).[112]

Despite its ubiquitous nature, the $Co^{2+}/Co^{1+}$ reduction continues to remain one of the insufficiently proven aspects of cobalamin chemistry. This is due in part to thermodynamic up-hill character of the $Co^{2+}/Co^{1+}$ process, because the reduction potential of the unbound base-off $Co^{2+}$Cbx (-500 mV vs standard hydrogen electrode (SHE)) is inaccessible to the common physiological reductants (-280 mV to -440 mV vs SHE) present in the cellular environments.[86,113] To rationalize the enzyme-induced tuning of the reduction process, formation of tetracoordinated square planar $Co^{1+}$Cbx has been advocated as the most reasonable mechanistic rationale because the axial ligand ($H_2O$)-bound $Co^{1+}$Cbl is found to be a thermodynamically unstable complex ($\Delta G$ = +1.96 kcal/mol) at the level of conventional DFT (i.e., PBE/TZP).[114] Existing EXAFS[115] and spectroscopic[111,114] data have been interpreted in favor of $Co^{1+}$Cbx being strictly a tetracoordinated square planar species. MetH-bound $Co^{1+}$Cbx has also been suggested to be a square planar complex, wherein the active site Y1139 residue catalyzes the formation of square planar MetH-bound $Co^{1+}$Cbx (Scheme 5).[111,116] Experimental[117-118] and spectroscopic[119-120]

precedence in the case of human-type ACA, even predict $Co^{2+}$Cbx to be a tetracoordinated species. The catalytic importance of Q112 of the *Lr*PduO enzyme, an ACA enzyme, in promoting the formation of tetracoordinated $Co^{2+}$Cbx is well-supported by the crystallographic data: the topological

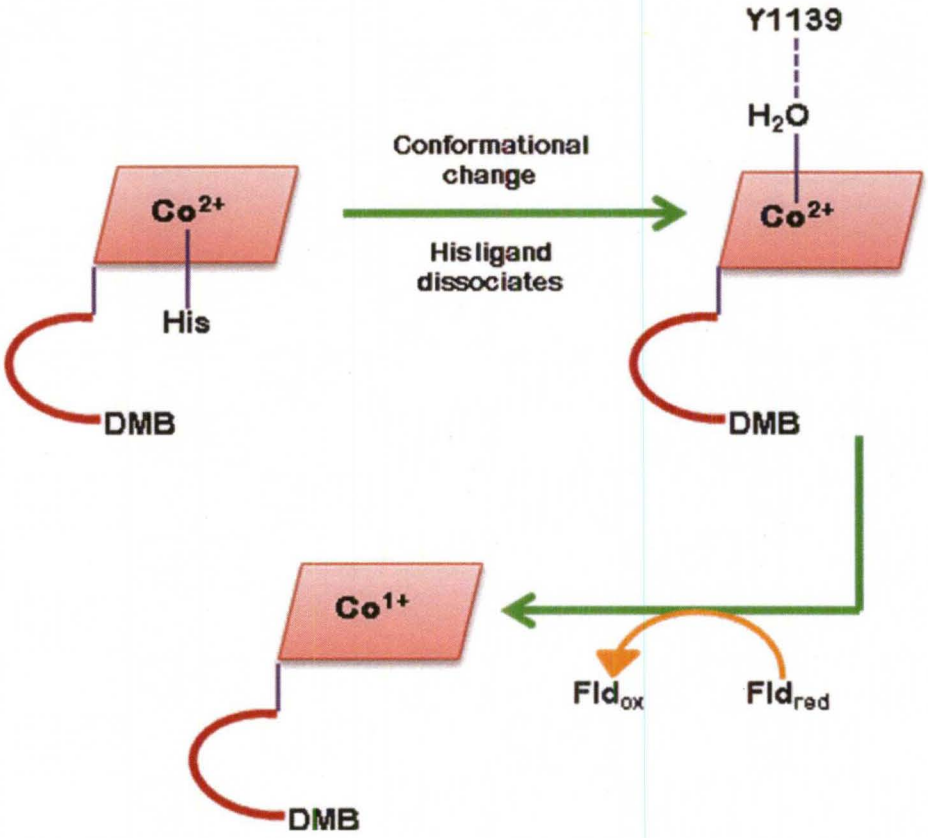


Scheme 5. MetH-induced formation of square planar $Co^{1+}$Cbx.

coordinates of Q112 in conjunction with its steric bulk has been postulated to dismiss any kind of the axial interaction of the cofactor.[118] Also, in the case of CFeSP enzyme, the QM/MM investigation of methylated $H_2O$-bound $Co^{2+}$Cbx model suggests that enzyme-bound $Co^{1+}$Cbx would be a tetracoordinated square

planar complex.[121] Surprisingly, the feasibility of a pentacoordinated $Co^{1+}$Cbx complex in the context of CFeSP enzyme (or in general for methyltransferases) has never been computationally tested using $H_2O$-bound $Co^{1+}$Cbx, rather the conclusions are based on the fact that the axial $H_2O$ ligand detachment in the case of $H_2O$-bound $Co^{2+}$Cbi is an energetically amenable process (< 4 kcal/mol).[121]

On the other hand, the X-ray structural characterization of two anionic pentacoordinated cob(I)aloximes namely $[pyCo^{1+}(dmgBF_2)_2]^-$,[122] and $[MeCNCo^{+1}(dmgBF_2)_2]^-$,[123] and, also of a $Co^{1+}$ clathrochelate ($[Co^{1+}(Cl_2g)_3(Bn\text{-}C_4H_9)_2]^-$)[124] in a trigonal prism arrangement, imply that $Co^{1+}$Cbx may also adapt to square pyramidal or octahedral coordination geometry in addition to the most widely embraced viewpoint of its square planarity. Note here that the biological importance of square pyramidal $Co^{1+}$ model compounds in the context of the catalytic cycle of MetH enzyme has also been discussed by Randaccio *et al.*[125] Interestingly, an increasing body of experimental and theoretical evidences suggests that the $d^8$ metal ions ($Co^{1+}$, $Ni^{2+}$, $Pt^{2+}$, $Pd^{2+}$ etc.) display an uncommon yet distinct ability of forming metal ion influenced H-bonds (i.e., $Co^{1+}$--H,[126,127,128] $Ni^{2+}$--H,[129] $Pt^{2+}$--H,[130,131,132-133] $Pd^{2+}$--H,[134,135] etc.)[136,137] that, in turn, empowers their complexes with an aptitude for square pyramidal coordination environment. The formation of such H-bonds is credited to the fact that the $d^8$ metal ions can utilize their preferentially oriented filled d-orbitals for interacting with the acidic hydrogens (H-X; X = N, O or C) of the axial ligands. For example, a $Ni^{2+}$--H-N interaction (2.45 Å; 158.2°) has been observed in square planar

$[Ni(NH_2Et)_3][NiL_2]$ (L = maleonitriledithiolato) complex where the hydrogen bound to N-hetero atom of the anionic ligand is engaged in cation-anion type interaction with the $Ni^{2+}$ center of the square planar complex.[129] A $Pt^{2+}$ ion-enforced charge-assisted H-bond (N-H---$Pt^{2+}$ interaction = 2.26 Å (167.3°)) has been identified in the $[PtCl_2(NH_2Me)_2][NPrn_4]_2[PtCl_4]$ complex.[132-133] It is worthy of mention that the axial $H_2O$ ligand in the trans-$[PtCl_2(NH_3)$(N-glycine)$].H_2O$ complex was found to be O-bound with the $Pt^{2+}$ ion during a prior X-ray diffraction study,[138] but this prediction has recently been reversed owing to a low temperature neutron diffraction study by Kozelka et al.,[133] wherein the accurate localization of H atoms has led to the confirmation that the $Pt^{2+}$ ion is rather H-bonded with $H_2O$ molecule. The PdClL.1.5$H_2O$ (L = glycyl-L-histidine-*N*,*N'*,*N''*) complex also displays a H-bond type interaction between the H-N segment of ligand and the square planar $Pd^{2+}$ center (N-H---$Pd^{2+}$ = 2.60 Å (137.5°)).[134]

The $Co^{1+}$ ion-induced charge-assisted H-bonds between the cobalt carbonyl anion ($Co(CO)_4^{-1}$) and its $NR_3H^+$ counterions have also been noted.[126-128] For example, the $[NMe_3H][Co(CO)_4]$ complex manifests a $Co^{1+}$--H-N interaction (2.51 Å - 2.52 Å; 179.5° - 179.7°), that is slightly weakened (2.61 Å - 2.68 Å) in the $[NEt_3H][Co(CO)_4]$ complex due to the greater steric size of the Et ligand.[126,127] The similar $Co^{1+}$--H-N interaction is also observed in crystalline $L_2L'[Co(CO)_4]$ (L = *N*-methylpiperazinium; L' = *N*-methylpiperazine) ($Co^{1+}$--H-N = 2.60 Å - 2.64 Å; 163.9° - 176.8°).[128]

These new fundamental organometallic and bioinorganic advances clearly imply that a significant amount of research effort has yet to be invested to provide

a comprehensive insight into coordination environment of $Co^{1+}$Cbx as well as into the details of the $Co^{2+}/Co^{1+}$ reduction process. The second part of this dissertation exclusively addresses the following mechanistically important question: is $Co^{1+}$Cbx intermediate really a square planar species as the existing data suggest? Or it can exist as a pentacoordinated square pyramidal or hexacoordinated octahedral complex owing to its plausible ability of communicating with the axial ligands via $Co^{1+}$ ion induced H-bonds? If yes, what could be the ensuing mechanistic prospects of such associative interactions in the context of $Co^{2+}/Co^{1+}$ reduction catalyzed by methyltransferases and ACAs? Finally, how is the thermodynamic stability of weak non-covalent $Co^{1+}$--H interactions affected by the enzyme environment? In specific, the purpose of the third study elaborated in Chapter IV is to probe the H-bond forming ability of $Co^{1+}$ ion which is a dominat $d^8$ configuration[39,40] with judiously oriented filled d-orbitals and can interact with the axial ligands in the $Co^{1+}$Cbx complexes. The DFT, natural bond orbital (NBO) and atoms in molecule (AIM) computational tools have been analyzed to investigate the coordination environments of model $Co^{1+}$Cbx complexes. The electrochemistry of $Co^{2+}/Co^{1+}$ reduction process has been computationally explored taking into account the square planar and square pyramidal geometries of $Co^{1+}$Cbx complexes.

Considering that the $d^8$ metal ion induced H-bonds are usually non-covalent in nature,[126-137] the formation of $Co^{1+}$--H bond may or may not be feasible inside the enzyme environment. To investigate the impact of biological environment of methyltransferase upon the thermodynamic stability of $Co^{1+}$--H

bond, DFT and QM/MM calculations in Chapter V have been performed to model the MetH-bound $Co^{2+}$Cbx and $Co^{1+}$Cbx complexes. The QM/MM calculations are performed using the most reasonable crystal structure available for the reaction complex of MetH-bound $Co^{2+}$Cbx (PDB-code: 3IVA @ 2.7 Å resolution)[116] to gain insight how the conformational change at the axial ligand is induced due to a change in the electronic configuration of the cobalt ion. The AIM calculations are carried out to characterize the nature of $Co^{1+}$--H interaction in model $Co^{1+}$Cbx complexes. The thermodynamic stability of H-bonded $Co^{1+}$Cbl complexes is analyzed within polarizable continuum model (PCM) of solvation where the chloroform solvent is used to mimick the enzyme environment.

In the next study in Chapter VI, DFT, AIM, NBO and QM/MM computational tools are applied to further probe the possibility of alternate coordination geometries of $Co^{1+}$Cbx. Two kinds of structural model namely simplified ($Co^{1+}$Cbl) as well as complete ($Co^{1+}$Cbi) models are considered in the DFT calculations wherein $H_2O$ and imidazole (Im) are mimicked as the axial ligands respectively. The nature of $Co^{1+}$--H interactions in the H-bonded $Co^{1+}$Cbl and $Co^{1+}$Cbi is characterized using AIM analysis. The reduction potentials of $Co^{2+}/Co^{1+}$ redox couple are calculated in three different solvents namely chloroform, acetonitrile and water while assuming all the possible coordination geometries of $Co^{1+}$Cbx complexes. The QM/MM calculations are performed on MetH-bound $Co^{1+}$Cbx complexes (PDB-code: 1BMT @ 3.0 Å resolution)[2] where the $\alpha$- and $\beta$-axial ligands are modeled by H759 and $H_2O$ respectively. The X-ray

crystal structure of the active sites of methyltransferases is analyzed to support our calculations.

Finally, the fourth study in Chapter VII focuses on understanding the possible involvement of the active site tyrosine residue (i.e., Y1139) of MetH enzyme[116,139] in the $Co^{1+}$--H bond formation. The DFT calculations are carried out on the $Co^{1+}$Cbi complexes testing two different β-axial ligands namely $H_2O$ and PhOH respectively. The PhOH motif is used to mimick the tyrosine Y1139 residue that has been found in the active site of the reactivation complex of MetH enzyme[116,139] and has been suggested to be catalytically important for the $Co^{2+}/Co^{1+}$ reduction process.[111,116] To model the local environment, an additional $H_2O$ molecule is considered in the vicinity of the β-axial ligands. The analysis of the existing crystallographic data available for the reactivation conformation of MetH enzyme has been carried out to evaluate the significance of our computational work.

# CHAPTER II

# ROLE OF TYROSINE RESIDUE IN $B_{12}$ CATALYSIS: A CASE STUDY OF ADENOSYLCOBALAMIN-DEPENDENT MUTASES

## 2.1 Introduction

AdoCbl catalyzes a variety of chemically difficult transformations involving 1,2-type intramolecular shift of a H-atom with a functional group such as alkyl, hydroxyl or amino (Scheme 1).[1-19] During the catalytic cycle the Co-C bond of AdoCbl cofactor is cleaved in a homolytic fashion leading to the formation of $Ado^{\bullet}$ and $Co^{2+}Cbx$.[41] The most remarkable aspect of AdoCbl-dependent enzyme catalysis is ~$10^{12}$ rate enhancement inside the enzyme environment.[22] Though it has been found that homolysis of the Co-C bond is rapid and is not a rate determining step[28] implying that its strength must be significantly reduced during catalytic turnover in comparison to free AdoCbl in solution,[29] yet the precise underlying mechanism responsible for such Co-C bond weakening remains elusive.

The Co-C bond in AdoCbl-dependent enzymes is not substantially destabilized in the absence of substrate. The most convincing argument supporting this notion comes from resonance Raman spectroscopy where vibrational data show that the Co-C stretching frequency is essentially the same in the case of isolated AdoCbl in solution as well as in the enzyme-bound AdoCbl.[67-69] Upon binding of substrate, the catalytic cycle is initiated with the homolysis of the Co-C bond which is followed by subsequent H-atom abstraction from the substrate. The manner in which the arrival of substrate triggers the enzymatic reaction remains an open question. Available crystallographic data for several AdoCbl-dependent enzymes[49,50,56,60,73,140,141] reveal that the substrate enters into the active site through channel positioned on the upper face of the corrin macrocycle.[49,50,56,73,140] It has further been postulated that the presence of substrate which induces a conformational switch[56] or the tight binding of the adenine binding pocket induces a marked distortion of the Co-C bond[49b,c] that can have implications with reference to the activation of Co-C bond. However, the crystal structures of AdoCbl-dependent enzymes have been determined under the condition that the Ado moiety is either not well-resolved or has been replaced by other groups. Furthermore, due to limited crystalographic resolution of available X-ray structures of $B_{12}$-dependent enzymes, one cannot get an obvious insight into how the structural changes observed upon substrate binding can be connected with AdoCbl-based catalytic activity.

On the other hand, closer inspection of crystallographic dataavailable for AdoCbl-based enzymes[49,50,56,62,73,140,141] reveals a very interesting and a common

thread connecting all these enzymes. In the vicinity of cofactor, the Y residue is present in the immediate surroundings of the active site at an average distance of ~7.5 Å from the cobalt center (see Table 1). Based upon structural information stored in protein data bank, Figure 2 sketches an overview of the local environment of the active site capturing the location of Y component in different enzymes. The –OH group of this motif is either directed towards the metal center of the cofactor or the substrate which might be significant from enzymatic catalysis point of view. Moreover, the site-specific Y89F mutation in the case of MCM,[57] has resulted in a significant drop (~$10^3$-$10^4$) in the catalytic activity.

An important question arises what can be the role of Y residue in the possible mechanism of Co-C bond activation accounting for ~$10^{12}$ enzymatic rate enhancement? Before turning our attention to this issue, it is important to emphasize that deprotonation of Y residue and its subsequent oxidation leading to the formation of neutral radical i.e., $Y \rightarrow Y^- \rightarrow Y^\bullet$, constitutes a key step in numerous enzymatic processes.[142] The participation of $Y^\bullet$ has been confirmed in many enzymes including PS-II,[143] prostaglandin H synthase,[144] galactose oxidase,[145] cytochrome c oxidase,[146] cytochrome $b_5$ reductase,[147] ribonucleotide reductase,[148] monoamine oxidase,[149] and charge transfer between the tyrosine and the tryptophan residues in proteins.[150] In all these enzymes, $Y^\bullet$ takes part in biological reactions via PCET, a phenomenon ubiquitous in biological systems and a topic of intense experimental and theoretical scrutiny. Thus, the role of the Y residue acting as a redox center has precedence in bioinorganic chemistry. This prompted us to investigate the importance of the Y residue as an internal

redox center inside the AdoCbl-dependent enzymes. If Y serves like a redox motif, an electron would be transferred to the AdoCbl cofactor leading to the formation of $\pi^*_{corrin}$ anion radical. Consequently, the cleavage of the enzyme-bound Co-C bond would be more in line with 1el-Red form of AdoCbl cofactor (i.e., $[AdoCbl]^{\bullet -}$) rather than its neutral analogue. It is well-documented in literature[86,89-90] that the electrochemical reduction of $B_{12}$ cofactors leads to significant lowering in the Co-C BDE. Such reduction of the bond strength, according to computational studies, [91-94] can be attributed to the involvement of two electronic states in the dissociation process: initially the addition of an electron to the cofactor leads to the formation of a $\pi^*_{corrin}$ anion radical, with the extra electron delocalized over the equatorial i.e. corrin ligand. As the Co-C bond

**Table 1**

Co••O(Y) distances (Å) in selected AdoCbl-dependent enzymes. Only the Y residues lying within a distance of 10 Å, from the Co center have been considered

| Enzymes | PDB-code | Tyr-code | Co••O(Y) | Ref. |
|---|---|---|---|---|
| MCM | 3REQ | Y89, Y243 | 8.71, 8.13 | 56 |
| | 4REQ | Y89, Y243 | 8.08, 6,95 | 56 |
| GLM | 1CB7 | Y181 | 7.54 | 73a |
| | 1CCW | Y181 | 7.43 | 73a |
| | 1I9C | Y181 | 7.21 | 73b |
| LAM | 1XRS | Y193 | 6.95 | 141 |
| DDH | 1DIO | Y226 | 7.20 | 49a |
| | 1EEX | Y226 | 7.23 | 49b |
| | 1EGM | Y226 | 7.19 | 49b |
| GDH | 1IWP | Y227 | 7.36 | 50a |
| | 1MMF | Y227 | 7.42 | 50b |

* MCM=MethylmalonylCoA Mutase; GLM=Glutamate Mutase; LAM= Lysine Amino Mutase; DDH=Diol Dehydratase; GDH=Glycerol Dehydratase

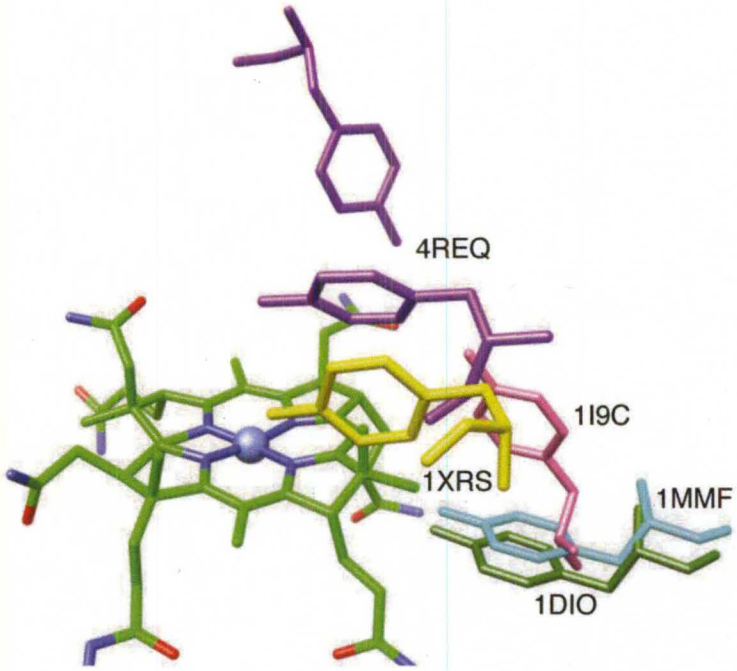


Figure 2. Close up view of the superimposition of the active site in AdoCbl-dependent enzymes depicting the location of Y residue relative to the corrin ring: 4REQ (Y89, Y213, purple), 1XRS (Y193, yellow), 1DIO (Y226, green), 1MMF (Y227, cyan), and 1I9C (Y181, pink). The corrin ring is shown only for MCM (4REQ) (see Table 1 for details).

is stretched, the extra electron relocates into the $\sigma^*_{Co\text{-}C}$ state, and the final cleavage involves a three-electron bond $(\sigma)^2(\sigma^*)^1$. Thus, according to this proposal, the main catalytic effect of AdoCbl-dependent enzymes may be due to the weakening of the Co-C bond via increased population of the $\sigma^*_{Co\text{-}C}$ orbital.

The purpose of the research described in this chapter is to investigate the redox role of the active site Y residue in the Co-C bond activation in AdoCbl-

dependent MCM and GLM mutases respectively. A variety of structural models while incorporating a varied degree of complexity associated with electronic structure calculations have been used to accomplish the research goals.

## 2.2 Computational Details

Three levels of sophistication with respect to theoretical framework as well as with regard to the structural models have been applied to elucidate the electronic properties of AdoCbl–Y complex. Specifically, first of all, the complex was investigated at DFT level of theory using realistic structural complexes of MCM and GLM mutases respectively. Since the diradical state of the complex can only approximately be described at a DFT level of theory, the analysis of AdoCbl–Y complex was also performed using multi-reference CASSCF wavefunction followed by second order multi-reference perturbation theory (QDPT2). In order to take enzymatic environment into consideration, QM/MM calculations were also carried out for the MCM enzyme. Finally, the effect of Y89F site-directed mutation of MCM enzyme on the electronic structure of the diradical state of the AdoCbl–Y complex was also probed.

### 2.2.1 DFT calculations

All the calculations reported in the present work have been carried out using the Gaussian03[151] suite of programs for electronic structure and properties calculations. To investigate the significance of Y being in the immediate vicinity of AdoCbl, we have carried out DFT-based computations using the structural models mimicking the active sites of MCM (PDB-code: 4REQ @ 2.2 Å resolution)

and GLM (PDB-code: 1I9C @ Å resolution) mutases (Table 1; Figure 2). The models have been constructed, first optimizing the structure of AdoCbl (simplified with respect to the side chains of corrin ring) and then placing the PhOH (an ideal structural mimick of the Y residue) in the locations consistent with the available crystallographic information (Figure 3). Both neutral (PhOH) and deprotonated phenol ($PhO^-$) were employed in the present theoretical investigation. BP86[152] and B3LYP[152a,153]-based DFT calculations have been performed assuming singlet electronic state, consistent with even number of total electrons, while allowing spin polarization between different molecular entities via unrestricted

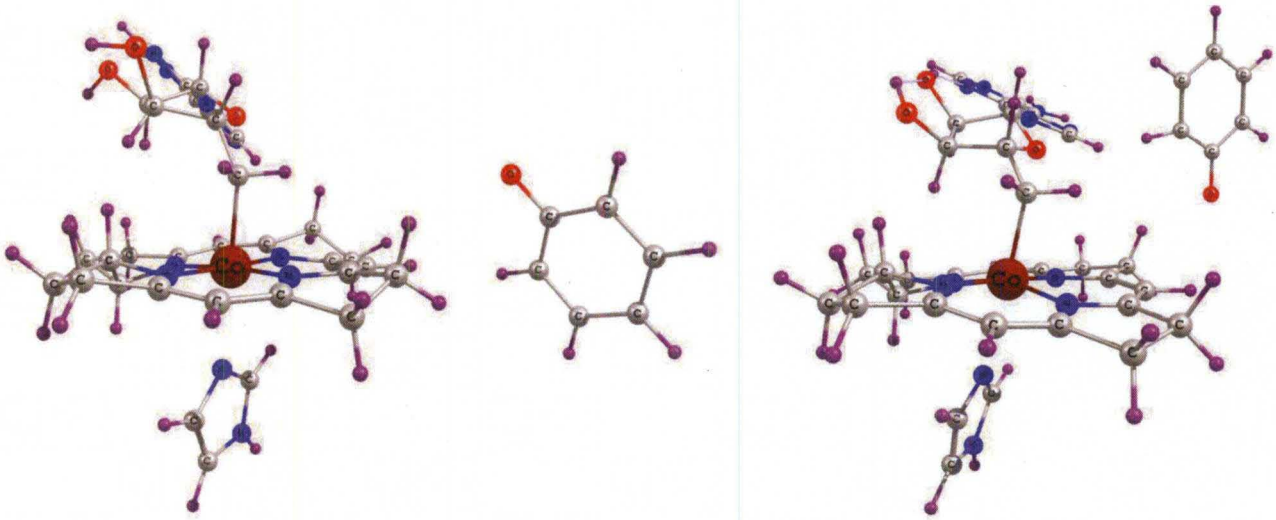

Figure 3. Structural models of GLM-(*left*) and MCM-bound (*right*) AdoCbl--$Y^-$ complexes.

Kohn-Sham formalism. The 6-31G(d) basis set (5d components) was used throughout the calculations. The use of BP86/6-31G(d) 5d level of theory is

inspired by the fact that it constitutes an appropriate platform for addressing the structural, electronic and spectroscopic properties of the alkyl-cobalt(III) complexes.[82,91-94,154,155,156]

### 2.2.2 CASSCF/MC-XQDPT2 calculations

Considering the fact that the diradical electronic state could only approximately be described using single-deterimantal wavefunction, CASSCF calculations followed by second-order perturbation theory were also applied to elucidate the electronic properties of AdoCbl–Y complex. Recently the modified version of quasi-degenerate perturbation theory with multiconfigurational self-consistent-field reference function (QDPT2)[157] referred to as MC-XQDPT2 as implemented in the PC GAMESS/Firefly QC package,[158] along with the SV(P) basis set was applied. In order to reduce the structural complexity of AdoCbl cofactor, Ado ligand was further simplified to $-CH_2CH_3$.[82]

### 2.2.3 QM/MM Calculations

The most complex and advanced calculations were carried out by taking into account the actual enzymatic environment of MCM enzyme where AdoCbl cofactor and Y89 residue were considered as a part of QM domain. Two different types of QM/MM calculations were performed with different QM and MM partitions. To prepare a structurally reasonable model for QM/MM calculations, we did initial model setting on the basis of the crystal structure (PDB-code: 4REQ @ 2.2 Å resolution) of MCM--substrate complex. The protonation states of

titratable residues at pH 7.5 were determined with the Generalized-Born method. The enzyme model included ligands, water molecules, and amino acids 38-728 of chain A, resulting in 12289 atoms in total. The system was heated and equilibrated at the CHARMM level of theory in three steps: (i) steepest descent optimization of the system, (ii) molecular dynamics (MD) for 15 ps heating from 50 to 300 K, and (iii) equilibration for 400 ps at 300 K with a time step of 1 fs. During the MD simulation, the coordinates of the QM-region atoms and of heavy atoms beyond 20 Å from the Co atom in the active site were kept fixed at the X-ray coordinates. The SHAKE algorithm was used to constrain bonds involving H-atoms.

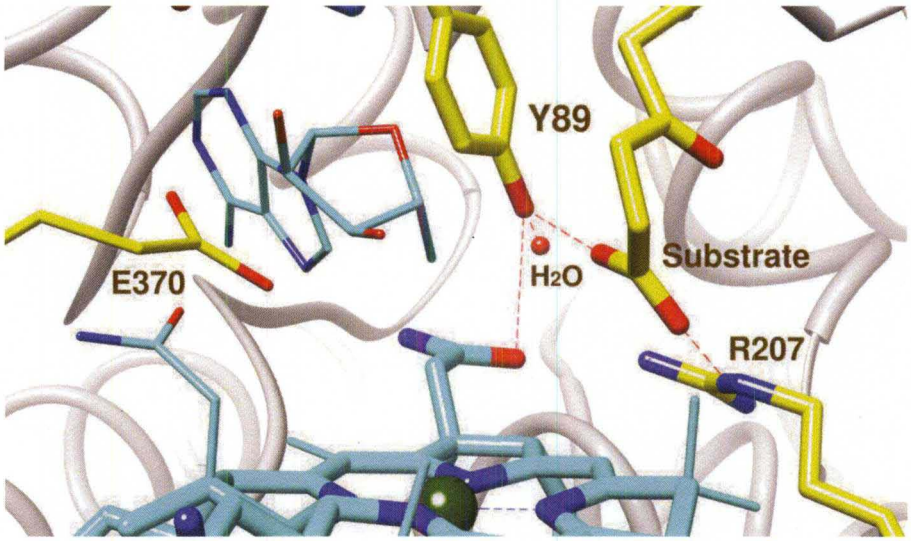


Figure 4. Active site view of MCM-bound AdoCbl cofactor (PDB-code: 4REQ @ 2.2 Å resolution).

Finally, the system was minimized with the adopted basis Newton-Raphson (ABNR) algorithm for 5000 steps. All calculations were carried out with Discovery Studio 2.0. The electronic structure of the AdoCbl-$Y^-$ complex was probed assuming QM matrix comprised of truncated coenzyme $B_{12}$ with respect to the side chains, part of substrate along with R207, H610, E370 and Y89 residues while treating rest of the enzyme at the MM level of theory (Figure 4). The enzyme model, employed in the present investigation, comprised of residues 38-78 of chain A, the AdoCbl cofactor, the truncated substrate, and the corresponding crystal water molecules closer to chain A, while the remaining flexible residues 3-37 of chain A, lying far from the cofactor and substrate were excluded from calculations. The effect of Y89F mutation was studied assuming Ado group, partial substrate along with Y89, R207, H244 and Q197 residues as the constituents of QM domain. BP86 functional was used to investigate the electronic properties of the AdoCbl-$Y^-$ complex while B3LYP was employed to analyze the effect of Y89F mutation.

All QM/MM calculations were performed with the ChemShell[159] interface using TURBOMOLE[160] for the DFT calculations along with CHARMM[161] force field. The basis set SV(P) (for all atoms) was used to carry out the geometry optimizations. The CHARMM force field running through the DL_POLY program was used for the MM part of the system. A standard electronic embedding scheme was chosen: the fixed MM atomic charges were included into the one-electron Hamiltonian of the QM calculations, and the QM/MM electrostatic interactions were evaluated from the QM electrostatic potential and the MM

atomic charges. No cutoffs were applied for the non-bonded MM and QM/MM interactions. We defined a region with 1308 and 1170 atoms to be fully optimized by including all the residues that have atoms within a distance of 10 Å from the Co atom for the Co–C bond cleavage and from the substrate for the rearrangement process, respectively, while keeping the remaining atoms fixed.

## 2.3 Results and Discussion

### 2.3.1 DFT Analysis of AdoCbl-Y Model Complexes

To investigate the significance of Y being in the vicinity of AdoCbl, first of all, we carried out DFT computations at the BP86/6-31G(d) 5D level of theory considering the structural replica of the active sites of MCM and GLM enzymes respectively. The structural replicas were modeled, by optimizing the simplified AdoCbl cofactor and then placing the structural mimicks of Y motif (i.e., PhOH and $PhO^-$) in positions consistent with available crystallographic data (Figure 2). DFT calculations were performed considering singlet electronic state while permitting spin polarization between different motives within the broken symmetry assumption. In structural models containing PhOH, the spin polarized solution couldn't be obtained while in the case of $PhO^-$ containing complexes (AdoCbl-$PhO^-$), the spin polarized solution pertained to the lowest energy structure implying that the complex has a diradical character and should be better described as $[AdoCbl]^{\bullet -}$-$PhO^{\bullet}$. This finding was further confirmed by using B3LYP functional (Tables A2 - A3), although numeric details were slightly different. The diradical character of the complex was further verified by

computing the triplet state and analyzing spin density pattern. Such spin polarization is indicative of the fact that the electronic configuration needed to describe AdoCbl-$PhO^-$ system (Figure 3), may require multi-configurational wave function. Careful analysis of spin polarized results reveals that the oxidation of $PhO^-$ takes place and the complex has a diradical character. More precisely, the AdoCbl-$PhO^-$ complex is better described as a diradical species, $[AdoCbl]^{\bullet -}$-$PhO^{\bullet}$ consistent with an open-shell singlet electronic configuration. This analysis further proves that the presence of the $Y^-$ residue in the proximity of AdoCbl cofactor induces ET between the two units, thus forming a diradical state. The formation of diradical complex is highly sensitive with respect to the location as well as orientation of the Y residue. When the Y motif was placed in orientation consistent with X-ray data, spin density was found to be equally distributed

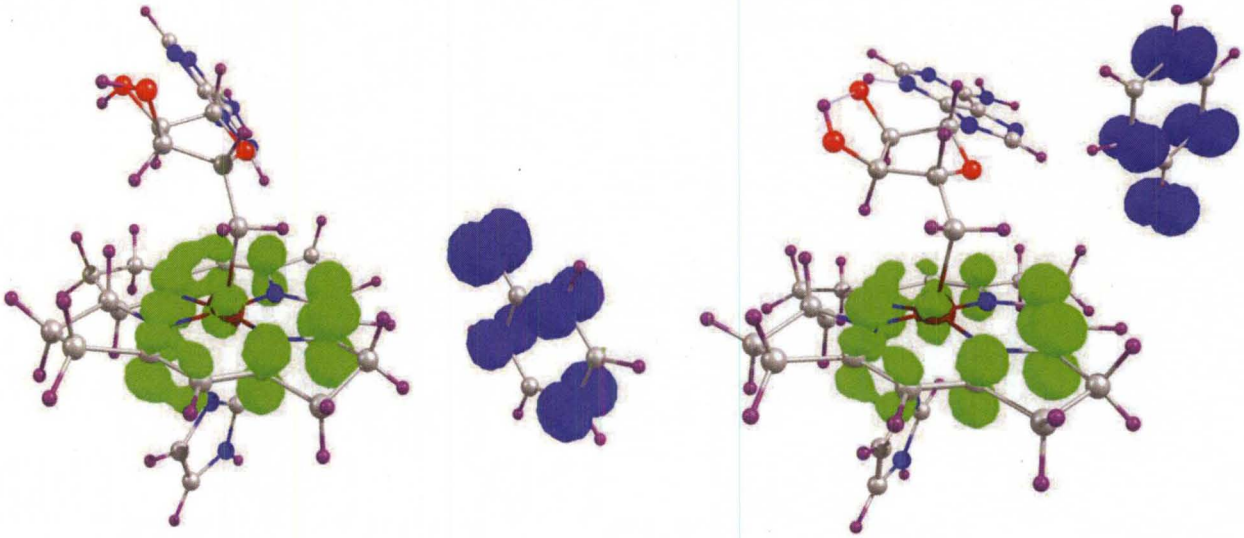

Figure 5. Spin density distribution in the structural models of GLM-(Left Panel) and MCM-bound (Right Panel) AdoCbl-$Y^-$ complexes where blue and green colors represent alpha and beta spin densities respectively.

between the Y residue and AdoCbl (Tables A1 - A2) but as the orientation of the Y motif was altered by means of rotation through different angles (but keeping the same location), we could not find the diradical state of the complex pointing that only a specific location and orientation of Y can induce the ET between the two motifs highlighting the enzyme specificity. To gain further insight, the isosurface spin density profiles were generated for structural models under consideration (Figure 5). In both cases, an unpaired electron is localized on the Y component with spin density distribution in odd-alternant manner, a typical characteristic of $Y^{\bullet}$, while the other electron is transferred onto the AdoCbl where it is mainly delocalized on the corrin ligand. The latter case represents a distribution consistent with the $\pi^*_{corrin}$ anion radical.

Clearly, the presence of the $PhO^-$ within ~7.5 Å distance from AdoCbl alters its electronic structure and the cleavage of the enzyme-bound Co-C bond would be more in line with 1el-Red form of AdoCbl (i.e. $[AdoCbl]^{\bullet -}$). Despite the potential relevance of the one-electron reduction of cofactor to the $B_{12}$ catalysis,[86,89-90] the reductive activation mechanism has never been considered as a valid mechanism mainly because the redox chemistry of $B_{12}$ cofactors is not accessible to the common biological reducing agents. [23,162] This argument is based on redox potentials obtained from electrochemical measurements in solution that cannot be directly applied to the enzyme-bound processes. Evidently interactions among the active site residues can appreciably alter the redox potential of the Y residue as well as that of the cofactor. For example, as has been found in case of PSII, the redox potentials of Y as well as that of $P680^+$

are appreciably tuned by the local protein invironment.[143] Indeed, as has been found here, the presence of the Y residue in the vicinity of AdoCbl might play the crucial role of a reducing agent causing the formation of $\pi^*_{corrin}$ anion radical in AdoCbl-dependent mutases. To further elaborate this proposal, we have performed three series of calculations: (1) dissociation energy curve was computed for neutral cofactor (2) similar analysis was performed for $[AdoCbl]^{\bullet -}$ in accordance with electrochemical measurements, and (3) energy curve was computed for AdoCbl in presence of $PhO^-$. Last series of calculations were performed with an additional constraint imposed on the orientation of $PhO^-$ with respect to the Co centre in accordance with 1I9C structure. Figure 6 displays the corresponding energy dissociation curves. In case of neutral cofactor, the energy

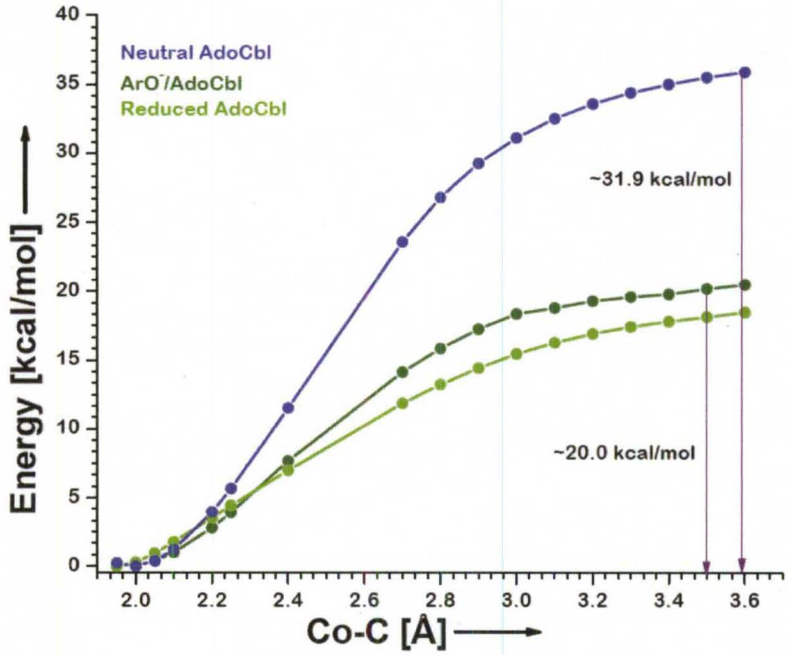


Figure 6. Co-C BDE curves for neutral AdoCbl, its 1-el-Red analogue (i.e., $[AdoCbl]^{\bullet -}$) and AdoCbl-$PhO^-$ complex.

required to cleave Co-C bond homolytically is 31.9 kcal/mol, in excellent agreement with experimental data of 31.5 ± 1.3 kcal/mol. However, in case of $[AdoCbl]^{\bullet -}$, the Co-C BDE is significantly reduced due to involvement of two electronic states: initially a $\pi^*_{corrin}$ state is formed with the extra electron delocalized over the corrin ligand, but as the Co-C bond is stretched (~2.50 Å), the extra electron transfers to the $\sigma^*_{Co\text{-}C}$ state. The mechanism of reductive cleavage for AdoCbl follows closely what has recently been reported for MeCbl[91,93-94] and its Pc analogue[92]. Since the final cleavage involves a three electron bond $(\sigma)^2(\sigma^*)^1$, the Co-C BDE decreases to 18.0 kcal/mol, implying 44% bond strength reduction. Interestingly, the dissociation energy curve for Co-C bond estimated in case of $[AdoCbl]^{\bullet -}$-$PhO^{\bullet}$ complex resembles very closely to that obtained for $[AdoCbl]^{\bullet -}$, and the BDE lowering essentially follows the same protocol. The presence of local enzyme environment near AdoCbl cofactor has resulted in ~41% lowering in the Co-C BDE which provides the logistic explanation why the formation of $[AdoCbl]^{\bullet -}$ can be one of the key ingredients of catalytic effect affiliated with AdoCbl-dependent mutases.

### 2.3.2 X-ray Structural Analysis of MCM and GLM Mutases

Up to now we have presented crystallographic details and computational evidences highlighting the critical importance of Y in the activation of Co-C bond in AdoCbl-dependent enzymes. According to DFT calculations, ET occurs only in case of $PhO^-$ (Figure 5), which makes the proton abstraction prerequisite for ET. Since the Y is present as a neutral residue inside the enzymes, it is reasonable

to postulate that upon substrate binding, the Y residue is deprotonated. The local environment around the active site provides important insight into how the deprotonation may take place (Figure 7). In case of MCM, Y89 residue lies in close proximity of substrate (i.e., MCA802) and a solvent HOH170 molecule, with the Y89 being at a distance of 2.60 Å and 2.69 Å, from the substrate and water molecule respectively.[56] The similar inspection of substrate-free crystal structure (PDB-code: 3REQ)[56] implies that the distance between the Y residue and the nearby H364 residue is significantly large enough (i.e., 4.09 Å) to discard the possibility of any H-bond formation using the phenolic proton of the Y residue (Figure 7c). This structural insight elucidates that the Y181 residue in case of GLM[73b] is at a distance of 3.38 Å and 3.41 Å from the substrate and the proximal histidine (H150) respectively. Thus it is expected that deprotonation of Y occurs upon substrate binding which serves to complete the PT pathway thereby promoting ET to cofactor. It is therefore reasonable to further postulate that PT step is coupled to ET which can be termed PCET (Scheme 6). There are two experimental findings which lend further support to PCET mechanism in case of AdoCbl-dependent mutases: in case of MCM enzyme, the Y89F mutation has lead to decrease in catalytic activity by 3-4 orders of magnitude.[57] Although this has been interpreted as the loss of stabilizing interactions upon mutation, the replacement Y $\rightarrow$ F appears to be more consistent with decrease in the rate of ET as Y is a comparatively electron rich systems. This implies that Y acts as a redox center transferring an electron to the cofactor, instead of just stabilizing the radicals formed upon the homolysis of Co-C bond. The further evidences

supporting PCET proposal comes from another experimental study[163] where the sensitivity of MCM catalytic activity with respect to the substrate modification was addressed. It was observed that the slight modifications in the structure of the substrate lead to substantial decrease in the catalytic rate which also underlines the significance of substrate in the activation process. The key feature of present proposal is that the Y motif acts as an internal redox center which transfers an electron to the AdoCbl cofactor leading to the formation of $\pi^*_{corrin}$ anion radical. Once the electron is transferred, the cleavage of the Co-C bond occurs from $[AdoCbl]^{\bullet -}$ involving a three electron bond $(\sigma)^2(\sigma^*)^1$, thereby yielding $Co^{1+}Cbx$ and $Ado^{\bullet}$. Although the $Y^{\bullet}$ as well as $Co^{1+}Cbx$ have never been observed during the experimental studies of AdoCbl-dependent enzymes, it does not rule out the possibility of the involvement of theY motif in the activation of Co-C bond. The lack of experimental $Y^{\bullet}$ detection can be explained by the back electron transfer involving $Co^{1+}Cbx$ and $Y^{\bullet}$ i.e. $Co^{1+}Cbx/Y^{\bullet} \rightarrow Co^{2+}Cbx/Y$ which is a thermodynamically feasible reaction because $Co^{1+}Cbx$ is a powerful reducing agent which favors the ET to the $Y^{\bullet}$. Thus the experimentally observed species would be $Co^{1+}Cbx$ instead of $Co^{2+}Cbx$. This type of ET reaction has chemical precedence in case of cobalamin-dependent MetH where $Co^{1+}Cbx$ is oxidized to $Co^{2+}Cbx$ in every 200 catalytic cycles.[108,112]

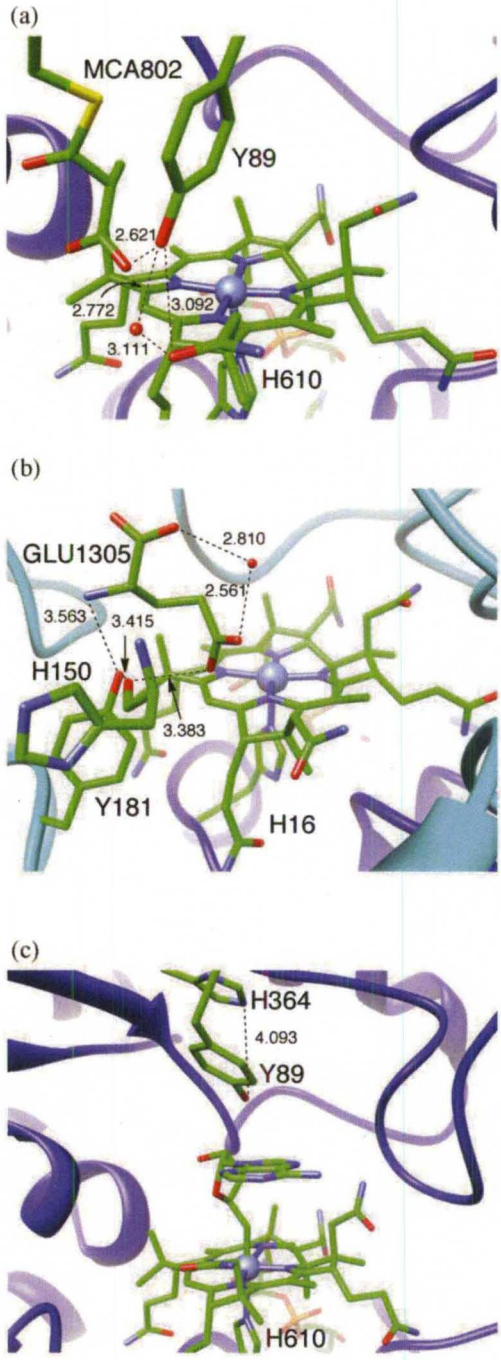


Figure 7. Close-up of the active site in AdoCbl-dependent mutases showing the location of Y residue relative to substrate and the corrin ring. (a) 4REQ crystal structure of MCM, (b) 1I9C crystal structure of GLM, (c) 3REQ crystal structure of substrate-free MCM.

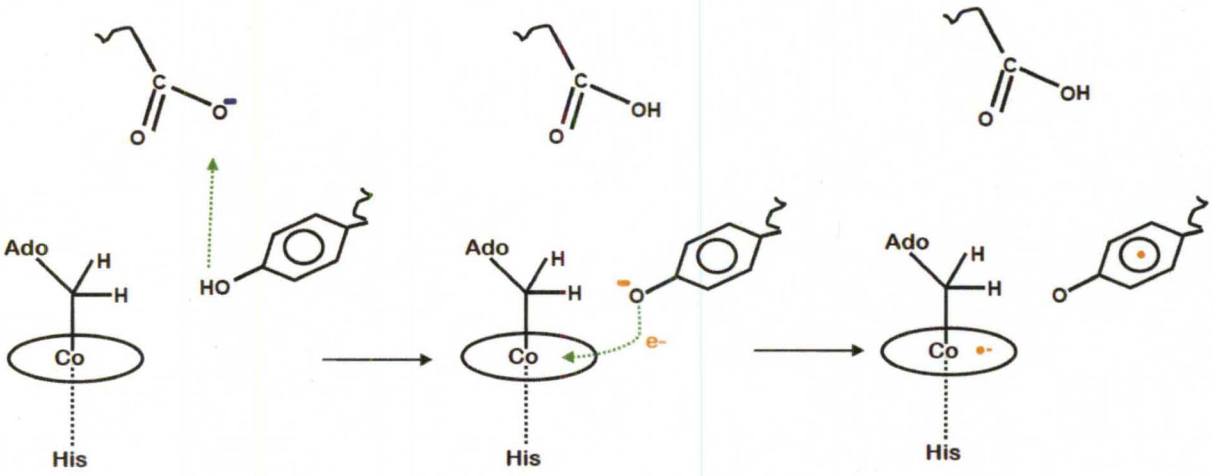


Scheme 6. PCET-inspired mechanistic pathway for the activation of Co-C bond in AdoCbl-dependent mutases.

### 2.3.3 CASSCF/MC-XQDPT2 Analysis of AdoCbl-$Y^-$ Complex

DFT-based investigation of electronic properties of the structural mimicks of two mutases under mention pointed out that the presence of the $Y^-$ in the vicinity of the AdoCbl cofactor alters its electronic structure by transferring an electron to the cofactor that gets delocalized over the corrin ring. This observation is based on UHF-type spin polarized solution with a noticeable value of $\langle S^2 \rangle$ that could be used for quantifying the extent of diradical character of a complex. Spin density is found to be evenly distributed between corrin and the Y aromatic rings. However, from the electronic structure point of view, multi-reference framework is required to describe the systems with diradical character as the open-shell singlet electronic configurations are only accurately captured using multi-reference wavefunctions. Since the Kohn-Sham formalism, which is

the basis for all DFT-based methodologies, is restricted to single-reference framework, we decided to perform CASSCF type analysis of the structural complex which is considered to be a more accurate theoretical way of addressing diradical-based problems.

In order to reduce the structural complexity, the Ado ligand of AdoCbl–$PhO^-$ complex was further simplified to $-CH_2CH_3$ group. Different active spaces were tested and analyzed based on initial orbitals generated from B3LYP/SV(P) calculations. Previously reported CASSCF calculations for $Co^{1+}$Cbx[39,40] and corroles[164] have provided important clues regarding how to select an active space for addressing such problems. Final active space selected in such a way had 12 active electrons distributed among 12 active orbitals as shown in Figure 8. The active space comprised of two doubly occupied corrin π–orbitals, $\sigma_{Co\text{-}C}$, $3d_{xz}$, *p* orbital of tyrosine oxygen, and tyrosine π–orbital plus oxygen-centred p-orbital. The respective correlating orbitals were three orrin π*–orbitals, $\sigma^*_{Co\text{-}C}$, $4d_{xz}$, and tyrosine π*–orbital. It is important to note that *p* orbital of tyrosine oxygen (lone pair) does not have correlating counterpart and thus corrin π*–orbital was selected. Using active space made-up of π spaces of Y as well as of corrin, our objective was to explore whether the formation of the diradical state is energetically feasible considering the close proximity between AdoCbl cofactor and the Y motif. However, performing CASSCF calculations that only accounted for the non-dynamical electron correlation was not enough and in addition dynamical correlation energy was needed to be incorporated in order to capture

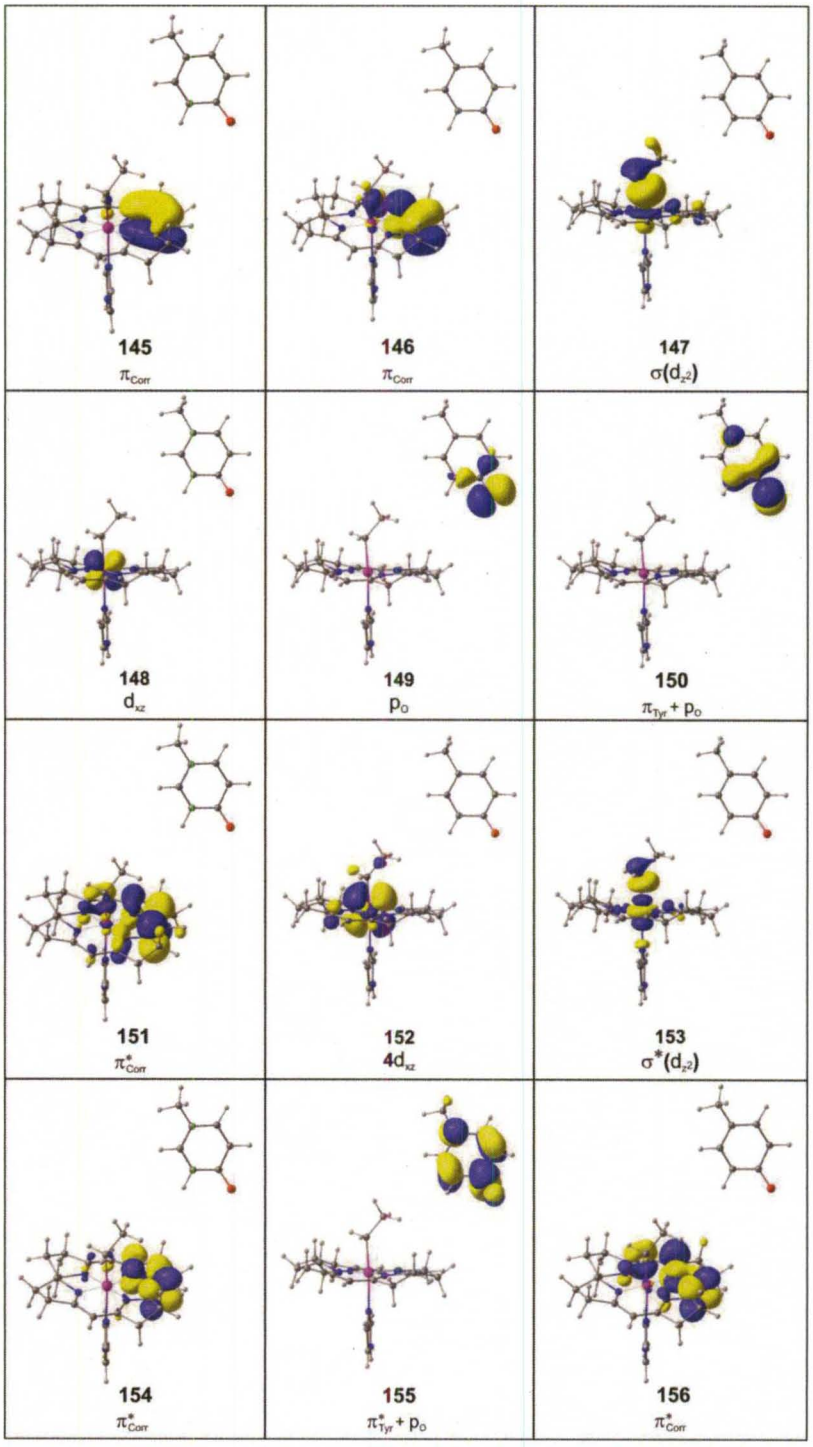


Figure 8. Orbitals in the active space for the $\Psi_{dirad}$ and $\Psi_{anionic}$ wave functions.

the essence of problem in hand. This was accomplished via using second order mutli-reference perturbation theory based on CASSCF wavefunction[157] where the efficient MC-XQDPT2 scheme was applied to account for the dynamical correlations.[158] To cover both anionic and diradical states we performed a series of state-average calculations (SA-CASSCF) testing different number of states. It is concluded that only three states are sufficient to describe the problem. Taking into account the fact that structure was taken from DFT calculation of the previous section and further truncation with respect to Ado group was applied, we also tested geometrical changes and their influence on final results. Since it has already been established that the displacement of axial base might have important influence on $\pi^*_{corrin}$ anion radical, we probed the energy dependence as a function of Co-$N_{ax}$ coordinate. As shown in Figure 9, all three states showed monotonic changes and the minima of energy occurred at Co-$N_{ax}$ ~2.3 Å.

The results based on CASSCF/MC-XQDPT2 calculations are fully consistent with conclusions derived from DFT analysis. Indeed, the lowest electronic state of the structural complex is found to be the diradical state i.e., $[AdoCbl]^{\bullet-}$-$PhO^{\bullet}$ while the anionic state is observed to be energetically 5.3 kcal/mol higher than the diradical state. The third electronic state probed in the current analysis also has diradical character but it is mainly due to excitation from the *p* orbital of tyrosyl oxygen to π–orbital of corrin. This state lies energetically much higher than the anionic state. It should be pointed out that energy differences between anionic and diradical states has only semi-quantitative meaning because the calculations are carried out using the geometry that was

optimized at DFT level of theory only. Taking into account the fact that neutral charges were not shielded by surrounding environment, the energy difference was most likely overestimated. However it serves as a proof of concept because the diradical state is found to be the lowest electronic state of the AdoCbl-$Y^-$ complex.

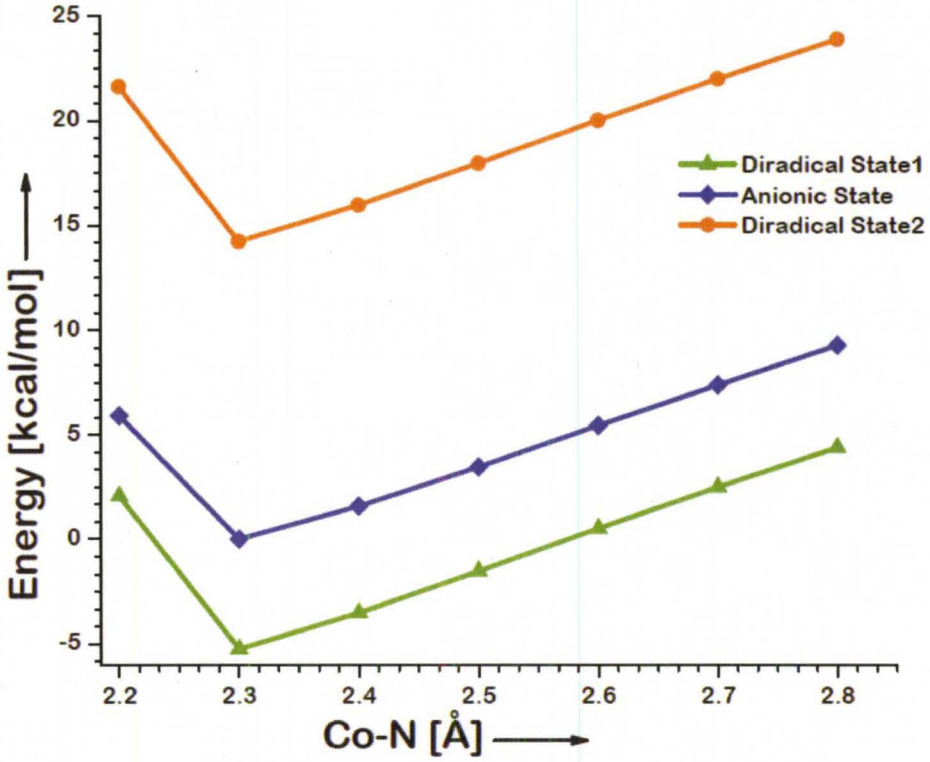


Figure 9. Diradical and anionic states of AdoCbl–$PhO^-$ complex computed along the Co-$N_{ax}$ coordinate at CASSCF/MP2 level of theory.

### 2.3.4 QM/MM Analysis of MCM-bound AdoCbl–$Y^-$ Complex

Up to this point, DFT and CASSCF/MC-XQDPT2 calculations were carried out for the isolated complexes in gas phase without the explicit inclusion of enzyme environment. Such models might artificially stabilize the diradical state and could give rise to anionic state due to the improperly balanced charges by the surrounding environment. To provide a more realistic description and to elucidate the energetic of the MCM-bound AdoCbl-$Y^-$ complex, we performed QM/MM calculations using the 4REQ crystal structure. It is important to recall that truncated AdoCbl with respect to the side chains, part of substrate together with R207, H610, E370 and Y89 residues were included in the QM part (Figure 4) while rest of the enzyme was treated at MM level. Several groups[81,84,85] have applied QM/MM framework to model the catalytic activity of AdoCbl-dependent enzymes but Y89 residue hasn't been considered as a part of QM region in any of these studies. Morokuma and co-workers[85] investigated the origin of catalysis in MCM enzyme where they considered several models to mimick the QM domain in terms of structural complexity but our present QM/MM set up containing Y89 residue is the largest model to be investigated till date.

Employing such a large QM region, structural analysis of the AdoCbl–Y complex was first carried out assuming the Y residue (Figure 10a). Of particular interest is the network of H-bonds around the Y residue and substrate with possible interaction exerted by the side chain of the AdoCbl cofactor. Although these chains were treated at the MM level of theory, yet the interactions involving these chains are nicely captured in the present study. The phenoxyl proton of

Y89 is directed towards the $-COO^-$ group of substrate and the YOH···$^-$OOC– optimized distance of 1.55 Å is relatively short. In addition, the –OH group of Y89 residue is involved in another H-bond with a solvent molecule (HOH170), present at a distance of 1.94 Å. The solvent molecule is also engaged in H-bond formation with the side chains of AdoCbl lying at 2.12 and 2.15 Å distances respectively. Thus the local environment around the Y motive (Y89) shows a network of H-bonds which might be important for efficient PT in order to facilitate ET process. Since objective of the present study is to explore the feasibility of tyrosine residue being oxidized, $Y^- \rightarrow Y^\bullet$, and of the AdoCbl cofactor being reduced (Scheme 6), we also optimized the anionic AdoCbl-$Y^-$ state. The deprotonation of the Y residue doesn't lead to the structural alternations as shown in Figure 10b. Using the anionic wavefunction, the triplet state calculations on AdoCbl-$Y^-$ were performed in order to generate an initial guess for probing the diradical state of the complex. Based on the triplet MOs the singlet state calculations on AdoCbl-$Y^-$ were performed while allowing spin polarization that could be used to describe diradical character of a given system. It is found that the optimized structure has wavefunction with $\langle S^2 \rangle = 0.30$ and the identity of the diradical state is further verified by the inspection of spin profiles. The spin density distribution of MCM-bound [AdoCbl]$^{\bullet -}$-$Y^\bullet$ is very similar to that calculated for the structural replica of active site of MCM in gas phase (see Sections 2.3.1 and 2.3.3).

Figure 10c displays QM/MM optimized structure of diradical analogue, showing that no significant differences in terms of key structural parameters are

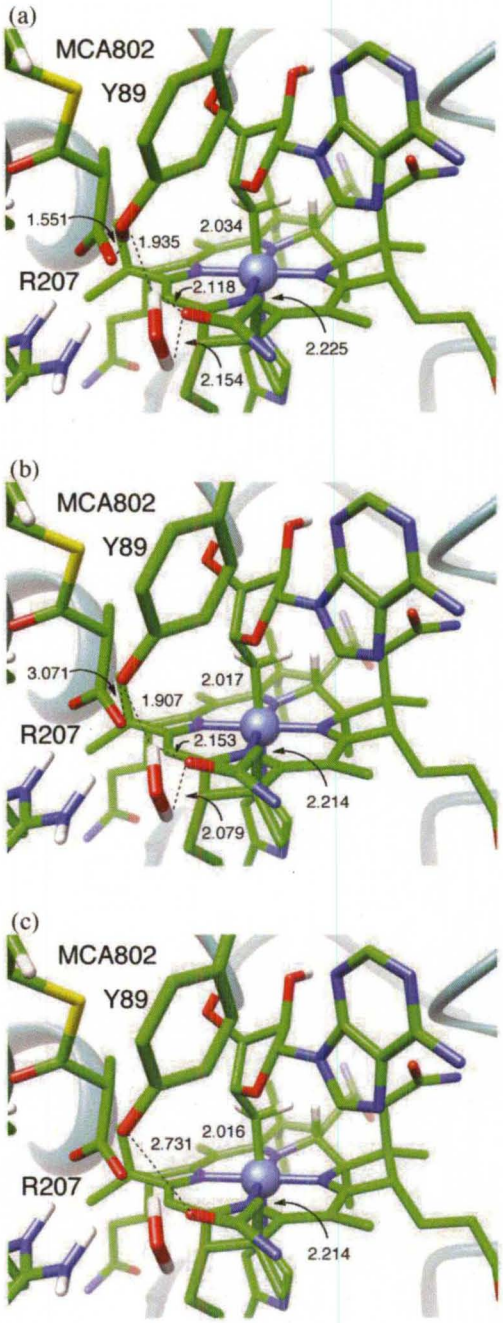


Figure 10. The active site for the reactant complex in different states. (a) AdoCbl-Y; (b) AdoCbl-Y$^-$, and (c) [AdoCbl]$^{\bullet-}$-Y$^{\bullet}$.

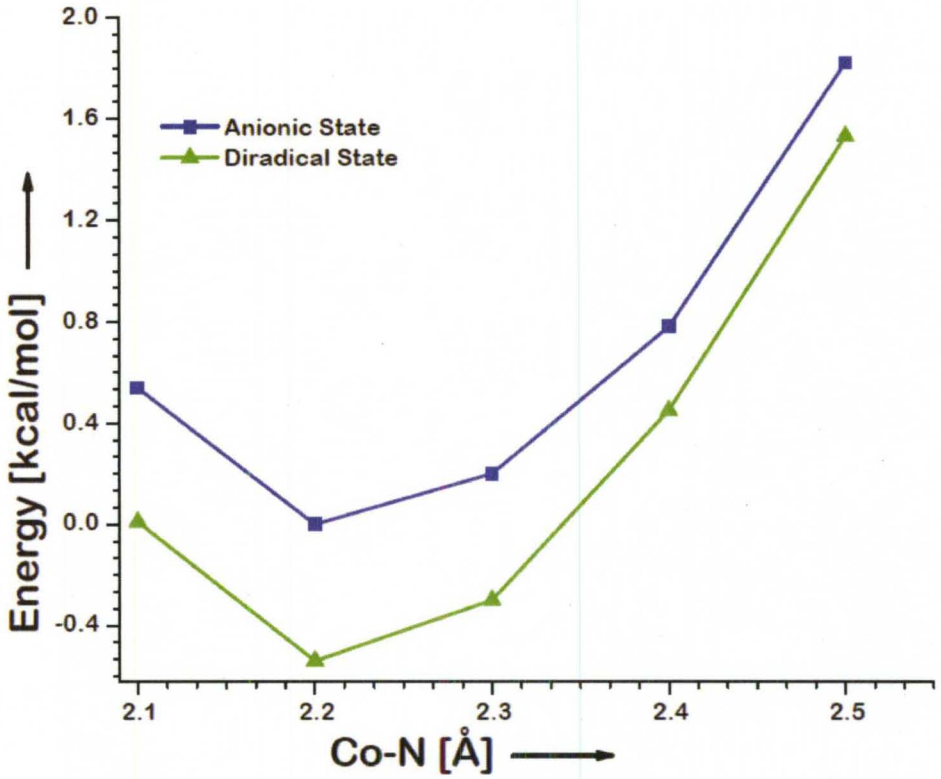


Figure 11. Anionic and diradical states of MCM-bound AdoCbl-Y complex as a function of the Co-$N_{ax}$(H610) bond distance.

noticed among them. In particular, the length of the Co-C bond is found to be 2.02 Å while the Co-N(H610) axial coordinate is 2.21 Å long. However it's important to notice that the distance between Y89 and the side chain of the AdoCbl cofactor in case of diradical complex is short enough (2.73 Å) to allow the efficient overlap required for the ET. The QM/MM optimized Co-N(H610) distance is observed to be noticeably shorter than that (2.47 Å) reported for 4REQ structure. Thus we performed two additional series of calculations where both the anionic and diradical states were optimized with energy being evaluated along

the Co-N(H610) coordinate. The minimum energy of the anionic state was used as a reference and energetic changes were plotted as a function of the Co-N(H610) distance (Figure 11). The energetic difference between the two states is found to be 0.53 kcal/mol implying that the energy gap between the two states in the presence of enzyme is significantly reduced; however, the diradical state is still dthe lowest electronic state of the system. Thus, the results of QM/MM analysis are in agreement with what is previously concluded for isolated complexes based on the gas phase calculations.

### 2.3.5 QM/MM Analysis of Y89F Mutation upon the Initial Step of $B_{12}$ Catalysis

There have been several reports documented in literature where the effect of mutation of Y89 residue[57] as well as a few others[165-166] near the corrin of MCM enzyme has been investigated. In particular, the crystal structure of Y89F mutant (PDB-code: 5REQ)[58] has been reported for mutant that is found to be essentially superimposable with that of wild-type, implying that the loss of the phenolic hydroxyl group has a minor impact on the structural properties, in particular on the active site environment of the coenzyme $B_{12}$. Interestingly, however, when the effect of mutation on the homolysis of the Co-C bond is studied, it has been found that ~$10^3$ to $10^4$ of the total $10^{12}$-fold acceleration of the homolysis rate might be derived from the contribution of a single Y89 residue.[57]

There are several possible explanations why the Y89F mutation might lead to a drop in catalytic activity. In the light of the present calculations, Y89

plays a critical role in the activation of the Co-C bond because the Y motive serves as an internal redox center and mutation alters its redox capacity. Similar types of mutation studies have been reported in the case of flavin enzymes[167] where it has been found that the Y98F mutation increases the mid-potential of redox couple due to the relatively lesser electron donating ability of the F residue. We think that a similar situation is being encountered in the MCM enzyme where the ET from the F (in the mutant enzyme) to the cofactor becomes comparatively difficult resulting in the rate reduction of four-orders of magnitude. In the case of human monoamine oxidase,[168] the site-specific mutation analysis has been used to probe the functional implications of tyrosine motif that also presents a quite similar picture: upon the Y435F replacement, the catalytic activity is hampered by one-fourth of its actual value (in case of wild-type enzyme) with no structural alterations being noticed in the active site architecture. Similarly Y430F substitution of one of the component of the aromatic cage in murine polyamine oxidase[169] has resulted in the reduced catalytic activity as compared to the wild–type.

However, there are some other possibilities that might cause reduction in the catalytic activity upon Y89F mutation. Some of them have been related to the Co-C post cleavage intermediates as well as substrate radical rearrangement step,[57,58] i.e. catalytic step where substrate radical, i.e., $Co^{2+}Cbx + AdoCH_3 + Sub^{\bullet}$, has already been formed. To provide deeper understanding of the Y89F mutation, we performed QM/MM calculations in which energy/structure relationship between $Sub^{\bullet}$ of MCM and corresponding TS was performed for

wild-type as well as for the Y89F mutant. The QM/MM set up was different than in the previous calculations. The QM part in addition to the Y89 includes the $AdoCH_3$, part of substrate along with R207, H244 and Q197 residues. Taking into account that only reactions between organic residues were analyzed, B3LYP functional was used to describe the energetic of TS as this hybrid functional is considered to be the most appropriate for modeling the organic reactions. Figure 12 summarized the main results of Y89F QM/MM calculations. Overall, the Y89F mutation doesn't lead to noticeable structural changes as could be judged from the QM/MM optimized structural parameters. The energy of radical rearrangement is predicted to be at 6.0 kcal/mol for wild-type and slightly higher (9.6 kcal/mol) for the Y89F mutant. The results of present investigation are in good agreement with the previously published by Loferer et al.,[170] though some minor differences are worth to notice. For example, in our optimized structure the H244 residue shares an H-bond between Q197 and the substrate thus supporting partial protonation of the C=O group (Figure 13).

Several important observations could be drawn from the current QM/MM calculations regarding the involvement of Y89 in the catalytic process. Overall, the Y89F mutation has minor influence on the radical rearrangement from energetic as well as structural standpoint. Any significant extent of H-bond between the Y residue and substrate has been found to have small influence on the radical rearrangement step. For example, before the rearrangement could actually take place, H-bond between the –OH group of Y89 residue and substrate is 1.55 Å long while in TS, this bond length changes to 1.62 Å.

Computational study predicts that the Y89F mutation has hardly any impact the flexibility of the bound substrate. Loss of the H-bond doesn't change orientation of the substrate because the $-COO^-$ group of substrate is engaged in additional electrostatic interaction via a two-pronged H-bonding contact with R207. Upon mutation these anchor type H-bond distances changes from 1.73 and 1.91 Å to 1.69 and 1.81 Å, respectively. Loss of the H-bonding interaction is predicted to increase the isomerization barrier from methylmalonyl-CoA to succinyl-CoA only by 3.6 kcal/mol. The interaction between the Y89 residue and Ado moiety is essentially negligible as could be judged from QM/MM optimized structure (Figure 13) and therefore any implications that Y might have in stabilizing the $Ado^{\bullet}$[57] have no structural justification. This is against the hypothesis that Y89 could function as a molecular wedge labilizing the Co-C bond.[58] This argument was derived from the crystallographic data, which revealed that substrate-driven barrel closure results in a large translational motion of this residue leading to the rupture of the adenine moiety and steric crowding above the corrin ring. This is very hard to reconcile considering the fact that the Ado ligand has not been accurately resolved in the case of MCM enzyme. In summary, the Y89 motif has minor influence on the cleavage step or in stabilizing the $Ado^{\bullet}$ which implies that this motif must be involved in the activation step via some different mechanism.

## 2.4 Conclusions

In the present theoretical study, the energetics of AdoCbl-$Y^-$ complex has been extensively investigated at various levels of theory (DFT, CASSCF/MC-

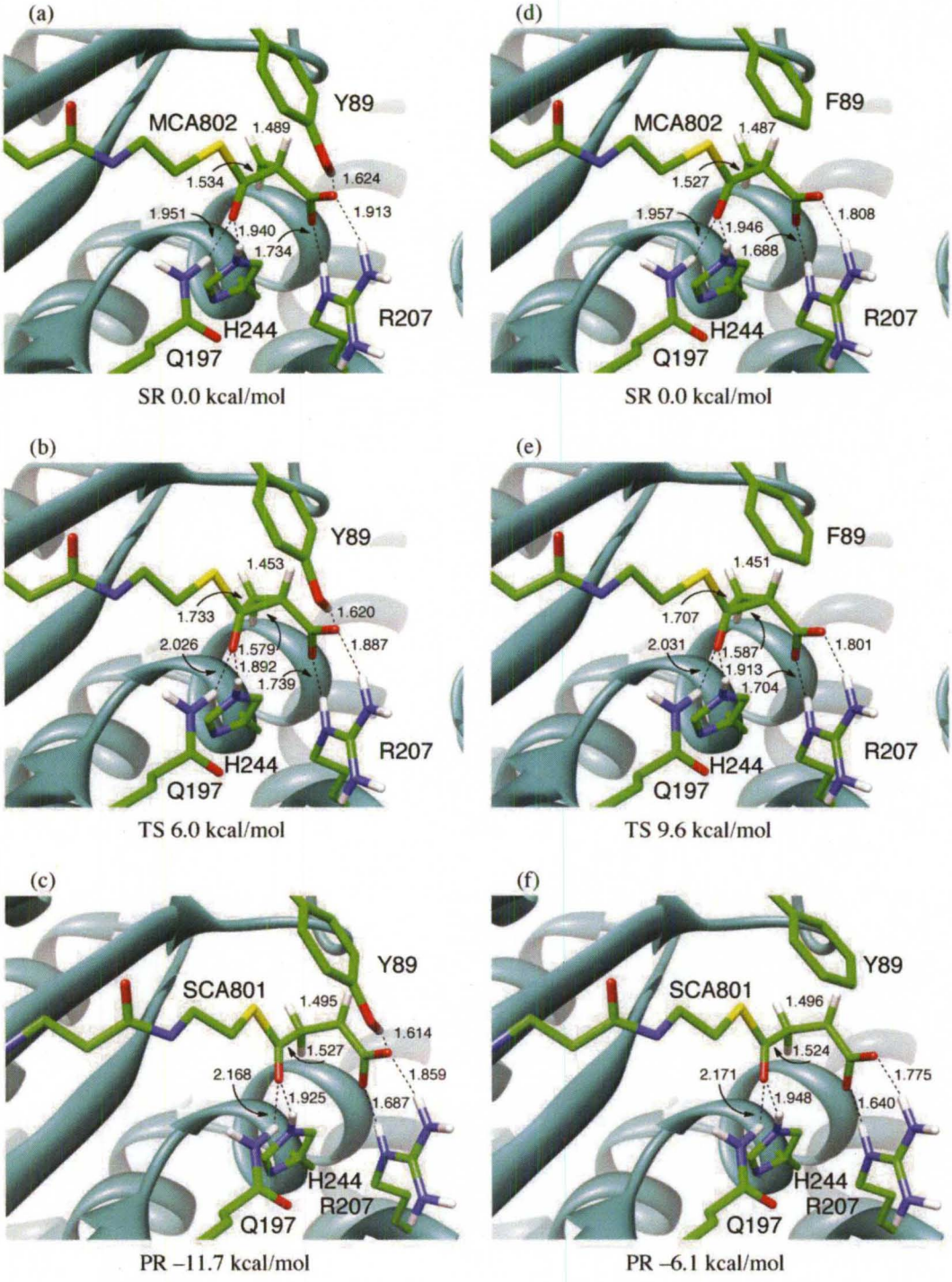


Figure 12. Key species involved in methylmalonyl-CoA to succinyl-CoA radical rearrangement (as catalyzed by MCM enzyme) corresponding to wild-type (a) – (c) and Y89F mutant (d) – (f), respectively. The Ado group has not been shown here for the sake of clarity.

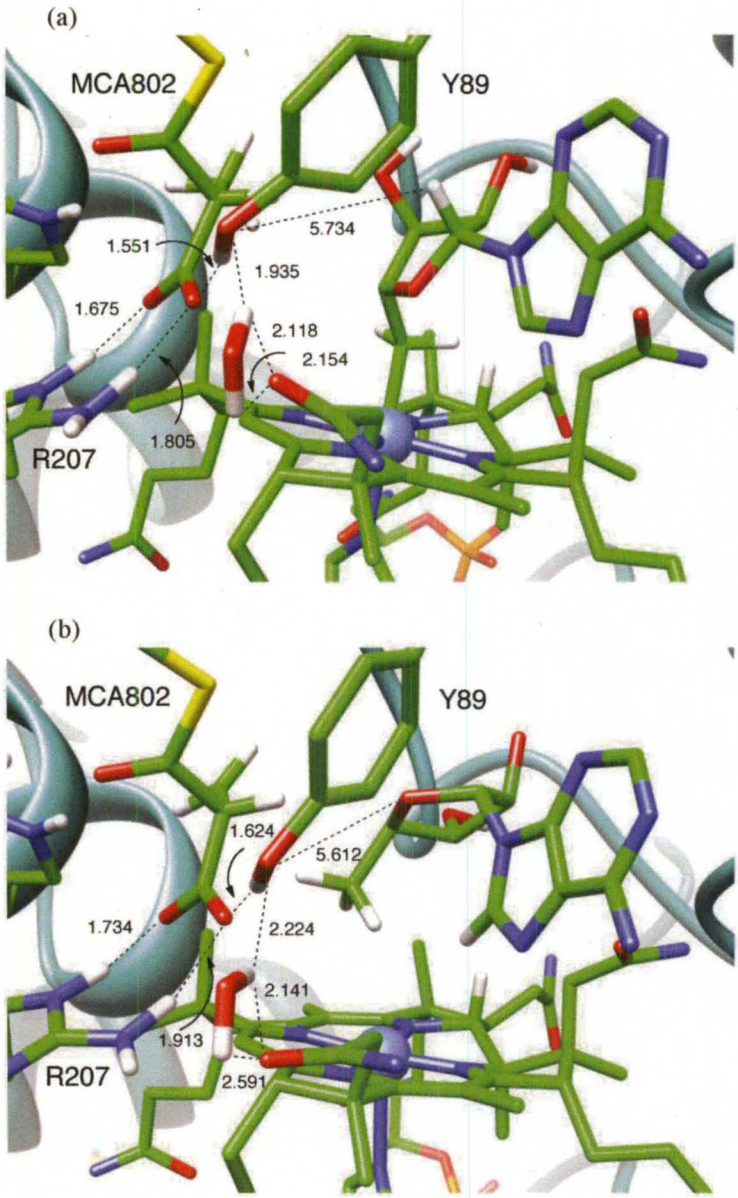


Figure 13. Close-up of QM/MM optimized MCM enzyme showing the location of the Y89 residue relative to the Ado moiety (a) before the Co–C bond cleavage, and (b) after Co-C bond cleavage and H-atom abstraction.

XQDPT2 and QM/MM) incorporating a varied degree of structural complexity. The QM/MM computations have been carried out for MCM enzyme with the Y89 residue being considered in the QM domain thereby making it a very first study where the role of the Y motif has been rigorously discussed in the context of AdoCbl-dependent enzyme catalysis. According to the computational results obtained (irrespective of the theoretical approach used), the diradical state i.e. $[AdoCbl]^{\bullet -}$-$Y^{\bullet}$ instead of AdoCbl-$Y^{-}$ has been found to be the lowest electronic state of the complex providing convincing evidence that ET can take place from the Y residue to the AdoCbl cofactor.

The involvement of $[AdoCbl]^{\bullet -}$ may have important consequence with regard to the cleavage of the Co-C bond in AdoCbl-dependent enzyme. It has been found that the electrochemical reduction of a $B_{12}$ cofactor weakens the Co-C bond.[86,89-90] However, it has been argued that the species like $[AdoCbl]^{\bullet -}$ can't be involved in the AdoCbl-dependent enzyme catalysis,[23,162] due to the very negative redox potentials of $B_{12}$ cofactors. It was reasoned that even the presence of a relatively strong reducing agent, such as a Fe-S cluster, can't facilitate the outer-sphere ET for reducing the $B_{12}$ cofactors. However, in the light of the present study as well as our increased understanding of redox processes inside enzymes, several arguments can be presented that speak against conclusions made during the earlier studies[23,162]. First of all, the redox potentials are usually computed employing the solution-based electrochemistry where two relevant redox components are considered to be infinitely separated. Certainly, this is not the situation being encountered inside the enzymes where several

types of interactions are taking place among the various entities, thereby invalidating the use of solution-based electrochemistry with reference to enzymatic processes. Thus the redox potentials derived from electrochemistry can provide some clue but can't be taken literarily to model enzymatic reaction. For example, in the case of SODs, it has been found that a single Gln residue plays a critical role of redox switch by inducing a redox tuning of ~1V range.[96] Even certain enzymatic processes can't take place if the redox potentials (from *in vitro* data) are taken into consideration. The best example is PS-II where the involvement of the Y residue in charge separation process is generally accepted.[143] However, the detailed thermodynamic study[97] showed that the redox potential of the $Y/Y^{\bullet}$ was far above that of $P_{680}$ literally negating the possibility of electron transfer from $Y_z$ to $P_{680}$ motif, but indeed the charge transfer occurs inside the enzyme where the electrostatic interactions such as dielectric effect and H-bond network play a key role of redox switch thereby altering the redox potentials of $Y_z$ and $P_{680}$ in order to make this charge separation process feasible. These theoretical studies reflect that the redox potentials of the active site residues are drastically modified when the enzymatic interactions are taken into consideration highlighting the existence as well as the significance of strong communication prevalent among the various motifs. Secondly, a strong reducing agent is not always required to facilitate the outer-sphere ET as the active site residues can also induce such ET via PCET route. PCET is thermochemically more favorable than processes involving the stepwise ET and PT often by $\geq$ 1eV. In the present study, it is thus proposed that the

presence of the active site Y residue plays a critical role of redox centre and can facilitate ET to the cofactor via PCET which may have implications in explaining the origin of catalysis in $B_{12}$-dependent mutases.

# CHAPTER III

# EFFECT OF REDUCED ADENOSYLCOBALAMIN COFACTOR UPON THE Co-C BOND CLEAVAGE AND SUBSEQUENT HYDROGEN ATOM ABSTRACTION FROM THE SUBSTRATE

## 3.1 Introduction

The origin of the enormous catalytic efficiency of the enzymes employing AdoCbl is of significant bioinorganic interest.[1-19] The AdoCbl-dependent catalysis is initiated by the homolytic cleavage of the Co-C5' bond leading to the formation of $Ado^{\bullet}$ and $Co^{2+}$Cbx that is coupled with subsequent H-atom abstraction from the substrate.[171] Precisely how the Co-C5' bond is activated and what mechanism is responsible for the observed ~12 orders of magnitude enzymatic rate enhancement[22] remains poorly understood. We recently proposed[172-173] that the active site tyrosine residue (e.g.,Y89 residue in case of MCM enzyme) plays a critical role in the activation of Co-C5' bond in the case of $B_{12}$-dependent mutases where the binding of the substrate induces the formation of 1el-Red form of AdoCbl cofactor (i.e. $[AdoCbl]^{\bullet-}$). The initial step of the proposed mechanism involves the PT coupled with the ET via PCET (Scheme 6), which

can be summarized as follows:

$$AdoCbl + YOH + XCOO^- \rightarrow [AdoCbl]^{\bullet -} + YO^{\bullet} + XCOOH \qquad (1)$$

The process is initiated by the PT which is an energetically uphill reaction. Although the catalytic step described by Eqn. (1) is thermoneutral, as revealed by DFT model calculations, there is an overall energy barrier for the initial PCET step. Due to nonadiabatic nature of the reaction, it is difficult to quantify the energy requirements for $[AdoCbl]^{\bullet -}$ formation. Considering there is an energy barrier associated with the PT and ET steps, it is expected that the energetic requirement would be lower when the PT and ET steps will occur in a concerted fashion, because the PCET pathway avoids the generation of charged intermediates minimizing the energetic demand of the reaction.

It should be noted that the reduction potentials of $B_{12}$ cofactors lie in the range of -1.31 to -1.60 V vs SCE.[86,87,88-90] Specifically, the reduction potential of MeCbl in the dimethylformamide (DMF):propanol solvent mixture has been estimated to be -1.47 to -1.60 V vs SCE, [86,89-90] while the reduction potential of AdoCbl in DMF:propanol mixture (-1.31 V vs SCE)[89] has been found to be relatively positive. Though the reduction potentials of isolated $B_{12}$ cofactors are significantly more negative than that of the tyrosine residue (+0.51 to +0.76 V vs SCE),[174] but it should be noted that the redox potential of an enzyme-bound cofactor can be significantly tuned by the various interactions operative inside the enzymes.[96-103] Our recent QM/MM computations also[173] suggest that the enzyme-bound $B_{12}$ cofactor can be reduced if a deprotonated tyrosine residue is

present in its vicinity. This implies that the redox chemistry of the AdoCbl-$Y^-$ complex is significantly altered by the enzymatic environment and consequently, the diradical state i.e. $[AdoCbl]^{\bullet-}$-$Y^{\bullet}$ (instead of AdoCbl-$Y^-$) becomes the lowest electronic state of the complex.

The main objective of the research detailed in this chapter is to further elaborate this proposal and provide energetic implications regarding the involvement of the $[AdoCbl]^{\bullet-}$ radical anion in the initial step of AdoCbl-dependent enzymatic catalysis that involves Co-C5' bond scission and subsequent H-atom abstraction from the substrate.

## 3.2 Computational Details

All the DFT calculations were performed using Gaussian03[151] suite of programs for electronic structure and properties calculations. To mimick the Co-C5' bond cleavage and subsequent H-atom abstraction from the substrate, the AdoCbl cofactor and the substrate were modeled by the simplified RibCbl where all the corrin amide side chains were substituted by H's, and the propanaldehyde respectively. To model the base-on forms of the AdoCbl cofactor, the Im was used as the axial base. The BP86/6-31G(d) 5d level of theory was used in all the computations considering its well-established usefulness in reproducing the structural, electronic and spectroscopic features of $B_{12}$ corrinoids.[82,91-94,154,155,156]

## 3.3 Results and Discussions

### 3.3.1 Co-C5' Bond Cleavage in RibCbl

In order to quantify the catalytic effect gained by the one-electron reduction of the cofactor, as a first step, the cleavage of Co-C5' bond was studied in the positively charged AdoCbl model represented by (Im-[$Co^{III}$(corrin)]-$Rib^+$; Figure 14) and its 1el-Red analogue where Im and ribosyl (Rib) were modeled as the lower and the upper axial ligands respectively. The Co-C5' bond cleavage was computationally investigated at the BP86 /6-31G(d) (5d) level of theory as this level of theory has been found to reproduce the structural aspects of $B_{12}$ cofactors and their electronic properties to a reliable degree of

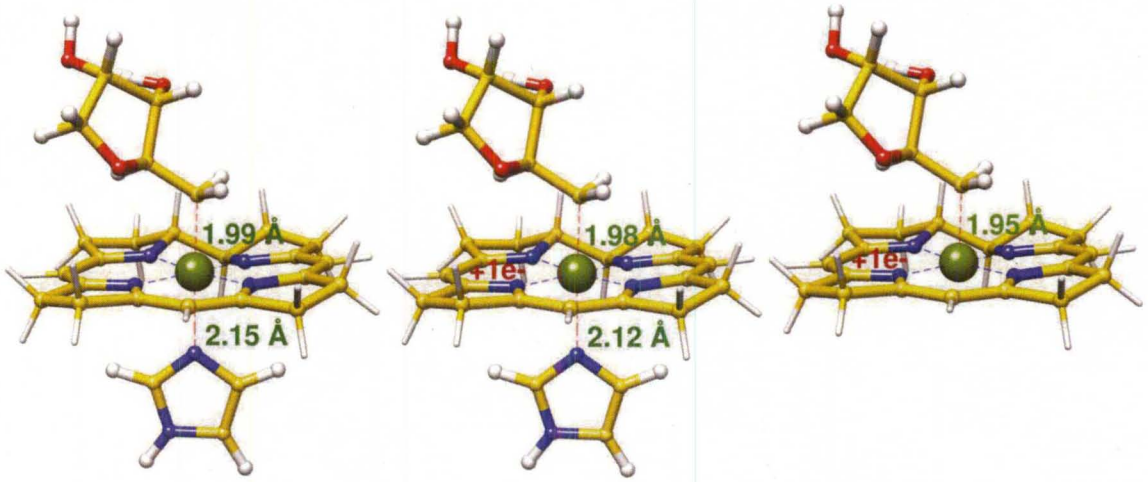


Figure 14. BP86-optimized structures of Im-[$Co^{III}$(corrin)]-$Rib^+$ (*left*), Im-[$Co^{III}$(corrin$^{\bullet}$)]-Rib (*middle*) and [$Co^{III}$(corrin$^{\bullet}$)]-Rib (*right*).

accuracy.[154,155,156] The bond dissociation energy (BDE) for Co-C5' homolytic cleavage in the Im-[$Co^{III}$(corrin)]-$Rib^+$ model has been calculated to be 37.2

kcal/mol,[82] that is in reasonable agreement with the experimental value of 31.5 ± 1.3 kcal/mol[26-29] estimated for AdoCbl cofactor.

Addition of an electron to AdoCbl cofactor initially lead to the formation of $\pi^*_{corrin}$ anion radical, that was modeled as Im-[$Co^{III}$(corrin$^{\bullet}$)]-Rib. Presence of an electron delocalized over the corrin ring had relatively small influence on the axial bond lengths as they were only slightly different from those in the Im-[$Co^{III}$(corrin)]-$Rib^+$ model (Figure 14). In order to illustrate the impact of one-electron reduction, the cleavage was studied in the Im-on and Im-off forms of the reduced cofactor where the axial bonds were repeatedly elongated and the geometry was reoptimized at each point. The previous theoretical studies[91-92] suggest that the cleavage of the Co-C5' bond in the 1el-Red $B_{12}$ cofactor models demands prior displacement of the axial base. The energy required for detaching DBI base from the neutral MeCbl in the aqueous solution has been experimentally estimated to be 6.5 - 7.6 kcal/mol.[175] However, the axial N-methylimidazole dissociation energy from the MeCbi(N-Im)$^+$ in the aqueous and ethylene glycol solution has been found to be 3.1 kcal/mol and 6.9 kcal/mol respectively.[176] A recent computational study quantified the energetic of the axial Im base detachment in the Im-[$Co^{III}$(corrin)]-$Me^+$ and the Im-[$Co^{III}$(corrin$^{\bullet}$)]-Me forms of MeCbl wherein the truncated cofactor models were employed.[91] It was concluded that the solvation effect has to be included in order to obtain results comparable with the experimental data. The Im detachment energy in the Im-[$Co^{III}$(corrin)]-$Me^+$ model was estimated to be 9.4 kcal/mol in the water solvent

which was lowered by ~58.5 % in the 1el-Red form (i.e., Im-[$Co^{III}$(corrin$^{\bullet}$)]-Me; 3.9 kcal/mol).

Herein we also computed the axial Im detachment energy for the positively charged Im-[$Co^{III}$(corrin)]-$Rib^{+}$ model and its 1el-Red analogue (i.e., Im-[$Co^{III}$(corrin$^{\bullet}$)]-Rib) in the gas phase as well as in the PCM-based water solvent ($\varepsilon$ = 78), respectively. Two different approaches were used to calculate the detachment energy: (i) the completely dissociated state was considered i.e., Im-[$Co^{III}$(corrin)]-$Rib^{+}$ $\rightarrow$ Im + [$Co^{III}$(corrin)]-$Rib^{+}$, and (ii) the axial Im base was repeatedly stretched for attaining the dissociated state. The approach (ii) was only explored for the Im-[$Co^{III}$(corrin$^{\bullet}$)]-Rib analogue. Following approach (i), the computed Im detachment energy for the Im-[$Co^{III}$(corrin)]-$Rib^{+}$ (14.4 kcal/mol (gas phase); 8.7 kcal/mol (water))

**Table 2**

Thermodynamic Data for Axial Imidazole Ligand Dissociation[a]

| Thermodynamic Quantity | Dissociation Reaction [kcal/mol] | |
|---|---|---|
| | Im-[$Co^{III}$(corrin)]-$Rib^{+}$ $\rightarrow$ Im + $Co^{III}$(corrin)]-$Rib^{+}$ | Im-[$Co^{III}$(corrin$^{\bullet}$)]-Rib $\rightarrow$ Im + [$Co^{III}$(corrin$^{\bullet}$)]-Rib |
| $\Delta E^{b}$ | 14.4 | 7.6 |
| ZPE Term | 1.5 | 1.1 |
| $\Delta E(PCM)^{c}$ | 8.7 | 4.6 |
| $\Delta H^{d}$ | 30.1 | 23.1 |
| $\Delta S^{d}$ | 44.6 | 40.0 |
| $\Delta G^{d}$ | 16.8 | 11.2 |

[a] Calculated using the BP86/6-31G(d) level of theory. [b] ZPE corrected. [c]The energetics for PCM model with dielectric constant for water as a solvent. [d] The thermodynamic data were calculated assuming ideal gas law validity.

was reduced by ~ 55 % in the Im-[$Co^{III}$(corrin$^{\bullet}$)]-Rib (7.6 kcal/mol (gas phase); 4.6 kcal/mol (water) (see Table 2 for details). This implied that the one-electron reduction favors the axial base detachment in the $B_{12}$ cofactors. The energy required to detach the axial Im base from the Im-[$Co^{III}$(corrin$^{\bullet}$)]-Rib model was also computed by repeatedly stretching the Co-$N_{Im}$ bond. The dissociated state (i.e., Im + [$Co^{III}$(corrin$^{\bullet}$)]-Rib) was found to be reached at a Co-$N_{Im}$ bond distance of 3.00 Å that corresponded to the Im detachment energy of 6.7 kcal/mol in gas phase and 5.3 kcal/mol in the aqueous solution, respectively. Considering that the elongated Co- $N_{axial}$ bond has also been observed in the $B_{12}$-dependent

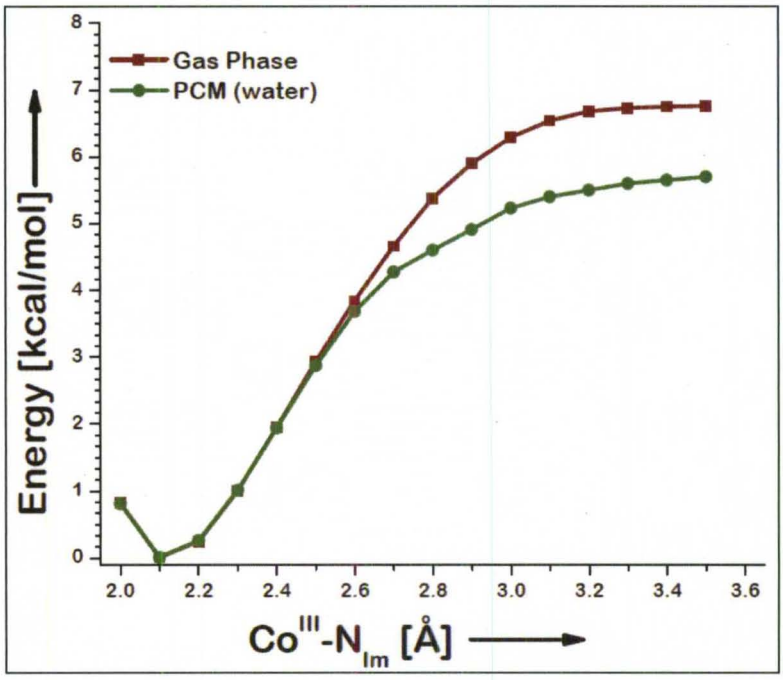


Figure 15. Estimation of the axial Im base detachment energy in the 1el-Red Im-[$Co^{III}$(corrin$^{\bullet}$)]-Rib.

mutases,[49,50,56,62,140,141] the activation of the enzyme-bound Co-C5' bond might also be occurring from the 1el-Red cofactor. Taking into account that the reductive cleavage of Co-C5' demands prior displacement of the axial Im base, the Co-C5' BDE for the 1el-Red cofactor was evaluated as the sum of energies associated with the axial Im base displacement, i.e., 7.6 kcal/mol and the dissociation reaction $[Co^{III}(corrin^{\bullet})]$-Rib $\rightarrow$ $[Co^{I}(corrin)]$ + $^{\bullet}$Rib i.e.,19.0 kcal/mol. The energy of the dissociation reaction is equivalent to the BDE of Co-C5' bond in the Im-off $[Co^{III}(corrin^{\bullet})]$-Rib (19.0 kcal/mol) which was lowered by ~48.9% as compared to the Im-$[Co^{III}(corrin)]$-$Rib^{+}$ model. The effective Co-C5' BDE in the Im-$[Co^{III}(corrin^{\bullet})]$-Rib thus came out to be 26.6 kcal/mol which indicated ~28.5% bond strength reduction in comparison to the positively charged Im-$[Co^{III}(corrin)]$-$Rib^{+}$. The Co-C5' BDE in the $[Co^{III}(corrin^{\bullet})]$-Rib as well as in the Im-$[Co^{III}(corrin^{\bullet})]$-Rib was also calculated by the systematic elongation of the Co-C5' and the (Co-C5' and Co-$N_{Im}$) bonds respectively (Figure 15). The significant lowering of Co-C5' BDE calculated with the 1el-Red analogues was due to involvement of the two electronic states in the cleavage event: initially a $\pi^{*}_{corrin}$ anion radical state was formed with the added electron delocalized over the equatorial corrin ligand. As the Co-C5' bond was stretched to ~2.35 Å, the electron relocated into the $\sigma^{*}_{Co\text{-}C5'}$ state and the final cleavage involved three electron bond $(\sigma)^2(\sigma^{*})^1$ (Figure 16b). The reductive cleavage mechanism of Co-C5' bond in Im-$[Co^{III}(corrin^{\bullet})]$-Rib is in line with what has recently been suggested for MeCbl[91] and Pc-based analogue[92] as well as for the MetH-bound MeCbl[94]. Especially in the case of MetH enzyme, the QM/MM computations[94] illustrated that the Hcy substrate can

reduce the cofactor that can potentially explain the considerable amount of catalytic effect associated with the MetH enzyme. The relevant electronic states and the spin density profiles associated with the corrin ring and the axial fragment (Co and C5' motives) of Im-[$Co^{III}$(corrin$^{\bullet}$)]-Rib are summarized in Figures 16 and 17. As could be observed, the reductive Co-C5' bond cleavage occurred only when both the axial bonds were stretched to represent the blue region which in turn corresponded to the situation when the added electron was localized in the axial Co-C5' bond (i.e., $\sigma^{*}_{Co\text{-}C5'}$ orbital). Initially when the Co-C5' bond was short (< 2.35 Å), the added electron was completely delocalized onto the corrin ring and the elongation of Co-$N_{Im}$ bond had no effect on the spin density distribution. As the Co-C5' bond was further lengthened, the Co-$N_{Im}$ bond started influencing the spin density distribution. For shorter Co-$N_{Im}$ bond (i.e.,< 2.25 Å), the spin density was mainly centered between the corrin ring and Co atom, but as the Co-$N_{Im}$ bond was stretched beyond 2.25 Å, the whole spin was migrated into the $\sigma^{*}_{Co\text{-}C5'}$ orbital. Since further elongation of the the Co-$N_{Im}$ bond had no noticeable impact upon the electronic states and the spin density distributions, the Co-$N_{Im}$ bond was only lengthened up to 2.60 Å. This implied that the elongated axial base is required to induce an efficient Co-C5' bond cleavage in the Im-[$Co^{III}$(corrin$^{\bullet}$)]-Rib cofactor. This is consistent with the electrochemical reduction studies in solution,[86-90] pointing out that the axial base has to be detached in order to effectively cleave the Co-C5' bond in the 1el-Red cofactor.

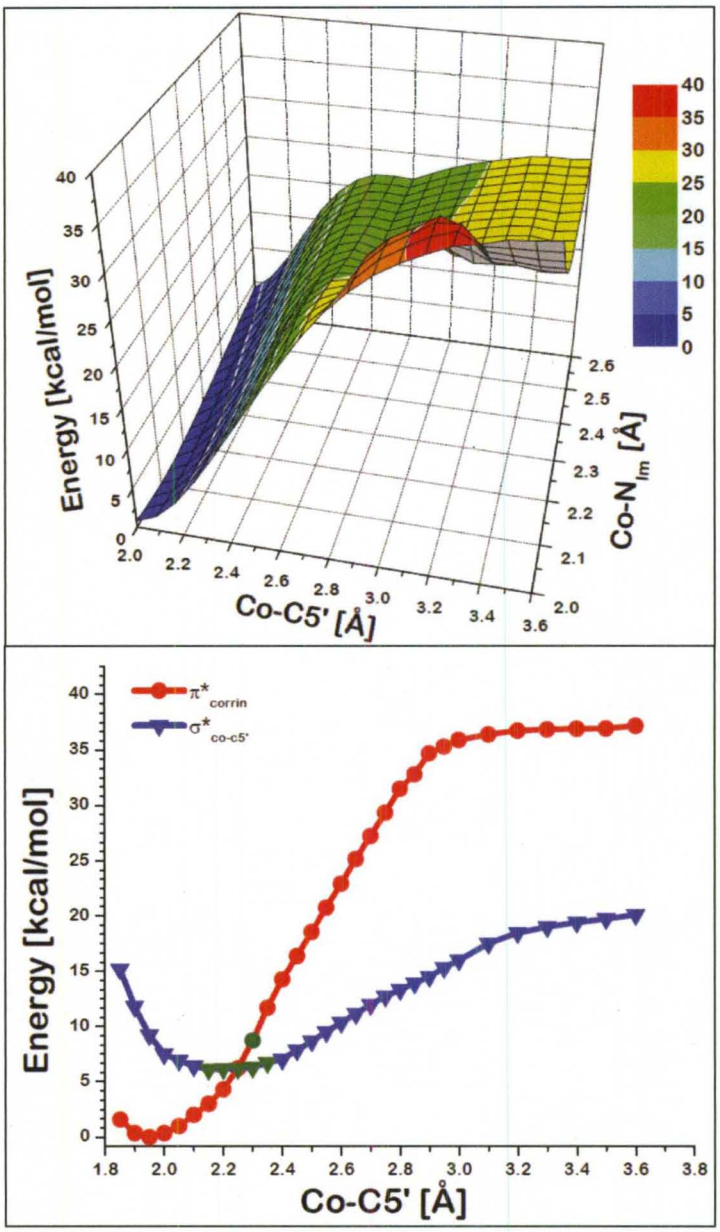


Figure 16. Three dimensional scan of the lowest electronic state (*upper panel*) involved in the Co-C5' Bond Cleavage in the 1el-Red Im-[$Co^{III}$(corrin$^{\bullet}$)]-Rib cofactor and (Lower Panel) two dimensional scan of the two lowest electronic states (*lower panel*) involved in the reductive cleavage of Co-C5' Bond in the Im-off [$Co^{III}$(corrin$^{\bullet}$)]-Rib. The olive circles correspond to the points of interpolation.

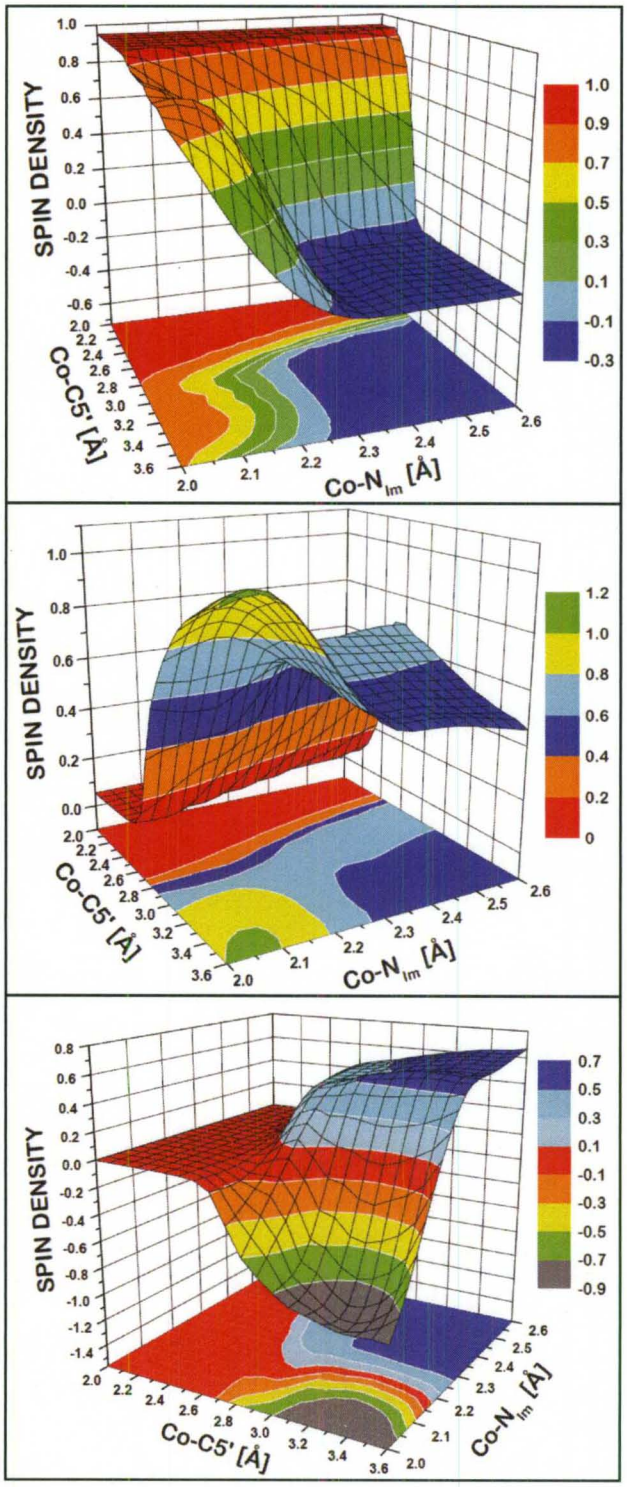


Figure 17. Spin density surfaces of the corrin ring (*top*), Co (*middle*) and C5' (*bottom*) moieties in the 1el-Red Im-[Co$^{III}$(corrin$^{\bullet}$)]-Rib.

### 3.3.2 Intrinsic Reaction Coordinate Analysis of Co-C Bond Cleavage and Subsequent H-atom Abstraction

As a next step, the reaction consisting of Co-C5' bond cleavage and subsequent H-atom abstraction was studied employing the 1el-Red Im-off structural model i.e., [$Co^{III}$(corrin$^{\bullet}$)]-Rib. To model the substrate, a structural replicate $CH_3$-C**H**H-CHO was used where **H** represents the H-atom that was abstracted by the cofactor during the course of reaction. The initial geometry of the TS was constructed on the basis of the optimized structure of [$Co^{III}$(corrin$^{\bullet}$)]-Rib as well as using the previously reported TS[82] involving the positively charged Im-[$Co^{III}$(corrin)]-Rib$^{+}$ model. The substrate was placed near the C5' atom of the [$Co^{III}$(corrin$^{\bullet}$)]-Rib for direct H-atom abstraction and a series of constrained optimizations were carried out followed by full optimization at the final stage. The location of the TS was confirmed by frequency calculations. It should also be noted that an attempt was made to probe the TS involving Im-on form of 1el-Red cofactor (i.e., Im-[$Co^{III}$(corrin$^{\bullet}$)]-Rib), but such a search was proved to be unsuccessful as it always involved the detachment of the axial Im ligand prior to the cleavage of Co-C5' bond. For that reason, the TS structure of the reaction involving Im-[$Co^{III}$(corrin)]-Rib$^{+}$ was compared with that of the Im-off [$Co^{III}$(corrin$^{\bullet}$)]-Rib mediated reaction. Such a comparative analysis would offer insight as to how differently the catalytic step consisting of Co-C5' bond cleavage and subsequent H-abstraction would be executed if the 1el-Red cofactor is taken into consideration.

The analysis of the TS structure furnished useful mechanistic details of the catalytic reaction. Figure 18 displays the TS involving Im-[$Co^{III}$(corrin)]-$Rib^+$ that primarily serves as a reference for the TS where the H-atom transfer is mediated by [$Co^{III}$(corrin$^\bullet$)]-Rib. A single imaginary frequency of 810*i* $cm^{-1}$ was found for the TS mediated by 1el-Red Im-off [$Co^{III}$(corrin$^\bullet$)]-Rib in comparison to 905*i* $cm^{-1}$ predicted for the TS involving Im-[$Co^{III}$(corrin)]-$Rib^+$. The TS structure in both cases displayed a reaction coordinate on catalytic path that represented

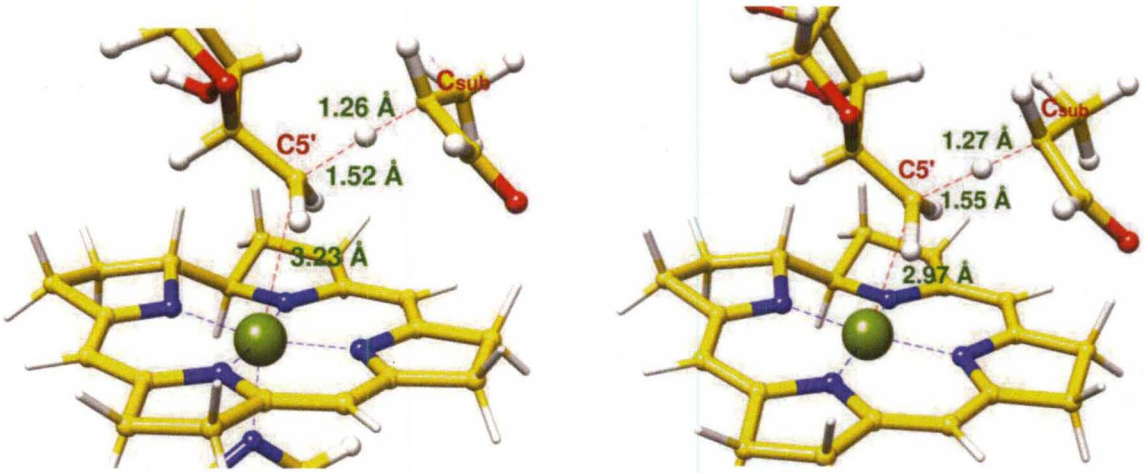


Figure 18. Close-ups of the transition state structures along with selected bond lengths (Å) representing homolytic Co-C5' bond cleavage concerted with H-atom abstraction for the Im-[$Co^{III}$(corrin)]-$Rib^+$ (*left*) and [$Co^{III}$(corrin$^\bullet$)]-Rib (*right*), respectively.

a stretched Co-C5' bond along with the partially linked **H**-atom between the $C_{sub}$ of the substrate and C5' atom of the cofactor. The Co-C5' bond in the TS

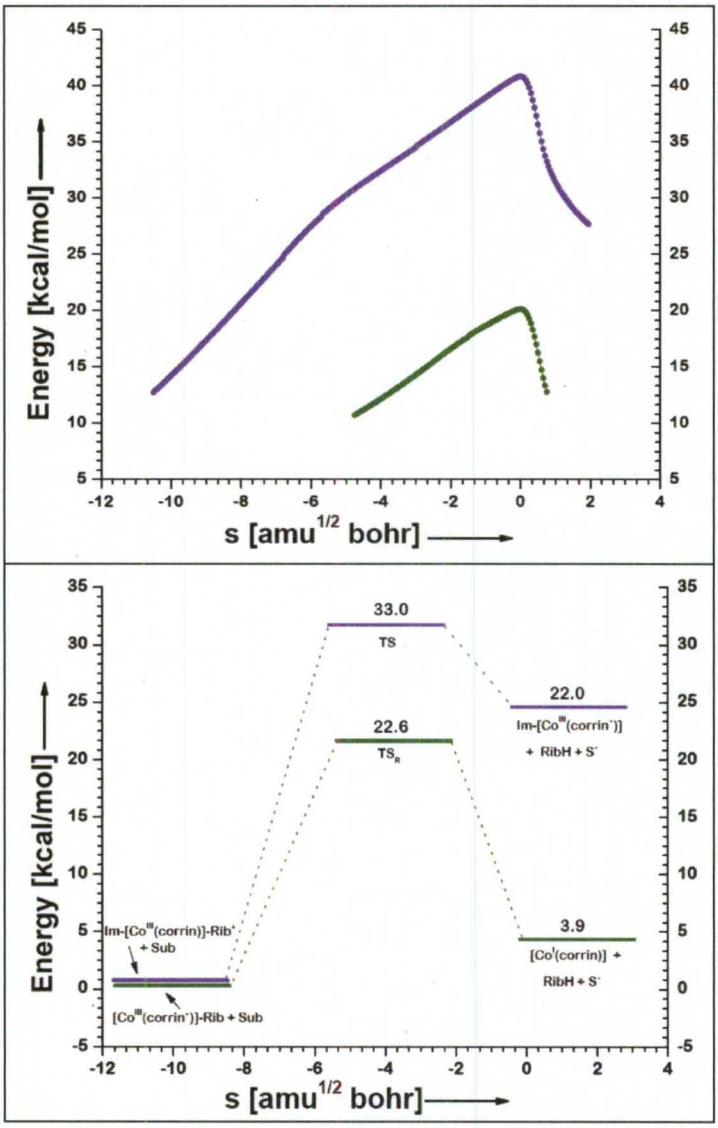


Figure 19. Energy profiles of the Co-C5' bond cleavage and subsequent H-abstraction. The upper panel corresponds to the IRC paths (not ZPE-corrected) for the concerted reaction of the Co-C5' bond cleavage and H-atom abstraction involving the Im-[$Co^{III}$(corrin)]-$Rib^+$ (violet) and its reduced analogue (olive). The distance along the IRC (s) is given in mass-scaled units and the TS is located at s=0. The lower panel shows the relative energies (ZPE-corrected) of the involved TSs and products.

structure involving the 1el-Red [$Co^{III}$(corrin$^{\bullet}$)]-Rib was 2.97 Å long that was identical to the one (2.99 Å) noticed in a synthetic analogue of coenzyme $B_{12}$.[177,178] The **H**-$C_{sub}$ bond was only slightly lengthened from 1.11 Å to 1.27 Å, while the C5'-**H** bond was still long i.e., 1.55 Å implying that the TS occurred late with respect to the Co-C5' coordinate while it appeared early with reference to H-atom transfer. In both the reactions, the homolytic cleavage of the Co-C5' bond and the subsequent H-atom abstraction was concerted. This was verified by the IRC calculations showing only single energy maximum connecting reactants and products (Figure 19).

The main finding of this computational investigation was the quantification of the significant amount of stabilization gained by the TS when the 1el-Red form is taken into consideration. Clearly, the energetic demand of the reaction was drastically reduced when the concerted reaction involved 1el-Red form of AdoCbl cofactor. The activation energy barrier of the reaction mediated by the Im-off [$Co^{III}$(corrin$^{\bullet}$)]-Rib, was found to be 15.0 kcal/mol (ZPE-corrected) that was lowered by approximately 50% in comparison to the reaction involving the Im-[$Co^{III}$(corrin)]-$Rib^{+}$ (energy barrier = 33.0 kcal/mol) (Figure 19). It is also important to mention that the concerted reaction involving the 1el-Red analogue could only be studied with the Im-off form, i.e., [$Co^{III}$(corrin$^{\bullet}$)]-Rib, as the Im base was always detached during the TS search. This implied that the computed activation energy barrier for the reductive pathway had to be corrected by adding the axial Im detachment energy (i.e., 7.6 kcal/mol). The effective activation barrier for the reaction was thus calculated to be 22.6 kcal/mol which reflected 31.5% energy

lowering in comparison to the reaction mediated by the Im-[$Co^{III}$(corrin)]-$Rib^+$. However, the energetic demand for the axial base elongation inside the enzyme environment is noticeably lower as has been shown by QM/MM calculations[179] implying that the catalytic effect of one-electron reduction in the enzyme-bound cofactor would be significantly higher than in model complexes. This could be of relevance for the enzyme catalysis that involves a rate enhancement of 12 orders of magnitude as compared to the uncatalyzed reaction in solution[22]. It should be noted that the reaction mediated by the [$Co^{III}$(corrin$^{\bullet}$)]-Rib is endothermic by 3.9 kcal/mol. The concerted nature of the reaction mechanism, as revealed by the present calculations, is also consistent with an experimental finding

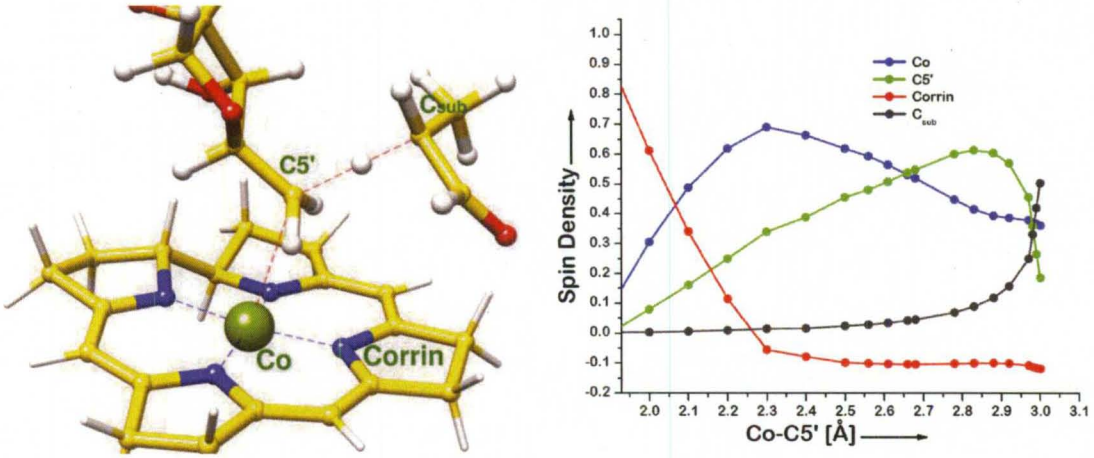


Figure 20. Spin density profiles of key entities along the Co-C5' stretching coordinate involved in the concerted reaction.

suggestive of the fact that the H-atom abstraction step is coupled with the homolytic cleavage of the Co-C5' bond.[47] The calculations exploring the 1el-Red

analogue of AdoCbl cofactor represented by Im-[$Co^{III}$(corrin$^{\bullet}$)]-Rib suggest that the axial Im base must be detached or Co-$N_{Im}$ bond distance significantly elongated in order to induce an efficient reductive cleavage of Co-C5' bond. Considering that the lengthened Co-$N_{axial}$ bond has been observed during the X-ray crystal structure studies of $B_{12}$-mutases namely MCM[56] and GLM[51b], the reductive mode of Co-C5' bond cleavage might also be operational inside these enzymes.

The analysis of the spin density profiles of the key entities along the Co-C5' bond (Figure 20) offers further insight into the molecular details of the reaction. The corrin macrocycle in the reaction mediated by the [$Co^{III}$(corrin$^{\bullet}$)]-Rib behaved as a non-innocent ligand. Initially, when an electron was added to the cofactor, it was entirely localized on the corrin ring. As the Co-C5' bond was stretched to ~ 2.35 Å, the added electron density was completely relocated into the axial bond, represented by $\sigma^*_{Co\text{-}C5'}$ orbital. Now Co centre had spin density of 0.7, acquiring $Co^{II}$ like character, while C5' had spin of 0.35. In order to initiate the **H**-atom transfer from the $C_{sub}$, C5' spin had to be further amplified. As the Co-C5' bond was stretched to ~2.90 Å, the spin density on C5' reached 0.65 values that enhanced its ability to abstract the **H**-atom from the substrate. This was also reflected in terms of the partial stretching of $C_{sub}$-**H** bond that lead to the spin build-up on $C_{sub}$ (~0.2). At a Co-C5' bond length of 2.97 Å corresponding to the TS, the **H**-atom was partially transferred to the C5' atom as could be gauged from the spin density values of C5' and $C_{sub}$, respectively. Beyond this point, the **H**-abstraction occurred very fast and Co ion mainly was present as cob(I)alamin.

Since the enhanced C5' spin played a key role in initiating the **H**-atom transfer and the 1el-Red amplified the electron density on C5' atom, it could explain why the TS occurred at relatively shorter Co-C5' bond distance when the reaction was mediated by the [$Co^{III}$(corrin$^{\bullet}$)]-Rib.

## 3.4 Conclusions

The impact of one-electron reduction of AdoCbl cofactor upon the preliminary step of $B_{12}$ catalysis has been investigated using density functional calculations. The IRC calculations indicate that the reaction consisting of Co-C5' bond

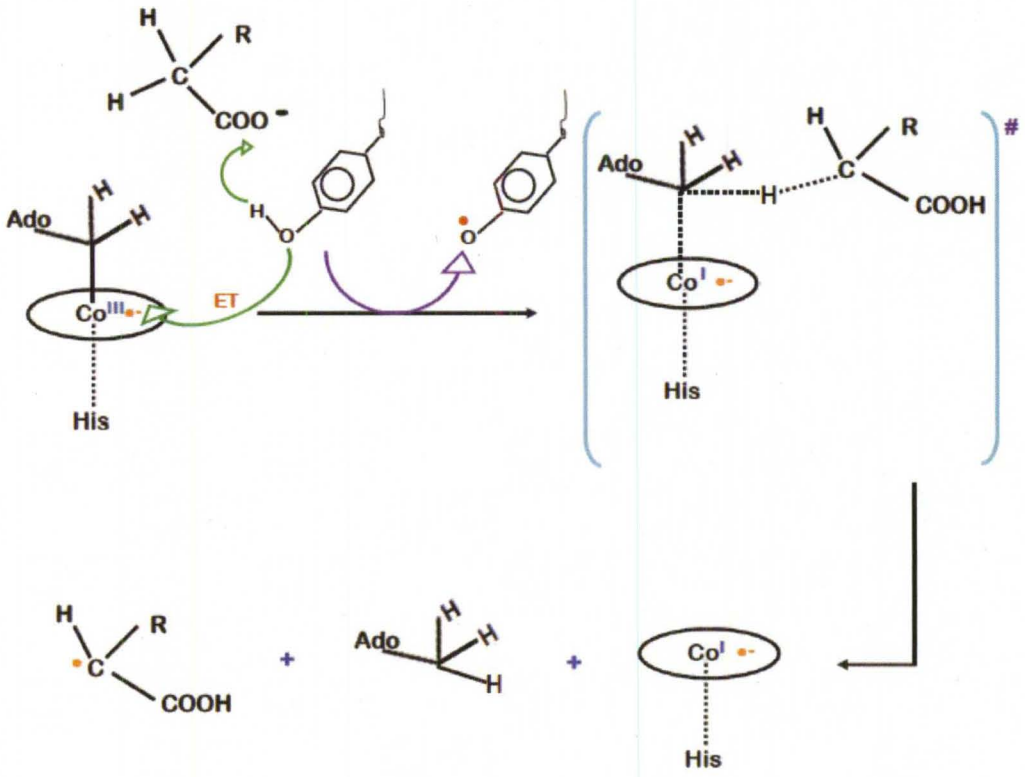


Scheme 7. PCET-inspired alternate mechanism for the initial step of catalysis in $B_{12}$-dependent mutases.

cleavage and the subsequent H-abstraction from the substrate occur in a concerted fashion. The activation energy barrier for the 1el-Red [$Co^{III}$(corrin$^{\bullet}$)]-Rib-mediated reaction (15.0 kcal/mol) is lowered by ~50 % in comparison to the reaction (33.0 kcal/mol) that involves the positively charged Im-[$Co^{III}$(corrin)]-$Rib^{+}$. Since the axial Im base is detached during the 1el-Red [$Co^{III}$(corrin$^{\bullet}$)]-Rib-mediated reaction, the energy barrier of the reaction needs to be corrected by adding the axial Im detachment energy (7.6 kcal/mol). As a result, the effective lowering in the activation barrier of the reaction induced by the one-electron reduction is estimated to be 31.5%. This catalytic effect of one-electron reduction is expected to be significantly higher in the case of enzyme-bound reactions because of the presence of elongated axial base (Scheme 7). These energetic implications associated with one-electron reduction of AdoCbl cofactor can play a major role in understanding the origin of AdoCbl-dependent enzyme catalysis.

# CHAPTER IV

# THEORETICAL STUDY OF THE ROLE OF $Co^{1+}$--H INTERACTION IN THE ENZYME-INDUCED REDOX TUNING OF $Co^{2+}/Co^{1+}$ REDUCTION PROCESS

## 4.1 Introduction

Although methyltransferases (e.g., MetH[31], CFeSP[32], MtaBC[33] etc.) and ACAs (e.g., CobA, PduO and EutT)[37-40] differ vastly in their catalytic functioning yet a common thread connects these two seemingly different classes of enzymes i.e., $Co^{2+}/Co^{1+}$ reduction serves as one of the key components of their catalytic cycles.[16] This is a thermodynamically challenging reaction because the midpoint reduction potentials of the physiological reducing agents (-260 to -440 mV vs SHE) are considerably more positive than that of the $Co^{2+}$Cbx cofactor (-490 mV vs SHE).[86,113] But this reaction is indeed observed[16] when the enzyme-bound $Co^{2+}$Cbx is considered implying that the enzyme must be exercising subtle mechanistic control over the reduction process. In spite of being a ubiquitous chemical event, the detailed mechanistic insight as to how $Co^{2+}/Co^{1+}$ reduction is accomplished inside the enzymes has yet to be fully revealed.

Based on spectroscopic[111,114,119-121] and X-ray structure studies,[116,117-118,139] the generation of tetra-coordinated square planar $Co^{1+}$Cbx has been invoked to be the key molecular determinant of the enzyme-mediated redox tuning of $Co^{2+}/Co^{1+}$ process. The reduction event in the case of ACAs is even postulated to be mediated by tetra-coordinated $Co^{2+}$Cbx.[117-120] However the possibility of penta-coordinated $Co^{2+}$Cbx displaying weak axial interactions has not been ruled out. In the case of MetH enzyme, the reduction process has been suggested to proceed via penta-coordinated $Co^{2+}$Cbx wherein the active site interactions, especially the Y1139 residue has been assessed of catalytic importance in weakening the interaction between the cofactor and β-axial $H_2O$ ligand that in turn will promote the reduction process.[111,114,116]

However an alternative catalytic strategy for driving $Co^{2+}/Co^{1+}$ reduction can be envisioned if we take into account recent studies[126-137] on $M^{n+}$--H bonds (M= Cu, Ni, Co, Pt or Pd; n=1 or 2) where it is shown that the filled d-orbitals of square planar $d^8$ metal ions can also serve as H-bond acceptors. In specific, the existence of a dispersion driven O-H--$Pt^{2+}$ interaction has been recently verified using low-temperature (20K) neutron diffraction technique.[133]

Considering that the ground state electronic structure of $Co^{1+}$Cbx also has a dominant component corresponding to closed-shell $d^8$ configuration,[39,40] an interesting question arises if a $Co^{1+}$ ion can also engage in metal-ion based H-bond formation via its filled d-orbitals. And if indeed, what could be the implications of such associative interactions in relation to $Co^{2+}/Co^{1+}$ reduction

process, a key catalytic conversion in a large variety of methyltransferases and ACAs?

The aim of the reseach work described in this chapter is to probe the abovementioned chemical issues using the DFT, NBO and AIM computational tools.

## 4.2 Computational Details

All calculations were performed using HF and a variety of DFT (BP86, B97-1,[180] B98,[181] B97-D,[182] ωB97X[183] and ωB97X-D[184]) functionals and two different basis sets (6-31G(d) (5d) and 6-31++G(d,p)) as embedded in Gaussian09[185] suite of program for electronic properties and structure calculations. The use of dispersion-corrected B97-D and ωB97X-D functionals was propelled by the fact that the dispersion interactions cannot be well-captured using conventional DFT functionals. The employed structural models were extracted from the high resolution X-ray crystal structure of isolated $Co^{2+}$Cbx[186] and were further augmented by performing geometry optimization. The simplified structural model ($Co^{1+}$Cbl) was prepared by removing all the amide side chains and the nucleotide loop of the cofactor while to mimic the *full* cofactor ($Co^{1+}$Cbi), the side chains were retained and only the nucleotide loop was trimmed off at the phosphodiester end (Figure 21). For optimizing penta-coordinated $Co^{1+}$Cbx complexes, two different starting geometries were considered: (1) $H_2O$ ligand with its O-end towards the $Co^{1+}$ ion ($Co^{1+}$Cbl--$OH_2$; $Co^{1+}$Cbi--$OH_2$) and (2) H-ended $H_2O$ bound to $Co^{1+}$Cbx ($Co^{1+}$Cbl--$H_2O$; $Co^{1+}$Cbi--$H_2O$). Both starting

geometries led to the same final conformation (i.e., $Co^{1+}$Cbl--**H**-O-H; $Co^{1+}$Cbi--**H**-O-H) wherein $H_2O$ axial ligand was **H**-bonded to the cofactor. To test the H-bond forming feature of $Co^{2+}$Cbx complexes, penta- and hexa-coordinated structural models of $Co^{2+}$Cbx were employed. To model penta-coordinated $Co^{2+}$Cbx complexes, two commonly suggested conformations[187] were used: (1) ($Co^{2+}$Cbl--$OH_2$; $Co^{2+}$Cbi--$OH_2$) where the $H_2O$ ligand was placed over the β-axial face of the cofactor and (2) ($Co^{2+}$Cbl--Im; $Co^{2+}$Cbi--Im) where Im, considered as an ideal structural mimick of His ligand, was modelled as α axial ligand. The hexa-coordinated $Co^{2+}$Cbx complexes were modelled as $H_2O$--$Co^{2+}$Cbl--Im and $H_2O$--$Co^{2+}$Cbi--Im respectively. For optimizing penta-coordinated $Co^{2+}$Cbl--$OH_2$ and $Co^{2+}$Cbi--$OH_2$ complexes, two different starting geometries were used: (1) H-ended as well as O-ended conformations of $H_2O$ axial ligand, and (2) optimized

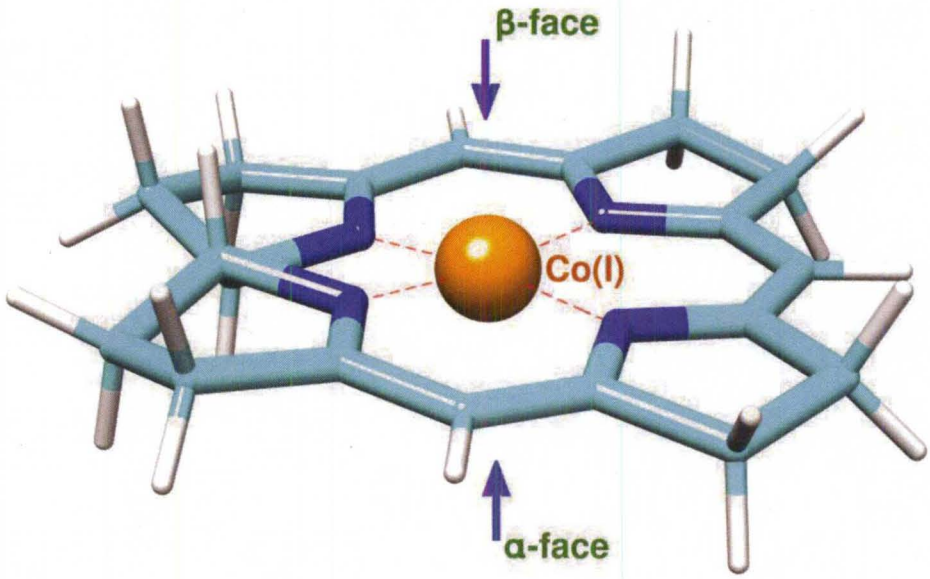


Figure 21. Structure of simplified square planar cob(I)alamin model.

**H**-bonded $Co^{1+}$Cbx ($Co^{1+}$Cbl--**H**-O-H and $Co^{1+}$Cbi--**H**-O-H) complexes. In all the optimized $Co^{2+}$Cbx complexes, the $H_2O$ axial ligand was found to be O-bound with the cofactor. The simplified structural models ($Co^{1+}$Cbl and $Co^{2+}$Cbl) were fully optimized using 6-31++G(d,p) basis set while in the case of the *full* complexes ($Co^{1+}$Cbi and $Co^{2+}$Cbi), geometry optimization was only carried out using 6-31G(d) (5d) basis set owing to the structural complexity of the cofactor model. The authenticity of all the optimized structural models was confirmed by frequency calculations. The solvation of **H**-bonded complexes was studied using chloroform ($\varepsilon$= 4.7), acetonitrile ($\varepsilon$= 32.7) and water ($\varepsilon$= 78) solvents as implemented in the PCM formalism of Gaussian09. The computed free energies of solvation were further corrected by adding the contribution of non-electrostatics terms (repulsion, cavitation, dispersion). The non-electrostatic terms were computed using SMD model of solvation.[188] The interaction energies of the penta-coordinated $Co^{1+}$Cbx complexes ($Co^{1+}$Cbl--$H_2O$; $Co^{1+}$Cbi--$H_2O$) were calculated as the difference between the total energies of the **H**-bonded complexes ($Co^{1+}$Cbl--**H**-O-H; $Co^{1+}$Cbi--**H**-O-H) and the sum of the total energies of the individual precursors ($Co^{1+}$Cbl, $H_2O$; $Co^{1+}$Cbi, $H_2O$). For computing the interaction energy profiles, the single point calculations at higher basis set (6-311++G(2df,2p)) were performed. The computed interaction energy profiles were corrected for basis set superposition error (BSSE) using the countpoise scheme of Gaussian09 software.

The AIM[189], NBO[190] and Wiberg bond index(WBI)[191] analysis of **H**-bonded complexes ($Co^{1+}$Cbl--**H**-O-H; $Co^{1+}$Cbi--**H**-O-H) was only performed at the BP86-optimized geometries.

In order to quantify the catalytic effect of $Co^{1+}$--**H** interaction, we computed the reduction potentials of $Co^{2+}/Co^{1+}$ couple considering two possible conformations of $Co^{1+}$Cbx ($Co^{1+}$Cbx and $Co^{1+}$Cbx--**H**-O-H). The reduction potentials were calculated using our recently calibrated computational protocol that predicts the redox chemistry of $B_{12}$ corrinoids within reliable degree of accuracy.[192] The following equation based on the Born-Haber cycle (Scheme 8) was used to compute the reduction potential of a $Co^{2+}/Co^{1+}$ couple

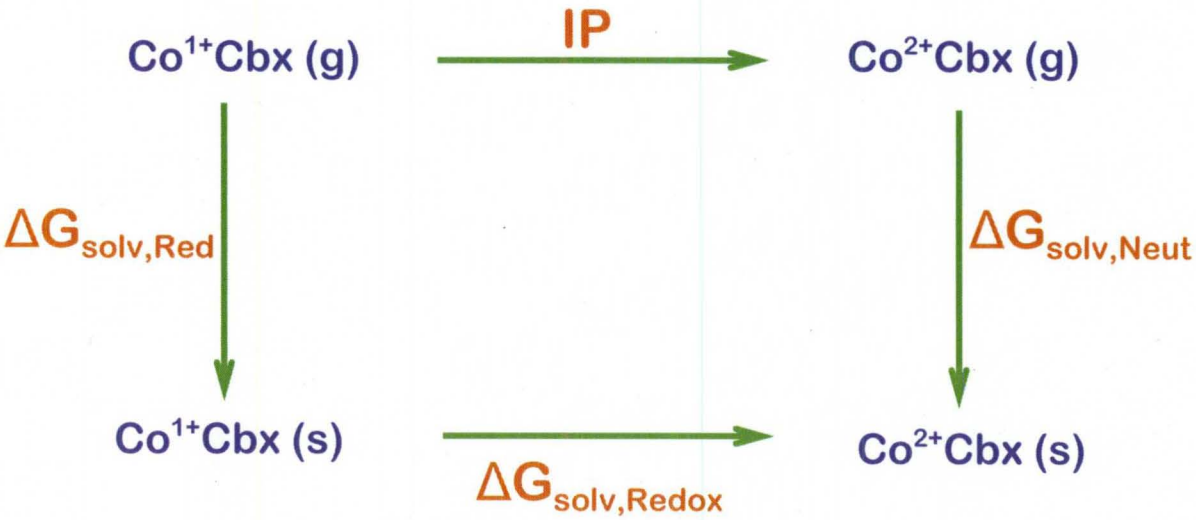


Scheme 8. Born-Haber cycle for $Co^{2+}$ Cbx/$Co^{1+}$Cbx couple.

$$E^0 \text{ (vs SHE)} = IP + 1/23.06(-T\Delta S + \Delta G_{\text{solvation, Redox}}) - 4.28$$

where IP corresponds to ionization potential.

For the SHE, the absolute potential has often been reported as –(4.44 ± 0.02) eV, as recommended by the International Union of Pure and Applied Chemistry in 1986.[193] However, recently Lewis et al.[194] reported a value of -4.28 eV that is considered to be the most accurate available and hence has been employed in the present analysis. Also, the entropy term (-TΔS) was dropped while computing reduction potentials as the ZPE/entropy corrections were relatively small and could be neglected as a first approximation.

## 4.3 Results and Discussions

### 4.3.1 DFT Structural analysis of $Co^{2+}$Cbx and $Co^{1+}$Cbx Model Complexes

Taking into account that $Co^{1+}$Cbx has only been spectroscopically characterized,[111,114,119-120] we turned our attention to computational modeling. As it's shown in the Figure 22, the axial $H_2O$ and Im ligands were O- and N-bound to the $Co^{2+}$ ion in the optimized $Co^{2+}$Cbx complexes (Tables A3 - A8). Note here that the axial $H_2O$ ligand in the $H_2O$--$Co^{2+}$Cbi--Im was significantly displaced (~4.00 - 4.30 Å) away from the $Co^{2+}$ ion indicating that the $H_2O$--$Co^{2+}$Cbi--Im complex is effectively a penta-coordinated complex. On the other hand, the $H_2O$ ligand in the $Co^{1+}$Cbx complexes ($Co^{1+}$Cbl--**H**-O-H; $Co^{1+}$Cbi--**H**-O- H) was ligated to the $Co^{1+}$ ion via its **H**-end (Figure 23 and Tables A9 - A10) which implies that H-bond forming tendency is only mandated by $d^8$ metal ions. The $Co^{1+}$--**H**-O motif in the optimized $Co^{1+}$Cbl--**H**-O-H and $Co^{1+}$Cbi--**H**-O-H complexes was found to be almost linear, a structural feature (<$M^{n+}$--**H**-X greater than 110°) that has

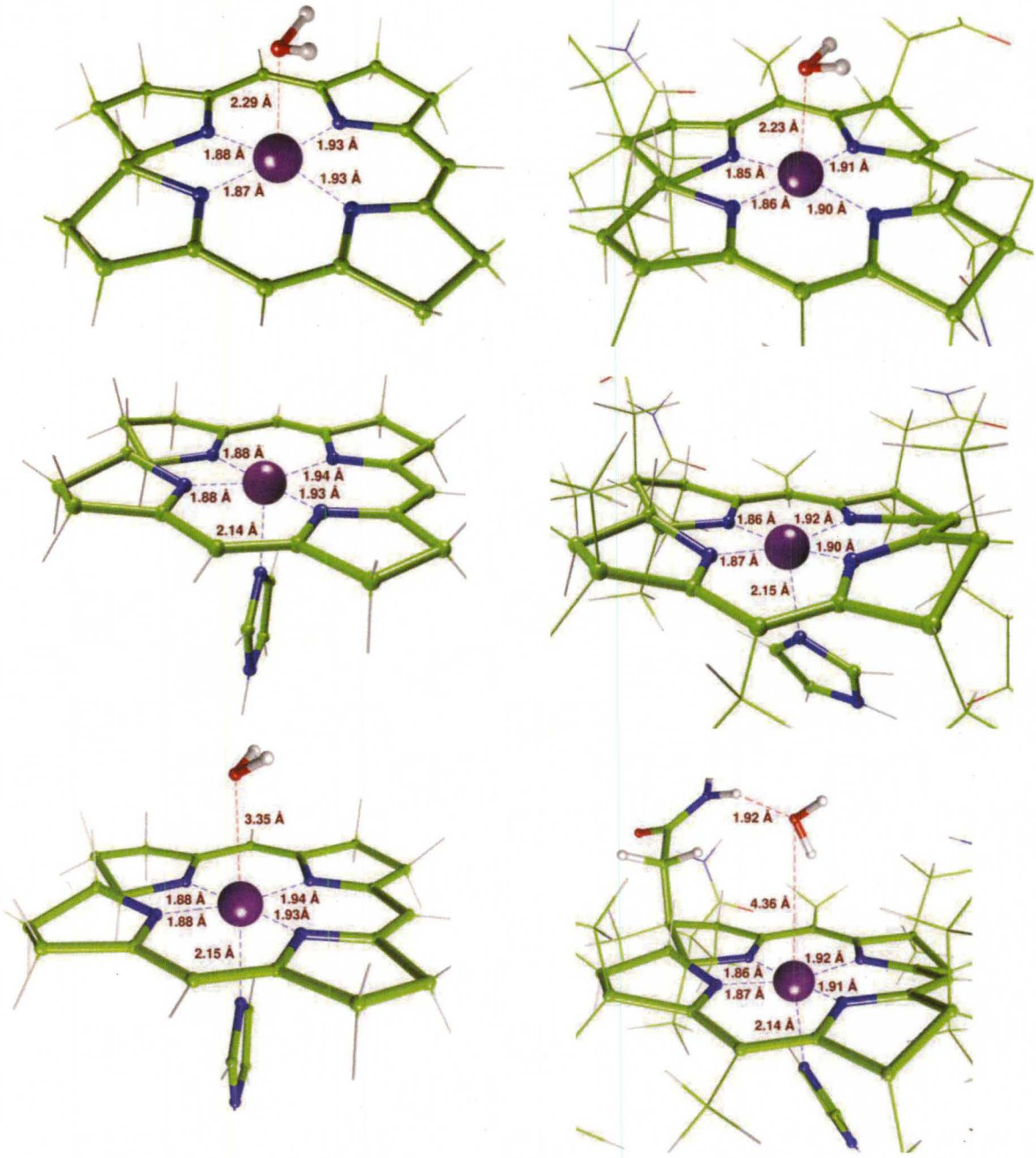


Figure 22. Close-ups of BP86-optimized $Co^{2+}$Cbx complexes ($Co^{2+}$Cbl (*left*); $Co^{2+}$Cbi (*right*)) wherein the regions of interest have been highlighted using ball-stick representation.

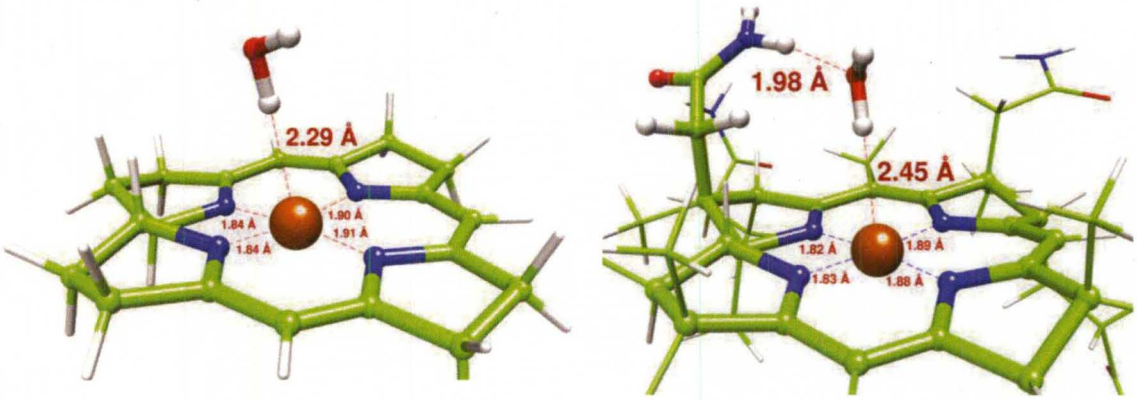


Figure 23. Close-ups of BP86-optimized H-bonded $Co^{1+}$Cbx ($Co^{1+}$Cbl--**H**-O-H (*left*); $Co^{1+}$Cbi--**H**-O-H (*right*)) complexes wherein the regions of interest have been highlighted using ball-stick representation.

usually been associated with **H**-bond forming complexes.[195] Notably the **H**-O bond of $H_2O$ axial ligand was found to be slightly lengthened as compared to its H-O bond that supported the development of $Co^{1+}$--**H** bond. The BP86-calculated harmonic vibrational frequencies further aided the elongation of **H**-O bond as the **H**-O stretching vibration (3328 $cm^{-1}$, 3352 $cm^{-1}$) was lower in energy than the H-O vibration (3747 $cm^{-1}$, 3670 $cm^{-1}$) in the **H**-bonded complexes. The WBI that probe for covalent interactions afforded useful quantitative information to compliment the $Co^{1+}$--**H** bond formation. The **H**-O bond had a lower bond index (0.711; 0.676) than the H-O bond (0.767; 0.761) while the $Co^{1+}$--**H** bond had a noticeable bond order of (0.040; 0.085) which signified the bonding interaction between the $Co^{1+}$ ion and **H**-O motif of the $H_2O$ axial ligand.

### 4.3.2 DFT Thermodynamic Analysis of $Co^{1+}$Cbx Model Complexes

To validate the stability of $Co^{1+}$--**H** bond, the static thermodynamic data for the complex formation reactions

$$Co^{1+}Cbl + \mathbf{H}\text{-O-H} \rightarrow Co^{1+}Cbl\text{--}\mathbf{H}\text{-O-H};$$

$$Co^{1+}Cbi + \mathbf{H}\text{-O-H} \rightarrow Co^{1+}Cbi\text{--}\mathbf{H}\text{-O-H}$$

were evaluated. Surprisingly, in the case of $Co^{1+}$Cbl--**H**-O-H complex, the reaction was found to be non-spontaneous when studied using HF or conventional DFT functionals (BP86, B97-1, B98) with the exception of ωB97X (Figure 24 and Table A11). This is in line with an earlier study,[111] suggesting that

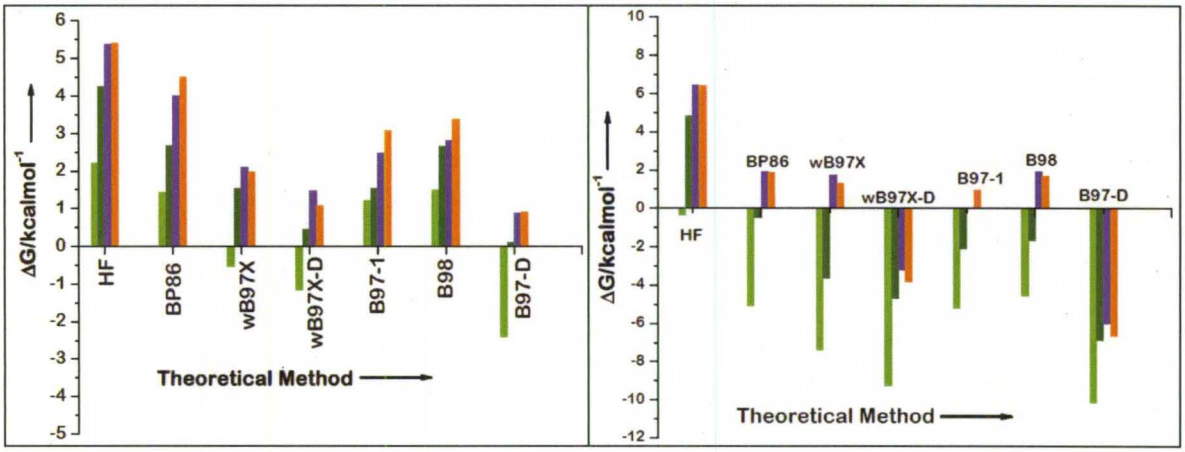


Figure 24. Computed thermodynamic data for the $Co^{1+}$Cbl--**H**-O-H (*upper panel*) and $Co^{1+}$Cbi--**H**-O-H (*lower panel*) complex (green: gas phase, olive: chloroform, violet: acetonitrile, orange: water).

such a complex formation ($Co^{1+}$Cbl--$H_2O$) is not possible from thermodynamic point of view ($\Delta G$ = +1.96 kcal/mol). The exothermicity calculated with ωB97X functional implied that the $Co^{1+}$--**H** linkage has long-range correlation component. When the thermodynamics of the complex was addressed using dispersion-corrected DFT, the complex formation was found to be a spontaneous phenomenon with B97-D functional while the exothermic effect noticed with ωB97X functional was enhanced by ~1 - 2 kcal/mol upon inclusion of dispersion interactions (i.e., with ωB97X-D functional). This indicates that the dispersion component of $Co^{1+}$--**H** linkage contributes noticeably towards the thermodynamic stability of the $Co^{1+}$Cbl--**H**-O-H complex. The importance of dispersion-corrected DFT has recently been illustrated in the case of transition metal complexes[196] and carbene-carbene complex formation reactions[197].

On the other hand, the $Co^{1+}$--**H** bond formation in the case of $Co^{1+}$Cbi--**H**-O-H complex was predicted to be an exothermic event at all levels of theory (Figure 24 and Table A12). It should be noted that though $Co^{1+}$--H bond in the $Co^{1+}$Cbi--**H**-O-H complex was weaker than in $Co^{1+}$Cbl--**H**-O-H, yet relatively a higher degree of exothermic effect was achieved in this case which was mainly due to the larger size of the cofactor ($Co^{1+}$Cbi) and an additional H-bond (-N-H--$OH_2$ = 1.98 Å) that the $H_2O$ axial ligand forms with one of the amide side chains of the cofactor (Figure 23).

To assess the stability of $Co^{1+}$--**H** linkage, the $Co^{1+}$Cbl--**H**-O-H and $Co^{1+}$Cbi--**H**-O-H complexes were solvated using chloroform (ε = 4.7), acetonitrile (ε = 32.7) and water (ε = 78) solvents respectively (Figure 24 and Tables A13-

A15 and A16-A18). The solvated $Co^{1+}$--**H** bond was found to be appreciably destabilized with lesser effect being noticed in the case of lesser polar solvent. The highly endothermic nature of $Co^{1+}$--**H** bond in water also provides a rationale why no such H-bond has been observed experimentally.[86] In spite of the weakening of $Co^{1+}$--**H** linkage upon solvation, the $Co^{1+}$Cbl--**H**-O-H complex formation reaction was found to be essentially a thermoneutral event ($\Delta G$ = +0.18-0.59 kcal/mol) when studies using B97-D and ωB97X-D functionals while the solvated $Co^{1+}$Cbi--**H**-O-H complex remained a thermodynamically stable entity. The solvent-induced destabilization of **H**-bonded complexes indicated that the $Co^{1+}$--**H** bonds are weaker interactions than $H_2O$--$H_2O$ H-bonds.

The existence of the stable $Co^{1+}$--**H** bond was further supported by the minima observed on the interaction energy curves of the $Co^{1+}$Cbl--**H**-O-H and

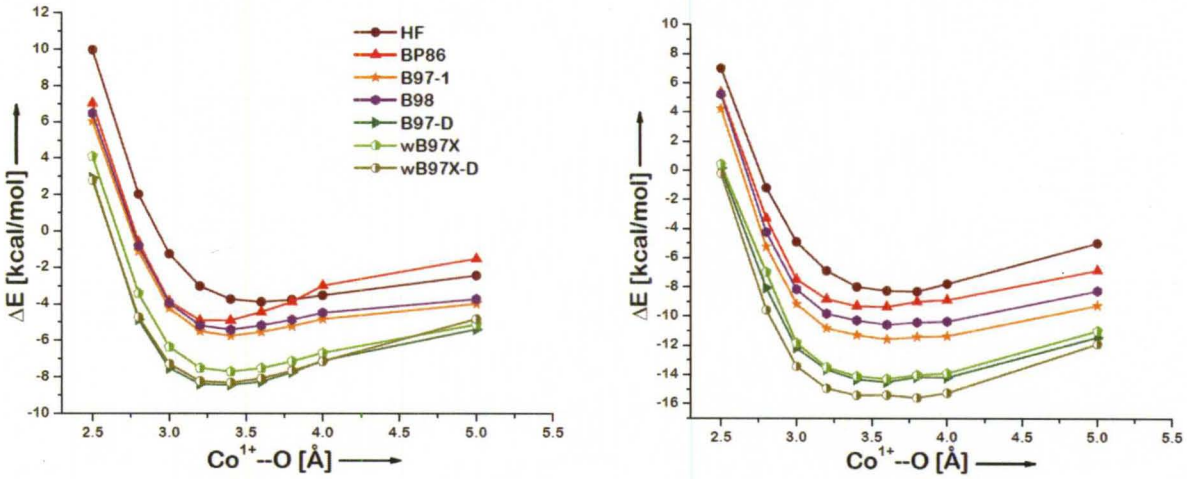


Figure 25. Computed interaction energy profiles of $Co^{1+}$Cbl--**H**-O-H (*left*) and $Co^{1+}$Cbi--**H**-O-H (*right*) complexes. Interaction energy profiles have been corrected with regard to BSSE error.

$Co^{1+}$Cbi--**H**-O-H complexes computed along the $Co^{1+}$--O coordinate (Figure 25). The interaction energies of the **H**-bonded complexes were calculated as the difference between the total energies of the complexes ($Co^{1+}$Cbl--**H**-O-H; $Co^{1+}$Cbi--**H**-O-H) and the sum of the total energies of their separated monomers ($Co^{1+}$Cbl, $H_2O$; $Co^{1+}$Cbi, $H_2O$). The occurrence of the HF minima further pointed out the electrostatic nature of the $Co^{1+}$--**H** bond while the deeper minima observed with DFT (BP86, B97-1, B98, B97-D, ωB97X and ωB97X-D) functionals implied that the $Co^{1+}$--**H** bond also has dispersion and correlation contribution.

### 4.3.3 AIM Analysis of $Co^{1+}$Cbx Model Complexes

In the AIM methodology, the topological properties of the electron density associated with bond critical point (BCP) are analyzed to define the bond path that connects the interacting atoms. Within the formalism of AIM theory, the sign of total energy density (H = G+V) at a BCP is used as an instructive parameter to classify the bonding type i.e., whether the interaction is purely electrostatic (H >0) or partially covalent (H <0). As a next step, we characterized the nature of $Co^{1+}$--**H** interaction using AIM analysis that was performed on the BP86-optimized geometries of the **H**-bonded complexes. For $Co^{1+}$--**H** interactions in the $Co^{1+}$Cbl--**H**-O-H and $Co^{1+}$Cbi--**H**-O-H complexes, the BCP could be located. Table 3 contains all the relevant BCP properties of $Co^{1+}$--**H** interactions. The $Co^{1+}$--**H** interaction in the $Co^{1+}$Cbl--**H**-O-H complex was found to be partially covalent in nature (H = -0.00092) while it was purely electrostatic (H = +0.00094) in the

$Co^{1+}$Cbi--**H**-O-H complex implying that the $Co^{1+}$--**H** interaction was stronger in the case of $Co^{1+}$Cbl--**H**-O-H complex. This is also reflected in terms of $Co^{1+}$--**H** bond distances depicted in Figure 23. This analysis further emphasized that the greater extent of exothermicity noticed in the case of $Co^{1+}$Cbi--**H**-O-H complex was largely due to its steric bulk and an additional binding interaction between the axial $H_2O$ ligand and the amide side chain of the cofactor.

**Table 3**

BCP Properties of $Co^{1+}$--**H** Interaction for $Co^{1+}$Cbl--**H**-O-H and $Co^{1+}$Cbi--**H**-O-H Complexes

| Complex | $\rho_{Co1+--H}$ [a] | $\nabla^2\rho_{Co1+--H}$ [b] | $-V_{Co1+--H}$ [c] | $G_{Co1+--H}$ [d] | $H_{Co1+--H}$ [e] $= -V_{Co1+--H} + G_{Co1+--H}$ |
|---|---|---|---|---|---|
| $Co^{1+}$Cbl--**H**-O-H | 0.02097 | 0.04105 | 0.01211 | 0.01119 | -0.00092 |
| $Co^{1+}$Cbi--**H**-O-H | 0.01530 | 0.03918 | 0.00791 | 0.00885 | 0.00094 |

[a]The electron density at the BCP ($\rho_{Co1+--H}$, e/au$^3$). [b]The Laplacian of the electron density at the BCP ($\nabla^2\rho_{Co1+--H}$, e/au$^5$). [c]The potential energy density at the BCP ($-V_{Co1+--H}$, hartrees/au$^3$). [d]The kinetic energy density at the BCP ($G_{Co1+--H}$, hartrees/au$^3$). [e]The total energy density at the BCP ($H_{Co1+--H}$, hartrees/au$^3$).

### 4.3.4 NBO Analysis of $Co^{1+}$Cbx Model Complexes

To gain insight into the electronic structure of the **H**-bonded complexes and to evaluate the role of orbital interaction between the $Co^{1+}$ ion and $H_2O$ ligand in stabilizing $Co^{1+}$--**H** interaction, NBO second-order perturbation analysis[190] was carried out on the BP86-optimized geometries of the $Co^{1+}$Cbl--**H**-O-H and $Co^{1+}$Cbi--**H**-O-H complexes. The calculated stabilization energy (5.6 kcal/mol; 10.4 kcal/mol) due to the $n_{Co1+}$ (filled d-orbitals of $Co^{1+}$ ion) $\rightarrow \sigma^*_{H-O}$ orbital interactions was significantly higher than that estimated for the $n_{Co1+} \rightarrow$

$\sigma^*_{H\text{-}O}$ interactions (0.82 kcal/mol; 0.2 kcal/mol). This indicated the presence of sizeable contribution of metal to ligand charge transfer component in the $Co^{1+}$--**H** linkage that was also reflected in terms of the orbital occupancies of the $\sigma^*_{H\text{-}O}$ (0.03; 0.06) and $\sigma^*_{H\text{-}O}$ (0.00; 0.00) orbitals (Table 4). Owing to the availability of metal antibonding orbitals ($n^*_{Co1+}$) and **H**-O bonding orbital ($\sigma_{H\text{-}O}$) of appropriate symmetry and energy, the ligand to metal charge transfer also contributed towards the stabilization of the $Co^{1+}$--**H** bond, though its impact was relatively lesser. The role of such orbital interactions in stabilizing non-covalent Se--N, Se--O and Se--F linkages is well documented in literature.[198]

**Table 4**

NBO Perturbation Analysis of $Co^{1+}$Cbl--**H**-O-H and $Co^{1+}$Cbi--**H**-O-H Complexes

| Complex | $\Delta E^{(2)}$ [kcalmol$^{-1}$]* | | | |
|---|---|---|---|---|
| | $n_{Co1+} \rightarrow \sigma^*_{H\text{-}O}$ | $n_{Co1+} \rightarrow \sigma^*_{O\text{-}H}$ | $\sigma_{H\text{-}O} \rightarrow n^*_{Co1+}$ | $\sigma_{O\text{-}H} \rightarrow n^*_{Co1+}$ |
| $Co^{1+}$Cbl--**H**-O-H | 5.6 | 0.8 | 4.1 | 0.3 |
| $Co^{1+}$Cbi--**H**-O-H | 10.4 | 0.2 | 3.0 | 0.8 |

*stabilization energy due to orbital interaction between the $Co^{1+}$ ion and the $H_2O$ axial ligand

### 4.3.5 Computational Electrochemistry of $Co^{2+}/Co^{1+}$ Process

Considering that the model calculations predict a stable $Co^{1+}$--H bond that has charge transfer, electrostatic, long-range correlation and empirical-dispersion contributions, an interesting question arises as to how it might impact the

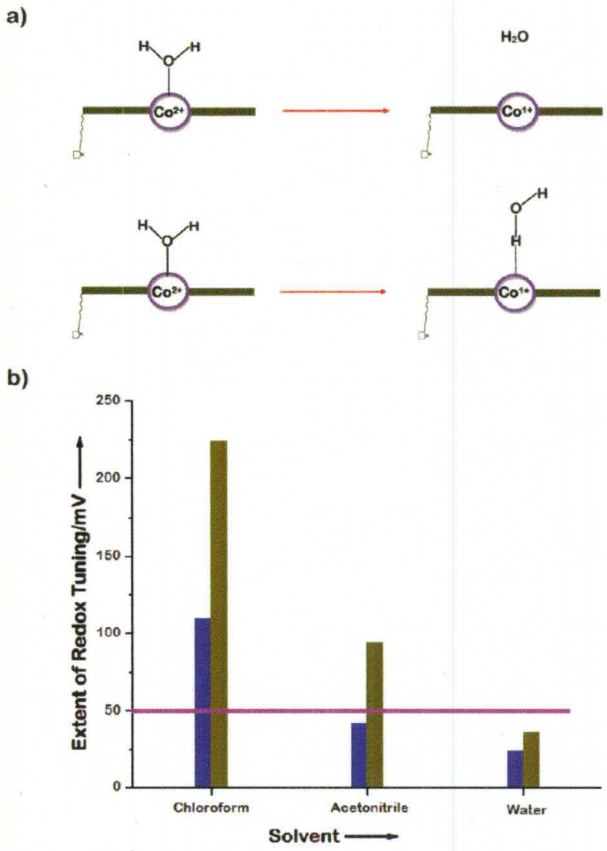


Figure 26. $Co^{1+}$--**H** interaction induced Redox Tuning (vs SHE) of $Co^{2+}/Co^{1+}$ process wherein the figure a) depicts the schematic of the studied reduction processes while figure b) illustrates the redox tuning computed as the difference between the reduction potentials of ($Co^{2+}$Cbl--$OH_2$/$Co^{1+}$Cbl;$Co^{2+}$Cbi--$OH_2$/$Co^{1+}$Cbi) and $Co^{2+}$Cbl--$OH_2$/$Co^{1+}$Cbl--$H_2O$;$Co^{2+}$Cbi--$OH_2$/$Co^{1+}$Cbi--$H_2O$) couples respectively (blue:$Co^{1+}$Cbl, dark yellow:$Co^{1+}$Cbi). The horizontal line (magenta color) in figure b) implies the biological redox gap corresponding to the reduction potential difference between the MetH-bound $Co^{2+}$Cbx cofactor ( -490 mV vs SHE) and the physiological reducing agents (-440 mV vs SHE) as discussed in ref. 111.

catalytic $Co^{2+}/Co^{1+}$ reduction, a key step in many enzymatic reactions? Earlier studies[111,114,116,117-121,139] indicate that the generation of tetra-coordinated square planar $Co^{1+}$Cbx is required to facilitate thermodynamically challenging $Co^{2+}/Co^{1+}$ reduction. But our computations suggest that $Co^{1+}$Cbx can indeed be penta-coordinated square pyramidal due to $Co^{1+}$--H bond formation. Thus to quantify the possible catalytic effect of $Co^{1+}$--**H** interaction, the reduction potentials for ($Co^{2+}$Cbl--$OH_2$/$Co^{1+}$Cbl; $Co^{2+}$Cbi--$OH_2$/$Co^{1+}$Cbi) and ($Co^{2+}$Cbl--$OH_2$/$Co^{1+}$Cbl--$H_2O$;$Co^{2+}$Cbi--$OH_2$/$Co^{1+}$Cbi--$H_2O$) couples were computed using a calibrated computational protocol (BP86/6-31+G*) that predicts the reduction potentials of $B_{12}$ cofactors within reliable degree of accuracy (Tables A19 - A24).[192] A significant amount of redox tuning (~100 - 225 mV vs SHE) was noticed when the **H**-bonded conformation of $Co^{1+}$Cbx was employed (Figure 26; Table A25)

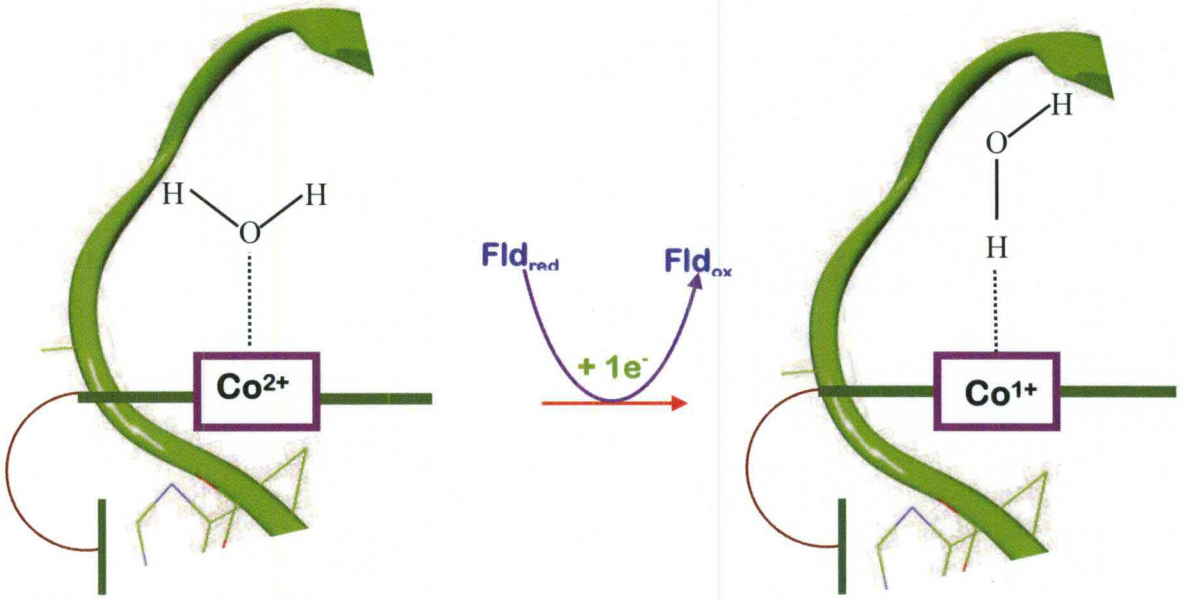


Scheme 9. An alternate mechanistic pathway for the enzyme-bound $Co^{2+}/Co^{1+}$ reduction.

which is appreciably higher than the redox gap (50 mV vs SHE) between the MetH-bound $Co^{2+}$Cbx cofactor and the physiological reducing agents.[111] This finding strongly suggests that $Co^{1+}$--H interaction driven H-bonded conformation of $Co^{1+}$Cbx can play a deterministic role in explaining as to how $Co^{2+}/Co^{1+}$ reduction is accomplished inside MetH enzyme. This reveals a novel catalytic strategy (Scheme 9) that might not only be deployed by MetH enzyme[31] during its reactivation cycle but also by other methyltransferases and a no. of ACAs during their biochemical pathways.[16] The axial H136 ligand in the case of MtaBC enzyme[33] is located at 2.51 Å distance from the $Co^{2+}$ ion and hence can serve as a potential H-bond donor for $Co^{1+}$--H bond formation. Similarily, in the case of PduO-type ACA, the topological location of F112 residue ($Co^{2+}$ --C = 3.8 Å)[118] also makes it an ideal H-donor to effectuate $Co^{1+}$--H bond formation.

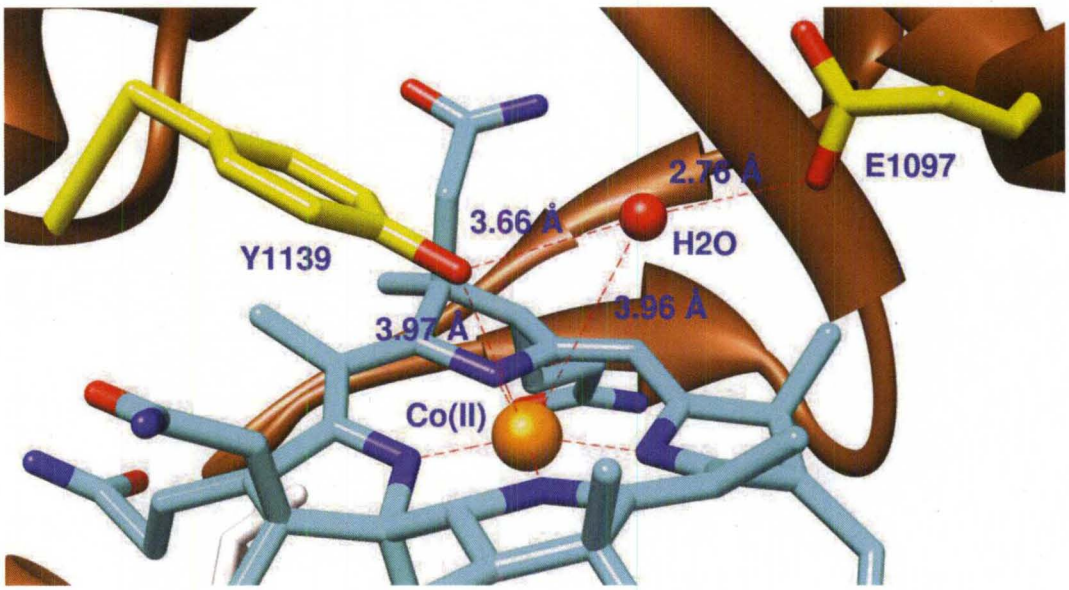


Figure 27. Active site view of the X-ray crystal structure of MetH-bound $Co^{2+}$Cbx (PDB-code: 3IVA @ 2.7 Å resolution).

Furthermore, the stability of such $Co^{1+}$--H linkages when formed inside the enzymes, may be enhanced due to the cooperativity effect exerted by the local protein environment. For example, the axial $H_2O$ ligand in the reactivation cycle of MetH enzyme[118] is engaged in extensive H-bond formation with the local protein domain (the active site Y1139 and E1097 residues) (Figure 27) and this H-bonded network may play a crucial role in stabilizing $Co^{1+}$--H interaction in the MetH-bound $Co^{1+}$Cbx.

## 4.4 Conclusions

The existence of an unanticipated $Co^{1+}$--H linkage that has charge transfer, electrostatic, long-range correlation and empirical-dispersion components is computationally validated using DFT, AIM and NBO tools. The usefulness of long-range correlation- and empirical dispersion-corrected DFT in the proper description of complexes containing $Co^{1+}$--H bonds is illustrated. The analysis of the computed reduction potentials indicated that the $Co^{1+}$ ion-induced H-bond can potentially fine-tune the thermodynamics of the enzyme-bound $Co^{2+}/Co^{1+}$ process which is an indispensable chemical event in a wide body of methyltransferases and ACAs.

# CHAPTER V

# ROLE OF THE AXIAL LIGAND CONFORMATIONAL CHANGE IN THE $Co^{2+}/Co^{1+}$ REDOX TUNING IN METHIONINE SYNTHASE ENZYME

## 5.1 Introduction

The $Co^{2+}/Co^{1+}$ reduction is a common corrinoid reaction in cytoplasmic methyltransferases and mitochondrial ACAs.[16] Despite its broad and general chemical appeal, the $Co^{2+}/Co^{1+}$ reduction remains poorly understood. This is because $Co^{2+}/Co^{1+}$ conversion is a thermodynamically challenging process due in part to the reduction potential of the unbound base-off $Co^{2+}$Cbx (-500 mV vs SHE) being inaccessible by the physiological reducing agents (-260 to -460 mV vs SHE) operative in cellular conditions.[86,113]

On the basis of structural[116,117-118,139] and spectroscopic evidence,[111,114,119-121] formation of tetracoordinated square planar $Co^{1+}$Cbx has been advocated as the most plausible mechanistic description to rationalize the enzyme-mediated tuning of the reduction process in the case of methyltransferases (Scheme 10a). Though such a mechanistic description significantly advances our understanding

of $Co^{2+}/Co^{1+}$ conversion, there are studies[199-201] indicating that $Co^{1+}$Cbx may also exist in other coordination geometries. Notably, two pentacoordinated $Co^{1+}$-model compounds (i.e., $[pyCo^{1+}(dmgBF_2)_2]^-$ and $[MeCNCo^{+1}(dmgBF_2)_2]^-$)[199-200] and a hexacoordinated $Co^{1+}$ clathrochelate ($[Co^{1+}(Cl_2g)_3(Bn\text{-}C_4H_9)_2]^-$)[201] in a trigonal prism arrangement have been structurally characterized. Further, a growing body of experimental and theoretical evidence[126-137] suggests that $d^8$ metal ions, such as $Pt^{2+}$ and $Co^{1+}$ can display pentacoordinated square pyramidality because of their distinct H-bond forming ability. Importantly, Kozelka et al.,[133] have provided the first conclusive evidence of a dispersion driven O-H--$Pt^{2+}$ interaction in an uncharged trans-$[PtCl_2(NH_3)(N\text{-glycine})].H_2O$ complex. Taking into account these findings, an alternative mechanistic preference has been recently proposed[205] as described in chapter IV wherein the H-bonded pentacoordinated $Co^{1+}$Cbx--$H_2O$ intermediate is invoked to tune the reduction process. Scheme 10b shows the proposed mechanistic route that involves a conformational change at the axial $H_2O$ ligand rather than its complete dissociation from the cofactor. The formation of $Co^{1+}$Cbx--$H_2O$ complex is facilitated by the fact that the $Co^{1+}$ ion, which is a dominant $d^8$ system,[39,40] prefers to deploy its filled d-orbitals for constructing a distinctive $Co^{1+}$--H interaction that has noticeable charge transfer, long-range correlation, dispersion and electrostatic components. The DFT calculations[202] indicate that the $Co^{1+}$--H interaction exerts a sizeable amount of redox tuning (50-225 mV vs SHE) upon the $Co^{2+}/Co^{1+}$ process thereby making it accessible by the common biological reductants.

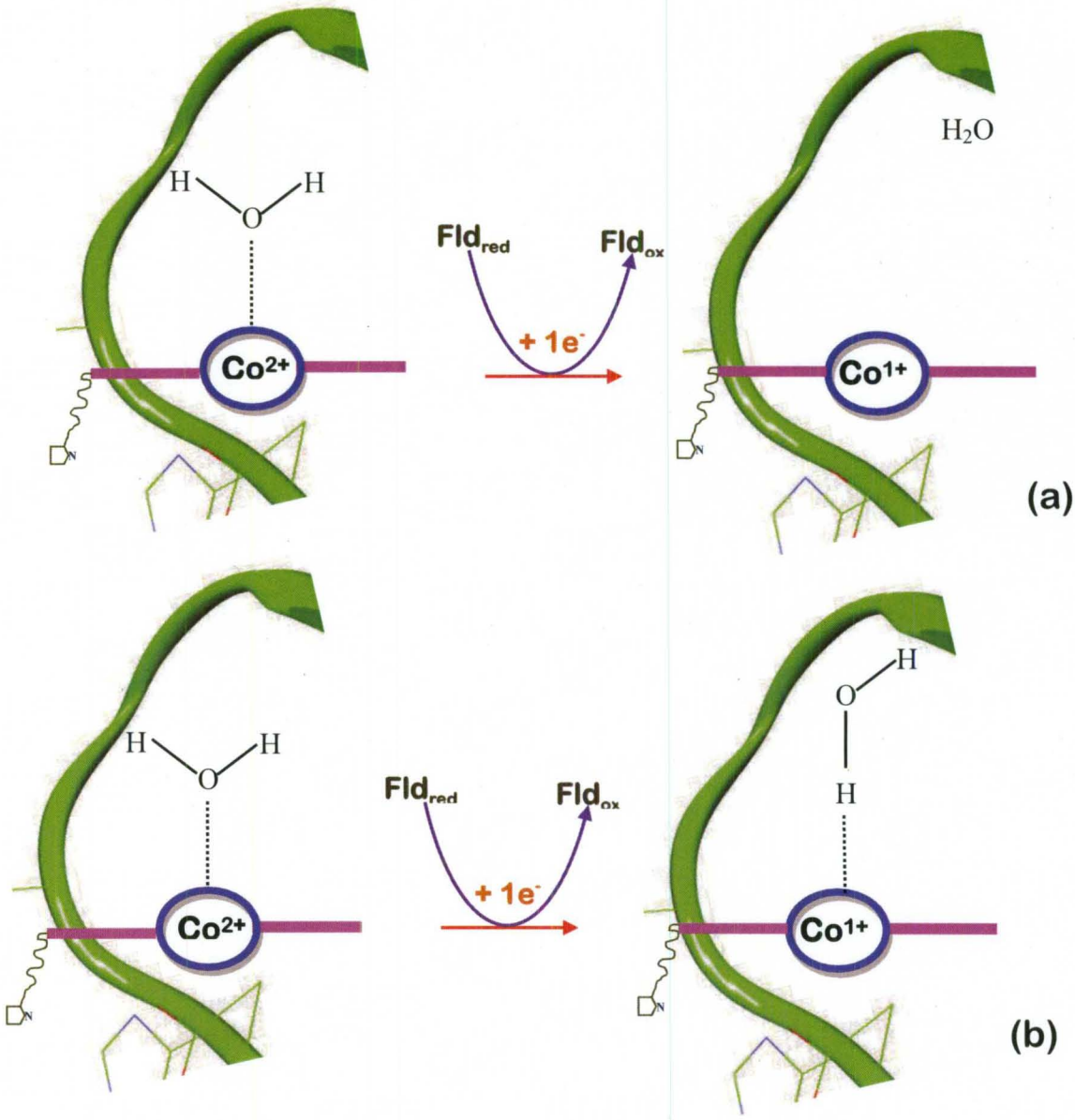


Scheme 10. Possible mechanistic routes for the enzyme-bound $Co^{2+}/Co^{1+}$ reduction in methyltransferases.

The computational work reported in this chapter demonstrates how the plausible mechanistic path shown in Scheme 9b may be realized inside the enzymes, i.e., precisely how the conformational change at the axial ligand may be induced en route to the formation of enzyme-bound $Co^{1+}$Cbx. Herein we employ DFT, AIM and ONIOM-based QM/MM computations to investigate the molecular details of a $Co^{1+}$--H bond formation during the reactivation cycle of MetH enzyme which is one of the better understood methyltransferases[33].

## 5.2 Computational Details

### 5.2.1 Model DFT Calculations

All calculations were performed using HF and a variety of DFT (BP86,[152] B97-1,[180] B98,[181] B97-D,[182] ωB97X[183] and ωB97X-D[184]) functionals and 6-31++G(d,p) basis set as embroidered into Gaussian09[185] quantum chemical suite of program for electronic structure and properties calculations except for the AIM analysis that was carried out using AIM2000[189] software. The use of the long-range correlation- and the empirical dispersion-corrected DFT functionals (ωB97X, ωB97X-D and B97-D) was motivated by the fact that the non-covalent interactions had not been faithfully reproduced using conventional DFT[116]. Considering that the crystal structure of $Co^{1+}$Cbx had yet not been resolved, the employed simplified structural models of $Co^{1+}$Cbx ($Co^{1+}$Cbl) as well as those of $Co^{2+}$Cbx ($Co^{2+}$Cbl) were prepared from the high resolution X-ray crystal structure of isolated $Co^{2+}$Cbx[186] and were further improved by performing the geometry optimization. These structural models were constructed by removing all the

amide side chains and the nucleotide loop of the cofactor. To mimic the possible active site interactions of the β-axial $H_2O$ ligand, two types of the structural models were considered: (1) $Co^{1+}$Cbl--$H_2O$--$H_2O$; $Co^{2+}$Cbl--$H_2O$--$H_2O$ where a $H_2O$ molecule, a universal H-bond donor, was placed in the vicinity of the axial ligand to replicate its H-bonding interaction with the proximal residues; (2) $Co^{1+}$Cbl--$H_2O$--HOPh; $Co^{2+}$Cbl--$H_2O$--HOPh where PhOH was used to model the local Y1139 residue of MetH enzyme. The latter kind of the structural models presented an excellent case study platform for extracting valuable insight into the catalytic role of Y1139 residue in relation to MetH-catalyzed reduction process. [111,116,139] All the structural models were fully optimized using 6-31++G(d,p) basis set and their optimized geometries were validated to be global minima via frequency calculations. It should be noted that the optimization of $Co^{2+}$Cbl and $Co^{1+}$Cbl complexes was initiated using O-ended as well as H-ended geometries of $H_2O$ or PhOH interacting with the axial $H_2O$ ligand. Both the starting points converged to the same final structure i.e., in $Co^{2+}$Cbl complexes, the neighbouring $H_2O$ or PhOH interacted with the axial ligand via its O-end while in $Co^{1+}$Cbl complexes, the local motif communicated through its H-end. To analyze the stability of $Co^{1+}$Cbl complexes, the static thermodynamic data was computed supposing a standard state convention of 1 atm and temperature of 298.15 K. The solvation of $Co^{1+}$Cbl complexes was studied using chloroform ($\varepsilon$ = 4.70) solvent as weaved into the PCM formalism of Gaussian09.

### 5.2.2 ONIOM QM/MM Calculations

A recently resolved X-ray crystal structure of MetH-bound $Co^{2+}$Cbx (PDB code: 3IVA @2.7 Å resolution)[116] was used to build a computational model. The experimental artifacts were deleted from the X-ray crystal structure and consequently, no counter ions were included in the models investigated. The protonation states of histidine residues were determined at pH = 7.0 using PROPKA suite of program[203] and visual inspection as follows: HID759, HID841, HID1028, HIE1104, HIE1145, HIE1184, HIP894, HIP927, HIP1021, HIP1027, HIP1080,

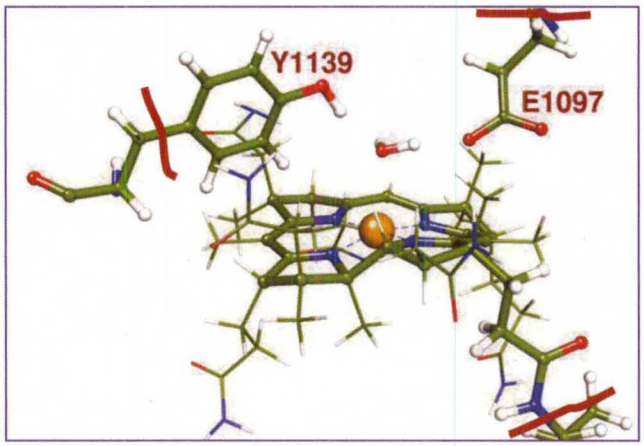


Figure 28. QM:MM partition scheme used in the present ONIOM analysis. The red color curly lines represent the boundaries between the QM and MM domains. Here QM region is described by DFT while MM part is analyzed using AMBER force field.

and HIP1160. HID and HIE were used here to mean that these were neutral histidine residues with the protonated $N_{\delta 1}$ and $N_{\delta 2}$ atoms, respectively, and HIP was a doubly protonated histidine. However, aspartic acid and glutamic acid residues were assumed as ionized, and lysine and arginine residues were assumed as protonated, and the crystal $H_2O$ molecules were also included in the model. The model structure was first pre-equilibrated and was subsequently subjected to geometry optimization of hydrogen atoms using the AMBER force field as implemented in Gaussian09. Subsequently, AMBER geometry optimization was performed for hydrogen atoms and heavy atoms of the side chains. Merz-Kollman electrostatic potential atomic charges were determined for the cofactor,[204] applying the ONIOM(B3LYP/6-31G(d):AMBER) mechanical embedding (ME) scheme. In this calculation, the cofactor was defined as the model system to which DFT was applied, and the radius for the Co ion was set at 0.79 Å. The residues within 20 Å from the Co center and hydrogen atoms were then geometry optimized with the ONIOM-ME method, where the cofactor was assumed the model system. The $Co^{2+}$Cbx model was turned out to be neutral. Then the model system was changed as shown in the Figure 28 and only the QM atoms were optimized using ONIOM-ME. After these preparatory calculations, ONIOM electronic embedding (EE) calculations were carried out where the QM part was analyzed using four different functionals (B3LYP, BP86, ωB97X and ωB97X-D).

## 5.3 Results and Discussion

### 5.3.1 DFT Analysis of MetH-bound $Co^{2+}$Cbx Model Complexes

The optimized isolated $Co^{2+}$Cbl complexes ($Co^{2+}$Cbl--$OH_2$--$OH_2$ and $Co^{2+}$Cbl--$OH_2$--HOPh) were found to be O-bound at the β face of the corrin ring with a strong $Co^{2+}$--O (~ 2.25 - 2.55 Å) bond (Figure 29; Tables A26 – A27) implying that MetH-bound $Co^{2+}$Cbx would prefer to be O-bound with the axial ligand endorsing prior structural,[116] spectroscopic and computational studies[111,114]. Note here that the axial $H_2O$ ligand in the optimized $Co^{2+}$Cbl--$OH_2$--HOPh complex was displaced by PhOH moiety that formed a relatively weak $Co^{2+}$--O bond (~2.32 – 2.46 Å).

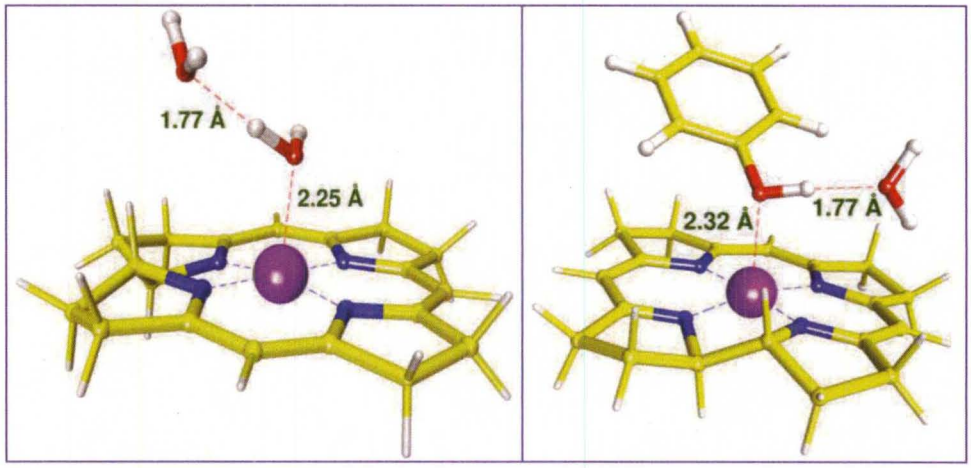


Figure 29. BP86-optimized $Co^{2+}$Cbl structural models ($Co^{2+}$Cbl--$OH_2$--$OH_2$ (*left*); $Co^{2+}$Cbl--$OH_2$--HOPh (*right*)).

### 5.3.2 QM/MM Analysis of MetH-bound $Co^{2+}$Cbx

With the ONIOM-based QM/MM calculations, a similar conceptual picture was obtained i.e., the axial $H_2O$ ligand communicated with the $Co^{2+}$ ion through its O-end (Figure 30). The QM/MM optimized $Co^{2+}$--O bond, ranging between 2.44 Å and 2.66 Å, was noticeably lengthened in comparison to that in the isolated structural models (~2.25 - 2.55 Å), implying that the enzyme environment would tend to weaken the interaction between the cofactor and the axial ligand. Furthermore, this computational finding was supported by the existing spectroscopic data of Brunold et al.,[111] where it had been shown that the enzyme environment would cause the elongation of $Co^{2+}$--O bond by 0.2 or 0.3 Å and would result in the formation of a weakly-bound penta-coordinated $Co^{2+}$Cbx--$OH_2$ state. It should be noted that the QM/MM optimized $Co^{2+}$--O bond distance was significantly deviated from the experimental value reported in ref. 116 (Figures 27 and 30). This discrepancy between the calculated and the experimental data might be due to the poor resolution of the X-ray crystal structure (i.e., 2.7 Å) of the reactivation complex of MetH-bound $Co^{2+}$Cbx[116] that is the most reasonable crystal structure available for this complex and was used as a reference point in the present work. The closer analysis of MetH-bound $Co^{2+}$Cbx revealed that the axial $H_2O$ ligand was engaged in a tightly coupled H-bonding network (Y1139--$H_2O$--E1097--R1094) with the local enzyme scaffold. Noteworthy were the direct H-bonding interactions between the axial $H_2O$ ligand and the local Y1139 and E1097 residues where the axial ligand constructed a relatively stronger interaction with the E1097 residue ($H_{H2O}$--$^{-}OOC_{E1097}$ ~1.69 Å; $O_{H2O}$--$HO_{Y1139}$

~1.95 Å). This suggested that the E1097 residue might be exerting a pull effect upon the axial ligand in order to disrupt its interaction with the cofactor, which in turn would be facilitated by the proximal R1094 residue owing to its strong salt-bridge interaction with the E1097 residue ($N_{R1094}$-H --$^{-}OOC_{E1097}$ = 1.78 Å). This was consistent with the prior studies[111,116] suggesting that the local enzyme scaffold, especially the Y1139 and E1097 residues, promote the generation of a weakly-coordinated square pyramidal MetH-bound $Co^{2+}$Cbx--$OH_2$ to combat the thermodynamic demand of the reduction process. It is important to mention that the axial $H_2O$ ligand would be detached from $Co^{2+}$Cbx inside the enzyme environment only if the active site of MetH-bound $Co^{2+}$Cbx would be hydrophobic in nature. But since the tyrosine (Y1139), glutamate (E1097) and arginine (R1094) residues were present in the binding pocket of MetH-bound $Co^{2+}$Cbx, the active site would be strongly hydrophilic. As a result, the axial $H_2O$ ligand would be retained in the active site.

### 5.3.3 DFT Analysis of MetH-bound $Co^{1+}$Cbx Model Complexes

The axial $H_2O$ ligand in the case of isolated $Co^{1+}$Cbl structural models ($Co^{1+}$Cbl--$H_2O$--$H_2O$ and $Co^{1+}$Cbl--$H_2O$--HOPh) (Figure 31, Tables A28 – A29), was found to be H-bonded with the $Co^{1+}$ ion of the cofactor documenting the unusual H-bond forming feature of $d^8$ $Co^{1+}$ ion. The binding motif ($Co^{1+}$--H-O) in the optimized $Co^{1+}$Cbl--$H_2O$--$H_2O$ ($\angle Co^{1+}$--H-O = 157.9°) and $Co^{1+}$Cbl--$H_2O$--HOPh ($\angle Co^{1+}$--H-O = 172.3°) complexes was found to be aligned in a strictly

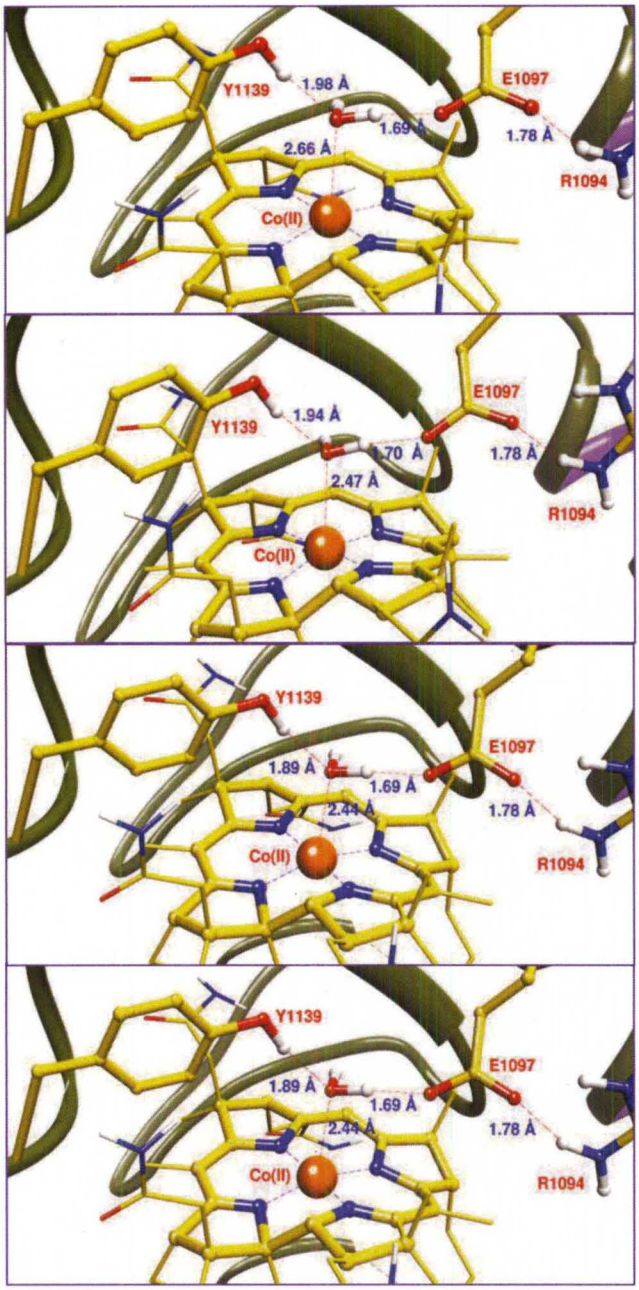


Figure 30. Active site view of the ONIOM (DFT:AMBER) optimized MetH-bound $Co^{2+}$Cbx (DFT = B3LYP/6-31G(d) (*top*), BP86/6-31G(d) (*middle1*), ωB97X/6-31G(d) (*middle 2*) and ωB97X-D/6-31G(d) (*bottom*)).

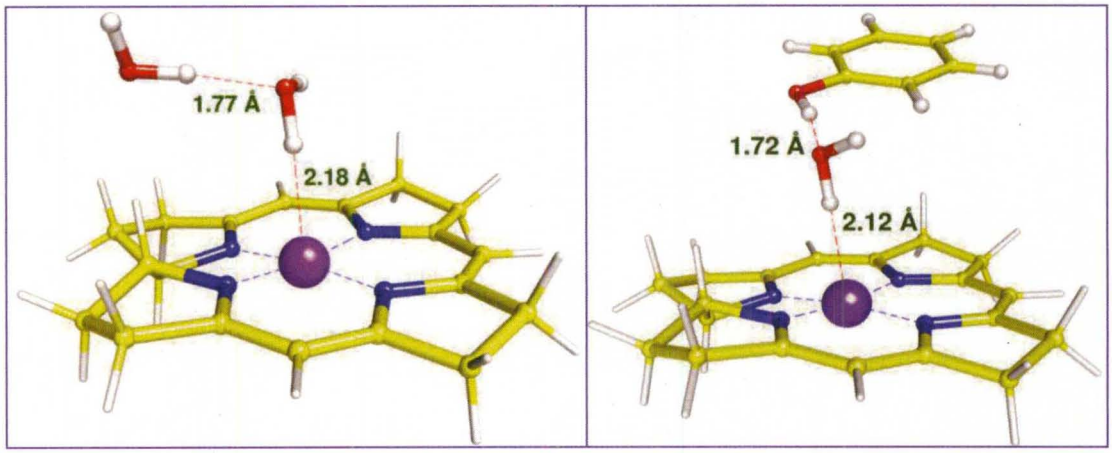


Figure 31. BP86-optimized $Co^{1+}$Cbl--$H_2O$--$H_2O$ (*left*) and $Co^{1+}$Cbl--$H_2O$--HOPh (*right*).

linear fashion which had been a typical structural signature of H-bond forming systems. The axial $H_2O$ ligand in the $Co^{1+}$Cbl--$H_2O$--HOPh complex remained coordinated to the $Co^{1+}$ ion in contrast to the analogous $Co^{2+}$Cbl complex where it was displaced by the tyrosine mimick (i.e., by PhOH). Notably the $Co^{1+}$--O bond distance (~3.13 – 3.29 Å) in the optimized H-bonded complexes was appreciably lengthened in comparison to the analogous $Co^{2+}$Cbl complexes implying that the weakening of $Co^{2+}$--O linkage was mandated to inudce a conformational change at the axial ligand for forming a $Co^{1+}$--H interaction, and should not be misinterpreted as a mechanistic prerequisite for generating square planar $Co^{1+}$Cbx. The optimized $Co^{1+}$--H linkage (~2.12 – 2.25 Å) in the $Co^{1+}$Cbl--$H_2O$--HOPh complex was stronger than in the $Co^{1+}$Cbl--$H_2O$--$H_2O$ complex ($Co^{1+}$--H ~2.18 – 2.37 Å) because the PhOH moiety, being a better H-donor, formed a stronger H-bonding contact with the axial $H_2O$ ligand (PhOH--$H_2O$ ~1.72 – 1.79

Å) and exerted a noticeable push to strengthen the communication between the $H_2O$ ligand and the $Co^{1+}$ ion.

### 5.3.4 DFT Thermodynamic Analysis of MetH-bound $Co^{1+}$Cbx Model Complexes

The computed thermodynamic data for the isolated $Co^{1+}$Cbl models further asserted the stable character of the $Co^{1+}$--H interaction (Figure 32 and Tables A30 – A33). The exothermicity affiliated with the H-bonded $Co^{1+}$Cbl complexes was validated only upon treatement with the long-range correlation- or the empirical-dispersion-corrected functionals (Tables A30 and A32) which signified the presence of a sizeable dispersion component in the $Co^{1+}$--H interaction. The formation of a similar $Co^{1+}$--H interaction had also been noted during a previous study,[114] but the thermodynamic feasibility of such a linkage could not be verified because the calculations were only performed using the conventional DFT functional. Upon solvation in chloroform ($\varepsilon$ = 4.70), an appreciable degree of destabilization was caused to the $Co^{1+}$--H linkage (Tables A31 and A33). As a result, the $Co^{1+}$Cbl--$H_2O$--$H_2O$ complex became endothermic at all levels of theory but the $Co^{1+}$Cbl--$H_2O$--HOPh complex, a realistic active site mimick of MetH-bound $Co^{1+}$Cbx, remained a thermodynamically viable entity, when analyzed with the dispersion-corrected functionals suggesting that the $Co^{1+}$--H interaction could be engineered inside the enzyme scaffold of MetH.

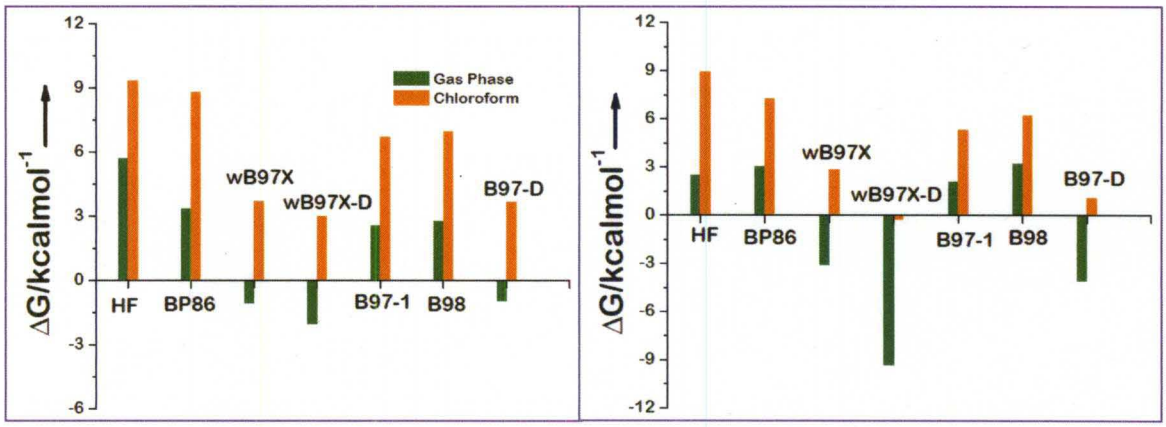


Figure 32. Computed Gibbs energy data for H-bonded $Co^{1+}$Cbl--$H_2O$--$H_2O$ (*left*) and $Co^{1+}$Cbl--$H_2O$--HOPh (*right*).

### 5.3.5 AIM Analysis of MetH-bound $Co^{1+}$Cbx Model Complexes

The AIM chemical tool could provide enriching quantitative insight into the precise nature of $Co^{1+}$--H interaction. Thus, as a next step, we performed AIM analysis on BP86 geometries of the $Co^{1+}$Cbl--$H_2O$--$H_2O$ and $Co^{1+}$Cbl--$H_2O$--HOPh models. The $\rho_{Co1+--H}$ estimated at the BCP of $Co^{1+}$--H interaction lied in the range of 0.02 - 0.03 e/au$^3$ (Table V-1) that had usually been suggested for normal H-bonds[205]. This indicated that the $Co^{1+}$--H interaction could be classified as a H-bond. The positive values of the $\nabla^2\rho_{Co1+--H}$ at the identified BCPs predicted $Co^{1+}$--H interaction to be a dominant electrostatic interaction. But it had been noted[206] that the total energy density (H) coupled with $\nabla^2\rho$ should be employed as a realistic descriptor of non-covalent interactions. The closer scrutiny of the AIM data instructed that the $Co^{1+}$--H interaction was partially covalent rather than being purely electrostatic. But since the absolute $H_{Co1+--H}$ values were very small;

the degree of partial covalence (electron sharing) should be treated as insignficant. It should be noted that the $Co^{1+}$--H interaction could not be categorized as an agostic-type because the transition metals that form such interactions were usually the early transition metals (e.g. Ti, Sc, Mo etc.) in high oxidation states[207]. Apparently, $Co^{1+}$ ion did not fall in this domain. On the other hand, the metal ion-induced H-bonds had been formed by the late transition metals in low oxidation states such as $Pt^{2+}$, $Ni^{2+}$, $Cu^{2+}$ ions etc.[128-139] The $Co^{1+}$--H interaction would clearly belong to this class.

**Table 5**

BCP Properties of $Co^{1+}$--H Interaction for $Co^{1+}$Cbl--$H_2O$--$H_2O$ and $Co^{1+}$Cbl--$H_2O$--HOPh Complexes

| Complex | $\rho_{Co1+--H}$ | $\Delta^2\rho_{Co1+--H}$ | $-V_{Co1+--H}$ | $G_{Co1+--H}$ | $H_{Co1+--H} = -V_{Co1+--H} + G_{Co1+--H}$ |
|---|---|---|---|---|---|
| $Co^{1+}$Cbl--$H_2O$--$H_2O$ | 0.02686 | 0.042775 | 0.01681 | 0.01375 | -0.00306 |
| $Co^{1+}$Cbl--$H_2O$--HOPh | 0.03027 | 0.04185 | 0.01971 | 0.01509 | -0.00462 |

### 5.3.6 QM/MM Analysis of MetH-bound $Co^{1+}$Cbx

Using the optimized structure of MetH-bound $Co^{2+}$Cbx as a starting point, a QM/MM analysis of MetH-bound $Co^{1+}$Cbx was carried out to investigate whether the axial $H_2O$ ligand would ligate to the $Co^{1+}$ ion via its O- or H-end. The computed QM/MM data clearly indicated the formation of a $Co^{1+}$--H interaction in MetH-bound $Co^{1+}$Cbx (Figure 33). The calculated $Co^{1+}$--H bond distance (2.33 – 2.54 Å) was in the domain of $d^8$ metal ion-induced H-bonds.[126-137] Notably, the $Co^{1+}$--H interaction was strengthened by ~0.1 – 0.2 Å with the ωB97X and

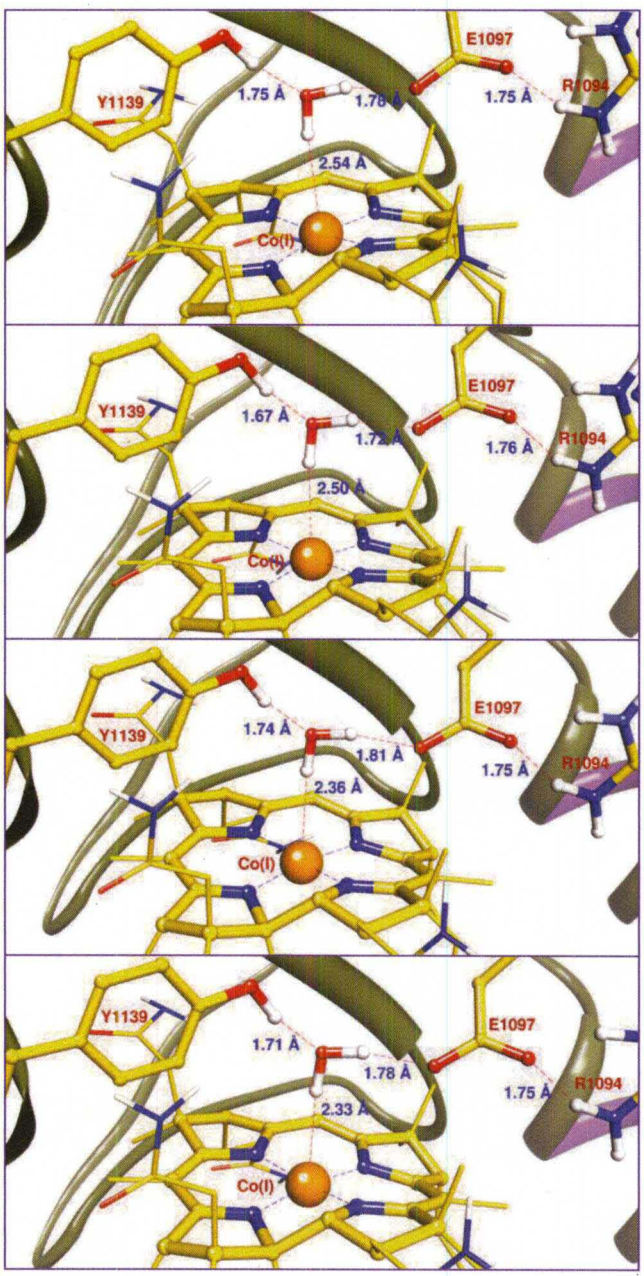


Figure 33. Active site view of the ONIOM (DFT:AMBER) optimized MetH-bound $Co^{1+}$Cbx (DFT = B3LYP/6-31G(d) (*top*), BP86/6-31G(d) (*middle1*), ωB97X/6-31G(d) (*middle 2*) and ωB97X-D/6-31G(d) (*bottom*)).

ωB97X-D functionals which pointed out the presence of a noticeable dispersion component in the $Co^{1+}$--H interaction. The QM/MM estimated $Co^{1+}$--H bond (~2.33 Å – 2.56 Å) was lengthened by ~ 0.2 – 0.3 Å in comparison to that in the active site mimicks ($Co^{1+}$--H ~2.18 – 2.37 Å ($Co^{1+}$Cbl--$H_2O$--$H_2O$) and $Co^{1+}$--H ~2.12 – 2.39 Å ($Co^{1+}$Cbl--$H_2O$--HOPh); Figures 31 and 33, Tables A28 – A29). The comparative analysis of the QM/MM optimized $Co^{2+}$Cbx and $Co^{1+}$Cbx complexes suggested how the $Co^{1+}$--H interaction could be formed inside MetH enzyme. The free H-end of the axial $H_2O$ ligand in MetH-bound $Co^{2+}$Cbx might undergo a conformational change (i.e., rotatory motion towards the metal ion) leading to the formation of a H-bonded $Co^{1+}$Cbx--$H_2O$ complex. This conformational switch would be mainly driven by a change in the electronic configuration of the metal ion (i.e., $Co^{2+}$ ($d^7$) → $Co^{1+}$ ($d^8$)) as no significant alteration was observed in the local environments of MetH-bound $Co^{2+}$Cbx and $Co^{1+}$Cbx. As a result of the $Co^{1+}$--H interaction, enzyme-bound $Co^{1+}$Cbx might adapt to alternative pentacoordinated square pyramidal ligation geometry in addition to the commonly accepted tetracoordinated square planar geometry[111,114,116]. Since the $Co^{1+}$--H interaction-driven square pyramidal $Co^{1+}$Cbx could tune the thermodynamics of the $Co^{2+}/Co^{1+}$ process,[202] the present QM/MM analysis might have implications for the reactivation cycles of methyltransferases as well as for the adenosylation pathways of ACAs. It is worth mentioning that the X-ray crystallographic methods cannot elucidate the formation of a $Co^{1+}$--H interaction because of their inability to resolve the electron density patterns associated with hydrogen atoms. In order to experimentally

validate the formation of a $Co^{1+}$--H linkage, a neutron diffraction technique must be used as has recently been demonstrated in the case of trans-[$PtCl_2(NH_3)$(N-glycine)].$H_2O$ complex.[133] An early X-ray study[138] on this complex predicted that the axial $H_2O$ ligand interacted with the $Pt^{2+}$ center through its O-end ($Pt^{2+}$--O = 3.52 Å), but a recent low temperature (20K) neutron diffraction study[133] led to the precise description of hydrogens and illustrated that the axial $H_2O$ ligand was rather H-bonded with the $Pt^{2+}$ ion ($Pt^{2+}$--H = 2.89 Å). We hope that our computational attempt would inspire an analogous neutron diffraction analysis of MetH-bound $Co^{2+}$Cbx that would experimentally confirm the existance of a $Co^{1+}$--H interaction.

## 5.4 Conclusions

The QM/MM analysis of MetH-bound $Co^{2+}$Cbx and $Co^{1+}$Cbx complexes indicate that the $Co^{1+}$ ion specifically constructs a $Co^{1+}$--H interaction that have implications for the reactivation cycle of MetH enzyme. Benefitting from this associative interaction, MetH-bound $Co^{1+}$Cbx would judiciously adapt to the square pyramidal coordination environment, which in turn might drive the otherwise inaccessible thermodynamically up-hill $Co^{2+}/Co^{1+}$ reduction.

# CHAPTER VI

# $Co^{1+}$--H INTERACTION INSPIRED ALTERNATE COORDINATION GEOMETRIES OF BIOLOGICALLY IMPORTANT COB(I)ALAMIN

## 6.1 Introduction

Recently, an unprecedented $Co^{1+}$--H bond in the neutral model as well as enzyme-bound $Co^{1+}$Cbx complexes has been theoretically validated[202,208] which suggests that $Co^{1+}$Cbx, a ubiquitous $B_{12}$ intermediate, may be a pentacoordinated square pyramidal complex. The $Co^{1+}$--H interaction alters the reduction potential of the $Co^{2+}/Co^{1+}$ couple via preferential stabilization of $Co^{1+}$Cbx. Taking this into account, an alternate mechanistic pathway has been suggested for the biological $Co^{2+}/Co^{1+}$ transformation (Scheme 8) that involves the conversion of pentacoordinated square pyramidal $Co^{2+}$Cbx into pentacoordinated square pyramidal $Co^{1+}$Cbx. The main feature of this mechanistic design is the conformational switch that may be induced at the axial ligand due to a change in the electronic configuration of the metal ion

(i.e., $Co^{2+}$ ($d^7$) → $Co^{1+}$ ($d^8$)). Precisely, this conformational change is inspired by the fact that a $Co^{1+}$ ion can act as a Lewis base due to the availability of judicious filled d-orbitals. This alternate mechanistic proposal may provide useful mechanistic insight into the molecular basis of thermodynamically demanding $Co^{2+}/Co^{1+}$ reduction which is a common occurrence in a large family of methyltransferases.

Building upon these new bioinorganic advances, herein we address a fundamentally important question: can $Co^{1+}$Cbx intermediate only be a pentacoordinated complex or can it also exist in hexacoordinated octahedral geometry owing to its plausible ability of communicating with the axial ligands via $Co^{1+}$ ion induced H-bonds? If yes, what could be the ensuing mechanistic prospects of such associative interactions in the context of $Co^{2+}/Co^{1+}$ reduction catalyzed by methyltransferases? Finally, what will be the impact of the enzyme environment upon the thermodynamic stability of weak non-covalent $Co^{1+}$--H interactions?

Considering that the crystallographic identification of $Co^{1+}$Cbx has yet not been possible owing to its highly transient nature, the profile of computational tools, especially DFT and QM/MM, gets magnified with regard to understanding the inherent structural and electronic properties of $Co^{1+}$Cbx. Herein this increased reliance of DFT and QM/MM methods along with the usefulness of AIM analysis in quantifying the degree of electron sharing has been explored to investigate the primary coordination environment of $Co^{1+}$Cbx.

## 6.2 Computational Details

### 6.2.1 Model DFT Calculations

To probe the issue, simplified ($Co^{1+}$Cbl) as well as complete ($Co^{1+}$Cbi) structural models of $Co^{1+}$Cbx were considered wherein $H_2O$ and Im were mimicked as the axial ligands respectively. $H_2O$ was modeled as α- as well as β-axial ligand while Im was only used as the β-axial ligand. The choice of the axial $H_2O$ ligand was inspired by the fact that the X-ray crystal structures of MetH- (3IVA, Res. 2.7 Å),[116] MtaBC- (2I2X, Res. 2.5 Å)[209] and CFeSP-bound $Co^{2+}$Cbx (2H9A, Res. 1.9 Å)[210] disclosed the presence of a β-axial $H_2O$ ligand in their active sites, while an α-axial $H_2O$ ligand had been revealed during a spectroscopic-cum-computational study of a CFeSP-bound methylated $Co^{2+}$Cbx intermediate[121]. The selection of Im ligand, an ideal structural replicate of His ligand was promoted by the fact that the MtaBC-bound $Co^{2+}$Cbx had recently been crystallized in His-on conformation.[209] Also, this conformation had been suggested as one of the possible binding modes for MetH-bound $Co^{2+}$Cbx.[211] Due to the lack of crystallographic data for $Co^{1+}$Cbx, the employed $Co^{1+}$Cbl and $Co^{1+}$Cbi models as well as $Co^{2+}$Cbl and $Co^{2+}$Cbi models were prepared from the high resolution X-ray crystal structure of isolated $Co^{2+}$Cbx[186] and were further improved by performing full geometry optimizations. To test the H-bond forming ability of $Co^{1+}$Cbx, the optimization of penta- and hexacoordinated $Co^{1+}$Cbx model complexes was commenced using two different starting geometries: (1) ligands (Im, $H_2O$) with their hetero atom-ends (N, O) towards the $Co^{1+}$ ion ($Co^{1+}$Cbl--$OH_2$, $Co^{1+}$Cbl--N(Im); $Co^{1+}$Cbi--$OH_2$, $Co^{1+}$Cbi--N(Im); $H_2O$--$Co^{1+}$Cbl--

$OH_2$, $H_2O$--$Co^{1+}$Cbi--$OH_2$; $H_2O$--$Co^{1+}$Cbl--N(Im), $H_2O$--$Co^{1+}$Cbi--N(Im)) and (2) H-ended ligands bound to $Co^{1+}$ ion ($Co^{1+}$Cbl--$H_2O$, $Co^{1+}$Cbl--HC(Im); $Co^{1+}$Cbi--$H_2O$, $Co^{1+}$Cbi--HC(Im); $OH_2$--$Co^{1+}$Cbl--$H_2O$, $OH_2$--$Co^{1+}$Cbi--$H_2O$; $OH_2$--$Co^{1+}$Cbl--HC(Im), $OH_2$--$Co^{1+}$Cbi--HC(Im)). All calculations were performed using Gaussian09[185] quantum chemical suite for electronic properties and structure computations. Considering that the metal ion influenced H-bonds are long-range interactions with noticeable dispersion components,[132-133,202] and since the non-covalent interactions are not faithfully reproduced using conventional DFT,[114] the complexes were also studied using ωB97X, ωB97X-D and B97-D functionals in addition to HF and BP86, B97-1 and B98 functionals. The $Co^{2+}$Cbl and $Co^{1+}$Cbl structural models were fully optimized using 6-31++G(d,p) basis set while the geometry optimizations of $Co^{2+}$Cbi and $Co^{1+}$Cbi complexes was only carried out with 6-31G(d) (5d) basis set owing to the structural complexity of model compounds. The optimized structural models were validated to be global minima via frequency calculations. To analyze thermodynamic behavior of the investigated complexes, the static thermodynamic data was computed assuming a standard state convention of 1 atm and temperature of 298.15 K. The solvation of the complexes was studied using chloroform ($\varepsilon$ = 4.70), acetonitrile ($\varepsilon$ = 32.70) and water ($\varepsilon$ = 78.36) solvents as weaved into the PCM formalism of Gaussian09. The computed solvation free energies were further corrected by adding the contributions of non-electrostatic terms that included repulsion, cavitation and dispersion. The non-electrostatic terms were calculated using SMD model of solvation as threaded into Gaussian09.

To gain deeper insight into the nature of interactions occurring between the $Co^{1+}$ ion and the axial ligands in the $Co^{1+}$Cbx models, the AIM analysis of the complexes was performed using AIM2000 software. The topological properties of the electron density at the relevant BCPs were characterized using the BP86 optimized geometries of $Co^{1+}$Cbl and $Co^{1+}$Cbi complexes respectively.

In order to evaluate the contribution of orbital interactions to the stability of complexes, NBO perturbation analysis was performed on the BP86 optimized geometries of $Co^{1+}$Cbl and $Co^{1+}$Cbi complexes. To probe the bond strength of key structural elements, the WBI were also calculated during NBO analysis.

To estimate the impact of the alternate coordination geometries of $Co^{1+}$Cbx model complexes upon the thermodynamics of the $Co^{2+}/Co^{1+}$ process, the reduction potentials of the $Co^{2+}/Co^{1+}$ couple were computed in three different solvents namely chloroform, acetonitrile and water using our calibrated computational protocol (BP86/6-31+G*) that had been found to reasonably describe the electrochemistry of $B_{12}$ corrinoids[192]. The whole redox treatment was based on the Born-Haber cycle (Scheme 7) and the reduction potentials were calculated as follows:

$$E^0 \text{ (vs NHE)} = IP + 1/23.06\ (-T\Delta S + \Delta G_{solvation,\ Redox}) - 4.28$$

## 6.2.2 ONIOM QM/MM Calculations

To investigate the possibility of $Co^{1+}$--H bond formation inside the enzymes, ONIOM-based QM/MM analysis was performed wherein the full

enzyme models for ONIOM (DFT:MM) calculations were constructed from a crystal structure of MetH enzyme (1BMT, Res.3.0 Å).[2] The methyl group bound to the Co center was removed. His residues were treated as HID in which the $N_\delta$ atom was protonated. After adding hydrogen atoms by VMD[212] and GaussView, the AMBER parameters developed by Marques et al.,[213] were assigned to a $B_{12}$ cofactor. Preparatory AMBER-MM geometry optimization was performed with only H atoms being allowed to move. Subsequently, the side chains of amino-acid residues were also subjected to geometry optimization. Assuming that the oxidation state of Co was +2 (i.e. doublet spin state), ONIOM(BP86/6-31G(d):AMBER)[214,215] single-point calculation was then performed to derive Merz-Kollman[204] atomic charges for the QM region. The entire cofactor was included in the QM region. The residues within 20 Å from the Co center in the X-ray structure were then geometry optimized by the ONIOM electronic-embedding method. Subsequently, the oxidation state of Co was changed to +1 (i.e., singlet spin state), and this geometry was optimized. A few rounds of energy scan calculations using the Co–N(His) distance as a reaction coordinate made the total energy lower, as the conformations of the amino acid residues and the corrin substituents were changed to more stable ones. A $H_2O$ molecule was added over the β-face of the $Co^{1+}$ center of MetH, and the resultant state was fully optimized.

## 6.3 Results and Discussion

### 6.3.1 DFT Structural Analysis of $Co^{1+}$Cbx Model Complexes

As a first step, we analyzed the structural features of the optimized $Co^{1+}$Cbx model compounds. Surprisingly, the axial ligands in all the optimized complexes displayed unusual coordination modes i.e., their **H**-ends rather than the expected O- or N-ends interacted with the $Co^{1+}$ ion thereby resulting in the formation of $Co^{1+}$--**H** interactions. The optimized geometries of the **H**-bonded

**Table 6**

Selected BP86 Computed Bond Distances in the **H**-bonded $Co^{1+}$Cbx Model Complexes and Their Corresponding Wiberg Bond Indices (WBI)

| H-bonded Complex | $Co^{1+}$--H [Å] | $Co^{1+}$--X* [Å] | WBI ($Co^{1+}$--H) | WBI ($Co^{1+}$--X) | WBI (H-X) | WBI (X-Y**; Y=H or C) |
|---|---|---|---|---|---|---|
| **1** | 2.25 | 3.19 | 0.04 | 0.03 | 0.71 | 0.76 |
| **1'** | 2.24 | 3.19 | 0.07 | 0.05 | 0.71 | 0.78 |
| **2** | 2.25 | 3.29 | 0.05 | 0.03 | 0.70 | 1.19 |
| **2'** | 3.55 | 4.60 | 0.01 | 0.01 | 0.91 | 1.25 |
| **3**(α)[a] | 2.32 | 3.30 | 0.03 | 0.35 | 0.72 | 0.77 |
| **3**(β)[b] | 2.32 | 3.30 | 0.03 | 0.35 | 0.72 | 0.77 |
| **3'**(α)[a] | 2.30 | 3.27 | 0.09 | 0.06 | 0.70 | 0.77 |
| **3'**(β)[b] | 2.44 | 3.41 | 0.08 | 0.05 | 0.68 | 0.76 |
| **4**(α)[a] | 2.28 | 3.32 | 0.04 | 0.03 | 0.71 | 1.24 |
| **4**(β)[b] | 2.33 | 3.31 | 0.03 | 0.03 | 0.72 | 0.77 |
| **4'**(α)[a] | 2.73 | 3.80 | 0.04 | 0.02 | 0.89 | 1.24 |
| **4'**(β)[b] | 3.53 | 4.05 | 0.01 | 0.02 | 0.71 | 0.74 |

* X = O, N or C

** Y = H or C

[a](α) corresponds to the contribution coming from the α-axial ligand

[b](β) corresponds to the contribution coming from the β-axial ligand

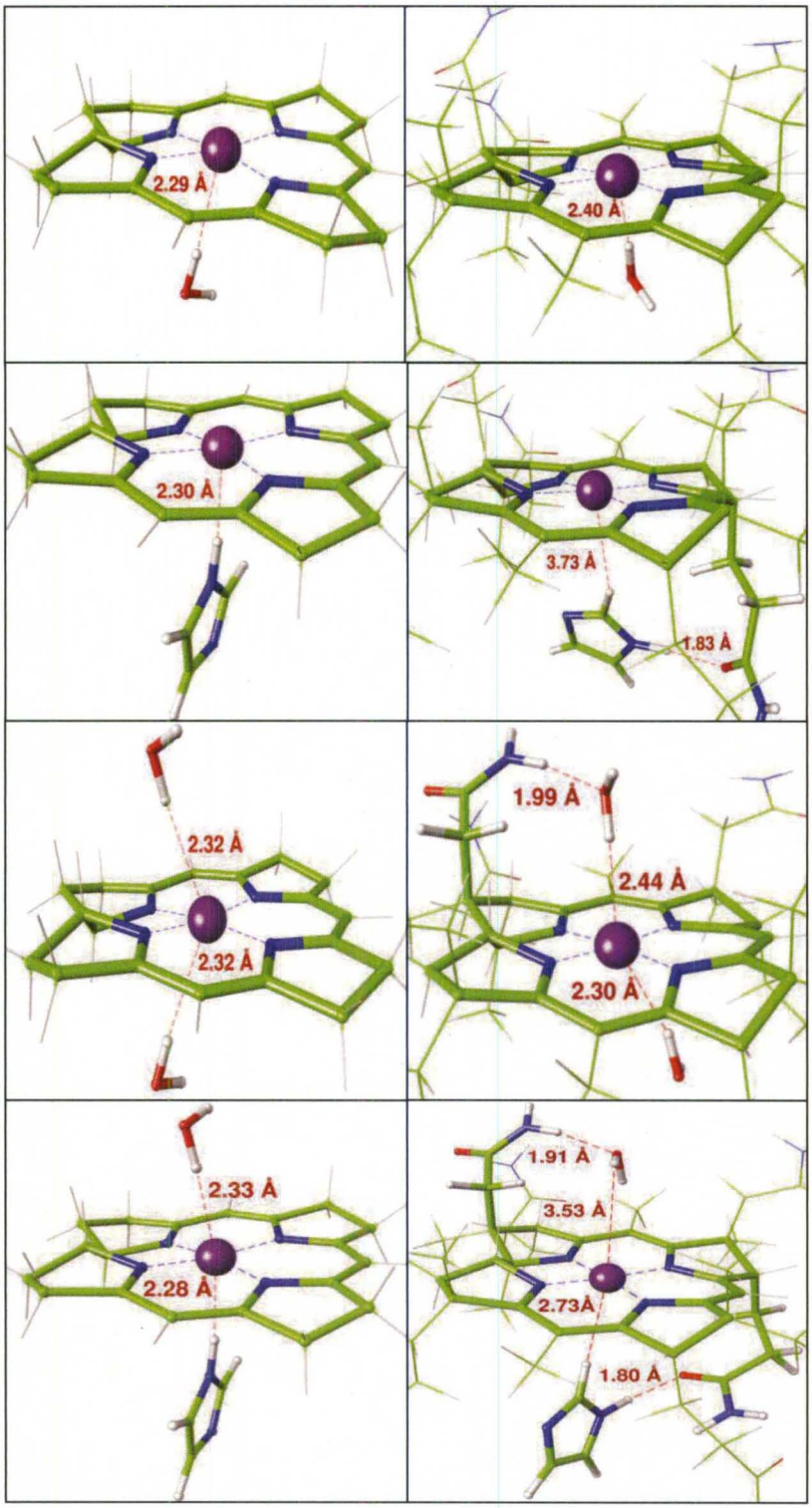


Figure 34. (*left*) Close-ups of BP86-optimized **H**-bonded $Co^{1+}$Cbl ($Co^{1+}$Cbl--**H**-O-H (**1**); $Co^{1+}$Cbl--**H**-N(Im) (**2**); H-O-**H**--$Co^{1+}$Cbl--**H**-O-H (**3**); H-O-**H**--$Co^{1+}$Cbl--**H**-N(Im) (**4**)) and (*right*) $Co^{1+}$Cbi ($Co^{1+}$Cbi--**H**-O-H (**1'**); $Co^{1+}$Cbi--**H**-C(Im) (**2'**); H-O-**H**--$Co^{1+}$Cbi--**H**-O-H (**3'**); H-O-**H**--$Co^{1+}$Cbi--**H**-C(Im) (**4'**)) structural models. The regions of interest have been highlighted using ball-stick representation.

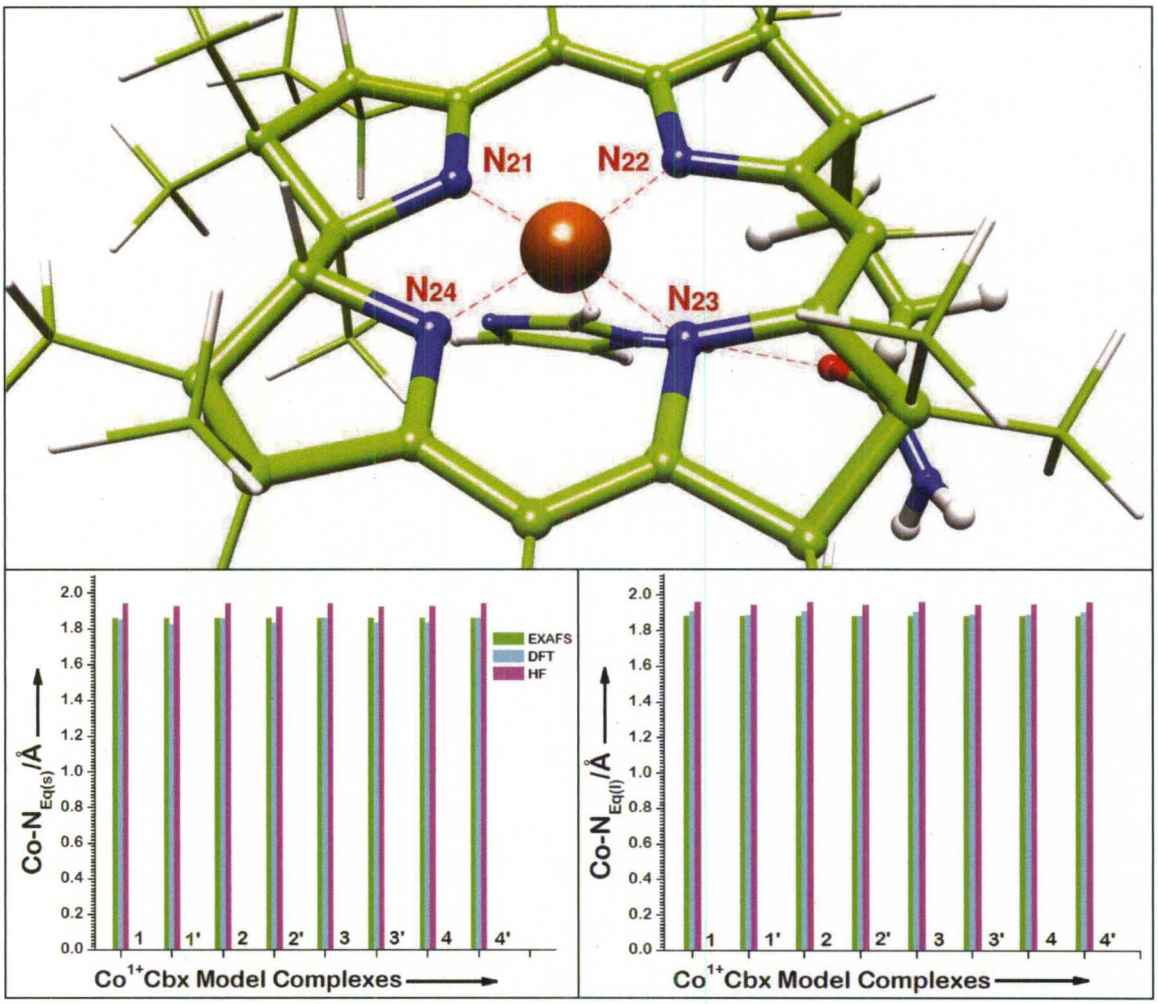


Figure 35. Numbering scheme commonly used in the case of $B_{12}$ cofactors (*upper panel*) and comparative analysis of calculated Co-$N_{eq}$ bond distances with the available EXAFS data (*lower panel*). Since Co-$N_{21}$ ~ Co-$N_{24}$ and Co-$N_{22}$ ~ Co-$N_{23}$, we used Co-$N_{Eq(s)}$ = (Co-$N_{21}$ + Co-$N_{24}$)/2; Co-$N_{Eq(l)}$ = (Co-$N_{22}$ + Co-$N_{23}$)/2 parameters to facilitate the discussion. The DFT values herein represent the average of Co-$N_{Eq(s)}$ and Co-$N_{Eq(l)}$ parameters computed using BP86, B97-1, B98, B97-D, ωB97X and ωB97X-D functionals respectively.

$Co^{1+}$Cbl and $Co^{1+}$Cbi structural models are depicted in Figure 34 with their detailed information being accessible via Tables 6 and A34 – A41 respectively. Though there is no experimental precedence for the **H**-bonded $Co^{1+}$Cbx complexes, yet the EXAFS analysis has been reported for the tetracoordinated square planar $Co^{1+}$Cbx[115] that was used as a reference point to test the accuracy of the employed theoretical methods. As illustrated in Figure 35, the DFT computed equatorial Co-$N_{Eq(s)}$ [(Co-$N_{21}$ + Co-$N_{24}$)/2] and Co-$N_{Eq(l)}$ [(Co-$N_{22}$ + Co-$N_{23}$)/2] bond distances were in excellent accord while analogous HF bond lengths were significantly deviated (i.e., by 0.05 – 0.09 Å) with regard to EXAFS values of 1.86 Å and 1.88 Å. This underscored the reliability of the applied DFT methods in reproducing the structural aspects of $Co^{1+}$Cbx model compounds. Since all the used DFT functionals predicted approximately identical geometries for the **H**-bonded complexes, we used DFT-averaged values to plot Figure 35. Note here although two different conformations of the axial ligands ($H_2O$ and/or Im) were explored for optimizing $Co^{1+}$Cbx mimicks, yet both the starting geometries led to the same final conformation (i.e., $Co^{1+}$Cbl--**H**-O-H (**1**), $Co^{1+}$Cbi--**H**-O-H (**1'**); $Co^{1+}$Cbl--**H**-N(Im) (**2**), $Co^{1+}$Cbi--**H**-C(Im) (**2'**); H-O-**H**--$Co^{1+}$Cbl--**H**-O-H (**3**), H-O-**H**--$Co^{1+}$Cbi--**H**-O-H (**3'**); H-O-**H**--$Co^{1+}$Cbl--**H**-N(Im) (**4**), H-O-**H**--$Co^{1+}$Cbi--**H**-C(Im) (**4'**)) wherein the axial ligands were **H**-bonded to the $Co^{1+}$ ion of the $Co^{1+}$Cbx models. The formation of $Co^{1+}$--**H**(Im) linkages in the **2'** and **4'** complexes was realized due to the interaction between the $Co^{1+}$ ion and the **H**-C fragment of the Im ligand while it was due to the interaction between the $Co^{1+}$ ion and the **H**-N fragment in the **2** and **4** complexes respectively. This difference in the

coordination modes of the axial Im ligand in $Co^{1+}$Cbl and $Co^{1+}$Cbi complexes was attributed to the fact that the Im ligand in $Co^{1+}$Cbi models was engaged in a sterically-driven H-bonding interaction with the proximal amide side chain of the corrin ring (N-H--O=C- ~ 1.80 Å) in addition to $Co^{1+}$--**H**(Im) interaction while such an interaction was not possible in $Co^{1+}$Cbl models. The computed $Co^{1+}$--**H** bond distances (except in complexes **2'** and **4'** where they were 3.53 Å – 3.73 Å) were in the regime of previously identified $d^8$ metal ion induced H-bonds (2.11 – 2.90 Å).[126-137,202,208] The length (~2.28 – 2.73 Å) and the approximate linearity (~154° – 172°) of the $Co^{1+}$--**H** linkages implied that these were reasonably strong interactions, which complemented the growing viewpoint that the $d^8$ metal ions could indulge in H-bond formation. The development of $Co^{1+}$--**H** bonds was further appreciated by the relative lengthening of **H**-X (X = O ($H_2O$), N (Im) or C(Im)) bonds of the axial ligands (Table 6). As a general trend, $Co^{1+}$--**H** bonds in $Co^{1+}$Cbi complexes were weaker than in the analogous $Co^{1+}$Cbls because the axial ligands in $Co^{1+}$Cbi models could engage in intramolecular multi-center hetero-acceptor H-bond formation with the $Co^{1+}$ ion and the nearby amide side chains of the corrin ring, which was not feasible in $Co^{1+}$Cbl complexes (Figure 34). Further, the α-axial Im ligand bound less strongly to the $Co^{1+}$Cbi complexes ($Co^{1+}$--**H** = 2.73 – 3.73 Å) than the α-axial $H_2O$ ligand ($Co^{1+}$--**H** = 2.30 – 2.44 Å) owing to its greater steric bulk, which in turn accounted towards its H-bonding interaction with the proximal amide side chain of the corrin macrocycle. The $Co^{1+}$--**H** linkages in the hexacoordinated $Co^{1+}$Cbl (**3**, **4**) and $Co^{1+}$Cbi (**3'**, **4'**) complexes were slightly weakened in comparison to the pentacoordinated ones (**1**, **2**; **1'**, **2'**)

indicating that the two axial ligands exerted the mutual weakening effect in the hexacoordinated complexes. Although the present computations suggest that $Co^{1+}$Cbx might exist in penta- as well as in hexacoordinated form, but since the axial Im ligands in the hexacoordinated $Co^{1+}$Cbi complex, that was the closer mimick of $Co^{1+}$Cbx, was significantly displaced away from the $Co^{1+}$ ion (i.e., by 2.73 Å), it seems plausible to suggest that enzyme-bound $Co^{1+}$Cbx might effectively be a pentacoordinated square pyramidal complex.

To provide further information into the bonding interactions between the $Co^{1+}$ ion and **H**-X motives of the axial ligands, WBI for the key structural elements of the BP86 optimized **H**-bonded complexes were calculated (Table 6). WBI probe covalent interactions and provide a quantitative measure of bond strength. The computed WBI for **H**-X bonds in the (**1** – **4**) and (**1'** – **4'**) complexes were lower by 0.04 – 0.08 than their values computed for the isolated axial ligands indicating the noticeable elongation of the complex-bound **H**-X bonds which, in turn, was reflected in their increased interactions with the $Co^{1+}$ ion in the **H**-bonded complexes (WBI ($Co^{1+}$--**H**) = 0.01 – 0.09).

Considering that $Co^{1+}$Cbx model complexes were $d^{16}$ electron systems, $Co^{1+}$ ion could participate in H-bond (4-electron 3-center) as well as in agostic bond (2-electron 3-center) formation, but the computational evidences suggested that $Co^{1+}$--**H** interaction was a H-bond, but not an agostic interaction because of the following reasons. (1) The **H**-atom of the axial ligands ($H_2O$ and/or Im) interacting with the $Co^{1+}$ ion was acidic in nature which was in line with the conventional H-bonds. However it is not a requirement for an agostic interaction

where H-atom is usually bonded to electropositive atoms (B, Li or Si).[137] (2) In an agostic interaction, the side-on interaction occurs between the metal ion and the ligand motif i.e., the interacting fragment typically orients perpendicular to the plane of the metal ion. But in the optimized $Co^{1+}$Cbl and $Co^{1+}$Cbi complexes, an approximate linear arrangement of $Co^{1+}$--**H**-X (149.9° – 175.7°) entities was observed which had been a typical characteristic of the metal ion induced H-bonded systems.[126-137,202,208] (3) It is well-documented in literature that a metal ion that forms H-bonds is usually a late transition metal in low oxidation state (i.e., $Pt^{2+}$, $Pd^{2+}$, $Cu^{1+}$, $Ni^{2+}$ or $Co^{1+}$ ion). Evidently $Co^{1+}$ ion belongs to this category. Apart from that, $Co^{1+}$Cbx, a $B_{12}$ intermediate, is considered as a supernucleophilic species[216] that plays a key role in methyl transfer reactions in methyltransferases and adenosyl group transfer reactions in ACAs. This lends further support to the fact that a $Co^{1+}$ ion may serve the role of a Lewis base for forming H-bond type interactions with its axial ligands. There have also been reports in literature indicating that the metal ion induced H-bonding interactions may solely be formed due to the steric constraints that are inherently imposed upon a complex-bound ligand.[217,218] But the $Co^{1+}$--**H** interaction could not be characterized as a sterically-driven interaction because the axial ligands in $Co^{1+}$Cbx model complexes were situated along the z-axis of the complex where they experienced the least amount of steric interaction. Moreover, the final conformations of the axial ligands in $Co^{1+}$Cbx complexes were determined by performing full geometry optimizations where the two different starting geometries of the axial ligands were used. This further eliminated the possibility

of a steric $Co^{1+}$--**H** interaction. This short discussion thus supplements our viewpoint that the $Co^{1+}$--**H** interaction should be classified as an H-bond.

### 6.3.2 AIM Analysis of $Co^{1+}$Cbx Model Complexes

To investigate the nature of $Co^{1+}$--**H** interactions from another point of view, AIM analysis was performed on the BP86 optimized geometries of **H**-bonded complexes. Within AIM methodology, the topological properties of electron density, $\rho(r)$ such as its gradient vector field, $\nabla\rho(r)$, Laplacian, $\nabla^2\rho(r)$ and total charge density, H(r) are analyzed to define the bond path between the interacting atoms. Chemical bonding is characterized by a BCP, where the $\rho(r)$ attains a

**Table 7**

Key BCP Properties of $Co^{1+}$--**H** Interactions in the **H**-bonded $Co^{1+}$Cbl and $Co^{1+}$Cbi Complexes

| Complex | $\rho_{Co1+--H}$ | $\nabla^2\rho_{Co1+--H}$ | $-V_{Co1+--H}$ | $G_{Co1+--H}$ | $H_{Co1+--H} = -V_{Co1+--H} + G_{Co1+--H}$ |
|---|---|---|---|---|---|
| 1 | 0.0210 | 0.0410 | 0.0121 | 0.0112 | -0.0009 |
| 1' | 0.0159 | 0.0451 | 0.0091 | 0.0102 | 0.0011 |
| 2 | 0.0230 | 0.0417 | 0.0138 | 0.0121 | -0.0017 |
| 2' | 0.0021 | 0.0073 | 0.0009 | 0.0014 | 0.0005 |
| 3 | 0.0211 | 0.0408 | 0.0127 | 0.0114 | -0.0012 |
| 3' | 0.0187 | 0.0519 | 0.0121 | 0.0125 | 0.0004 |
| 4 | 0.0211 | 0.0408 | 0.0127 | 0.0114 | -0.0012 |
| 4' | 0.0089 | 0.0256 | 0.0037 | 0.0050 | +0.0014 |

minimum value along the bond path. For all $Co^{1+}$--**H** interactions of **H**-bonded complexes, the BCPs were located, with Table 7 summarizing their key properties. The ρ(r) at a BCP correlates with the strength of an atomic interaction. The values of $\rho_{Co1+--H}$ obtained for the $Co^{1+}$--**H** interactions ranged from 0.02 to 0.03 $ea^{-3}$, which were similar to that for neutral hydrogen bonds ($\rho_{H\text{-}bond} \sim 0.002 - 0.04\ ea^{-3}$),[205] suggesting that the strength of the $Co^{1+}$--**H** interactions competes with that of hydrogen bonds. In accordance with the empirical guidelines suggested by Popelier et al.,[219] the value of the $\nabla^2\rho_{Co1+--H}$ (r) at the BCP should be between 0.024 and 0.139 au for a particular interaction to be classified as a H-bond. The results enlisted in Table 7 clearly instructs that the $Co^{1+}$--**H** interactions in $Co^{1+}$Cbl and $Co^{1+}$Cbi complexes belongs to this category authenticating $Co^{1+}$--**H** contacts as genuine H-bonds. The behavior of the $\nabla^2\rho(r)$ at the BCP also serves as a useful source of information for understanding the nature of interaction. If $\nabla^2\rho(r) < 0$, the interaction is referred to as a shared-electron (covalent) interaction, and if $\nabla^2\rho(r) > 0$, the interaction is called closed-shell (electrostatic) interaction. The values of $\nabla^2\rho_{Co1+--H}(r)$ listed in Table 7 are all positive, suggesting that the $Co^{1+}$--**H** interactions in $Co^{1+}$Cbl and $Co^{1+}$Cbi complexes have a dominant electrostatic character. However, it has been noted[207] that H(r) at a BCP, along with its $\nabla^2\rho(r)$, constitutes a more appropriate probe for accessing deeper insight into non-bonded interactions i.e. (i) for pure electrostatic weak H-bonds, $\nabla^2\rho(r) > 0$; $H(r) > 0$; (ii) for partial covalent H-bonds, $\nabla^2\rho(r) > 0$; $H(r) < 0$; and (iii) for covalent strong H-bonds, $\nabla^2\rho(r) < 0$; $H(r) < 0$.

Thus, within the framework of the AIM theory, the $Co^{1+}$--**H** interactions in **1 – 4** complexes had partial covalence while they were purely electrostatic weak H-bonds in **1' – 4'** complexes. However, the absolute values of $H_{Co1+--H}(r)$ obtained for $Co^{1+}$--**H** interactions were very small, indicating that the degree of electron sharing calculated for **1 – 4** complexes must be considered negligible.

### 6.3.3 NBO Analysis of $Co^{1+}$Cbx Model Complexes

The linear propensity of the $Co^{1+}$--**H**-X (X = O, N or C) interactions (Figure 34 and Table 6) suggests a significant contribution of the orbital interactions between the $n_{Co1+}$ and the $\sigma^*_{H-X}$ to the stability of $Co^{1+}$--**H** linkages. Thus to gain a further level of insight into the principal interacting functionals, NBO analysis was performed on the BP86 optimized geometries of the **H**-bonded complexes. The NBO analysis provides a quantitative picture of donor-acceptor delocalization in terms of the second order delocalization energy correction to the donor NBO. The $\Delta E^{(2)}_{CT}$ energies due to the $n_{Co1+} \rightarrow \sigma^*_{H-X}$ interactions are listed in Table 8. Depending upon the availability of empty $n^*_{Co1+}$ metal orbitals and bonding $\sigma_{H-X}$ orbitals of appropriate energy and symmetry, the orbital interactions involving back bonding might also contribute appreciably to the stability of $Co^{1+}$--**H**-X interactions. To estimate the magnitude of such dative interactions, the $\Delta E^{(2)}_{BCT}$ energies due to the $\sigma_{H-X} \rightarrow n^*_{Co1+}$ interactions were also evaluated (Table 8). Because $Co^{1+}$ ion had more than one filled and empty d-orbitals participating in dipolar interactions, the $\Delta E^{(2)}_{CT}$ and $\Delta E^{(2)}_{BCT}$ energies were evaluated as the sum of all such possible interactions.

**Table 8**

NBO Perturbation Analysis of H-bonded $Co^{1+}$Cbx Model Complexes

| H-bonded Complex | $\Delta E_{CT}^{(2)}$/kcal/mol | $\Delta E_{BCT}^{(2)}$/kcal/mol | $n_{\sigma H\text{-}X}$ | $n_{\sigma^* H\text{-}X}$ |
|---|---|---|---|---|
| 1 | 3.1 | 3.5 | 1.987 | 0.030 |
| 1' | 5.6 | 3.7 | 1.987 | 0.053 |
| 2 | 10.6 | 4.1 | 1.978 | 0.058 |
| 2' | 0.8 | 0.4 | 1.982 | 0.023 |
| 3(α) | 4.3 | 6.2 | 1.985 | 0.025 |
| 3(β) | 4.3 | 6.2 | 1.985 | 0.025 |
| 3'(α) | 6.4 | 7.9 | 1.984 | 0.058 |
| 3'(β) | 7.2 | 4.8 | 1.988 | 0.057 |
| 4(α) | 8.4 | 4.9 | 1.976 | 0.052 |
| 4(β) | 5.4 | 4.3 | 1.985 | 0.023 |
| 4'(α) | 1.4 | 3.2 | 1.974 | 0.038 |
| 4'(β) | 0.6 | 1.5 | 1.995 | 0.021 |

According to the NBO analysis, the orbital interactions between the $n_{Co1+}$ orbitals and the $\sigma^*_{H\text{-}X}$ orbitals contributed significantly to the stabilization of $Co^{1+}$--**H** interactions: $\Delta E^{(2)}_{CT}$ was in the range of 0.8 – 10.6 kcal/mol for the pentacoordinated complexes and was 1.9 – 13.7 kcal/mol for the hexacoordinated complexes. Though the values were slightly lower, the orbital interactions involving the $\sigma_{H\text{-}X}$ and the $n^*_{Co1+}$ orbitals ($\Delta E^{(2)}_{BCT}$ (**1**, **1'**, **2**, **2'**) = 0.4 – 4.1 kcal/mol; $\Delta E^{(2)}_{BCT}$ (**3'**, **3**, **4**, **4'**) = 4.6 – 12.8 kcal/mol) also imparted noticeable stabilization effect to $Co^{1+}$--**H** interactions. However the orbital interactions involving **H**-C fragment of the Im ligand in the **2'** and **4'** complexes contributed very less towards the stabilization of the $Co^{1+}$--**H** linkages owing to relatively weaker communication between the $Co^{1+}$ ion and the Im ligand (2.73 – 3.73 Å).

The appreciable role of analogous dipole-dipole interactions in stabilizing the non-covalent contacts has also been observed in the case of Se--O, Se--F and Se--N linkages.[198] The net electronic populations of the $\sigma_{H\text{-}X}$ and $\sigma^*_{H\text{-}X}$ orbitals of the axial ligands provided a quantitative measure of a charge transfer component of $Co^{1+}$--**H** interactions. The appearance of noticeable electronic charge in the $\sigma^*_{H\text{-}X}$ orbitals (0.02 – 0.06) implied the charge transfer from the $Co^{1+}$ ion to the axial ligands while the appreciable decrease in the orbital occupancies of $\sigma_{H\text{-}O}$ orbitals (0.01 – 0.02) indicated the extent of back charge transfer from the axial ligands to the $Co^{1+}$ ion.

### 6.3.4 DFT Thermodynamic Analysis of $Co^{1+}$Cbx Model Complexes

Taking into account that the $Co^{1+}$--**H** bonds are weak interactions that have critical dispersion contributions,[33] the formation of the **H**-bonded complexes might not be feasible from a thermodynamic standpoint owing to the unfavorable entropic factors. Thus to provide a convincing evidence of $Co^{1+}$--**H** bond formation, the static thermodynamic data for the complex formation reactions was computed (Figure 36, Tables A42 – A73) for all the complexes using a theoretical protocol as outlined in the Computational Section. The **H**-bonded $Co^{1+}$Cbl complexes (**1** – **4**) were found to be endothermic entities at conventional DFT level of theory (BP86, B97-1 and B98) with the exception of ωB97X, which was in line with a previous study[114] suggesting that the formation of a

pentacoordinated $Co^{1+}$Cbl complex was not feasible from thermodynamic perspective. Note here that ωB97X functional correctly captured the long-range character of $Co^{1+}$--**H** linkages and hence validated the exothermicity of the **H**-bonded $Co^{1+}$Cbl complexes. When the thermodynamics of the **H**-bonded $Co^{1+}$Cbl complexes was studied with the dispersion-corrected functionals (ωB97X-D and B97-D), the exothermic effect affiliated with the **H**-bonded $Co^{1+}$Cbl complexes was appreciably enhanced (by ~1.0 – 6.0 kcal/mol). This implied that the long-range and/or the dispersion-corrected DFT functionals must be used in order to correctly describe the complexes containing $Co^{1+}$--**H** linkages. Further, the computed ΔG values for the hexacoordinated $Co^{1+}$Cbl complexes (**3** – **4**) were only 0.3 – 1.0 kcal/mol less than twice for the pentacoordinated $Co^{1+}$Cbl complexes (**1** - **2**) implying that the $Co^{1+}$--**H** linkages were only slightly weakened in the hexacoordinated $Co^{1+}$Cbl complexes.

On the other hand, the **H**-bonded $Co^{1+}$Cbi complexes with the exception of **1'** – **2'** were predicted to be exothermic (ΔG = -ve) even with the conventional DFT functionals. The driving force associated with the **H**-bonded $Co^{1+}$Cbi complexes was found to be significantly enhanced upon the inclusion of long range and/or dispersion effects via ωB97X (ΔG ~ -1.8 to -15.0 kcal/mol), ωB97X-D (ΔG ~ -1.8 to -22.0 kcal/mol) and B97-D (ΔG ~ -4.8 to -24.0 kcal/mol) functionals. Although $Co^{1+}$--**H** linkages in the $Co^{1+}$Cbi complexes were weaker by ~5% in comparison to $Co^{1+}$Cbl ones, yet the **H**-bonded hexacoordinated $Co^{1+}$Cbi complexes (**3'** – **4'**) were found to possess ΔG values that were appreciably higher than twice the values computed for the pentacoordianted $Co^{1+}$Cbi

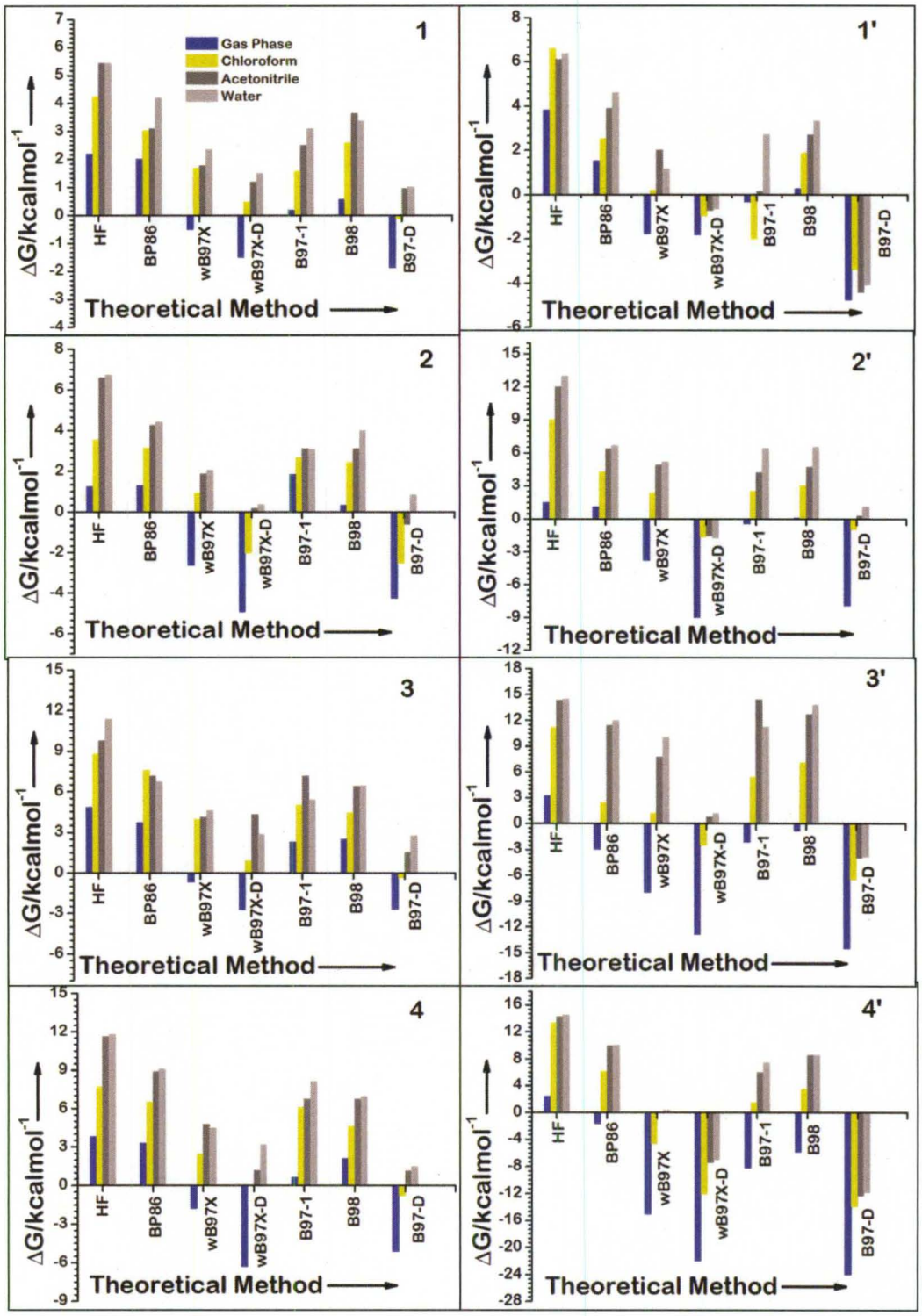


Figure 36. Computed Gibbs free energy data for **H**-bonded $Co^{1+}$Cbl (*left*) and $Co^{1+}$Cbi (*right*) complexes.

complexes (**1'** – **2'**). This significant increase in the thermodynamic stability of hexacoordinated $Co^{1+}$Cbi complexes was attributed to the combined effect of steric bulk of the cofactor and capacity of the axial ligands to indulge in intramolecular multi-site H-bond formation with the metal ion and the proximal amide side chains of the corrin nucleus.

Upon solvation, the **H**-bonded $Co^{1+}$Cbl and $Co^{1+}$Cbi complexes were significantly destabilized with the optimum effect being noted in the case of water solvent. In particular, the $Co^{1+}$Cbl complexes were found to be endothermic entities in water at all levels of theory suggesting that $H_2O$--$H_2O$ interaction is stronger than a $Co^{1+}$--**H**($H_2O$) or $Co^{1+}$--**H**(Im) interaction. This also explained why a tetracoordinated square planar $Co^{1+}$Cbx complex had been observed during electrochemical experiments.[86] Despite the solvent-induced destabilization of $Co^{1+}$--**H** interactions, the **H**-bonded $Co^{1+}$Cbl and $Co^{1+}$Cbi complexes were predicted to be thermodynamically amenable entities in chloroform solution with the dispersion-corrected functionals (ωB97X-D and B97-D) that hinted towards their feasibility in the presence of the enzyme environment. Note here that **1** (ΔG = +0.5 kcal/mol) and **3** (ΔG = +0.9 kcal/mol) complexes were found to be slightly endothermic with the ωB97X-D functional.

### 6.3.5 Computational Electrochemistry of $Co^{2+}/Co^{1+}$ Redox Process

Considering that the present computations suggest the existence of alternate $Co^{1+}$Cbx coordination geometries, an apparent question arises: how

these uncommon H-bonded complexes may impact $B_{12}$ catalysis? It is believed that the coordination number of a $Co^{n+}$ ion (n = 1, 2 or 3) in a cofactor state follows a direct correlation with its oxidation state.[220-222] However, as found/unveiled here as well as during recent studies,[202,208] $Co^{1+}$Cbx intermediate may represent an exception to this correlation as the electronic richness of the $Co^{1+}$ ion rather than its net positive charge seems controlling the coordination chemistry of $Co^{1+}$Cbx. Consequently it may also exist in square pyramidal or octahedral coordination environment in addition to the commonly accepted tetracoordinated square planar geometry. The H-bonded $Co^{1+}$Cbx complexes may also provide invaluable chemical tools for accessing atomistic insight into the thermodynamically unrealistic $Co^{2+}/Co^{1+}$ reduction that forms a vital part of the reactivation cycles of methyltransferases as well as of the biochemical pathways of ACAs. To comply with the thermodynamic demand of the $Co^{2+}/Co^{1+}$ reaction, formation of square planar $Co^{1+}$Cbx has been suggested as the most plausible mechanistic rationale.[111,114,116,117,119-121] However, recently an alternate mechanistic proposal[202,208] has been postulated that takes advantage of the driving force associated with the $Co^{1+}$--H interaction (Scheme 8) and bypasses the generation of highly energetic tetracoordinated square planar $Co^{1+}$Cbx. Owing to the significant thermodynamic advantages, the **H**-bonded square pyramidal or octahedral $Co^{1+}$Cbx complexes may further illustrate the usefulness of this alternate mechanistic scheme. To assess the catalytic impact of $Co^{1+}$--**H** interactions, the reduction potentials of the $Co^{2+}/Co^{1+}$ couple were computed assuming all the possible coordination geometries of $Co^{1+}$Cbx model complexes

(square planar, and **H**-bonded square pyramidal and octahedral) (Table A69). The electrochemistry of the $Co^{2+}/Co^{1+}$ process was explored in three different solvents using a calibrated procedure (BP86/6-31+G*)[192] as mentioned in the Computational

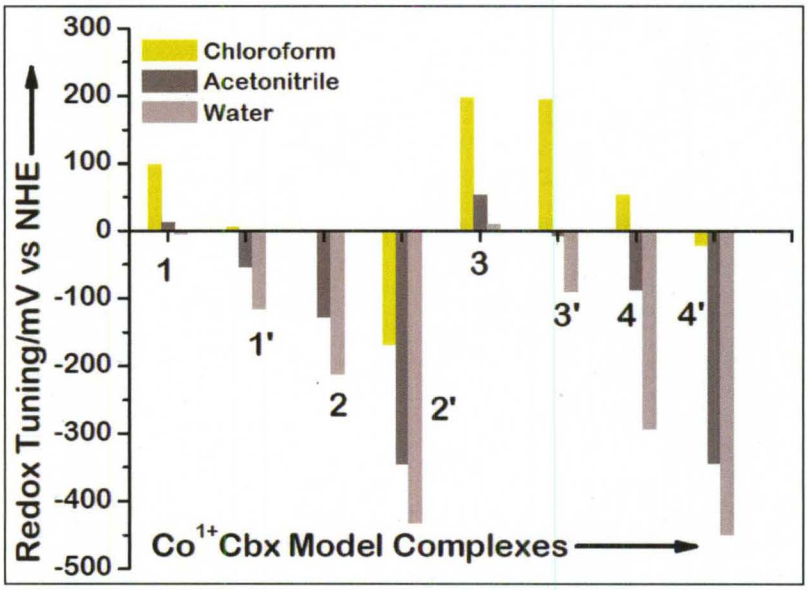


Figure 37. Computed $Co^{1+}$--**H**-induced redox tuning $Co^{2+}/Co^{1+}$ process.

Section. The extent of redox tuning achieved with the **H**-bonded square pyramidal and octahedral $Co^{1+}$Cbl and $Co^{1+}$Cbi complexes relative to the square planar analogues, is illustrated in Figure 37 (check Table A74 for a detailed information). The axial $H_2O$ ligand-mediated $Co^{1+}$--**H**($H_2O$) interaction exerted a greater anodic shift (atleast in chloroform solvent) than the analogous $Co^{1+}$--**H**(Im) interaction (except in complexes **2'** and **4'** where the Im ligand even caused cathodic shifts**)** in the reduction potentials of the $Co^{2+}/Co^{1+}$ couple. This

was due to the higher solvation cost of the Im ligand which in turn was rooted in its greater steric bulk. This may also be the reason why an axial $H_2O$ ligand, rather than a His ligand, has specifically been observed in the active sites of methyltransferases as revealed by the high resolution X-ray studies of MetH,[116] MtaBC[209] and CFeSP[210] methyltransferases. It should be noted that 50 mV vs SHE is the estimated redox gap that has to be bridged in order to eventualize MetH-bound $Co^{2+}/Co^{1+}$ process.[111,114,116] However the anodic shift induced by $Co^{1+}$--**H** interaction in the **1**, **3**, **3'** and **4** complexes was higher than 50 mV vs SHE (in chloroform solution), suggesting that $Co^{1+}$--**H** interaction might help in combating the thermodynamic demand of the enzyme-bound $Co^{2+}/Co^{1+}$ process. The greater amount of redox modulation calculated with the complexes **3** and **3'** in comparison to **1** and **1'** suggested that the two $Co^{1+}$--**H**($H_2O$) bonds were catalytically more potent than the one. Interestingly, the anodic shift induced by the α-axial $H_2O$ ligand in **1'** complex (5 mV vs SHE in chloroform solution) was significantly lower than that noted recently[202,208] with the β-axial $H_2O$ ligand (224 mV vs SHE in chloroform solution). This indicates the functional importance of a ubiquitous β-axial $H_2O$ ligand that has been identified in the active sites of methyltransferases.

### 6.3.6 QM/MM Analysis of MetH-bound $Co^{1+}$Cbx Complex

Although, according to the current understanding,[113,116,117,118,121-123] $H_2O$ or His ligands interact with $Co^{2+}$Cbx via their conventional O- or N-ends, and dissociate completely in the $Co^{1+}$Cbx intermediate state, herein presented model DFT

calculations suggest that the axial ligands in $Co^{1+}$Cbx may potentially undergo a conformational change rather than the complete dissociation, resulting in the formation of $Co^{1+}$--H bonds because such a conformational change is thermodynamically feasible. The presented DFT data indicates the possibility of the His ligand undergoing slight rotation in order to provide its C-H (or N-H) fragment for H-bond formation with the $Co^{1+}$ ion of $Co^{1+}$Cbx. However the feasibility of such an H-bond formation would strongly depend upon the conformational freedom permissible to the His ligand inside the enzyme environment.

In order to access a realistic description of the coordination environment of the enzyme-bound $Co^{1+}$Cbx, ONIOM-based QM/MM computations wereperformed where the X-ray crystal structure of MetH-bound MeCbl (PDB-code:1BMT@ 3.0 Å resolution)[2] was employed as a reference point. Owing to the absence of crystallographic data for the $Co^{1+}$Cbx intermediate, MeCbl binding module of MetH was used by removing the Me ligand and adjusting the number of electrons of the QM system, consistent with the $Co^{1+}$ oxidation state. For the QM/MM treatment, His759-on pentacoordinated MetH-bound $Co^{1+}$Cbx was considered while to model the hexacoordinated form, an additional $H_2O$ ligand was incorporated over the β sector of the corrin ring. Although the His ligand in pentacoordinated MetH-bound $Co^{1+}$Cbx ligated via its conventional N-end, but the β-axial $H_2O$ ligand in MetH-bound octahedral $Co^{1+}$Cbx (an effective pentacoordinated square pyramidal complex due to long $Co^{1+}$--N(His759) bond (~3.35 Å)) manifested an unconventional binding mode i.e., it ligated to the $Co^{1+}$

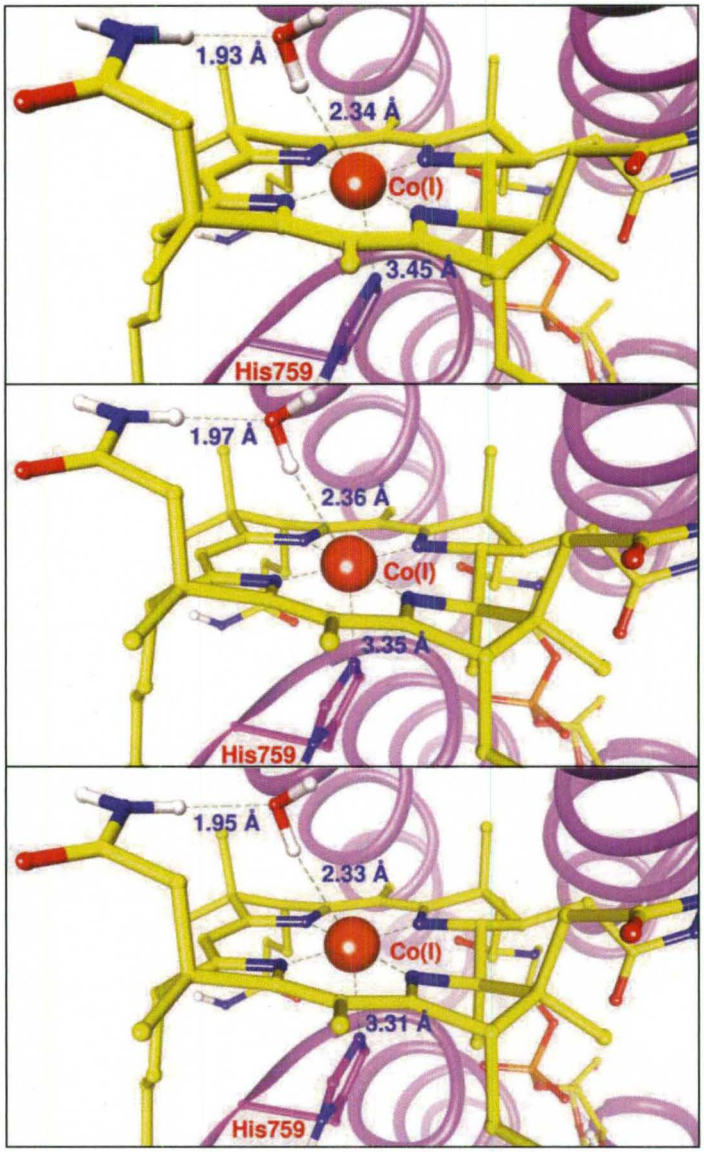


Figure 38. Close-ups of the ONIOM-based QM(BP86(*top)*, ωB97X(*middle*) and ωB97X-D(*bottom*))/MM-optimized MetH-bound $Co^{1+}$Cbx complex.

ion via its **H**-end (Figure 38) that rendered a definitive evidence of $Co^{1+}$--**H** bond formation inside the enzyme scaffold of methyltransferases. The length (~2.34 Å) and the linearity (~166°) of $Co^{1+}$--**H**-O bonding motif implied that it was a fairly strong interaction that falls within the domain of $d^8$ metal ion influenced H-bonds[126-137,202,208]. This adds an important piece to the emerging picture that H-bond forming feature is a *bona fide* signature of the low spin $d^8$ metal ions. Interestingly, the QM/MM estimated $Co^{1+}$--**H** bond distance was ~20% shorter than the analogous $Pt^{2+}$--H (~2.80 Å)[132-133] which suggested that $Co^{1+}$ ion constructs relatively stronger H-bonding contacts giving an impressive testimony of its well-known supernucleophilic character[216]. Though all three DFT functionals (BP86, ωB97X and ωB97X-D) provided an identical description of the **H**-bonded $Co^{1+}$Cbx complex, yet the ωB97X-D functional predicted $Co^{1+}$--**H** interaction (~2.33 Å) to be slightly stronger implying the presence of a noticeable dispersion component. The axial $H_2O$ ligand in MetH-bound $Co^{1+}$Cbx participated in intramolecular multi-center H-bond formation as it not only communicated with the cofactor via $Co^{1+}$--**H** interaction, but also through the propanamide side chain of the corrin ring where it formed a strong H-bonding contact (~1.95 Å) with the $-NH_2$ tail of the amide chain (Figure 38). Taking into account that $Co^{1+}$Cbx is an intermediate species with a uniquely rich and diverse portfolio of biological activities, and since its ligation geometry has been poorly understood, the present QM/MM analysis unraveling its primary coordination sphere may considerably improve our understanding about the catalytic functioning of a broad family of methyltransferases.

### 6.3.7 X-ray Crystal Structure Analysis of Methyltransferases

The present theoretical study indicates the possibility of the binding interaction between $Co^{1+}$Cbx and its plausible axial ligands that may have catalytic relevance for methyltransferases such as MetH, CFeSP and MtaBC as well as for ACAs. This viewpoint is also fostered by the analysis of the existing X-ray crystal structures of MetH-,[116] MtaBC-[209] and CFeSP-bound $Co^{2+}$Cbx[210] that encage an axial $H_2O$ ligand on their β-faces (Figures 27 and 39). In the case of MetH-bound complex of $Co^{2+}$Cbx,[116] the β-axial $H_2O$ ligand is located at 3.94 Å from the $Co^{2+}$ ion and is intensely involved in H-bonding network with the local Y1139 and E1097 residues (Figure 27). Notably, the $Co^{2+}$--O bond is significantly lengthened inside the enzyme. It has been suggested based on spectroscopic[111] and X-ray studies[116] that the Y1139 residue serves to weaken the interaction between $Co^{2+}$Cbx and the axial $H_2O$ ligand. However the present calculations suggest that the enzyme-induced lengthening of the $Co^{2+}$--O bond may be mandated to cause a conformational change at the axial ligand leading to the $Co^{1+}$--H bond formation. The β-axial $H_2O$ ligand is localized at a distance of 3.24 Å from the $Co^{2+}$ ion in the case of MtaBC-bound $Co^{2+}$Cbx[209] that also implies the inclination of enzyme scaffold towards nurturing $Co^{1+}$--H interaction and advocates another strong case where the $Co^{1+}$--H interaction-driven $Co^{1+}$Cbx might be participating in an analogous chemical reaction. Though, the axial $H_2O$ ligand in the case of methylated CFeSP-bound $Co^{2+}$Cbx has been predicted in

the lower axial coordination site,[121] a recent high resolution crystal structure of CFeSP-bound $Co^{2+}$Cbx indicates a β-axial $H_2O$ ligand bound to the $Co^{2+}$ ion

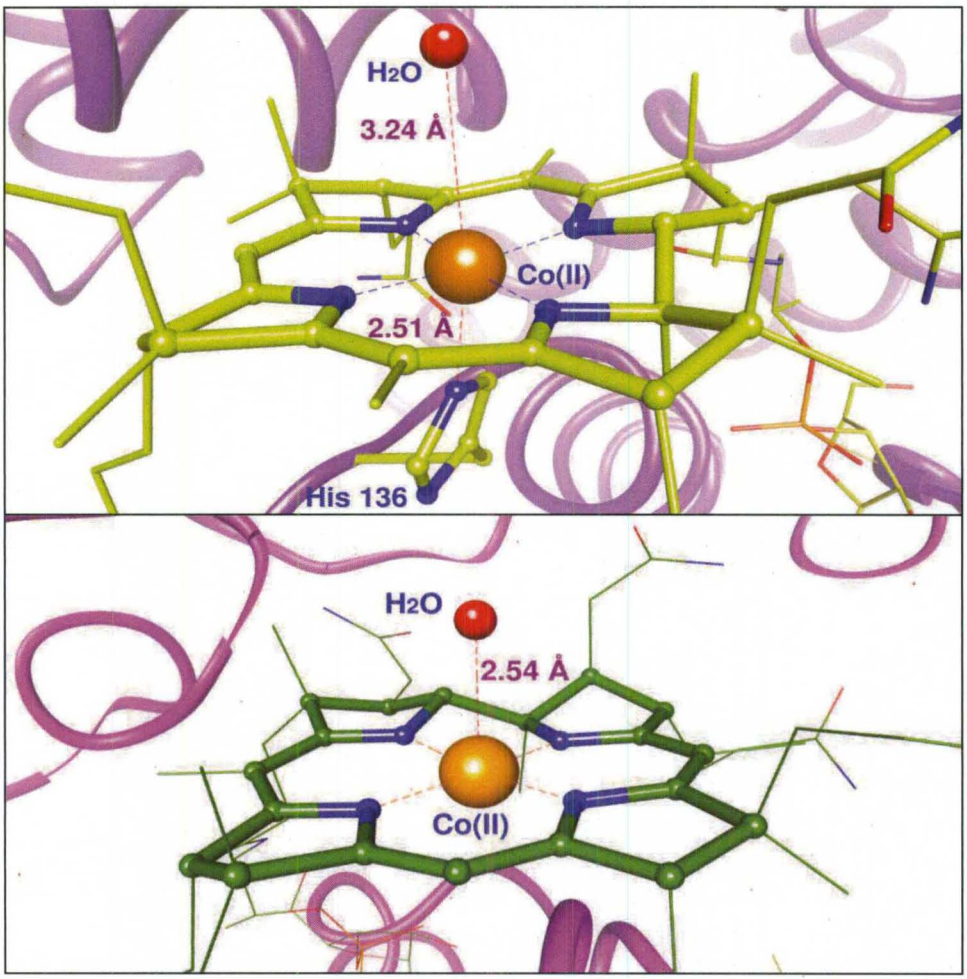


Figure 39. Active site view of the X-ray crystal structures of MtaBC-(*upper panel*) and CFeSP-bound $Co^{2+}$Cbx (*lower panel*). Check Figure 27 for MetH-bound $Co^{2+}$Cbx.

($Co^{2+}$ --O = 2.54 Å).[210] This is clearly suggestive of the fact that the $Co^{1+}$--H interaction might also be formed in the case of CFeSP-bound $Co^{1+}$Cbx. The rich

indirect experimental precedence in conjunction with the present calculations thus implies that the $Co^{1+}$--H interaction may be an unanticipated ubiquitous signature of methyltransferases.

## 6.4 Conclusions

The existence of square pyramidal or octahedral coordination environment of $Co^{1+}$Cbx, a key intermediate in a broad class of methyltransferases and ACAs is computationally explored using DFT, AIM and QM/MM tools. Taking into account the non-bonding nature of $Co^{1+}$--H interactions (~2.28 – 3.73 Å) and the enhanced thermodynamic stability of H-bonded $Co^{1+}$Cbx model complexes calculated with ωB97X, ωB97X-D and B97-D DFT functionals, it is be concluded that the long-range- and/or the empirical dispersion-corrected functionals must be employed to correctly capture the thermodynamic essence of such complexes. The AIM analysis of the H-bonded $Co^{1+}$Cbl and $Co^{1+}$Cbi complexes predicts the $Co^{1+}$--H interactions to be H-bonding type interactions that either have a dominant electrostatic component or a very small covalent character. The larger extent of redox modulation computed for the $H_2O$-bound model complexes indicate that the $Co^{1+}$--H($H_2O$) interaction is catalytically more effective than the $Co^{1+}$--H(Im) interaction with regard to the enzyme-bound $Co^{2+}/Co^{1+}$ process and signifies the functional importance of the β-axial $H_2O$ ligand commonly observed in the crystal structures of the methyltransferases. The QM/MM analysis of MetH-bound $Co^{1+}$Cbx indeed implies that a β-axial $H_2O$ ligand may coordinate to the $Co^{1+}$ ion through its unusual H-end resulting in the formation of an effective

square pyramidal complex which would favor the formation of $Co^{1+}$--H interaction inside the biological environments of methyltransferases. In summary, the H-bonded $Co^{1+}$Cbx complexes may provide significant insight into the thermodynamically challenging $Co^{2+}/Co^{1+}$ reduction which is a key component of the reactivation cycles of methyltransferases, and also of the biochemical pathways of ACAs.

# CHAPTER VII

# POSSIBLE INVOLVEMENT OF THE LOCAL ENZYME SCAFFOLD IN THE $Co^{1+}$--H BOND FORMATION: THE CURIOUS CASE OF METHIONINE SYNTHASE-BOUND COB(I)ALAMIN

## 7.1 Introduction

E. Coli MetH[31] is a cobalamin-dependent modular methyltransferase that carries out the Me group transfer from $CH_3$-folate to Hcy forming methionine (Met).[16] The reaction cycle of MetH enzyme is composed of two components namely the main catalytic cycle and the reactivation cycle (Scheme 4) respectively. The main catalytic cycle involves the transfer of a Me group from $CH_3$-folate to Hcy resulting in the formation of Met with MeCbl cofactor providing the intermediate platform for this reaction. Precisely, during the first half of the catalytic cycle, the methyl group is transferred from MeCbl to Hcy resulting in the formation of Met and $Co^{1+}$Cbx, while during the other half of the catalytic cycle, $Co^{1+}$Cbx is methylated by $CH_3$-folate and catalytically competent MeCbl form is regenerated. $Co^{1+}$Cbx is an unsually strong nucleophile which is often referred to as a "supernucleophile"[216] due to its very high Karl-Pearson constant (14). However this supernucleophilicity of $Co^{1+}$Cbx under microaerophilic

circumstances also makes it a prime target for sporadic oxidation which results in a catalytically incompetent $Co^{2+}$Cbx form. This deactivation reaction is reported to occur once every 2000 turnover cycles.[108] In a related methyltransferase namely Fe-S corrinoid,[32] the similar deactivation occurs every 100 catalytic cycles.[109] In order to maintain the efficient reaction cycle, the activated MeCbl form must be recovered. This mandatory reactivation which is achieved by the reductive methylation of $Co^{2+}$Cbx, involves a two-step process: (i) initially, the $\alpha$-axial His (H759) ligand is displaced from the MetH-bound $Co^{2+}$Cbx[110] and is substituted by the axial $H_2O$ ligand on the $\beta$-face of the cofactor[111]. This step is the rate limiting step of the reactivation process and involves a significant amount of conformational motion of the interacting domains.[110] (ii) In the subsequent step, $Co^{2+}$Cbx is reduced to $Co^{1+}$Cbx by the physiological electron donors such as flavodoxins, followed by the subsequent methylation by AdoMet.[112]

Though the molecular basis of the first step of the reactivation cycle is relatively well-understood, yet the mechanistic details of the second step continue to remain elusive. This is mainly attributed to the fact that the $Co^{2+}/Co^{1+}$ reduction is an endergonic process under the cellular conditions due to its inaccessible redox chemistry.[11] The reduction potential of $Co^{2+}/Co^{1+}$ couple is -500 mV vs SHE which is more cathodic than that of the common biological reducing agents (-280 to -440 mV vs SHE) operational inside the methyltransferases.[86,113] Evidently this reaction should not take place. But this reaction is indeed observed inside the enzymes indicating the rigorous control of the enzyme over the reduction process. The computational, structural and

spectroscopic studies suggest that the formation of tetracoordinated square planar $Co^{1+}$Cbx drives the $Co^{2+}/Co^{1+}$ reduction.[111,114,115,116] Especially, the catalytic role of Y1139 residue in the MetH-bound $Co^{2+}/Co^{1+}$ reduction is well-documented in literature:[111,116] the Y1139 residue serves to weaken the communication between the axial $H_2O$ ligand and the $Co^{2+}$ ion of the cofactor and thus promotes the generation of square planar $Co^{1+}$Cbx. In summary, the existing conventional wisdom indicates that the MetH-bound $Co^{2+}/Co^{1+}$ reduction involves the conversion of nearly square planar $Co^{2+}$Cbx into square planar $Co^{1+}$Cbx. Though the $Co^{2+}/Co^{1+}$ reduction would occur in a spontaneous fashion if the participation of the square planar $Co^{2+}$Cbx and $Co^{1+}$Cbx is assumed, but in that case the supernucleophile $Co^{1+}$Cbx may engage in the unwanted side reactions which will have a negative impact on the overall functioning of the reaction cycle.

On the other hand, a recently proposed alternate mechanism[202,208] suggests that the activation of enzyme-bound $Co^{2+}$Cbx may involve the conversion of pentacoordinated square pyramidal $Co^{2+}$Cbx into pentacoordinated square pyramidal $Co^{1+}$Cbx and the preferential stabilization of $Co^{1+}$Cbx state via $Co^{1+}$--H bond formation may provide the necessary driving force for the $Co^{2+}/Co^{1+}$ reduction process (Scheme 8). The major thermodynamic advantage of this mechanistic path is that it avoids the generation of highly energetic square planar $Co^{1+}$Cbx and may ensure that the supernucleophilicity of $Co^{1+}$Cbx remains protected from the deleterious side reactions to be selectively utilized for the subsequent methylation reaction. The QM/MM analysis of the MetH-bound

$Co^{n+}$Cbx (n = 1 or 2) complex described in chapters V and VI indicates that the $Co^{1+}$--H linkage may also be constructed in the presence of enzyme environment which further advocates a case of a pentacoordinated square pyramidal $Co^{1+}$Cbx.

Although these recent developments imply that the β-axial $H_2O$ ligand may be H-bonded with MetH-bound $Co^{1+}$Cbx, but the closer analysis of the available crystallographic data about this MetH conformation (Figure 40) [116,139] implies that the local scaffold, especially Y1139 residue may also act as an H-donor for a $Co^{1+}$--H bond formation because of its active site presence. This viewpoint is supported by the fact that the Y1139 residue in the X-ray crystal structure of MetH-bound $Co^{2+}$Cbx is located at a distance of 4.41 Å from the $Co^{2+}$ ion (PDB-code = 1K7Y @ 3.0 Å resolution)[139] and this distance is significantly shortened upon binding of AdoMet substrate (PDB-code: 1K98 @ 3.8 Å resolution; Y1139--$Co^{2+}$ = 3.97 Å). However it should be noted that these crystal structures were determined at poor resolutions of 3.0 Å and 3.8 Å respectively as a result of which the identity of the β-axial ligand could not be confirmed. However this problem has been resolved to some extent in a recently determined X-ray crystal structure of the MetH-bound reactivation complex (PDB-code: 3IVA @ 2.7 Å resolution).[116] The electron density map near the β-axial coordination site has been interpreted in favor of the $H_2O$ ligand stabilized by a H-bond with the E1097 residue. Interestingly, the axial $H_2O$ ligand and the Y1139 residue were localized at a similar distance from the $Co^{2+}$ ion ($H_2O$--$Co^{2+}$ = 3.96 Å; Y1139--$Co^{2+}$ = 3.97 Å) indicating that the axial ligand may be substituted by the Y1139 residue.

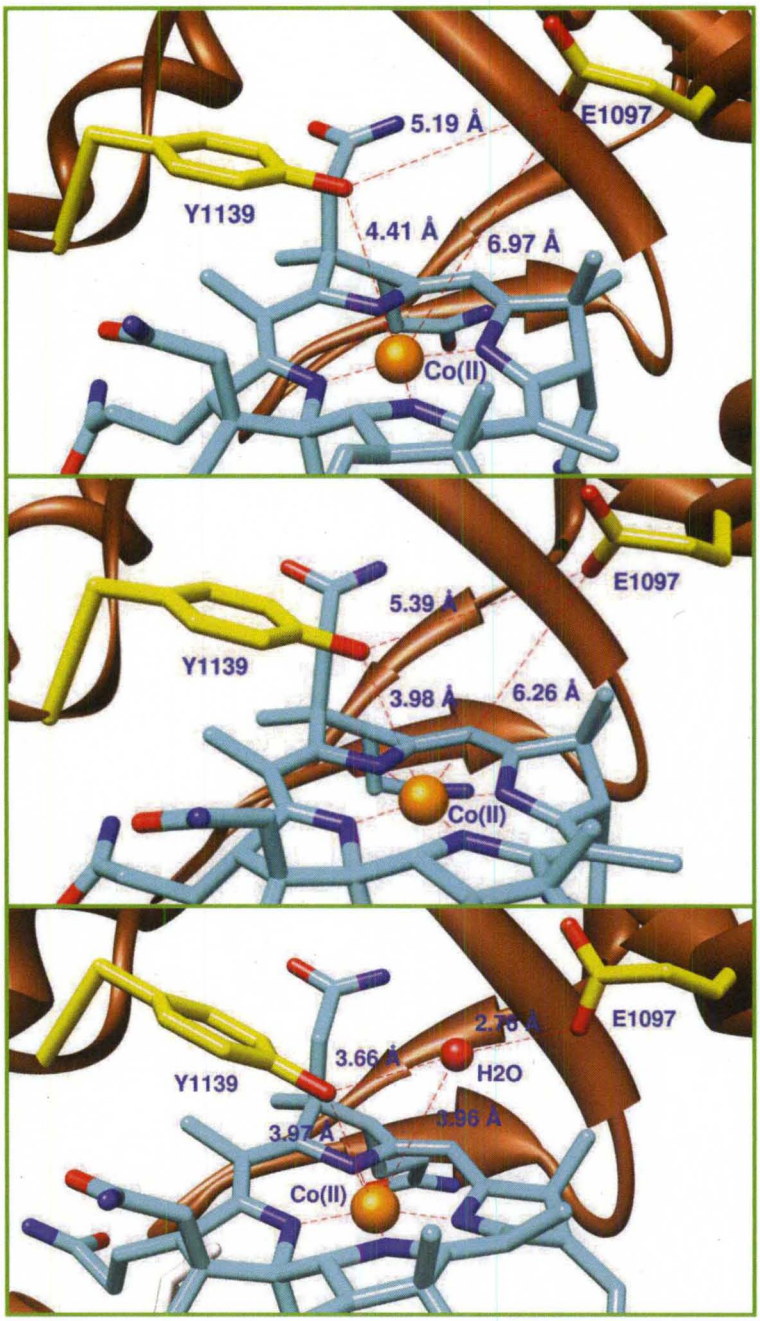


Figure 40. Active site view of the MetH-bound $Co^{2+}$Cbx complex. The *top panel* corresponds to the situation when the substrate AdoMet is not present (1K7Y, 3.0 Å), the *middle panel* represents a binary complex of MetH-bound $Co^{2+}$Cbx and AdoMet substrate (1K98, 3.8 Å) while the *bottom panel* shows the better resolved active site of the same binary complex (3IVA, 2.7 Å).

Building upon these crystallographic developments, herein we explore the computational tools to address the following mechanistically important issue: what will happen if the β-axial $H_2O$ ligand is replaced by the active site Y1139 residue? Will it communicate better with the $Co^{1+}$ ion of $Co^{1+}$Cbx? If yes, will it be O-bound with the $Co^{1+}$ ion or will it be offering its H-end for constructing a $Co^{1+}$--H linkage? And if it will be H-bonded, what will be the thermodynamic consequences in the context of $Co^{2+}/Co^{1+}$ reduction i.e., will the Y1139-induced $Co^{1+}$--H interaction be catalytically more efficient than that mediated by the axial $H_2O$ ligand?

## 7.2 Computational Details

All the calculations were performed using the Gaussian09 suite of program for the electronic structure and properties calculations. In order to perform the computational modeling of the MetH-bound $Co^{1+}$Cbx, the cobinamide type models ($Co^{1+}$Cbi) were used in which all the corrin amide side chains were retained and only the nucleotide loop was truncated at the phosphodiester end. To test the possibility of an alternate β-axial ligand, pentacoordinated square pyramidal as well as hexacoordinated octahedral $Co^{1+}$Cbi complexes were investigated where $H_2O$ and PhOH were used as the β-axial ligands. The use of β-axial PhOH ligand is promoted by the fact that the Y1139 residue is situated in the active site of MetH-bound $Co^{2+}$Cbx complex and has been shown to be catalytically important in the reactivation cycle of MetH enzyme[111,116]. In the octahedral complexes, the other axial ligand i.e., α-axial ligand was modeled by

$H_2O$ molecule. To understand how the presence of local enzyme environment will impact the stability of $Co^{1+}$Cbi complexes, the square pyramidal and octahedral complexes containing an additional $H_2O$ molecule in the proximity of the β-axial ligands were also considered. The geometry optimization of the $Co^{1+}$Cbi complexes was carried out using HF, BP86, ωB97X and ωB97X-D functionals respectively. Taking into account the structural complexity of the $Co^{1+}$Cbi models (Total no. of atoms = 143-159), the 6-31G(d) 5d basis set was used in the optimizations. It should be noted that all the $Co^{1+}$Cbi complexes were exclusively treated at the QM level of theory in contrast to the earlier studies[121] where only certain part of the cofactor was investigated at the QM level of theory while the rest of the system was given molecular mechanics treatment. The static thermodynamic data for all the $Co^{1+}$Cbi complexes were computed assuming a standard state convention of 298.15 K and 1 atm. Taking into account recent studies[202,208] that show that the long-range correlation- and the empirical-dispersion-corrected DFT functionals must be used for properly describing the non-covalent $Co^{1+}$--H interactions, we optimized the $Co^{1+}$Cbi complexes using ωB97X (long-range-corrected functional) and ωB97X-D (empirical-dispersion-corrected functional) in addition to the HF and conventional DFT (BP86) functionals. The use of BP86 functional as a conventional DFT representative is inspired by its well-established usefulness in reproducing the structural, electronic, spectroscopic and electrochemical properties of $B_{12}$ corrinoids.

## 7.3 Results and Discussion

### 7.3.1 DFT Structural Analysis of $Co^{1+}$Cbi Complexes

The Figure 41 displays the ωB97X-D optimized $Co^{1+}$Cbi structural models. The calculated $Co^{1+}$-O bond distance lies in the range of 3.30 - 3.40 Å. Though the crystallographic identification of MetH-bound $Co^{1+}$Cbx has not been feasible due to its transient nature, but the activation complex of MetH-bound $Co^{2+}$Cbx and AdoMet has been well-investigated[116,139] that provides a reasonable reference point for analyzing the computed structural data. The experimental value for the MetH-bound $Co^{2+}$-O bond has been determined to be ~3.97 Å. This hints towards the noticeable elongation of $Co^{1+}$-O bond inside the MetH enzyme. This structural aspect of MetH-bound $Co^{1+}$Cbx is discussed in detail in the computational study reported in chapter V where the presence of the enzyme was shown to elongate the $Co^{1+}$-O bond by 0.2 - 0.3 Å. The analogous role of the enzyme environment in weakening the interaction between the cobalt cofactor and the axial $H_2O$ ligand has been illustrated in a spectroscopic study by Brunold et al.,[111] where the local enzyme scaffold, especially Y1139 residue and AdoMet substrate accounted for a $Co^{2+}$-O bond lengthening of 0.05 Å.

In all the optimized model complexes, the axial ligands were H-bonded with the $Co^{1+}$ ion of the cofactor through their unusual binding centers in contrast to their traditional hetero O-atom ligation sites. The formation of the $Co^{1+}$--H bonds had no effect upon the geometry of the equatorial corrin ring i.e. the corrin structure remained essentially unaffected in the presence of $Co^{1+}$--H linkages as

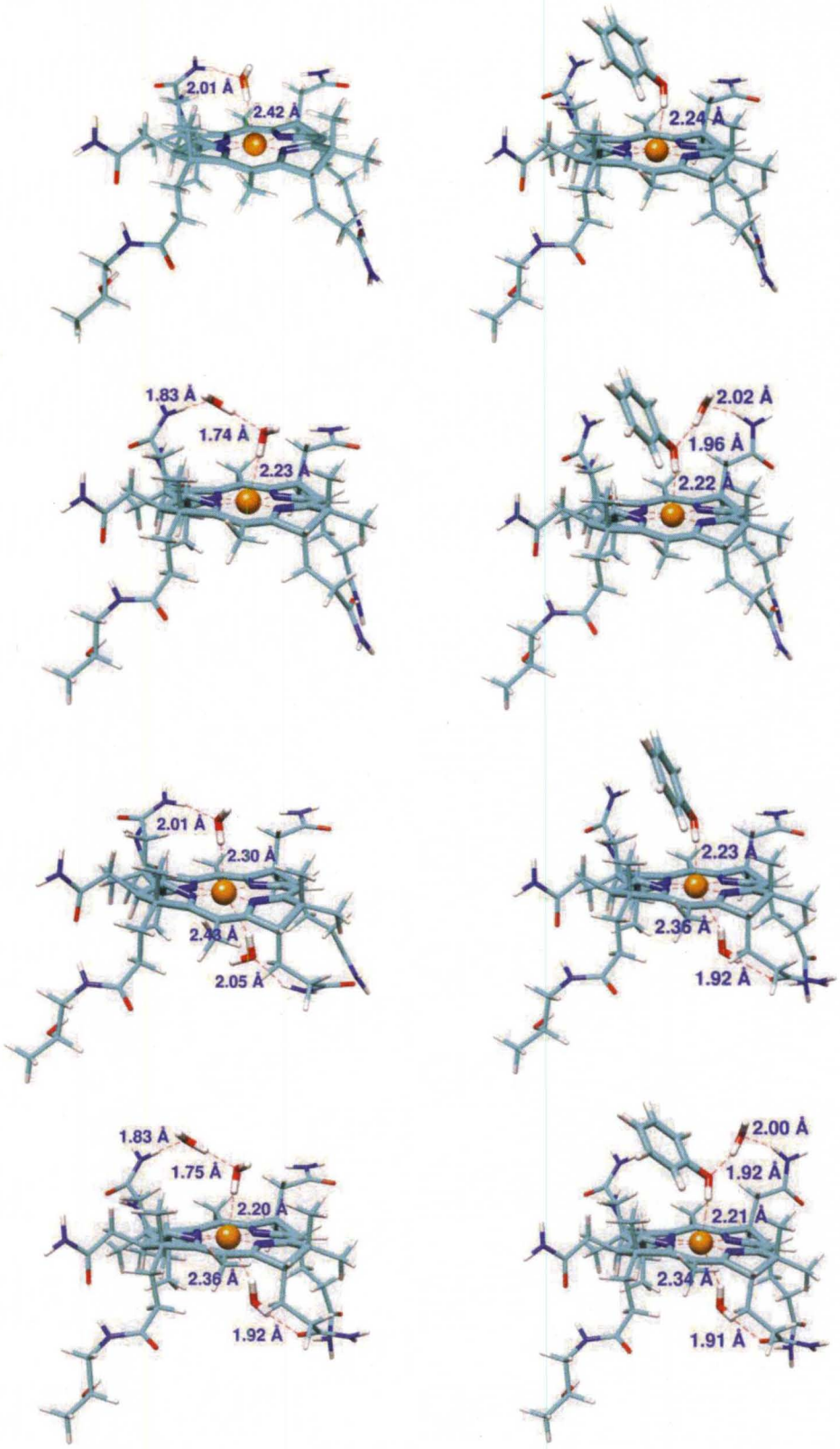


Figure 41. ωB97X-D optimized H-bonded β-axial $H_2O$-(*left*) and PhOH-ligated (*right*) $Co^{1+}$Cbi complexes.

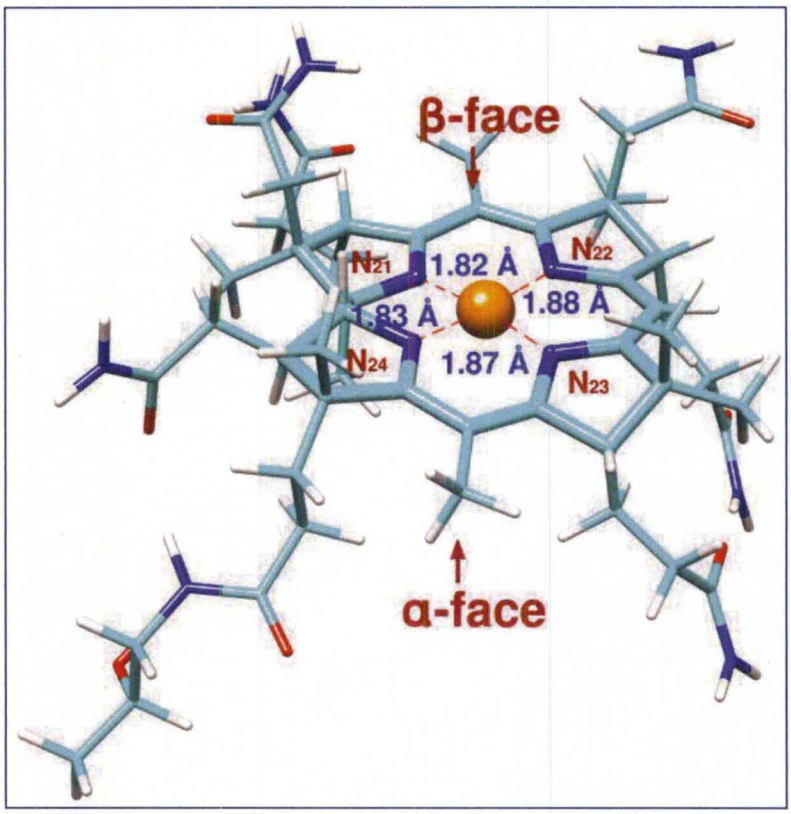


Figure 42. ωB97X-D-optimized structure of tetracoordinated square planar $Co^{1+}$Cbi complex. The relevant part of the corrin ring is also labeled using the numbering scheme commonly used for $B_{12}$ corrinoids.

their impact was specifically localized in the axial region (Figure 42; Tables A75-A83). The computed $Co^{1+}$-- H bond distances showed a reasonable agreement with the previously computed or experimentally determined values for the $d^8$ metal ion-influenced H-bonds.[126-137,202,208] The scatter plots of $\angle Co^{1+}$--H-O vs $Co^{1+}$--H and $\angle Co^{1+}$--H-O vs $Co^{1+}$--O for the H-boned $Co^{1+}$Cbi complexes are

illustrated in Figure 43. The linear structural arrangement of $Co^{1+}$--H-O binding motives in the optimized structural models imply that the $Co^{1+}$--H linkages fall in the bracket of conventional hydrogen bonds. The β-axial PhOH ligand in the $Co^{1+}$Cbi models had a better interaction with $Co^{1+}$ ion than the β- or α-axial $H_2O$ ligand. This was due to the better H-donating capacity of the PhOH motif which was also reflected in terms of the directional character of $Co^{1+}$--H-O binding units. The degree of $Co^{1+}$--H-O motif linearity in the PhOH-ligated $Co^{1+}$Cbx complexes was found to be higher than in the $H_2O$-ligated $Co^{1+}$Cbx complexes. The strength of $Co^{1+}$--H interactions was noticeably impacted in going from the pentacoordinated to the hexacoordinated complexes. The α-axial $H_2O$ ligand in the octahedral $Co^{1+}$Cbi complexes constructed relatively stronger intramolecular H-bond with the carbonyl group of the nearby propanamide side chain (i.e., H-O-H--O=C- ~ 1.91 Å) which might be the reason that the α-axial $H_2O$ ligand bound less strongly to the $Co^{1+}$ ion of $Co^{1+}$Cbi than the β-axial ligand. To model the impact of the local enzyme environment, $Co^{1+}$Cbi models enclosing an additional $H_2O$ molecule in the vicinity of the β-axial ligand were also optimized. The local $H_2O$ molecule acted as an H-donor and formed an associative interaction with the β-axial ligand (i.e., H–O-H--O(PhOH or $H_2O$) = 2.20 – 2.30 Å). This hydrophilic interaction strengthened the $Co^{1+}$--H bonds. The β-axial $H_2O$ ligand in $Co^{1+}$Cbi--$H_2O$ and $H_2O$--$Co^{1+}$Cbi--$H_2O$ complexes also interacted with the peripheral amide side chains of the corrin ring via H-bond i.e., they formed a strong H-bond with the amino group (–$NH_2$) of the proximal acetamide side chain (i.e., -N-H--$OH_2$ ~ 2.01 Å). In the complexes where the local environment effect

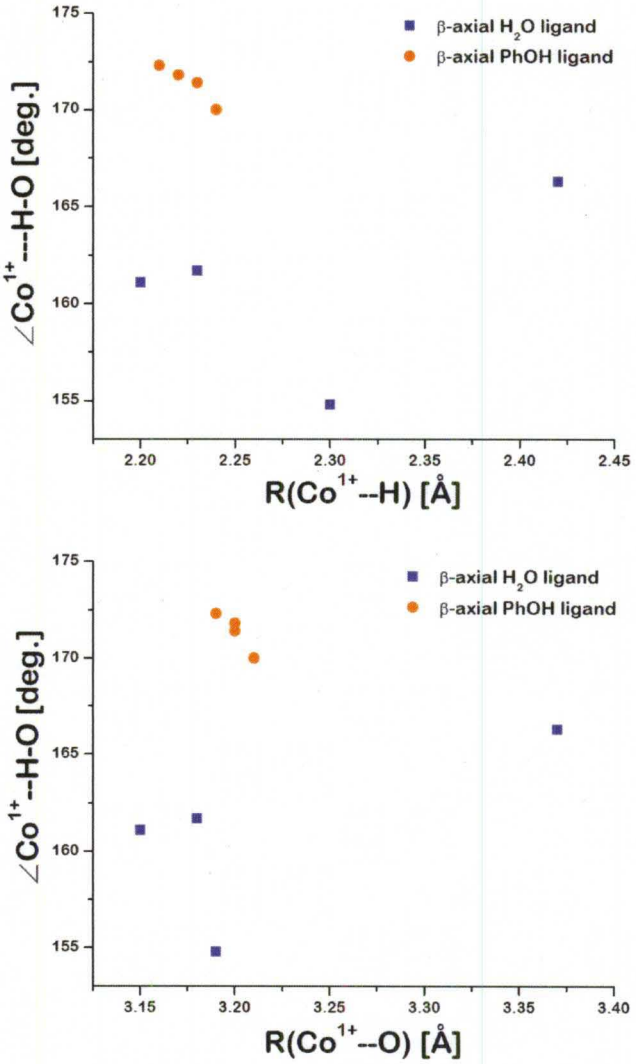


Figure 43. ∠$Co^{1+}$--H-O vs $Co^{1+}$--H (*upper panel*) and ∠$Co^{1+}$--H-O vs $Co^{1+}$--O (*lower panel*) in the H-bonded $Co^{1+}$Cbi complexes. The ωB97X-D/6-31G(d) 5d calculated data have been shown.

was taken into account, the β-axial $H_2O$ ligand did not directly interact with the side chain, but the local residue, mimicked by $H_2O$ molecule, formed a H-bonding interaction with the $-NH_2$ end of the acetamide chain (i.e., $H_2O$--H-N- = 1.83 Å). The local $H_2O$ molecule in the PhOH-coordinated complexes formed a similar H-bond but with the $NH_2$- end of a different corrin side chain (i.e., $H_2O$--H-N- ~ 2.01 Å) due to the bulkier β-axial PhOH ligand which inhibited its interaction with the acetamide chain. This H-bond was found to be longer by ~0.2 Å than that in the $H_2O$-ligated complexes. This structural analysis suggests that the Y1139-mediated $Co^{1+}$--H interactions may result in a better H-bonded $Co^{1+}$Cbx complex. Further, the presence of the local enzyme scaffold may augment the strength of these interactions which might have thermodynamic implications for the MetH-bound $Co^{2+}/Co^{1+}$ reduction.

### 7.3.2 DFT Thermodynamics Analysis of $Co^{1+}$Cbi Complexes

As a next step, we computed the gas phase thermodynamic data for the H-bonded $Co^{1+}$Cbi complexes. The comparative analysis of $Co^{1+}$Cbi model complexes with the β-axial $H_2O$ and PhOH ligands, is illustrated in Figure 44 respectively (also check Tables A84 - A91 for further details). The complex formation reactions

i.e., $Co^{1+}Cbi + H_2O$ or PhOH $\rightarrow$ $Co^{1+}Cbi$--$H_2O$ or $Co^{1+}Cbi$--HOPh

were found to be exothermic in nature when the complexes were probed using the ωB97X and ωB97X-D functionals that indicated the presence of long-range correlation and empirical-dispersion components in the $Co^{1+}$--H interactions. The PhOH-ligated $Co^{1+}$Cbi complexes were more stable than the $H_2O$-ligated $Co^{1+}$Cbi ones due to better coordinating ability of PhOH motif which resulted in the relatively tightly-bound H-bonded $Co^{1+}$Cbi complexes. The $Co^{1+}$--H interactions in the hexacoordinated $Co^{1+}$Cbi complexes were appreciably weakened in comparison to the pentacoordinated ones revealing that the two axially directed $Co^{1+}$--H interactions exert a mutual weakening influence. The computed driving force ($\Delta G^{o}$) for the $OH_2$--$Co^{1+}$Cbi--$H_2O$ complex ($\Delta G^{o}$ = -12.9 kcal/mol) was 5.7 kcal/mol less than twice the value calculated for the $Co^{1+}$Cbi--$H_2O$ complex ($\Delta G^{o}$ = -9.3 kcal/mol). The similar weakening effect was also evident in case of PhOH-ligated complexes as the $\Delta G^{o}$ value for the PhOH--$Co^{1+}$Cbi--$H_2O$ complex ($\Delta G^{o}$ = -14.9 kcal/mol) was only slightly higher than that for the PhOH--$Co^{1+}$Cbi complex ($\Delta G^{o}$ = -12.3 kcal/mol). The α-axial $H_2O$ ligand bound less efficiently to the $Co^{1+}$ ion than the β-axial $H_2O$ or PhOH ligand in the octahedral complexes because of its tendency to engage in the formation of stronger hydrophilic interaction with the proximal propanamide side chain which might also have contributed towards the observed weakening effect. However this destabilizing effect is expected to be completely diminished inside the cellular environments of MetH as only the β-face of the enzyme-bound cofactor is exposed to the solvent.[223] The presence of local environment that was modeled by placing an additional $H_2O$ molecule in the vicinity of the β-axial ligand noticeably improved the driving force available for the

H-bonded $Co^{1+}$Cbi complexes which is rooted in the fact that the additional stabilizing contacts were formed and the communication between the corrin ring side chain and the axial ligand was either strengthened (in the case of $H_2O$-ligated complexes) or established (in the case of PhOH-ligated complexes). For example, in the case of $Co^{1+}$Cbi--$H_2O$--$H_2O$ and $OH_2$--$Co^{1+}$Cbi--$H_2O$--$H_2O$ complexes, the local $H_2O$ constructed a strong H-bonding interaction with the β-axial $H_2O$ ligand (i.e., $H_2O$--$H_2O$(local) ~1.75 Å). Besides that, it also formed a H-bond with the corrin amide side chain (i.e., -$NH_2$--$OH_2$(local) ~1.83 Å) which is a stronger interaction than that noticed between the β-axial $H_2O$ ligand and the corrin side chain (i.e., -$NH_2$--$OH_2$ (axial ligand) ~2.05 Å). As a result, the $\Delta G^o$ values for the $Co^{1+}$Cbi--$H_2O$--$H_2O$ and $OH_2$--$Co^{1+}$Cbi--$H_2O$--$H_2O$ complexes were increased by 5.3 kcal/mol and 2.2 kcal/mol respectively. Similarly, the local $H_2O$ molecule in the $Co^{1+}$Cbi--PhOH--$H_2O$ and $OH_2$--$Co^{1+}$Cbi--PhOH--$H_2O$ complexes constructed multi-center hetero acceptor H-bonds (i.e., PhOH--$H_2O$ ~1.94 Å; $H_2O$--$H_2N$ ~2.01 Å) that accounted towards the observed increase in the $\Delta G^o$ values of these complexes. However they were relatively less strong than those formed in the $H_2O$-ligated $Co^{1+}$Cbi complexes. It should be noted that the two additional H-bonding interactions were gained in the $Co^{1+}$Cbi--PhOH--$H_2O$ and $OH_2$--$Co^{1+}$Cbi--PhOH--$H_2O$ complexes due to the involvement of local $H_2O$ molecule as compared to the $Co^{1+}$Cbi--PhOH and $OH_2$--$Co^{1+}$Cbi--PhOH complexes which had no interaction between the PhOh ligand and the corrin side chain. The stabilization impact exerted by the local environment in the case of $Co^{1+}$Cbi complexes is interesting because these complexes closely resemble

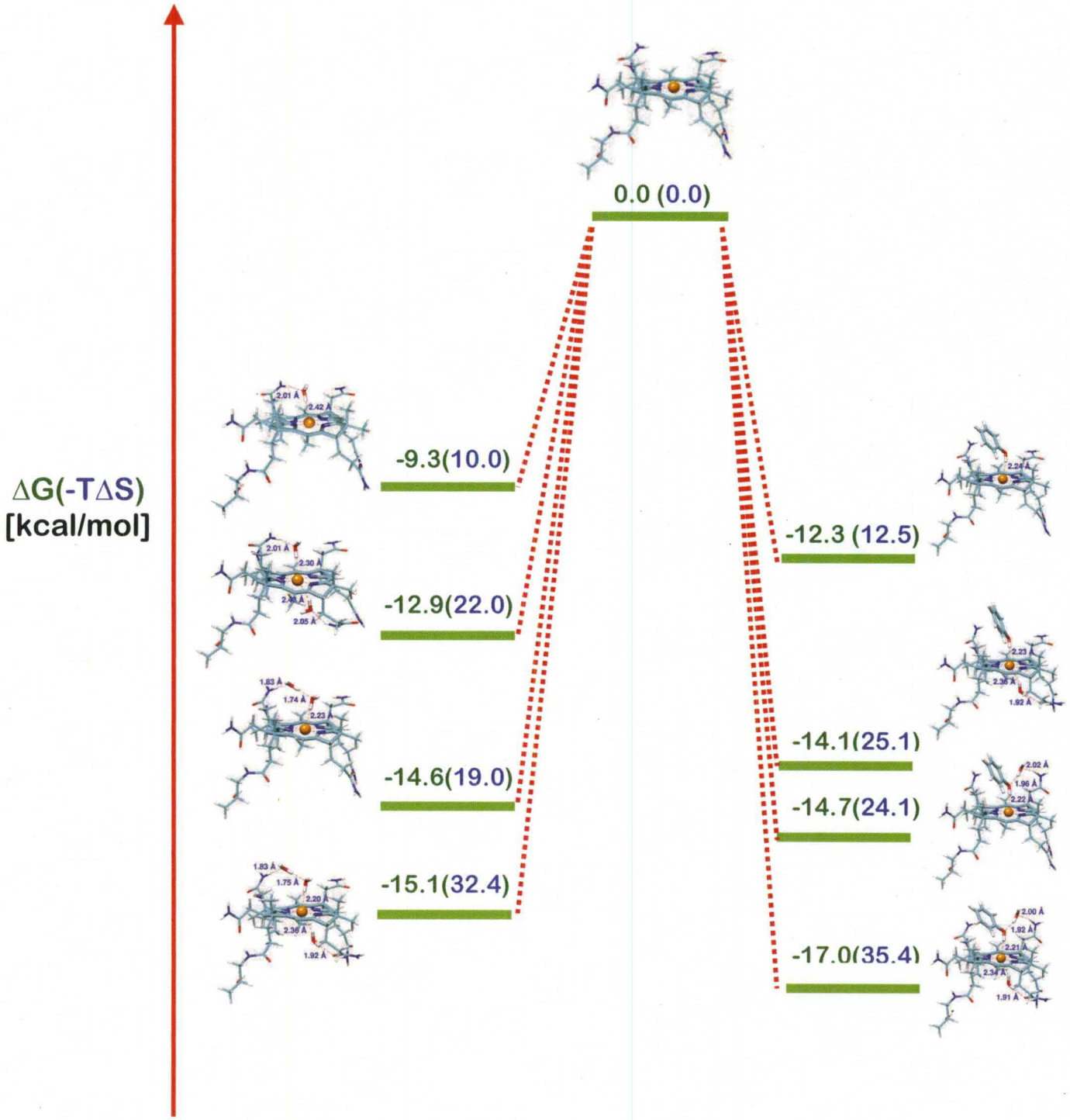


Figure 44. ωB97X-D-computed thermodynamic data for H-bonded β-axial $H_2O$- (*left*) and PhOH-ligated (*right*) $Co^{1+}$Cbi complexes.

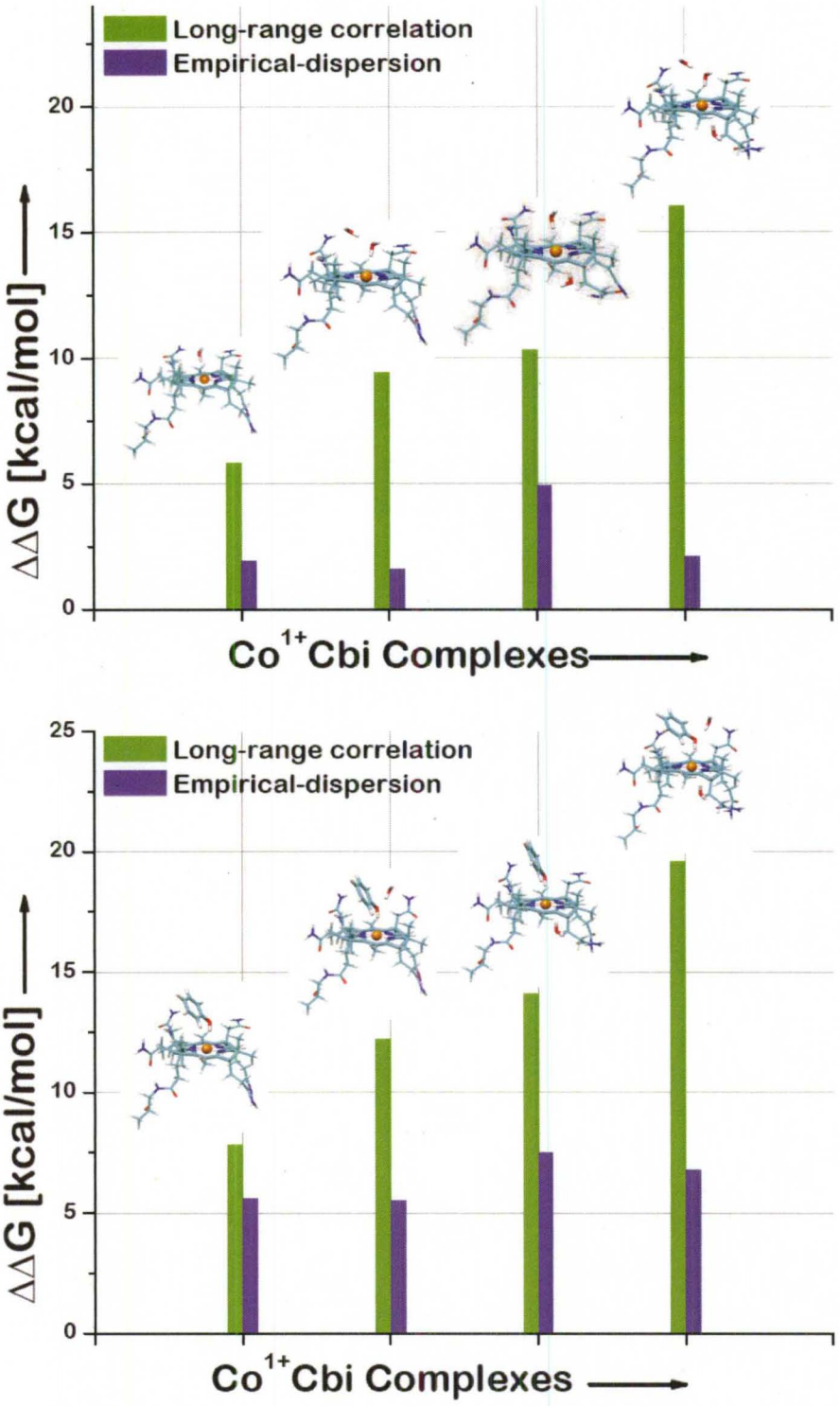


Figure 45. Degree of long-range correlation and empirical-dispersion in the H-bonded β-axial $H_2O$-(*upper panel*) and PhOH-ligated (*lower panel*) $Co^{1+}$Cbi model complexes.

with the biologically active $Co^{1+}$Cbx intermediate and tends to suggest that the $Co^{1+}$--H(HOPh) interaction may be strengthened in the presence of enzyme environment.

The difference between the HF and ωB97X computed $\Delta G^{o}$ and that between the ωB97X and ωB97X-D functionals-based $\Delta G^{o}$ values provided us a quantitative estimate of the long-range correlation and the empirical-dispersion component involved in the $Co^{1+}$--H interactions respectively. As shown in the Figure 45, the H-bonded $Co^{1+}$Cbi complexes contained a significant amount of correlation component that was primarily stored in the $Co^{1+}$--H interactions. The $Co^{1+}$Cbi model compounds with the PhOH axial ligand (8.0 – 19.5 kcal/mol) were found to be richer in correlation than those with the axial $H_2O$ ligand (7.0 – 17.0 kcal/mol). The degree of correlation component was found to be directly proportional to the structural complexity of a $Co^{1+}$Cbi complex. For example, the β-axial $H_2O$-ligated octahedral $Co^{1+}$Cbi complexes (i.e., $OH_2$--$Co^{1+}$Cbi--$H_2O$; $\Delta\Delta G^{o}$= 12.0 kcal/mol) and $OH_2$--$Co^{1+}$Cbi--$H_2O$--$H_2O$; $\Delta\Delta G^{o}$ = 17.0 kcal/mol) as well as the $Co^{1+}$Cbi--PhOH--$H_2O$ ($\Delta\Delta G^{o}$ = 14.0 kcal/mol) and $OH_2$--$Co^{1+}$Cbi--PhOH--$H_2O$ ($\Delta\Delta G^{o}$ = 19.5 kcal/mol) complexes had more correlation component than their corresponding pentacoordinated analogues because of the presence of two $Co^{1+}$--H bonds. The comparison between ωB97X and ωB97X-D computed thermodynamics indicated that $Co^{1+}$Cbi models had 2.0 - 8.3 kcal/mol dispersion contributions in the computed $\Delta G^{o}$ values. However the effect of empirical-dispersion was less pronounced than the long-range correlation. The β-axial PhOH-ligated $Co^{1+}$Cbi complexes ($\Delta\Delta G^{o}$ = 5.3 – 8.0 kcal/mol) had greater

dispersion contribution than the β-axial $H_2O$-ligated $Co^{1+}$Cbi complexes ($\Delta\Delta G^o$ = 2.5 – 5.0 kcal/mol) which might be due to its better $Co^{1+}$--H bond forming ability as well as due to its greater steric bulk. The recent DFT and QM/MM calculations have also suggested the presence of a dispersion component in the $Co^{1+}$--H interactions in the model as well as MetH-bound $Co^{1+}$Cbx complexes respectively.[202,208] The significance of dispersion interactions in the $d^8$ metal ion-induced H-bonds in the case of $Pt^{2+}$ complexes has also been recently illustrated where the MP2 calculations revealed the presence of dispersion interactions in the $Pt^{2+}$--H bonds.[132-133] The present analysis thus supports the previous studies[202,208] that the $Co^{1+}$--H interactions contain a significant amount of long-range correlation and a noticeable amount of empirical-dispersion components, and the right kind of DFT functionals must be used to accurately describe the $Co^{1+}$Cbx complexes containing such interactions.

## 7.4 Conclusions

The possible alternate role of the active site tyrosine (i.e., Y1139) residue in the context of $Co^{1+}$--H bond formation has been computationally investigated using DFT calculations. The calculated data suggest that the PhOH, an ideal structural mimick of tyrosine residue, constructs thermodynamically more stable $Co^{1+}$--H interactions than the axial $H_2O$ ligand which may have relevance for the reactivation cycle of the MetH enzyme. In the reactivation cycle, the thermodynamically unfavorable $Co^{2+}/Co^{1+}$ reduction need to be executed to recover the catalytically active $Co^{1+}$Cbx form, however the mechanistic base of

this process is yet to be fully understood. The exisiting spectroscopic[111,114] and structural[116] studies on the reactivation conformation of MetH enzyme imply that the active site Y1139 residue plays a major catalytic role in the reduction process by promoting the dissociation of the β-axial ligand from the cofactor. However the presented calculations suggest that this residue may not only displace the axial ligand, but may also provide better H-donor facilities for constructing $Co^{1+}$--H interactions. This finding is interesting in the wake of recent computational studies[202,208] which suggests that the preferential stabilization of $Co^{1+}$Cbx state via $Co^{1+}$--H interactions may drive the thermodynamically difficult reduction process. From thermodynamic perspective, the axial PhOH-induced $Co^{1+}$--H interactions are found to be more stable than the axial $H_2O$ ligand-influenced ones which may result in the enhanced driving force available for the reduction process if the active site Y1139 residue is engaged in $Co^{1+}$--H bond formation. So far two X-ray studies[116,139] have been reported on the MetH-bound $Co^{2+}$Cbx state and both seem to support this conceptual picture (Figure 40). In the first study,[139] the active site Y1139 was localized at a distance of 4.41 Å from the $Co^{2+}$ ion of MetH-bound $Co^{2+}$Cbx (PDB-code = 1K7Y @ 3.0 Å resolution) and no other direct axial interaction involving metal center was detected. Apparently the Y1139 was the judicious β-axial ligand. The Y1139--$Co^{2+}$ bond distance was significantly reduced upon binding of AdoMet substrate i.e. (Y1139)O--$Co^{2+}$ = 3.97 Å (PDB-code: 1K98 @ 3.8 Å resolution). Though in the subsequent X-ray analysis[116] that afforded a better resolved reactivation complex of MetH-bound $Co^{2+}$Cbx with AdoMet (PDB-code: 3IVA @ 2.7 Å resolution), a β-axial $H_2O$ ligand

was identified, but it was 3.96 Å distance away from the $Co^{2+}$ ion. The active site Y1139 residue was also located at an identical distance (i.e., 3.97 Å) from the $Co^{2+}$ ion. The axial $H_2O$ ligand that is displaced in the MetH-bound $Co^{2+}$Cbx, is not only nteracting with Y1139 residues ($H_2O$--Y1139 = 3.30 Å) but is also be involved in an H-bonding interaction with the $COO^-$ end of the E1097 residue (($H_2O$)O--$^-$OOC = 3.10 Å) which is a slightly stronger interaction than Y1139--$H_2O$ interaction and may be providing the additional driving force for rupturing the binding interaction between the axial $H_2O$ ligand and the cofactor. The recent QM/MM calculations[208] also implied the feasibility of an intensive communication between the axial $H_2O$ ligand and the active site E1097 residue ((H-O-H--$^-$OOC = 2.70 - 2.80 Å).[21] Also, the spectroscopic study of Brunold et al.,[111] has established that the binding of the AdoMet substrate results in the translational motion of the Y1139 residue towards the binding pocket of the cofactor. It seems reasonable to suggest that the Y1139 residue may be sterically in a better position to interact with the $Co^{1+}$ ion through $Co^{1+}$--H interactions. These non-classical $Co^{1+}$--H bonds may considerably stabilize $Co^{1+}$Cbx and may play a part in ensuring the driving force for the $Co^{2+}/Co^{1+}$ reduction. In summary, the present DFT calculations and X-ray crystallographic analysis of the reactivation conformation of MetH enzyme suggest the possible involvement of Y1139 residue as an H-donor in the $Co^{1+}$--H bond formation. This may be one of the possible catalytic strategies that the MetH enzyme uses to carry out the thermodynamically challenging $Co^{2+}/Co^{1+}$ reduction during its reactivation cycle.

# CHAPTER VIII

# SUMMARY AND CONCLUSIONS

In this dissertation, the various aspects of $B_{12}$–dependent reaction cycles have been investigated using state of the art computational methods. In particular two problems are specifically studied: (i) Activation of Co-C bond in adenosylcobalamin (AdoCbl)-dependent mutases; and (ii) cob(II)alamin($Co^{2+}$Cbx)/cob(I)alamin($Co^{1+}$Cbx) redox process in methyltransferases.

The mechanism of Co-C bond activation as well as the initial step of $B_{12}$ catalysis that consists of Co-C bond cleavage and subsequent hydrogen atom (H-atom) abstraction from the substrate are studied by means of density functional theory, complete active space self-consistent field and quantum mechanics/molecular mechanics computational methodologies respectively. The solvation correction by polarizable continuum solvation model is applied as needed.

The detailed theoretical study of Chapter II along with the X-ray crystal structure analysis of two of the most important adenosylcobalamin (AdoCbl)-dependent mutases namely methylmalonyl coenzymeA mutase (MCM) and

glutamate mutase (GLM) showed that the diradical state, $[AdoCbl]^{\bullet -}$-$Y^{\bullet}$, is the lowest electronic state of the AdoCbl--$Y^{-}$ complex providing strong evidence that the electron transfer (ET) from the active site tyrosine (Y) residue to the AdoCbl cofactor is feasible. The diradical character of AdoCbl--$Y^{-}$ model complex is also approved by the complete active space self-consistent field calculations. The quantum mechanics/molecular mechanics (QM/MM) calculations indicated that the active site Y89 residue of MCM enzyme does indeed induce ET onto the AdoCbl cofactor when present in its deprotonated form. The crystallographic analysis of the active sites of MCM and GLM enzymes revealed that the substrate binding can play a critical role in displacing the hydroxyl proton of Y residue (Y89 in case of MCM enzyme and Y181 in case of GLM enzyme) that will facilitate the ET, and the Co-C bond cleavage will preferably occur via proton-coupled electron transfer (PCET) pathway. Thus the initial step of $B_{12}$ catalysis is proposed to involve the one-electron reduced form of AdoCbl cofactor (i.e. $[AdoCbl]^{\bullet -}$) that provides an efficient mode of cleavage and can help in understanding the origin of catalysis in $B_{12}$ mutases.

As a next step, the energetic implications of the possible involvement of the $[AdoCbl]^{\bullet -}$ in the initial step of $B_{12}$ catalysis that involves Co-C bond cleavage and subsequent H-abstraction from the substrate are investigated. The intrinsic reaction coordinate computations predicted that the reaction consisting of Co-C bond cleavage and subsequent H-atom abstraction occurs in a concerted fashion if the reduced form of AdoCbl cofactor is involved in the reaction. The computed activation energy barrier of the reaction was significantly lowered (by ~31.5%) in

comparison to the reaction involving the neutral cofactor model that lent further support to our PCET-based mechanistic pathway for the origin of catalysis in AdoCbl-dependent mutases.

In the second part of the dissertation, the alternate coordination environments of cob(I)alamin ($Co^{1+}$Cbx) as well the mechanistic pathways of the $Co^{2+}/Co^{1+}$ reduction process in the context of methyltransferases are evaluated by means of density functional (DFT), atoms in molecule (AIM), natural bond orbital (NBO) and QM/MM computational tools respectively. The polarizable continuum solvation model is adopted to investigate the thermodynamics of $Co^{1+}$Cbx complexes where the non-electrostatic contributions are computed within the formalism of SMD solvation model.

The detailed research described in Chapter IV showed that the $Co^{1+}$ ion in $Co^{1+}$Cbx model complexes engage in the formation of H-bond with the beta-axial $H_2O$ ligand. The H-bond forming capacity of $Co^{1+}$ ion is rooted in the fact that it is dominant $d^8$ electronic configuration system that has appropriately oriented filled d-orbitals for interacting with the acidic ends of the axial ligands. The DFT and NBO analysis indicated that the $Co^{1+}$--H interaction has noticeable amount of electrostatic, charge transfer, long-range correlation and dispersion contributions respectively. The AIM analysis indicated the presence of dominant electrostatic or partial covalent character in the $Co^{1+}$--H interactions. As a result of this binding interaction, the $Co^{1+}$Cbx complexes adapt to an unprecedented pentacoordinated square planar coordination environement in addition to their well-established tetracoordinated square planarity. The computed reduction potentials of the

$Co^{2+}/Co^{1+}$ couple assuming the possible coordination geometries of $Co^{1+}$Cbx indicated that the $Co^{1+}$--H interaction exerts a significant amount of redox tuning upon the electrochemistry of the $Co^{2+}/Co^{1+}$ reduction process. Based on these calculations, an alternate mechanistic pathway for the $Co^{2+}/Co^{1+}$ reduction process was proposed that involves the conversion of the square pyramidal $Co^{1+}$Cbx into the square pyramidal $Co^{1+}$Cbx rather than its square planar form. The analysis of the existing X-ray crystallographic data about the reaction complex of methionine synthase (MetH) enzyme indicated that the axial $H_2O$ ligand is located in the binding pocket of the cofactor and can interact with the cobalt center that provided experimental support to our proposed mechanistic scheme.

As a next step, the possibility of $Co^{1+}$--H bond formation inside the biological environment of MetH enzyme is investigated with the help of DFT, AIM and ONIOM-based QM/MM computational tools. The DFT and AIM calculations asserted the dominant electrostatic character of $Co^{1+}$--H linkages in the model complexes of MetH-bound $Co^{1+}$Cbx. The QM/MM computations indicated that the axial $H_2O$ ligand in the MetH-bound $Co^{2+}$Cbx (PDB-code:3IVA @ 2.7 Å resolution) with the $Co^{2+}$ ion through its O-end while it coordinates to the $Co^{1+}$ ion of the MetH-bound $Co^{1+}$Cbx via its H-end which provides the first conclusive evidence of the formation of $Co^{1+}$--H interaction inside the enzyme environment. The comparative analysis of the QM/MM optimized $Co^{2+}$Cbx and $Co^{1+}$Cbx complexes revealed that the free H-end of the axial $H_2O$ ligand in the MetH-bound $Co^{2+}$Cbx undergoes a conformational change en route to the $Co^{1+}$Cbx

complex formation. This conformational switch is primarily driven by the change in the electronic configuration of the metal ion (i.e., $Co^{2+}$ ($d^7$) → $Co^{1+}$ ($d^8$)). Benefiting from the $Co^{1+}$--H interaction, the MetH-bound $Co^{1+}$Cbx adapts to the unique square pyramidal coordination environment.

The further computational analysis of the primary coordination environment of $Co^{1+}$Cbx suggested that $Co^{1+}$Cbx can also exist in octahedral coordination environment in addition to its square pyramidal and square planar geometries. The QM/MM calculations predicted that a β-axial $H_2O$ in the QM/MM optimized hexacoordinated octahedral MetH-bound $Co^{1+}$Cbx (1BMT, Res. 3.0 Å) is coordinated to $Co^{1+}$ ion via its unusual H-end ($Co^{1+}$--H($H_2O$) ~ 2.34 Å (166°)) while the α-axial His ligand is significantly displaced away ($Co^{1+}$--N(His) = 3.51 Å), thereby resulting in the formation of an effective H-bonded square pyramidal complex. The theoretical validation of H-bonded $Co^{1+}$Cbx complexes implied that the electron richness of $Co^{1+}$ ion rather than its net charge starts playing a deterministic role in governing the primary ligation sphere of the $Co^{1+}$ ion. The AIM analysis of the H-bonded $Co^{1+}$Cbl and $Co^{1+}$Cbi complexes predicted that the $Co^{1+}$--H interactions in the square pyramidal or octahedral complexes are H-bonding type interactions that either have a dominant electrostatic component or a very small covalence character. The computed reduction potentials of the $Co^{2+}/Co^{1+}$ couple using the possible coordination geometries of $Co^{1+}$Cbx model complexes implied that the $Co^{1+}$--H($H_2O$) interaction exerts a greater anodic shift (5 - 98 mV vs standard hydrogen electrode (SHE) in chloroform solvent) than the analogous $Co^{1+}$--H(Im) interaction (1 mV vs SHE) upon the reduction potential of

the $Co^{2+}/Co^{1+}$ couple. This provided an explanation as to why a β-axial $H_2O$ ligand has specifically been identified during the X-ray studies of certain methyltransferases such as MetH, Fe-S corrinoid proteins and methanol:cobalamin.

The DFT calculations and the X-ray crystal structure analysis described in the final chapter of this dissertation addressed the possibile involvement of the local enzyme scaffold especially that of the active site Y1139 residue of MetH enzyme in the $Co^{1+}$--H bond formation. The calculations on the $Co^{1+}$Cbi complexes indicated that the β-axial $H_2O$ or PhOH ligand tends to construct $Co^{1+}$--H interactions that contain a significant amount of long-range correlation and a noticeable amount of dispersion components respectively, and the PhOH ligand, a Y1139 mimick, forms stronger $Co^{1+}$--H contacts than $H_2O$ ligand due to its better H-donor capacity and supports the possibility of an alternate scenario where the PhOH ligand may be a β-axial ligand in the MetH-bound $Co^{2+}$Cbx. The analysis of the existing crystallographic data available for the reactivation conformation of MetH enzyme (1K7Y (3.0 Å); 1K98 (3.8 Å) and 3IVA (2.7 Å)) also corroborated our calculations as the Y1139 residue and the β-axial $H_2O$ ligand in the MetH-bound $Co^{2+}$Cbx complex are located at a similar distance from the $Co^{2+}$ ion (Y1139--$Co^{2+}$ = 3.97 Å; $H_2O$--$Co^{2+}$ = 3.96 Å). Taking into account that the $Co^{1+}$--H interactions tend to stabilize $Co^{1+}$Cbx, and the Y1139-induced $Co^{1+}$--H linkages are thermodynamically more stable than the $H_2O$-induced ones, the possibility of the Y1139 residue being the β-axial ligand in the catalytically competent reactivation conformation of MetH enzyme has been suggested.

# REFERENCES


(1) D. Dolphin, *$B_{12}$*; Wiley-Interscience: New York, **1982**.

(2) Drennan, C. L.; Huang, S.; Drummond, J. T.; Matthews, R. G.; Ludwig, M. L. *Science* **1994**, *266*, 1669-1674.

(3) Banerjee, R. *Chem. Biol.* **1997**, *4*, 175-186.

(4) Ludwig, M. L.; Matthews, R. G. *Annu. Rev. Biochem.* **1997**, *66*, 269-313.

(5) *Vitamin $B_{12}$ and $B_{12}$ Proteins* (Eds.: B. Kräutler, D. Arigoni, B. T. Golding), Wiley-VCH, New York, **1998** (Lectures Presented at the 4$^{th}$ European Symposium on Vitamin $B_{12}$ and $B_{12}$ Proteins).

(6) Marzilli, L. G. In *Bioinorganic Catalysis*; Reedijk, J.; Bouwman, E.; Eds.; Marcel Dekker: New York, **1999**; pp 423-468.

(7) Banerjee, R. *Chemistry and Biochemistry of $B_{12}$*, Wiley, New York, **1999**.

(8) Toraya, T. *Cell. Mol. Life Sci.* **2000**, *57*, 106-127.

(9) Banerjee, R. *Biochemistry* **2001**, *40*, 6191-6198.

(10) Matthews, R. G. *Acc. Chem. Res.* **2001**, *34*, 681-689.

(11) Banerjee, R.; Ragsdale, S. W. *Annu. Rev. Biochem.* **2003**, *72*, 209-247.

(12) Banerjee, R. *Chem. Rev.* **2003**, *103*, 2083-2094.

(13) Toraya, T. *Chem. Rev.* **2003**, *103*, 2095-2127.

(14) Brown, K. L. *Chem. Rev.* **2005**, *105*, 2075-2149.

(15) Randaccio, L.; Geremia, S.; Nardin, G.; Wuerges, J. *Coord. Chem. Rev.* **2006**, *250*, 1332-1350.

(16) Matthews, R. G.; Koutmos, M.; Datta, S. *Curr. Opin. Struct. Biol.* **2008**, *18*, 658-666.

(17) Randaccio, L.; Geremia, S.; Demitri, N.; Wuerges, J. *Trends Inorg. Chem.* **2009**, *11*, 1-19.

(18) Matthews, R. G. in *Metal Ions in Life Sciences*, Sigel, A.; Sigel, H.; Sigel, R. K. O., Eds.; Royal Society of Chemistry: Cambridge, UK, **2009**; Volume 6, pp. 53-114.

(19) Randaccio, L.; Geremia, S.; Demitri, N.; Wuerges, J. *Molecules* **2010**, *15*, 3228-3259.

(20) Shell, T. A.; Lawrence, D. S. *J. Am. Chem. Soc.* **2011**, *133*, 2148-2150.

(21) Kräutler, B.; Puffer, B. *Angew. Chem. Int. Ed. Engl.* **2011**, *50*, 2-4.

(22) R. G. Finke in *vitamin $B_{12}$ and $B_{12}$ Proteins* (Eds.: B. Krautler, D. Arigoni, B. T. Golding), Wiley-VCH, Weinheim, **1998**, chap. 25; b) S. Chowdhury, R. Banerjee, *Biochem.*, **2000**, 39, 7998-8006.

(23) Martin, B. D. ; Finke, R. G. *J. Am. Chem. Soc.* **1992**, *114*, 585-592.

(24) Hung, R. R.; Grabowski, J. J. *J. Am. Chem. Soc.* **1999**, *121*, 1359-1364.

(25) Halpern, J.; Kim, S. -H.; Leung, T. W. *J. Am. Chem. Soc.* **1984**, *106*, 8317-8319.

(26) Hay, B. P.; Finke, R. G. *Polyhedron* **1988**, *7*, 1469-1481.

(27) (a) Chen, L. H.; Yan, H.; Luo, L.; Cui, X. X.; Tang, W. X. *J. Inorg. Chem.* **1997**, *66*, 219. (b) Luo, L. B.; Li, G.; Chen, H. L.; Fu, S. W.; Zhang, S. Y. *J. Chem. Soc. Dalton Trans.* **1998**, 2103-2107. (c) Chen, H.; Li, G. Shang, F. F. Sun, L.; Chen. J. L.; Shang. S. Y. *Spectrochim. Acta A* **2003**, *59*, 2767.

(28) (a) Padmakumar, R.; Padmakumar, R.; Banerjee, R. *Biochemistry* **1998**, *37*, 11864-11872; (b) Marsh, E. N. G.; Ballou, D. P. *Biochemistry* **1998**, *37*, 11864-11872; (c) Hollaway, M. R.; White, H. A.; Joblin, K. N.; Johnson, A. W.; Lappert, A. W.; Wallis, O. C. *Eur. J. Biochem.* **1978**, *82*, 143-154; (d) Licht, S. S.; Booker, S.; Stubbe, J. *Biochemistry* **1999**, *38*, 1221-1233.

(29) Hay, B. P.; Finke, R. G. *J. Am. Chem. Soc.* **1986**, *108*, 4820-4829.

(30) Herein $Co^{2+}$Cbx and $Co^{1+}$Cbx have been used as abbreviations for the full cob(II)alamin and cob(I)alamin respectively. $Co^{2+}$Cbl and $Co^{1+}$Cbl represent their simplified versions where the corrin side chains as well as the nucleotide loop have been replaced by H's while $Co^{2+}$Cbi and $Co^{1+}$Cbi represent their mimicks where only the nucleotide loop of the corrin ring has been terminated at the phosphodiester end.

(31) Goulding, C. W.; Postigo, D.; Matthews, R. G. *Biochemistry* **1997**, *36*, 8082-8091.

(32) Ragsdale, S. W.; Wood, H. G. *J. Biol. Chem.* **1985**, *260*, 3970-3977.

(33) Sauer, K.; Thauer, R. K. *Chemistry and Biochemistry of $B_{12}$*, Ed Banerjee, R. Wiley, New York, **1999**, pp 655.

(34) (a) Burke, S. A.; Lo, S. L.; Krzycki, J. A. *J. Bacteriol.* **1998**, *180*, 3432-3440; (b) Ferguson Jr., D. J.; Gorlatova, N.; Grahame, D. A.; Krzycki, J. A. *J. Biol. Chem.* **2000**, *275*, 29053-29060; (c) Paul, L.; Ferguson, D. J.; Kryzycki, J. A. *J. Bacteriol.* **2000**, *182*, 2520-2529; (d) Tallant, T. C.; Paul, L.; Krzycki, J. A. *J. Biol. Chem.* **2001**, *276*, 4485-4493.

(35) Escalante-Semerena, J. C.; Suh, S. -J.; Roth, J. R. *J. Bactriol.* **1990**, *172*, 273-280.

(36) Suh, S.; Escalante-Semerena, J. C. *J. Bactriol.* **1995**, *177*, 921-925.

(37) Johnson, C. L.; Buszako, M. L.; Bobik, T. A. *J. Bactriol.* **2004**, *186*, 7781-7787.

(38) Buan, N. R.; Escalante-Semerena, J. C. *J. Biol. Chem.* **2006**, *281*, 16971-16977.

(39) Jensen, K. P. *J. Phys. Chem. B* **2005**, *109*, 10505-10512.

(40) Kumar, N.; Prieto, M. A-.; Rovira, C.; Lodowski, P.; Jaworska, M.; Kozlowski, P. M. *J. Chem. Theory Comput.* **2011**, *7*, 1541-1551.

(41) Halpern, J. *Science* **1985**, *227*, 869-875.

(42) Brown, K. L.; Zou, X. *J. Inorg. BioChem.* **1999**, *77*, 185-195.

(43) Padmakumar, R.; Padmakumar, R.; Banerjee, R. *Biochemistry* **1997**, *36*, 3713-3718.

(44) Bandarian, V.; Reed, G. H. *Biochemistry* **2000**, *39*, 12069-12075.

(45) Meier, T. W.; Thoma, N. H.; Leadlay, P. F. *Biochemistry* **1996**, *35*, 11791-11796.

(46) Chih, H. –W.; Marsh, E. N. G. *Biochemistry* **1999**, *38*, 13684-13691.

(47) Buckel, W.; Golding, B. T.; Kratky, C. *Chem. Eur. J.* **2006**, *12*, 352-362.

(48) Golding, B. T.; Radom, L. *J. Am. Chem. Soc.* **1976**, *98*, 6331-6338.

(49) (a) Shibata, N.; Masuda, J.; Tobimatsu, T.; Toraya, T.; Suto, K.; Morimoto, Y.; Yasuoka, N. *Structure* **1999**, *7*, 997-1008; (b) Masuda, J.; Shibata, N.; Morimoto, Y.; Toraya, T.; Yasuoka, N. *Structure* **2000**, *8*, 775-788; (c) Shibata, N.; Masuda, J.; Morimoto, Y.; Yasuoka, N.; Toraya, T. *Biochemistry* **2002**, *41*, 12607-12617; (d) Shibata, N.; Nakanishi, Y.; Fukuoka, M.; Yamanishi, M.; Yasuoka, N.; Toraya, T. *J. Biol. Chem.* **2003**, *278*, 22717-22725.

(50) (a) Yamanishi, M.; Yunoki, M.; Tobimatsu, T.; Sato, H.; Matsui, J.; Dokiya, A.; Luchi, Y.; Oe, K.; Suto, K.; Shibata, N.; Morimoto, Y.; Yasuoka, N.; Toraya, T. *Eur. J. Biochem.* **2002**, *269*, 4484-4494; (b) Liao, D. -I.; Dotson G.; Turner, Jr I.; Reiss, L.; Emptage, M. *J. Inorg. Biochem.* **2003**, *93*, 84-91.

(51) Hill, H. A. O.; Pratt, J. M.; Williams, R. J. P. *Chem. Br.* **1969**, *5*, 169-172.

(52) Grate, J. H.; Schrauzer, G. N. *J. Am. Chem. Soc.* **1979**, *101*, 4601-4611.

(53) De Ridder, D. J. A.; Zangrando, E.; Bürgi, H. -B. *J. Mol. Struct.* **1996**,*374*, 63-83.

(54) Dong, S. L.; Padmakumar, R.; Banerjee, R.; Spiro, T. G. *J. Am. Chem. Soc.* **1999**, *121*, 7063-7070.

(55) Bresciana-Pahor, N.; Forcolin, M.; Marzilli, L. G.; Randaccio, L.; Summers,M. F.; Toscano, P. J. *Coord. Chem. Rev.* **1985**, *63*, 1-47.

(56) Mancia, F.; Evans, P. R. *Structure* **1998**, *6*, 711-720.

(57) Vlasie, M. D.; Banerjee, R. *J. Am. Chem. Soc.* **2003**, *125*, 5431-5435.

(58) Thoma¨, N. H.; Meier, T. W.; Evans, P. R.; Leadlay, P. F. *Biochemistry* **1998**, *37*, 14386-14393.

(59) Toraya, T.; Ishida, A. *Biochemistry* **1988**, *27*, 7677-7682.

(60) Zhu, L.; Kostic, N. M. *Biochemistry* **1987**, *26*, 6-15.

(61) Scheuring, E.; Padmakumar, R.; Banerjee, R.; Chance, M. R. *J. Am. Chem. Soc.* **1997**, *119*, 12192-12200.

(62) Mancia, F.; Keep, N. H.; Nakagawa, A.; Leadlay, P. F.; McSweeney, S.; Rasmussen, B.; Bösecke, P.; Diat, O.; Evans, P. R. *Structure* **1996**, *4*, 339-350.

(63) Tollinger, M.; Konrat, R.; Hilbert, B. H.; Marsh, E. N. G.; Kräutler, B. *Structure* **1998**, *6*, 1021-1033.

(64) Trommel, J. S.; Warncke, K.; Marzilli, L. G. *J. Am. Chem. Soc.* **2001**,*123*, 3358-3366.

(65) Brooks, A. J.; Vlasie, M.; Banerjee, R.; Brunold, T. C. *J. Am. Chem. Soc.* **2004**, *126*, 8167-8180.

(66) Champloy, F.; Jogl, G.; Reitzer, R.; Buckel, W.; Bothe, H.; Beatrix, B.; Broeker, G.; Michalowicz, A.; Meyer-Klaucke, W.; Kratky, C. *J. Am. Chem. Soc.* **1999**, *121*, 11780-11789.

(67) (a) Dong, S.; Padmakumar, R.; Banerjee, R.; Spiro, T. G. *J. Am. Chem. Soc.* **1996**, *118*, 9182-9183; (b) Dong, S.; Padmakumar, R.; Banerjee, R.; Spiro, T. G. *Inorg. Chim. Acta* **1998**, *270,* 392-398; (c) Dong, S.; Padmakumar, R.; Maiti, N.; Banerjee, R.; Spiro, T. G. *J. Am. Chem. Soc.* **1998**, *120,* 9947-9948.

(68) Huhta, M. S.; Chen, H. -P.; Hemann, C.; Hille, C. R.; Marsh, E. N. G. *Biochemistry* **2001**, *355*, 131-137.

(69) The Co-C stretching vibration originally proposed for AdoCbl has been re-assigned; see Kozlowski, P. M.; Andruniow, T.; Jarzecki, A. A.; Zgierski, M. Z.; Spiro, T. G. *Inorg. Chem.* **2006**, *45,* 5585-5590.

(70) Jensen, K. P.; Ryde, U. *J. Mol. Struct. (THEOCHEM)* **2002**, *585*, 239-255.

(71) Dölker, N.; Maseras, F.; Lledos, A. *J. Phys. Chem. B* **2001**, *105*, 7564-7571.

(72) Sirovatka, J. M.; Rappe´, A. K.; Finke, R. G. *Inorg. Chim. Acta* **2000**, *300-302*, 545-555.

(73) (a) Reitzer, R.; Gruber, K.; Jogl, G.; Wagner, U. G.; Bothe, H.; Buckel, W.; Kratky, C. *Structure* **1999**, *7*, 891-902; (b) Gruber, K.; Reitzer, R.; Kratky, C. *Angew. Chem. Int. Ed. Engl.* **2001**, *40*, 3377-3380.

(74) Smith, D. M.; Golding, B. T.; Radom, L. *J. Am. Chem. Soc.* **1999**, *121*, 1037-1044.

(75) Smith, D. M.; Golding, B. T.; Radom, L. *J. Am. Chem. Soc.* **1999**, *121*, 1383-1384.

(76) Smith, D. M.; Golding, B. T.; Radom, L. *J. Am. Chem. Soc.* **1999**, *121*, 9388-9399.

(77) Wetmore, S. D.; Smith, D. M.; Radom, L. *ChemBioChem* **2001**, *2*, 919-922.

(78) Wetmore, S. D.; Smith, D. M.; Golding, B. T.; Radom, L. *J. Am. Chem. Soc.* **2001**, *123*, 7963-7972.

(79) Loferer, M. J.; Webb, B. M.; Brand, G. H.; Liedl, K. R. *J. Am. Chem. Soc.* **2003**, *125*, 1072-1078.

(80) Kamaschi, T.; Toraya, T.; Yoshizawa, K. *J. Am. Chem. Soc.* **2004**, *126*, 16207-16216.

(81) Jensen, K. P.; Ryde, U. *J. Am. Chem. Soc.* **2005**, 127, 9117-9128.

(82) Kozlowski, P. M.; Kamachi, T.; Toraya, T.; Yoshizawa, K. *Angew. Chem. Int. Ed. Engl.* **2007**, *46*, 980-983.

(83) Durbeej, B.; Sandala, G. M.; Bucher, D.; Smith, D. M.; Radom, L. *Chem. Eur. J.* **2009**, *15*, 8578-8585.

(84) Sharma, P. K.; Chu, Z. T.; Olsson, M. H. M.; Warshel, A. *Proc. Natl. Acad. Sci. USA* **2007**, *104*, 9661-9666.

(85) Li, X.; Chung, L. W.; Paneth, P.; Morokuma, K. *J. Am. Chem. Soc.* **2009**, *131*, 5115-5125.

(86) (a) Lexa, D.; Savéant, J-M. *J. Am. Chem. Soc.* **1978**, *100*, 3220-3222; (b) Lexa, D.; Savéant, J-M. *Acc. Chem. Res.* **1983**, *16*, 235-243.

(87) Kim, M. -H.; Birke, R. L. *J. Electroanal. Chem.* **1983**, *144*, 331-350.

(88) Ohkubo, K.; Fukuzumi, S. *J. Phys. Chem. A* **2005**, *109*, 1105-1113.

(89) Birke, R. L.; Huang, Q.; Spataru, T.; Gosser Jr, D. K. *J. Am. Chem. Soc.* **2006**, *128*, 1922-1936.

(90) Spataru, T.; Birke, R. L. *J. Electroanal. Chem.* **2006**, *593*, 74-86.

(91) Kozlowski, P. M.; Kuta, J.; Galezowski, W. *J. Phys. Chem. B* **2007**, *111*, 7638-7645.

(92) Galezowski, W.; Kuta, J.; Kozlowski, P. M. *J. Phys. Chem. B* **2008**, *112*, 3177-3183.

(93) Kumar, N.; Jaworska, M.; Lodowski, P.; Kumar, M.; Kozlowski, P. M. *J. Phys. Chem. B* **2011**, *115*, 6722-6731.

(94) Alfonso-Prieto, M.; Biarnés, X.; Kumar, M.; Rovira, C.; Kozlowski, P. M. *J. Phys. Chem. B* **2010**, *114*, 12965-12971.

(95) Jensen, K. P.; Ryde, U. *J. Am. Chem. Soc.* **2003**, *125*, 13970-13971.

(96) (a) Yikilmaz, E.; Porta, J.; Grove, L. E.; Vahedi-Faridi, A.; Bronshteyn, Y.; Brunold, T. C.; Borgstahl, G. E. O.; Miller, A. -F. *J. Am. Chem. Soc.* **2007,** *129*, 9927-9940; (b) Miller, A. -F. *Acc. Chem. Res.* **2008,** *41*, 501-510.

(97) Blomberg, M. R. A.; Siegbahn, P. E. M.; Babcock, G. T. *J. Am. Chem. Soc.* **1998**, *120*, 8812-8824.

(98) Shifman, J. M.; Gibney, B. R.; Sharp, R. E.; Dutton, P. L. *Biochemistry* **2000**, *39*,14813-14821.

(99) Kennedy, M. L.; Gibney, B. R. *Curr. Opin. Struct. Biol.* **2001**, 11, 485-490.

(100) Cowley, A. B.; Kennedy, M. L.; Silchenko, S.; Lukat-Rodgers, G. S.; Rodgers, K. R.; Bensen, D. R. *Inorg. Chem.* **2006**, *45*, 9985-10001.

(101) Fisher, M. T.; Sligar, S. G. *J. Am. Chem. Soc.* **1985**, *107*, 5018-5019.

(102) Tezcan, F. A.; Winkler, J. R.; Gray, H. B. *J. Am. Chem. Soc.* **1998**, *120*, 13383-13388.

(103) Battistuzzi, G.; Borsari, M.; Cowan, J. A.; Ranieri, A.; Sola, M. *J. Am. Chem. Soc.* **2002**, *124*, 5315-5324.

(104) Burris, D. R.; Delcomyn, C. A.; Smith, M. H.; Roberts, A. L. *Environ. Sci. Technol.* **1996**, *30*, 3047-3052.

(105) Burris, D. R.; Delcomyn, C. A.; Deng, B. L.; Buck, L. E.; Hatfield, K. *Environ. Toxicol. Chem.* **1998**, *17*, 1681-1688.

(106) Shey, J.; van der Donk, W. A. *J. Am. Chem. Soc.* **2000**, *122*, 12403-12404.

(107) Doherty, R. E. *Environ. Forensics* **2000**, *1*, 69-81.

(108) Drummond, J. T.; Huang, S.; Blumenthal, R. M.; Matthews, R. G. *Biochemistry* **1993**, *32*, 9290-9295.

(109) Menon, S.; Ragsdale, S. W. *J. Biol. Chem.* **1999**, *274*, 11513-11518.

(110) Jarrett, J. T.; Hoover, D. M.; Ludwig, M. L.; Matthews, R. G. *Biochemistry* **1998**, *37*, 12649-12658.

(111) Liptak, M. D.; Datta, S.; Matthews, R. G.; Brunold, T. C. *J. Am. Chem. Soc.* **2008**, *130*, 16374-16381.

(112) Fujii, K.; Galivan, J. H.; Huennekens, F. M. *Arch. Biochem. Biophys.* **1977**, *178*, 662-670.

(113) Wolthers, K. R.; Scrutton, N. S. *J. FEBS* **2009**, *276*, 1942-1951.

(114) Liptak, M. D.; Brunold, T. C. *J. Am. Chem. Soc.* **2006**, *128*, 9144-9156.

(115) Wirt, M. D.; Sagi, I.; Chance, M. R. *Biophys. J.* **1992**, *63*, 412-417.

(116) Koutmos, M.; Datta, S.; Pattridge, K. A.; Smith, J. L.; Matthews, R. G. *Proc. Natl. Acad. Sci. USA* **2009**, *106*, 18527-18532.

(117) Maurice, M. St; Mera, P. E.; Park, K.; Brunold, T. C.; Escalante-Semerena, J. C.; Rayment, I. *Biochemistry* **2008**, *47*, 5755-5766.

(118) Mera, P. E.; Maurice, M. St; Rayment, I.; Escalante-Semerena, J. C. *Biochemistry* **2009**, *48*, 3138-3145.

(119) Stich, T. A.; Yamanishi, M.; Banerjee, R.; Brunold, T. C. *J. Am. Chem. Soc.* **2005**, *127*, 7660-7661.

(120) Stich, T. A.; Buan, N. R.; Escalante-Semerena, J. C.; Brunold, T. C. *J. Am. Chem. Soc.* **2005**, *127*, 8710-8719.

(121) Stich, T. A.; Seravalli, J.; Venkateshrao, S.; Spiro, T. G.; Ragsdale, S. W.; Brunold, T. C. *J. Am. Chem. Soc.* **2006**, *128*, 5010-5020.

(122) Shi, S.; Daniels, L. M.; Espenson, J. H. *Inorg. Chem.* **1991**, *30*, 3407-3410.

(123) Hu, X. L.; Brunschwig, B. S.; Peters, J. C. *J. Am. Chem. Soc.* **2007**, *129*, 8988-8998.

(124) Voloshin, Y. Z.; Varzatskii, O. A.; Vorontsov, I. I.; Antipin, M. Y. *Angew. Chem. Int. Ed. Engl.* **2005**, *44*, 3400-3402.

(125) Dreos, R.; Geremia, S.; Randaccio, L.; Seiga, P. *The Chemistry of hydroxylamines, oximes and hydroxamic acids*, John Wiley & Sons Ltd., *Vol. 2*, chapter 15, page 903.)

(126) Calderazzo, F.; Facchinetti, G.; Marchetti, F.; Zanazzi, P. F. *J. Chem. Soc., Chem. Commun.* **1981**, 181.

(127) Brammer, L.; McCann, M. C.; Bullock, R. M.; McMullan, R. K.; Sherwood, P. *Organometallics* **1992**, *11*, 2339-2341.

(128) Brammer, L.; Zhao, D.; Ladipo, F. T.; Braddock-Wilking, J. *Acta Crystallogr. Sect.* B **1995**, *B51*, 632-640.

(129) Keum, C.; Kim, C.; Kim, C.; Kwak, H.; Moonhee Kwon, M.; Namgung, H. *Bull. Kor. Chem. Soc.* **1992**, *13*, 695-699.

(130) Brammer, L.; Charnock, J. M.; Goggin, P. L.; Goodfellow, R. J.; Koetzle, T. F.; Orpen, A. G. *J. Chem. Soc., Chem. Commun.* **1987**, 443.

(131) Brammer, L.; Charnock, J. M.; Goggin, P. L.; Goodfellow, R. J.; Koetzle, T. F.; Orpen, A. G. *J. Chem. Soc., Dalton Trans.* **1991**, 1789.

(132) Kozelka, J.; Bergès, J.; Attias, R.; Fraitag, J. *Angew. Chem. Int. Ed. Engl.* **2000**, *39*, 198-201.

(133) Rizzato, S.; Bergès, J.; Mason, S. A.; Albinati, A.; Kozelka, J. *Angew. Chem. Int. Ed. Engl.* **2010**, *49*, 7440-7443.

(134) Wienken, M.; Zangrando, E.; Randaccio, L.; Menzer, S.; Lippert, B. *J. Chem. Soc., Dalton Trans.* **1993**, 3349-3357.

(135) Baidina, A.; Podberezskaya, N. V.; Krylova, L. F.; Borisov, S. V. *J. Struct. Chem.* **1981**, *22*, 463-465.

(136) Braga, D.; Grepioni, F.; Tedesco, E.; Biradha, K.; Desiraju, G. R. *Organometallics* **1997**, *16,* 1846-1856.

(137) Brammer, L. *J. Chem. Soc., Dalton Trans.* **2003**, 3145-3157.

(138) Baidina, I. A.; Podberezskaya, N. V.; Krylova, L. F.; Borisov, S. V. *J. Struct. Chem.* **1981**, *22*, 463.

(139) Bandarian, V.; Pattridge, K. A.; Lennon, B. W.; Huddler, D. P.; Matthews, R. G.; Ludwig, M. L. *Nat. Struct. Biol.* **2002**, 9, 53-56.

(140) Mancia, F.; Smith, G. A.; Evans, P. R. *Biochemistry* **1999**, *38*, 7999-8005.

(141) Berkovitch, F.; Behshad, E.; Tang, K. H.; Enns, E. A.; Frey, P. A.; Drennan, C. L. *Proc. Natl. Acad. Sci. USA* **2004**, *101*, 15870-15875.

(142) (a) Stubbe, J.; van der Donk, W. A. *Chem. Rev.* **1998**, *98*, 705-762; (b) Pesavento, R. P.; van der Donk, W. A. *Adv. Protein Chem.* **2001**, *58*, 317-385.

(143) (a) Barry, B. A.; Babcock, G. T. *Proc. Natl. Acad. Sci. USA* **1987**, *84*, 7099-7103; (b) Barry, B. A.; El-Deeb, M. K.; Sandusky, P. O.; Babcock, G. T. *J. Biol. Chem.* **1990**, *265*, 20139-20143; (c) Meyer, T. J.; Huynh, M. H. V.; Thorp, H. H. *Angew. Chem. Int. Ed. Engl.* **2007**, *46*, 5284-5304.

(144) (a) Tsai, A. -L.; Kulmacz, R. J.; Palmer, G. *J. Biol. Chem.* **1995**, *270*, 10503-10508; (b) Tsai, A. -L.; Palmer, G.; Kulmacz, R. J. *J. Biol. Chem.* **1992**, *276*, 17753-17759; (c) Tsai, A. -L.; Palmer, G.; Xiao, G.; Swinney, D. C.; Kulmacz, R. J. *J. Biol. Chem.* **1998**, *273*, 3888-3894; (d) His, L. C.; Hoganson, C. W.; Babcock, G. T.; Smith, W. L. *Biochem. Biophys. Res. Commun.* **1994**, *202*, 1592-1598.

(145) (a) Whittaker, M. M.; Whittaker, J. W. *J. Biol. Chem.* **1990**, *265*, 9610-9613; (b) Himo, F.; Erikkson, L. A.; Maseras, F.; Siegbahn, P. E. M. *J. Am. Chem. Soc.* **2000**, *122*, 8031-8036; (c) Lee, Y. -K.; Whittaker, M. M.; Whittaker, J. W. *Biochemistry* **2008**, *47*, 6637-6649.

(146) (a) Ferguson-Miller, S.; Babcock, G. T. *Chem. Rev.* **1996**, *96*, 2889 - 2907; (b) Gamelin, D. R.; Randall, D. W.; Hay, M. T.; Houser, R.

P.; Mulder, T. C.; Canters, G. W.; de Vries, S.; Tolman, W. B.; Lu, Y.; Solomon, E. I. *J. Am. Chem. Soc.* **1998**, *120*, 5246-5263; (c) Proshlyakakov, D. A.; Pressler, M. A.; DeMaso, C.; Leykam, J. F.; Dewitt, D. L.; Babcock, G. T. *Science* **2000**, *290*, 1588-1591.

(147) Marohnick, C. C.; Crowley, L. J.; Davis, C. A.; Smith, E. T.; Barber, M. J. *Biochemistry* **2005**, *44*, 2449-2461.

(148) (a) Ehrenberg, A.; Reichard, P. *J. Biol. Chem.* **1972**, *247*, 3485-3488; (b) Sjöberg, B. –M.; Reichard, P.; Gräslund, A.; Ehrenberg, A. *J. Biol. Chem.* **1978**, *253*, 6863-6865; (c) Sahlin, M.; Gräslund, A.; Ehrenberg, A.; Sjöberg, B. –M. *J. Biol. Chem.* **1982**, *257*, 366-369; (d) Griepenburg, U.; Lassmann, G.; Auling, G. *Free Radical Res.* **1996**, *26*, 473-481; (e) Stubbe, J.; Nocera, D. G.; Yee, C. S. *Chem. Rev.* **2003**, *103*, 2167-2201.

(149) Rigby, S. E. J.; Hynson, R. M. G.; Ramsay, R. R.; Munro, A. W.; Scrutton, N. S. *J. Biol. Chem.* **2005**, *280*, 4627-4631.

(150) Chen, X.; Zhang, L.; Zhang, L.; Wang, J.; Liu, H.; Bu, Y. *J. Phys. Chem. B* **2009**, *113*, 16681-16688.

(151) Frisch, M. J.; Trucks, G. W.; Schlegel, H. B.; Scuseria, G. E.; Robb, M. A.; Cheeseman, J. R.; Montgomery, J. A., Jr.; Vreven, T.; Kudin, K. N.; Burant, J. C.; Millam, J. M.; Iyengar, S. S.; Tomasi, J.; Barone, V.; Mennucci, B.; Cossi, M.; Scalmani, G.; Rega, N.; Petersson, G. A.; Nakatsuji, H.; Hada, M.; Ehara, M.; Toyota, K.; Fukuda, R.; Hasegawa, J.; Ishida, M.; Nakajima, T.; Honda, Y.;

Kitao, O.; Nakai, H.; Klene, M.; Li, X.; Knox, J. E.; Hratchian, H. P.; Cross, J. B.; Bakken, V.; Adamo, C.; Jaramillo, J.; Gomperts, R.; Stratmann, R. E.; Yazyev, O.; Austin, A. J.; Cammi, R.; Pomelli, C.; Ochterski, J. W.; Ayala, P. Y.; Morokuma, K.; Voth, G. A.; Salvador, P.; Dannenberg, J. J.; Zakrzewski, V. G.; Dapprich, S.; Daniels, A. D.; Strain, M. C.; Farkas, O.; Malick, D. K.; Rabuck, A. D.; Raghavachari, K.; Foresman, J. B.; Ortiz, J. V.; Cui, Q.; Baboul, A. G.; Clifford, S.; Cioslowski, J.; Stefanov, B. B.; Liu, G.; Liashenko, A.; Piskorz, P.; Komaromi, I.; Martin, R. L.; Fox, D. J.; Keith, T.; Al-Laham, M. A.; Peng, C. Y.; Nanayakkara, A.; Challacombe, M.; Gill, P. M. W.; Johnson, B.; Chen, W.; Wong, M. W.; Gonzalez, C.; Pople, J. A. *Gaussian 03*, revision C.02; Gaussian, Inc.: Wallingford, CT, **2004**.

(152) (a) Becke, A. D. *J. Chem. Phys.* **1986**, *84*, 4524-4529; (b) Perdew, J. P. *Phys. Rev. B* **1986**, *33*, 8822-8824.

(153) Lee, C.; Yang, W.; Parr, R. G. *Phys. Rev. B* **1988**, *37*, 785.

(154) Jensen, K. P.; Ryde, U. *J. Phys. Chem. A* **2003**,*107*, 7539-7545.

(155) Dölker, N.; Morreale, A.; Maseras, F. *J. Biol. Inorg. Chem.* **2005**, *10*, 509-517.

(156) Kuta, J.; Patchkovskii, S.; Zgierski, M. Z.; Kozlowski, P. M. *J. Comput. Chem.* **2006**, *27*, 1429-1437.

(157) Nakano, H. *J. Chem. Phys.* **1993**, *99*, 7983-7992.

(158) Granovsky, A. A. PC GAMESS/Firefly version 7.1.F, www.http://classic.chem.msu.su/gran/gamess/index.html

(159) ChemShell, a Computational Chemistry Shell, see www.chemshell.org

(160) (a) Ahlrichs, R.; Bär, M.; Häser, M.; Horn, H.; Kölmel, C. Electronic structure calculations on workstation computers: The program system Turbomole, *Chem. Phys. Lett.* **1989**, *162*, 165-169. (b) Treutler, O.; Ahlrichs, R. *J. Chem. Phys.* **1995**, *102*, 346. (c) Furche, F.; Ahlrichs, R. *J. Chem. Phys.* **2002**, *117*, 7433. (d) Furche, F.; Rappoport, D. Density functional methods for excited states: equilibrium structure and electronic spectra, ch. III of "Computational Photochemistry", ed. by M. Olivucci, vol. 16 of "Theoretical and Computational Chemistry", Elsevier, Amsterdam, 2005. (e) TURBOMOLE has been designed by the Quantum Chemistry Group, University of Karlsruhe, Germany, since 1988. The following members of the group have made contributions: Reinhart Ahlrichs, Michael Bär, Hans-Peter Baron, Rüdiger Bauernschmitt, Stephan Böcker, Nathan Crawford, Peter Deglmann, Michael Ehrig, Karin Eichkorn, Simon Elliott, Filipp Furche, Frank Haase, Marco Häser, Christof Hättig, Arnim Hellweg, Hans Horn, Christian Huber, Uwe Huniar, Marco Kattannek, Andreas Köhn, Christoph Kölmel, Markus Kollwitz, Klaus May, Paola Nava, Christian Ochsenfeld, Holger Öhm, Holger Patzelt, Dmitrij

Rappoport, Oliver Rubner, Ansgar Schäfer, Uwe Schneider, Marek Sierka, Oliver Treutler, Barbara Unterreiner, Malte von Arnim, Florian Weigend, Patrick Weis, Horst Weiss, http://www.turbomole.com.

(161) CHARMM: A Program for Macromolecular Energy, Minimization, and Dynamics Calculations; Brooks, B. R.; Bruccoleri, R. E.; Olafson, B. D.; States, D. J.; Swaminathan, S.; Karplus, M. *J. Comput. Chem.* **1983,** *4,* 187-217.

(162) Finke, R. G.; Martin, B. D. *J. Inorg. Biochem.* **1990**, *40*, 19-22.

(163) Abend, A.; Illich, V.; Retey, J. *Eur. J. Biochem.* **1997**, *249*, 180-186.

(164) Roos, B. O.; Veryazov, V.; Conradie, J.; Taylor, P. R.; Ghosh, A. *J. Phys. Chem. B* **2008**, *112*, 14099-14102.

(165) Vlasie, M. D.; Banerjee, R. *Biochemistry* **2004**, *43*, 8410-8417.

(166) Padovani, D.; Banerjee, R. *Biochemistry* **2006**, *45*, 2951-2959.

(167) Swenson, R. P.; Krey, G. D. *Biochemistry* **1994**, *33*, 8505-8514.

(168) Li, M.; Binda, C.; Mattevi, A.; Edmondson, D. E. *Biochemistry* **2006**, *45*, 4777-4784.

(169) Royo, M.; Fitzpatrick, P. Fl. *Biochemistry* **2005**, *44*, 7079-7084.

(170) Loferer, M. J.; Webb, B. M.; Grant, G. H.; Leidl, K. R. *J. Am. Chem. Soc.* **2003**, *125*, 1072-1078.

(171) Zydowsky, T. M.; Courtney, L. F.; Frasca, V.; Kobayashi, K.; Shimizu, H.; Yuen, L. –D.; Matthews, R. G.; Benkovic, S. J.; Floss, H. G. *J. Am. Chem. Soc.* **1986**,*108*, 3152-3153.

(172) Kumar, M.; Kozlowski, P. M. *J. Phys. Chem. B* **2009**, *113*, 9050-9054.

(173) Kozlowski, P. M.; Kamachi, T.; Kumar, M.; Nakayama, T.; Yoshizawa, K. *J. Phys. Chem. B* **2010**, *114*, 5928-5937.

(174) Vass, I.; Styring, S. *Biochemistry* **1991**, *30*, 830-839.

(175) Brown, K. L.; Peck-Siler, S. *Inorg. Chem.* **1988**, *27*, 3548-3555.

(176) Sirovatka-Dorweiler, J.; Matthews, R. G.; Finke, R. G. *Inorg. Chem.* **2002**, *41*, 6217-6224.

(177) Schosser, S. G.; Hannak, R. B.; Konrat, R.; Gruber, K.' Mikl, C.; Kratky, C.; Kräutler, B. *Chem. Eur. J.* **2003**, *11*, 81-93.

(178) Fukuoka, M.; Nakanishi, Y.; Hannak, R. B.; Kräutler, B.; Toraya, T. *FEBS J.* **2005**, 272, 4787-4796.

(179) Friendorf, M.; Kozlowski, P. M. *J. Am. Chem. Soc.* **2004**, *126*, 1928-1929.

(180) (a) Becke, A. D. *J. Chem. Phys.* **1997**, *107*, 8554; (b) Hamprecht, F. A.; Cohen, A. J.; Tozer, D. J.; Handy, N. C. *J. Chem. Phys.* **1998**, *109*, 6264.

(181) Schmider, H. L.; Becke, A. D. *J. Chem. Phys.* **1998**, *108*, 9624.

(182) Grimme, S. J. *J. Comput. Chem.* **2006**, *27*, 1787-1799.

(183) Chai, J.-D.; Head-Gordon, M. *J. Chem. Phys.* **2008**, *128*, 084106.

(184) Chai, J. -D.; Head-Gordon, M. *Phys. Chem. Chem. Phys.* **2008**, *10*, 6615.

(185) Frisch, M. J. et al. *Gaussian 09*, revision C.02; Gaussian, Inc.: Wallingford, CT, **2009**.

(186) Kräutler, B.; Keller, W.; Kratky, C. *J. Am. Chem. Soc.* **1989**, *111*, 8938-8940.

(187) Ragsdale, S. W.; Wood, H. G. *J. Biol. Chem.* **1985**, *260*, 3970-3977.

(188) Marenich, A. V.; Cramer, C. J.; Truhlar, D. G. *J. Phys. Chem.* **2009**, *113*, 6378-6396.

(189) Bader, R. F. W. *Atoms in Molecules: A Quantum Theory*; Oxford University Press: New York **1990**.

(190) Reed, A. E.; Curtiss, L. A.; Weinhold, F. *Chem. Rev.* **1988**, *88*, 899-926.

(191) Wiberg, K. *Tetrahedron* **1968**, *24*, 1083-1096.

(192) Kumar, M.; Galezowski, W.; Kozlowski, P. M. *Int. J. Quant. Chem.* **2012** (accepted).

(193) Trasatti, S. *Pure Appl. Chem.* **1986**, *58*, 955-966.

(194) (a) Lewis, A.; Bumpus, J. A.; Truhlar, D. G.; Cramer, C. J. *J. Chem. Edu.* **2004**, *81*, 596-604; (b) Lewis, A.; Bumpus, J. A.; Truhlar, D. G.; Cramer, C. J. *J. Chem. Edu.* **2007**, *84*, 934.

(195) Yao, W.; Eisenstein, O.; Crabtree, R. H. *Inorg. Chim. Acta* **1997**, *254*, 105-111.

(196) Lonsdale, R.; Harvey, J. N.; Mullholand, A. J. *J. Phys. Chem. Lett.* **2010**, *1*, 3232-3237.

(197) Moss, R. A.; Wang, L.; Odorisio, C. M.; Jespersen, K. K-. *J. Am. Chem. Soc.* **2010**, *132*, 10677-10679.

(198) (a) Iwaoka, M.; Komatsu, H.; Katsuda, T.; Tomoda, S. *J. Am. Chem. Soc.* **1996**, *118*, 8077-8084; (b) Iwaoka, M.; Komatsu, H.; Katsuda, T.; Tomoda, S. *J. Am. Chem. Soc.* **2004**, *126*, 5309-5317; (c) Iwaoka, M.; Komatsu, H.; Katsuda, T.; Tomoda, S. *J. Am. Chem. Soc.* **2002**, *124*, 1902-1909.

(199) Shi, S.; Daniels, L. M.; Espenson, J. H. *Inorg. Chem.* **1991**, *30*, 3407.

(200) Hu, X. L.; Brunschwig, B. S.; Peters, J. C. *J. Am. Chem. Soc.* **2007**, *129*, 8988-8998.

(201) Voloshin, Y. Z.; Varzatskii, O. A.; Vorontsov, I. I.; Antipin, M. Y. *Angew. Chem. Int. Ed. Engl.* **2005**, *44*, 3400-3402.

(202) Kumar, M.; Kozlowski, P. M. *Angew. Chem. Int. Ed. Engl.* **2011**, *50*, 8705-8707.

(203) (a) Li, H.; Robertson, A. D.; Jensen, J. H. *Proteins* **2005**, *61*, 704-721; b) Bas, D. C.; Rogers, D. M.; Jensen, J. H. *Proteins* **2008**, *73*, 765-783.

(204) Besler, B. H.; Merz, K. M.; Kollman, P. A. *J. Comput. Chem.* **1990**, *11*, 431-439.

(205) Popelier, P. *Atoms in Molecules: An Introduction*; Pearson Education: Harlow **2000**.

(206) Rozas, I.; Alkorta, I.; Elguero, J. *J. Am. Chem. Soc.* **2000**, *122*, 11154-11161.

(207) Brookharta, M.; Green, M. L. H.; Parkin, G. *Proc. Natl. Acad. Sci. USA* **2007**, *104*, 6908-6914.

(208) Kumar, M.; Kumar, N.; Hirao, H.; Kozlowski, P. M. *Inorg. Chem.* **2012** (accepted).

(209) Hagemeier, C. H.; Kruer, M.; Thauer, R. K.; Warkentin, E.; Ermler, U. *Proc. Natl. Acad. Sci. USA* **2006**, *103*, 18917-18922.

(210) Svetlitchnaia, T.; Svetlitchnyi, V.; Meyer, O.; Dobbek, H. *Proc. Natl. Acad. Sci. USA* **2006**, *103*, 14331-14336.

(211) Jarrett, J. T.; Huang, S.; Matthews, R. G. *Biochemistry* **1998**, *37*, 5372-5382.

(212) Humphrey, W.; Dalke, A.; Schulten, K. *J. Mol. Graphics* **1996**, *14*, 33-38.

(213) Marques, H. M.; Ngoma, B.; Eganb, T. J.; Brown, K. L. *J. Mol. Struct.* **2001**, *561*, 71-91.

(214) (a) Svensson, M.; Humbel, S.; Froese, R. D. J.; Matsubara, T.; Sieber, S.; Morokuma, K. *J. Phys. Chem.* **1996**, *100*, 19357-19363; (b) Vreven, T.; Byun, K. S.; Komáromi, I.; Dapprich, S.; Montgomery, J. A.; Morokuma, K.; Frisch, M. J. *J. Chem. Theory Comput.* **2006**, *2*, 815-826.

(215) Cornell, W. D.; Cieplak, P.; Bayly, C. I.; Gould, I. R.; Merz Jr., K. M.; Ferguson, D. M.; Spellmeyer, D. C.; Fox, T.; Caldwell, J. W.; Kollman, P. A. *J. Am. Chem. Soc.* **1995**, *117*, 5179-5197.

(216) Schrauzer, G. N.; Deutsch, E. *J. Am. Chem. Soc.* **1969**, *91*, 3341-3350.

(217) Saillard, J. -Y.; Hoffmann, R. *J . Am. Chem. Soc.* **1984**, *106,* 2006-2026.

(218) Sundquist, W. I.; Bancroft, D. P.; Lippard, S. J. *J. Am. Chem. Soc.* **1990**, *112*, 1590-1596.

(219) Koch, U.; Popelier, P. L. A. *J. Phys. Chem.* **1995**, *99*, 9747-9754.

(220) Brown, K. L.; Hakimi, J. M.; Nuss, D. M.; Montejano, Y. D.; Jacobsen, D. W. *Inorg. Chem.***1984**, *23*, 1463-1471.

(221) Brown, K. L.; Pecksiler, S. *Inorg. Chem.* **1988**, *27*, 3548-3555.

(222) Fleischhacker, A. S.; Matthews, R. G. *Biochemistry* **2007**, *46*, 12382-12392.

(223) Liptak, M. D.; Fleischhacker, A. S.; Matthews, R. G.; Brunold, T. C. *Biochemistry* **2007**, *46*, 8024-8035.

# LIST OF ABBREVIATIONS

| | |
|---|---|
| XCbl | general cobalamin |
| RCbl | alkylcobalamin |
| AdoCbl | adenosylcobalamin |
| Ado | adenosyl group |
| Ado$^{\bullet}$ | adenosyl radical |
| MeCbl | methylcobalamin |
| Me | methyl group |
| CNCbl | cyanocobalamin |
| $B_{12}$ cofactors | MeCbl and AdoCbl |
| Vitamin $B_{12}$ | CNCbl |
| Coenzyme $B_{12}$ | AdoCbl |
| $\alpha$-face | lower face |
| $\beta$-face | upper face |
| DBI | dimethylbenzimidazole |
| BDE | bond dissociation energy |
| MCM | methylmalonyl coA mutase |
| GLM | glutamate mutase |
| QM/MM | quantum mechanics/molecular mechanics |
| DFT | density functional theory |
| CASSCF | complete active space self-consistent field |
| $Co^{2+}$Cbx | enzyme-bound cob(II)alamin |
| $Co^{2+}$Cbi | cob(II)alamin with only nucleotide group truncated |
| $Co^{2+}$Cbl | cob(II)alamin with all side chains truncated |
| $Co^{1+}$Cbx | enzyme-bound cob(I)alamin |
| $Co^{1+}$Cbi | cob(I)alamin with only nucleotide group truncated |
| $Co^{1+}$Cbl | cob(I)alamin with all side chains truncated |
| $Co^{2+}/Co^{1+}$ | cob(II)alamin/cob(I)alamin |
| MetH | methionine synthase |
| CFeSP | corrinoid iron-sulfur protein |
| ACAs | ATP:corrinoid adenosyltransferases |
| Y | active site tyrosine residue |
| F | phenylalanine |
| Y$^{\bullet}$ | tyrosyl radical |
| ET | electron transfer |
| PT | proton transfer |
| PCET | proton-coupled electron transfer |

| | |
|---|---|
| H-atom | hydrogen atom |
| TS | transition state |
| SCE | saturated calomel electrode |
| Gln | glutamine residue |
| SOD | superoxide dismutase |
| PS-II | photosystem-II |
| PDB | protein data bank |
| RibCbl | ribosecobalamin |
| Rib | ribosyl group |
| $Rib^{\bullet}$ | ribosyl radical |
| AdoMet | adenosyl-L-methionine |
| SHE | standard hydrogen electrode |
| PCM | polarizable continuum model |
| AIM | atoms in molecule |
| NBO | natural bond orbital |
| PhOH | phenol |
| PhO- | phenolate anion |
| $PhO^{\bullet}$ | phenoxyl radical |
| 1el-Red | one-electron reduced |
| $[AdoCbl]^{\bullet-}$ | 1el-Red AdoCbl |
| UHF | unrestricted hartree Fock |
| $<S^{**2}>$ | expectation value of the square of spin |
| His | histidine residue |
| $-COO^{-}$ | carboxylate anion |
| DMF | dimethylformamide |
| Im | imidazole |
| ZPE | zero point energy |
| $N_{ax}$ | axial nitrogen |
| IRC | intrinsic reaction coordinate |
| $C_{sub}$ | carbon atom of the substrate |
| BSSE | basis set superposition error |
| WBI | Wiberg bond index |
| BCP | bond critical point |
| E | active site glutamate residue |
| R | active site arginine residue |
| Res. | Resolution |
| $\rho(r)$ | electron density |
| $\nabla\rho(r)$ | gradient of electron density |
| $\nabla^2\rho(r)$ | Laplacian of electron density |
| H(r) | total charge density |
| $\varepsilon$ | dielectric constant |
| CT | charge transfer |
| BCT | back charge transfer |
| $\Delta E^{(2)}_{CT}$ | second order stabilization energy due to CT |
| $\Delta E^{(2)}_{BCT}$ | second order stabilization energy due to BCT |
| Met | methionine |

| | |
|---|---|
| Hcy | homocysteine |

# APPENDIX

**Table A1:** BP86 computed Spin Density Distribution in the structural mimics of GLM and MCM

| Model Complex | <S*²> value | Corrin spin | Tyrosine spin (odd-alternant pattern) | | | |
|---|---|---|---|---|---|---|
| | | | O7 | C1 | C4 | C8 |
| AdoCbl-PhOH (GLM) | 0.0000 | 0.000499 | 0.0000 | 0.0000 | 0.0000 | 0.000 |
| AdoCbl-PhO⁻ (GLM) | 1.0028 | -0.994421 | 0.5349 | 0.2118 | 0.1753 | 0.1739 |
| AdoCbl-PhOH (MCM) | 0.0000 | 0.00010 | 0.0000 | 0.0000 | 0.0000 | 0.0000 |
| AdoCbl-PhO⁻ (MCM) | 1.0007 | -0.989755 | 0.5405 | 0.2340 | 0.1997 | 0.1945 |

**Table A2:** B3LYP Computed Spin Density Distribution in the Structural Mimics of GLM and MCM

| Model Complex | <S*²> value | Corrin spin | Tyrosine spin (odd-alternant pattern) | | | |
|---|---|---|---|---|---|---|
| | | | O7 | C1 | C4 | C8 |
| AdoCbl-PhOH (GLM) | 0.0002 | 0.000446 | 0.0000 | 0.0000 | 0.0000 | 0.0000 |
| AdoCbl-PhO⁻ (GLM) | 0.6278 | -0.60327 | 0.3968 | 0.1669 | 0.1535 | 0.1520 |
| AdoCbl-PhOH (MCM) | 0.0002 | 0.000524 | 0.0000 | 0.0000 | 0.0000 | 0.0000 |
| AdoCbl-PhO⁻ (MCM) | 0.7356 | -0.707306 | 0.4522 | 0.1986 | 0.1794 | 0.1742 |

**Table A3**: Key structural features of the optimized $Co^{2+}$Cbi--$OH_2$ complex (bond lengths and bond angle are expressed in Å and degree respectively)

| Theoretical Method | Co-$N_{21}$ | Co-$N_{22}$ | Co-$N_{23}$ | Co-$N_{24}$ | Co-$O_{H2O}$ |
|---|---|---|---|---|---|
| HF/6-31++G(d,p) | 1.93 | 1.96 | 1.96 | 1.93 | 2.53 |
| BP86/6-31++G(d,p) | 1.88 | 1.93 | 1.93 | 1.87 | 2.29 |
| ωB97X/6-31++G(d,p) | 1.89 | 1.92 | 1.93 | 1.89 | 2.36 |
| ωB97X-D/6-31++G(d,p) | 1.88 | 1.92 | 1.92 | 1.88 | 2.35 |
| B97-1/6-31++G(d,p) | 1.88 | 1.94 | 1.94 | 1.88 | 2.39 |
| B98/6-31++G(d,p) | 1.89 | 1.94 | 1.94 | 1.88 | 2.40 |
| B97-D/6-31++G(d,p) | 1.88 | 1.94 | 1.94 | 1.88 | 2.30 |

**Table A4**: Key structural features of the optimized $Co^{2+}$Cbi--$OH_2$ complex (bond lengths and bond angle are expressed in Å and degree respectively)

| Theoretical Method | Co-$N_{21}$ | Co-$N_{22}$ | Co-$N_{23}$ | Co-$N_{24}$ | Co-$O_{H2O}$ |
|---|---|---|---|---|---|
| HF/6-31G(d) 5d | 1.93 | 1.96 | 1.95 | 1.94 | 2.42 |
| BP86/6-31G(d) 5d | 1.85 | 1.91 | 1.90 | 1.86 | 2.23 |
| ωB97X/6-31G(d) 5d | 1.87 | 1.91 | 1.90 | 1.88 | 2.28 |
| Ωb97X-D/6-31G(d) 5d | 1.86 | 1.91 | 1.90 | 1.87 | 2.28 |
| B97-1/6-31G(d) 5d | 1.87 | 1.93 | 1.91 | 1.88 | 2.31 |
| B98/6-31G(d) 5d | 1.87 | 1.93 | 1.91 | 1.88 | 2.31 |
| B97-D/6-31G(d) 5d | 1.85 | 1.92 | 1.91 | 1.86 | 2.28 |

**Table A5**: Key structural features of the optimized $Co^{2+}$Cbl--Im complex (bond lengths and bond angle are expressed in Å and degree respectively)

| Theoretical Method | Co-$N_{21}$ | Co-$N_{22}$ | Co-$N_{23}$ | Co-$N_{24}$ | Co-$N_{Im}$ |
|---|---|---|---|---|---|
| HF/6-31++G(d,p) | 1.94 | 1.97 | 1.97 | 1.94 | 2.40 |
| BP86/6-31++G(d,p) | 1.88 | 1.94 | 1.93 | 1.88 | 2.14 |
| ωB97X/6-31++G(d,p) | 1.89 | 1.94 | 1.93 | 1.90 | 2.22 |
| ωB97X-D/6-31++G(d,p) | 1.88 | 1.93 | 1.93 | 1.89 | 2.18 |
| B97-1/6-31++G(d,p) | 1.89 | 1.95 | 1.94 | 1.89 | 2.22 |
| B98/6-31++G(d,p) | 1.89 | 1.95 | 1.94 | 1.89 | 2.23 |
| B97-D/6-31++G(d,p) | 1.88 | 1.94 | 1.94 | 1.88 | 2.12 |

**Table A6**: Key structural features of the optimized $Co^{2+}$Cbi--Im complex (bond lengths and bond angle are expressed in Å and degree respectively)

| Theoretical Method | Co-$N_{21}$ | Co-$N_{22}$ | Co-$N_{23}$ | Co-$N_{24}$ | Co-$N_{Im}$ |
|---|---|---|---|---|---|
| HF/6-31G(d) 5d | 1.95 | 1.98 | 1.96 | 1.96 | 2.45 |
| BP86/6-31G(d) 5d | 1.86 | 1.92 | 1.90 | 1.87 | 2.15 |
| ωB97X/6-31G(d) 5d | 1.88 | 1.92 | 1.90 | 1.89 | 2.25 |
| ωB97X-D/6-31G(d) 5d | 1.87 | 1.92 | 1.90 | 1.88 | 2.21 |
| B97-1/6-31G(d) 5d | 1.88 | 1.94 | 1.92 | 1.89 | 2.27 |
| B98/6-31G(d) 5d | 1.88 | 1.94 | 1.92 | 1.89 | 2.27 |
| B97-D/6-31G(d) 5d | 1.86 | 1.92 | 1.91 | 1.86 | 2.12 |

**Table A7**: Key structural features of the optimized $H_2O$--$Co^{2+}$Cbl--Im complex (bond lengths and bond angle are expressed in Å and degree respectively)

| Theoretical Method | Co-$N_{21}$ | Co-$N_{22}$ | Co-$N_{23}$ | Co-$N_{24}$ | Co-$N_{Im}$ | Co-$O_{H2O}$ |
|---|---|---|---|---|---|---|
| HF/6-31++G(d,p) | 1.94 | 1.97 | 1.97 | 1.94 | 2.48 | 2.96 |
| BP86/6-31++G(d,p) | 1.88 | 1.94 | 1.93 | 1.88 | 2.15 | 3.35 |
| ωB97X/6-31++G(d,p) | 1.89 | 1.94 | 1.93 | 1.89 | 2.28 | 2.61 |
| ωB97X-D/6-31++G(d,p) | 1.89 | 1.93 | 1.93 | 1.89 | 2.25 | 2.57 |
| B97-1/6-31++G(d,p) | 1.89 | 1.95 | 1.94 | 1.89 | 2.29 | 2.79 |
| B98/6-31++G(d,p) | 1.89 | 1.95 | 1.94 | 1.89 | 2.29 | 2.83 |
| B97-D/6-31++G(d,p) | 1.88 | 1.94 | 1.94 | 1.88 | 2.14 | 2.97 |

**Table A8**: Key structural features of the optimized $H_2O$--$Co^{2+}$Cbi--Im complex (bond lengths and bond angle are expressed in Å and degree respectively)

| Theoretical Method | Co-$N_{21}$ | Co-$N_{22}$ | Co-$N_{23}$ | Co-$N_{24}$ | Co-$N_{Im}$ | Co-$O_{H2O}$ |
|---|---|---|---|---|---|---|
| HF/6-31G(d) 5d | 1.94 | 1.97 | 1.96 | 1.95 | 2.53 | 3.65 |
| BP86/6-31G(d) 5d | 1.86 | 1.92 | 1.91 | 1.87 | 2.14 | 4.36 |
| ωB97X/6-31G(d) 5d | 1.88 | 1.92 | 1.90 | 1.89 | 2.23 | 4.13 |
| ωB97X-D/6-31G(d) 5d | 1.87 | 1.92 | 1.90 | 1.88 | 2.21 | 3.98 |
| B97-1/6-31G(d) 5d | 1.88 | 1.94 | 1.91 | 1.89 | 2.25 | 4.26 |
| B98/6-31G(d) 5d | 1.88 | 1.94 | 1.91 | 1.89 | 2.25 | 4.26 |
| B97-D/6-31G(d) 5d | 1.85 | 1.92 | 1.91 | 1.86 | 2.12 | 4.18 |

**Table A9**: Key structural features of the optimized $Co^{1+}$Cbl--**H**-O-H complex (bond lengths and bond angle are expressed in Å and degree respectively)

| Theoretical Method | Co-$N_{21}$ | Co-$N_{22}$ | Co-$N_{23}$ | Co-$N_{24}$ | Co-H | Co-O | Co-H-O |
|---|---|---|---|---|---|---|---|
| HF/6-31++G(d,p) | 1.94 | 1.96 | 1.96 | 1.94 | 2.62 | 3.54 | 164.61 |
| BP86/6-31++G(d,p) | 1.84 | 1.91 | 1.91 | 1.84 | 2.29 | 3.29 | 170.32 |
| ωB97X/6-31++G(d,p) | 1.86 | 1.91 | 1.91 | 1.86 | 2.41 | 3.37 | 168.90 |
| ωB97X-D/6-31++G(d,p) | 1.85 | 1.90 | 1.90 | 1.85 | 2.39 | 3.33 | 162.98 |
| B97-1/6-31++G(d,p) | 1.86 | 1.91 | 1.91 | 1.86 | 2.39 | 3.36 | 170.36 |
| B98/6-31++G(d,p) | 1.86 | 1.91 | 1.91 | 1.85 | 2.39 | 3.35 | 170.77 |
| B97-D/6-31++G(d,p) | 1.85 | 1.92 | 1.91 | 1.85 | 2.44 | 3.40 | 168.06 |

**Table A10**: Key structural features of the optimized $Co^{1+}$Cbi--**H**-O-H complex (bond lengths and bond angle are expressed in Å and degree respectively)

| Theoretical Method | Co-$N_{21}$ | Co-$N_{22}$ | Co-$N_{23}$ | Co-$N_{24}$ | Co-H | Co-O | Co-H-O |
|---|---|---|---|---|---|---|---|
| HF/6-31G(d) 5d | 1.92 | 1.95 | 1.94 | 1.93 | 2.55 | 3.48 | 166.24 |
| BP86/6-31G(d) 5d | 1.82 | 1.89 | 1.88 | 1.83 | 2.45 | 3.42 | 166.11 |
| ωB97X/6-31G(d) 5d | 1.83 | 1.88 | 1.88 | 1.84 | 2.44 | 3.40 | 167.04 |
| ωB97X-D/6-31G(d) 5d | 1.82 | 1.88 | 1.87 | 1.84 | 2.42 | 3.37 | 166.27 |
| B97-1/6-31G(d) 5d | 1.83 | 1.90 | 1.89 | 1.84 | 2.52 | 3.47 | 164.70 |
| B98/6-31G(d) 5d | 1.83 | 1.90 | 1.89 | 1.84 | 2.52 | 3.47 | 164.64 |
| B97-D/6-31G(d) 5d | 1.82 | 1.90 | 1.89 | 1.83 | 2.56 | 3.51 | 160.93 |

**Table A11:** Computed thermodynamic data for the $Co^{1+}$Cbl--**H**-O-H complex formation reaction studied in **gas phase** while assuming standard state convention of 1atm and 298.15 K (all thermodynamic parameters are given in kcal/mol units)

| Theoretical Method | $Co^{1+}$Cbl + $H_2O$ ⟶ $Co^{1+}$Cbl--H-O-H | | | | |
|---|---|---|---|---|---|
| | ΔE | ΔU | ΔH | -TΔS | ΔG |
| HF/6-31++G(d,p) | -4.12 | -3.30 | -3.89 | 6.10 | 2.21 |
| BP86/6-31++G(d,p) | -5.54 | -4.91 | -5.51 | 6.94 | 1.43 |
| ωB97X/6-31++G(d,p) | -8.09 | -7.48 | -8.07 | 7.53 | -0.54 |
| ωB97X-D/6-31++G(d,p) | -8.80 | -8.18 | -8.77 | 7.61 | -1.16 |
| B97-1/6-31++G(d,p) | -6.18 | -5.54 | -6.13 | 7.34 | 1.21 |
| B98/6-31++G(d,p) | -5.84 | -5.21 | -5.80 | 7.30 | 1.49 |
| B97-D/6-31++G(d,p) | -9.14 | -8.40 | -8.99 | 6.56 | -2.42 |

**Table A12:** Computed thermodynamic data for the $Co^{1+}$Cbi--**H**-O-H complex formation reaction studied in **gas Phase** while assuming standard state convention of 1atm and 298.15 K (all thermodynamic parameters are given in kcal/mol units)

| Theoretical Method | $Co^{1+}$Cbi + $H_2O$ ⟶ $Co^{1+}$Cbi--H-O-H | | | | |
|---|---|---|---|---|---|
| | ΔE | ΔU | ΔH | -TΔS | ΔG |
| HF/6-31G(d) 5d | -9.60 | -9.57 | -10.16 | 9.81 | -0.35 |
| BP86/6-31G(d) 5d | -13.91 | -14.04 | -14.63 | 9.57 | -5.06 |
| ωB97X/6-31G(d) 5d | -17.04 | -17.23 | -17.82 | 10.43 | -7.39 |
| ωB97X-D/6-31G(d) 5d | -18.62 | -18.64 | -19.23 | 9.97 | -9.26 |
| B97-1/6-31G(d) 5d | -1447 | -14.59 | -15.18 | 9.97 | -5.21 |
| B98/6-31G(d) 5d | -13.88 | -13.98 | -14.57 | 10.01 | -4.56 |
| B97-D/6-31G(d) 5d | -19.09 | -19.03 | -19.63 | 9.46 | -10.16 |

**Table A13:** Computed Thermodynamic Data for the $Co^{1+}$Cbl--**H**-O-H Complex Formation Reaction studied in **Chloroform solution** assuming standard state convention of 1atm and 298.15 K (all thermodynamic parameters are given in kcal/mol units).

| Theoretical Method | $Co^{1+}$Cbl + $H_2O$ ⟶ $Co^{1+}$Cbl--H-O-H | | | | |
|---|---|---|---|---|---|
| | ΔE | ΔU | ΔH | -TΔS | ΔG |
| HF/6-31++G(d,p) | -2.00 | -1.16 | -1.75 | 6.01 | 4.30 |
| BP86/6-31++G(d,p) | -4.38 | -3.74 | -4.34 | 7.04 | 2.67 |
| ωB97X/6-31++G(d,p) | -5.92 | -5.25 | -5.84 | 7.37 | 1.66 |
| ωB97X-D/6-31++G(d,p) | -6.92 | -6.20 | -6.80 | 7.23 | 0.59 |
| B97-1/6-31++G(d,p) | -4.78 | -4.00 | -4.59 | 6.15 | 1.56 |
| B98/6-31++G(d,p) | -4.33 | -3.64 | -4.23 | 6.89 | 2.67 |
| B97-D/6-31++G(d,p) | -7.50 | -6.91 | -7.50 | 7.60 | 0.18 |

**Table A14:** Computed thermodynamic data for the $Co^{1+}$Cbl--**H**-O-H complex formation reaction studied in **acetonitrile solution** while assuming standard state convention of 1atm and 298.15 K (all thermodynamic parameters are given in kcal/mol units)

| Theoretical Method | $Co^{1+}$Cbl + $H_2O$ ⟶ $Co^{1+}$Cbl--H-O-H | | | | |
|---|---|---|---|---|---|
| | ΔE | ΔU | ΔH | -TΔS | ΔG |
| HF/6-31++G(d,p) | -0.92 | -0.01 | -0.60 | 5.99 | 5.38 |
| BP86/6-31++G(d,p) | -3.82 | -3.71 | -4.31 | 8.54 | 4.02 |
| ωB97X/6-31++G(d,p) | -4.94 | -4.23 | -4.82 | 6.94 | 2.12 |
| ωB97X-D/6-31++G(d,p) | -5.89 | -5.26 | -5.85 | 7.32 | 1.42 |
| B97-1/6-31++G(d,p) | -3.98 | -3.25 | -3.84 | 6.32 | 2.31 |
| B98/6-31++G(d,p) | -3.69 | -2.95 | -3.54 | 6.34 | 2.61 |
| B97-D/6-31++G(d,p) | -6.93 | -6.41 | -7.00 | 7.89 | 0.77 |

**Table A15:** Computed thermodynamic data for the $Co^{1+}$Cbl--**H**-O-H complex formation reaction studied in **water solution** while assuming standard state convention of 1atm and 298.15 K (all thermodynamic parameters are given in kcal/mol units)

| Theoretical Method | $Co^{1+}$Cbl + $H_2O$ ⟶ $Co^{1+}$Cbl--H-O-H | | | | |
|---|---|---|---|---|---|
| | ΔE | ΔU | ΔH | -TΔS | ΔG |
| HF/6-31++G(d,p) | -0.82 | 0.10 | -0.49 | 5.88 | 5.26 |
| BP86/6-31++G(d,p) | -3.76 | -3.65 | -4.24 | 8.46 | 4.52 |
| ωB97X/6-31++G(d,p) | -4.84 | -4.11 | -4.70 | 6.68 | 2.03 |
| ωB97X-D/6-31++G(d,p) | -5.88 | -5.19 | -5.79 | 6.88 | 1.21 |
| B97-1/6-31++G(d,p) | -3.89 | -3.19 | -3.78 | 6.86 | 3.38 |
| B98/6-31++G(d,p) | -3.58 | -2.88 | -3.47 | 6.85 | 3.71 |
| B97-D/6-31++G(d,p) | -6.88 | -6.36 | -6.95 | 7.86 | 1.08 |

**Table A16:** Computed Thermodynamic Data for the $Co^{1+}$Cbi--**H**-O-H Complex Formation Reaction studied in **Chloroform solution** while assuming standard state convention of 1atm and 298.15 K (all thermodynamic parameters are given in kcal/mol units)

| Theoretical Method | $Co^{1+}Cbi + H_2O \longrightarrow Co^{1+}Cbi$--H-O-H | | | | |
|---|---|---|---|---|---|
| | ΔE | ΔU | ΔH | -TΔS | ΔG |
| HF/6-31G(d) 5d | -4.50 | -4.43 | -5.02 | 9.69 | 4.85 |
| BP86/6-31G(d) 5d | -10.00 | -10.11 | -10.70 | 10.09 | -0.48 |
| ωB97X/6-31G(d) 5d | -12.76 | -12.86 | -13.45 | 9.69 | -3.64 |
| ωB97X-D/6-31G(d) 5d | -14.63 | -14.67 | -15.26 | 10.40 | -4.69 |
| B97-1/6-31G(d) 5d | -10.90 | -10.81 | -11.40 | 9.14 | -2.09 |
| B98/6-31G(d) 5d | -10.22 | -10.11 | -10.71 | 8.85 | -1.69 |
| B97-D/6-31G(d) 5d | -20.08 | -20.62 | -21.21 | 13.62 | -6.85 |

**Table A17:** Computed thermodynamic data for the $Co^{1+}$Cbi--**H**-O-H complex formation reaction studied in **acetonitrile solution** while assuming standard state convention of 1atm and 298.15 K (all thermodynamic parameters are given in kcal/mol units)

| Theoretical Method | $Co^{1+}Cbi + H_2O \longrightarrow Co^{1+}Cbi$--H-O-H | | | | |
|---|---|---|---|---|---|
| | ΔE | ΔU | ΔH | -TΔS | ΔG |
| HF/6-31G(d) 5d | -2.35 | -2.15 | -2.74 | 9.09 | 6.45 |
| BP86/6-31G(d) 5d | -8.12 | -8.39 | -8.98 | 10.84 | 1.93 |
| ωB97X/6-31G(d) 5d | -9.79 | -10.32 | -10.92 | 12.53 | 1.76 |
| ωB97X-D/6-31G(d) 5d | -12.55 | -12.57 | -13.61 | 9.79 | -3.19 |
| B97-1/6-31G(d) 5d | -8.84 | -8.94 | -9.53 | 9.42 | -0.03 |
| B98/6-31G(d) 5d | -7.99 | -8.17 | -8.76 | 10.56 | 1.93 |
| B97-D/6-31G(d) 5d | -19.01 | -19.49 | -20.09 | 13.34 | -6.00 |

**Table A18:** Computed thermodynamic data for the $Co^{1+}$Cbi--**H**-O-H complex formation reaction studied in **water solution** while assuming standard state convention of 1atm and 298.15 K (all thermodynamic parameters are given in kcal/mol units)

| Theoretical Method | $Co^{1+}Cbi + H_2O \longrightarrow Co^{1+}Cbi$--H-O-H | | | | |
|---|---|---|---|---|---|
| | ΔE | ΔU | ΔH | -TΔS | ΔG |
| HF/6-31G(d) 5d | -2.08 | -1.92 | -2.51 | 9.47 | 6.40 |
| BP86/6-31G(d) 5d | -7.87 | -8.18 | -8.77 | 11.31 | 1.85 |
| ωB97X/6-31G(d) 5d | -9.54 | -10.09 | -10.69 | 12.60 | 1.32 |
| ωB97X-D/6-31G(d) 5d | -12.38 | -12.43 | -13.02 | 9.69 | -3.81 |
| B97-1/6-31G(d) 5d | -8.50 | -8.67 | -9.26 | 10.90 | 0.97 |
| B98/6-31G(d) 5d | -7.82 | -7.99 | -8.58 | 10.94 | 1.69 |
| B97-D/6-31G(d) 5d | -18.83 | -19.37 | -19.97 | 13.78 | -6.64 |

**Table A19.** Reduction Potentials of MeCbl Cofactor computed using a variety of DFT functionals and 631G(d) 5d basis set.

| | Reduction Potential [V units] vs SCE | | | | | | | | | | | |
|---|---|---|---|---|---|---|---|---|---|---|---|---|
| Functional | Naked MeCbl Cofactor | | | | | | Full MeCbl Cofactor | | | | | |
| | DMF | DMSO | MeOH | $H_2O$ | DMF + Propanol | DMF + MeOH | DMF | DMSO | MeOH | $H_2O$ | DMF + Propanol | DMF + MeOH |
| BP86 | -1.81 | -1.80 | -1.79 | -1.79 | -1.78 | -1.79 | -1.76 | -1.88 | -1.92 | -1.81 | -1.81 | -1.81 |
| B3LYP | -1.86 | -1.86 | -1.85 | -1.86 | -1.84 | -1.85 | -1.85 | -1.98 | -2.02 | -1.91 | -1.90 | -1.91 |
| B3LYP-D | -2.10 | -2.00 | -1.99 | -2.01 | -2.11 | -2.11 | -1.98 | -2.01 | -1.83 | -1.91 | -1.98 | -1.98 |
| B3PW91 | -1.84 | -1.83 | -1.81 | -1.82 | -1.80 | -1.81 | -1.84 | -1.96 | -2.01 | -1.89 | -1.89 | -1.89 |
| PBE1PBE | -1.84 | -1.83 | -1.82 | -1.82 | -1.81 | -1.81 | -1.86 | -1.98 | -2.03 | -1.91 | -1.91 | -1.91 |
| mPW1PBE | -1.84 | -1.83 | -1.82 | -1.82 | -1.81 | -1.81 | -1.86 | -1.98 | -1.71 | -2.29 | -1.91 | -1.91 |
| mPW 3PBE | -1.82 | -1.81 | -1.79 | -1.80 | -1.78 | -1.79 | -1.83 | -1.95 | -1.99 | -1.88 | -1.87 | -1.87 |
| mPW1PW91 | -1.83 | -1.82 | -1.80 | -1.81 | -1.79 | -1.80 | -1.84 | -1.97 | -2.01 | -1.89 | -1.89 | -1.89 |

**Table A20.** Reduction Potentials of MeCbl Cofactor computed using a variety of DFT functionals and 631+G basis set.

| | Reduction Potential [V units] vs SCE | | | | | | | | | | | |
|---|---|---|---|---|---|---|---|---|---|---|---|---|
| Functional | Naked MeCbl Cofactor | | | | | | Full MeCbl Cofactor | | | | | |
| 6-31G* | DMF | DMSO | MeOH | $H_2O$ | DMF + Propanol | DMF + MeOH | DMF | DMSO | MeOH | $H_2O$ | DMF + Propanol | DMF + MeOH |
| BP86 | -2.01 | -2.00 | -1.99 | -1.98 | -1.98 | -1.98 | -2.12 | -2.14 | -2.16 | -2.15 | -2.16 | -2.16 |
| B3LYP | -1.87 | -1.86 | -1.85 | -1.86 | -2.02 | -2.02 | -2.00 | -2.01 | -2.02 | -2.03 | -2.03 | -2.03 |
| B3LYP-D | -2.20 | -2.17 | -2.16 | -2.17 | -2.19 | -2.19 | -2.14 | -2.20 | -2.02 | -2.08 | -2.16 | -2.17 |
| B3PW91 | -2.01 | -2.00 | -1.98 | -1.99 | -1.97 | -1.97 | -1.97 | -1.97 | -1.99 | -1.99 | -2.00 | -1.99 |
| PBE1PBE | -2.01 | -2.00 | -1.98 | -1.98 | -1.97 | -1.97 | -2.14 | -2.15 | -2.17 | -2.18 | -2.18 | -2.18 |
| mPW1PBE | -2.07 | -2.06 | -2.04 | -2.04 | -2.02 | -2.03 | -1.99 | -1.99 | -2.01 | -2.03 | -2.02 | -2.03 |
| mPW 3PBE | -1.93 | -1.92 | -1.90 | -1.98 | -1.89 | -1.89 | -1.98 | -2.08 | -2.00 | -2.01 | -2.00 | -2.00 |
| mPW1PW91 | -2.02 | -2.02 | -2.00 | -1.99 | -1.98 | -1.98 | -2.01 | -2.02 | -2.03 | -2.05 | -2.04 | -2.04 |

**Table A21.** Reduction Potentials of MeCbl Cofactor computed using a variety of DFT functionals and 631+G* basis set.

| | Reduction Potential [V units] vs SCE | | | | | | | | | | | |
|---|---|---|---|---|---|---|---|---|---|---|---|---|
| Functional | Naked MeCbl Cofactor | | | | | | Full MeCbl Cofactor | | | | | |
| | DMF | DMSO | MeOH | $H_2O$ | DMF + Propanol | DMF + MeOH | DMF | DMSO | MeOH | $H_2O$ | DMF + Propanol | DMF + MeOH |
| BP86 | -1.76 | -1.76 | -1.74 | -1.75 | -1.74 | -1.74 | -1.63 | -1.77 | -1.81 | -1.71 | -1.71 | -1.71 |
| B3LYP | -1.84 | -1.83 | -1.82 | -1.84 | -1.82 | -1.83 | -1.77 | -1.87 | -1.92 | -1.81 | -1.80 | -1.80 |
| B3LYP-D | -2.10 | -2.00 | -1.99 | -2.01 | -2.11 | -2.11 | -1.91 | -1.93 | -1.91 | -1.84 | -1.91 | -1.91 |
| B3PW91 | -1.80 | -1.79 | -1.78 | -1.79 | -1.77 | -1.78 | -1.74 | -1.85 | -1.89 | -1.79 | -1.78 | -1.78 |
| PBE1PBE | -1.81 | -1.80 | -1.78 | -1.79 | -1.78 | -1.78 | -1.75 | -1.87 | -1.91 | -1.80 | -1.80 | -1.80 |
| mPW1PBE | -1.81 | -1.80 | -1.78 | -1.79 | -1.78 | -1.78 | -1.75 | -1.87 | -1.91 | -1.80 | -1.80 | -1.80 |
| mPW 3PBE | -1.78 | -1.77 | -1.76 | -1.77 | -1.75 | -1.76 | -1.72 | -1.83 | -1.87 | -1.77 | -1.80 | -1.79 |
| mPW1PW91 | -1.79 | -1.79 | -1.77 | -1.78 | -1.77 | -1.77 | -1.74 | -1.85 | -1.90 | -1.79 | -1.79 | -1.79 |

**Table A22.** Reduction Potentials of AdoCbl Cofactor computed using a variety of DFT functionals and 631G(d) 5d basis set.

| Functional | Naked AdoCbl Cofactor | | | | Full AdoCbl Cofactor | | | |
|---|---|---|---|---|---|---|---|---|
| | DMF | DMSO | MeOH | $H_2O$ | DMF | DMSO | MeOH | $H_2O$ |
| BP86 | -1.71 | -1.86 | -1.75 | -1.76 | -1.81 | -1.92 | -1.94 | -2.04 |
| B3LYP | -1.84 | -1.87 | -1.87 | -1.88 | -1.93 | -1.91 | -2.07 | -1.91 |
| B3LYP-D | -1.76 | -1.76 | -175 | -1.77 | -1.84 | -1.84 | -1.85 | -1.84 |
| B3PW91 | -1.72 | -1.75 | -1.75 | -1.75 | -1.75 | -1.85 | -1.89 | -2.00 |
| PBE1PBE | -1.81 | -1.84 | -1.84 | -1.85 | -1.56 | -1.66 | -1.70 | -1.79 |
| mPW1PBE | -1.75 | -1.78 | -1.78 | -1.78 | -1.69 | -1.79 | -1.83 | -1.92 |
| mPW 3PBE | -1.64 | -1.66 | -1.67 | -1.67 | -1.69 | -1.79 | -1.83 | -1.94 |
| mPW1PW91 | -1.78 | -1.80 | -1.81 | -1.81 | -1.79 | -1.90 | -1.93 | -2.02 |

**Table A23.** Reduction Potentials of AdoCbl Cofactor computed using a variety of DFT functionals and 631+G basis set.

| Functional | Naked AdoCbl Cofactor | | | | Full AdoCbl Cofactor | | | |
|---|---|---|---|---|---|---|---|---|
| 6-31+G | DMF | DMSO | MeOH | $H_2O$ | DMF | DMSO | MeOH | $H_2O$ |
| BP86 | -1.57 | -1.60 | -1.60 | -1.61 | -1.55 | -1.40 | -1.72 | -1.83 |
| B3LYP | -1.65 | -1.68 | -1.69 | -1.71 | -1.60 | -1.73 | -1.78 | -1.90 |
| B3LYP-D | -1.59 | -1.59 | -1.58 | -1.60 | -1.68 | -1.68 | -1.68 | -1.67 |
| B3PW91 | -1.61 | -1.64 | -1.64 | -1.66 | -1.60 | -1.72 | -1.78 | -1.89 |
| PBE1PBE | -1.60 | -1.63 | -1.63 | -1.64 | -1.59 | -1.72 | -1.77 | -1.89 |
| mPW1PBE | -1.61 | -1.63 | -1.64 | -1.65 | -1.60 | -1.73 | -1.78 | -1.90 |
| mPW 3PBE | -1.58 | -1.61 | -1.61 | -1.63 | -1.57 | -1.70 | -1.75 | -1.87 |
| mPW1PW91 | -1.60 | -1.62 | -1.51 | -1.64 | -1.59 | -1.71 | -1.77 | -1.88 |

**Table A24.** Reduction Potentials of AdoCbl Cofactor computed using a variety of DFT functionals and 631+G* basis set.

| Functional | Naked AdoCbl Cofactor | | | | Full AdoCbl Cofactor | | | |
|---|---|---|---|---|---|---|---|---|
| | DMF | DMSO | MeOH | $H_2O$ | DMF | DMSO | MeOH | $H_2O$ |
| BP86 | -1.56 | -1.59 | -1.60 | -1.60 | -1.45 | -1.56 | -1.61 | -1.70 |
| B3LYP | -1.67 | -1.70 | -1.71 | -1.72 | -1.51 | -1.62 | -1.67 | -1.79 |
| B3LYP-D | -1.60 | -1.61 | -1.60 | -1.62 | -1.58 | -1.58 | -1.58 | -1.57 |
| B3PW91 | -1.62 | -1.64 | -1.65 | -1.66 | -1.50 | -1.61 | -1.66 | -1.60 |
| PBE1PBE | -1.61 | -1.63 | -1.58 | -1.65 | -1.49 | -1.60 | -1.65 | -1.76 |
| mPW1PBE | -1.62 | -1.64 | -1.65 | -1.66 | -1.50 | -1.62 | -1.67 | -1.78 |
| mPW 3PBE | -1.59 | -1.61 | -1.62 | -1.63 | -1.47 | -1.59 | -1.63 | -1.74 |
| mPW1PW91 | -1.61 | -1.63 | -1.64 | -1.65 | -1.63 | -1.22 | -1.65 | -1.76 |

**Table A25.** Computed Reduction Potentials of $Co^{2+}/Co^{1+}$ Couple assuming tetra- and penta-coordinated Conformations of $Co^{1+}$Cbx

| $Co^{2+}/Co^{1+}$ Redox Couple | Reduction Potential [mV] vs SHE | | |
|---|---|---|---|
| | Chloroform | Acetonitrile | Water |
| $Co^{2+}$Cbl--$OH_2$/$Co^{1+}$Cbl | -220 | -275 | -303 |
| $Co^{2+}$Cbi--$OH_2$/$Co^{1+}$Cbi | -239 | -328 | -291 |
| $Co^{2+}$Cbl--$OH_2$/$Co^{1+}$Cbl--H-O-H | -110 | -223 | -279 |
| $Co^{2+}$Cbi--$OH_2$/$Co^{1+}$Cbi--H-O-H | -15 | -236 | -255 |

**Table A26**: Key Structural Features of the Complex $Co^{2+}$Cbl--$OH_2$--$OH_2$ optimized using a variety of theoretical methods (bond lengths and bond angles are expressed in Å and degrees respectively).

| Theoretical Method | Co-$N_{21}$ | Co-$N_{22}$ | Co-$N_{23}$ | Co-$N_{24}$ | Co-O |
|---|---|---|---|---|---|
| HF/6-31++G(d,p) | 1.93 | 1.95 | 1.95 | 1.93 | 4.29 |
| BP86/6-31++G(d,p) | 1.88 | 1.93 | 1.93 | 1.88 | 2.25 |
| ωB97X/6-31++G(d,p) | 1.89 | 1.92 | 1.93 | 1.89 | 2.44 |
| ωB97X-D/6-31++G(d,p) | 1.86 | 1.91 | 1.90 | 1.87 | 2.28 |
| B97-1/6-31++G(d,p) | 1.89 | 1.94 | 1.94 | 1.89 | 2.52 |
| B98/6-31++G(d,p) | 1.88 | 1.94 | 1.94 | 1.89 | 2.55 |
| B97-D/6-31++G(d,p) | 1.85 | 1.92 | 1.91 | 1.86 | 2.28 |

**Table A27**: Key Structural Features of the Complex $Co^{2+}$Cbl--$OH_2$--HOPh optimized using a variety of theoretical methods (bond lengths and bond angles are expressed in Å and degrees respectively).

| Theoretical Method | Co-$N_{21}$ | Co-$N_{22}$ | Co-$N_{23}$ | Co-$N_{24}$ | Co-O |
|---|---|---|---|---|---|
| HF/6-31++G(d,p) | 1.93 | 1.95 | 1.95 | 1.93 | 3.34 |
| BP86/6-31++G(d,p) | 1.88 | 1.93 | 1.93 | 1.87 | 2.32 |
| ωB97X/6-31++G(d,p) | 1.89 | 1.92 | 1.93 | 1.89 | 2.40 |
| ωB97X-D/6-31++G(d,p) | 1.88 | 1.92 | 1.93 | 1.88 | 2.40 |
| B97-1/6-31++G(d,p) | 1.89 | 1.93 | 1.94 | 1.89 | 2.45 |
| B98/6-31++G(d,p) | 1.89 | 1.93 | 1.94 | 1.89 | 2.46 |
| B97-D/6-31++G(d,p) | 1.88 | 1.93 | 1.93 | 1.88 | 2.32 |

**Table A28**: Key Structural Features of the Complex $Co^{1+}Cbl$--$H_2O$--$H_2O$ optimized using a variety of theoretical methods (bond lengths and bond angles are expressed in Å and degrees respectively).

| Theoretical Method | Co-H | Co-O | Co-H-O | $O_{H2O}$--$H_{H2O}$ | $O_{H2O}$--$O_{H2O}$ |
|---|---|---|---|---|---|
| HF/6-31++G(d,p) | 2.54 | 3.43 | 115.62 | 1.97 | 2.92 |
| BP86/6-31++G(d,p) | 2.18 | 3.17 | 167.09 | 1.77 | 2.76 |
| ωB97X/6-31++G(d,p) | 2.35 | 3.25 | 153.60 | 1.81 | 2.78 |
| ωB97X-D/6-31++G(d,p) | 2.30 | 3.21 | 154.47 | 1.80 | 2.78 |
| B97-1/6-31++G(d,p) | 2.37 | 3.29 | 157.44 | 1.83 | 2.81 |
| B98/6-31++G(d,p) | 2.33 | 3.27 | 160.62 | 1.83 | 2.80 |
| B97-D/6-31++G(d,p) | 2.26 | 3.18 | 154.08 | 1.79 | 2.78 |

**Table A29**: Key Structural Features of the Complex $Co^{1+}Cb$--$H_2O$--HOPh optimized using a variety of theoretical methods (bond lengths and bond angles are expressed in Å and degrees respectively).

| Theoretical Method | Co-H | Co-O | Co-H-O | $O_{H2O}$--$H_{PhOH}$ | $O_{H2O}$--$O_{PhOH}$ |
|---|---|---|---|---|---|
| HF/6-31++G(d,p) | 2.39 | 3.34 | 174.12 | 1.90 | 2.85 |
| BP86/6-31++G(d,p) | 2.12 | 3.13 | 175.69 | 1.72 | 2.71 |
| ωB97X/6-31++G(d,p) | 2.15 | 3.13 | 174.51 | 1.77 | 2.74 |
| ωB97X-D/6-31++G(d,p) | 2.25 | 3.21 | 164.74 | 1.77 | 2.74 |
| B97-1/6-31++G(d,p) | 2.20 | 3.19 | 175.83 | 1.79 | 2.77 |
| B98/6-31++G(d,p) | 2.17 | 3.16 | 175.83 | 1.75 | 2.74 |
| B97-D/6-31++G(d,p) | 2.17 | 3.15 | 166.93 | 1.74 | 2.73 |

**Table A30:** Computed thermodynamic data for the $Co^{1+}Cbl$--$H_2O$--$H_2O$ complex formation reaction studied in **gas phase** while assuming standard state convention of 1atm and 298.15 K (all thermodynamic parameters are given in kcal/mol units)

| Theoretical Method | $Co^{1+}Cbl + H_2O + H_2O \longrightarrow Co^{1+}Cbl$--$H_2O$--$H_2O$ | | | | |
|---|---|---|---|---|---|
| | ΔE | ΔU | ΔH | -TΔS | ΔG |
| HF/6-31++G(d,p) | -9.36 | -8.47 | -9.65 | 15.36 | 5.71 |
| BP86/6-31++G(d,p) | -13.00 | -12.54 | -13.73 | 17.06 | 3.33 |
| ωB97X/6-31++G(d,p) | -18.15 | -17.78 | -18.96 | 17.91 | -1.05 |
| ωB97X-D/6-31++G(d,p) | -19.01 | -18.59 | -19.78 | 17.77 | -2.01 |
| B97-1/6-31++G(d,p) | -14.21 | -13.73 | -14.91 | 17.47 | 2.56 |
| B98/6-31++G(d,p) | -13.58 | -13.01 | -14.19 | 16.96 | 2.77 |
| B97-D/6-31++G(d,p) | -18.40 | -18.13 | -19.32 | 18.38 | -0.94 |

**Table A31:** Computed thermodynamic data for the $Co^{1+}Cbl$--$H_2O$--$H_2O$ complex formation reaction studied in **chloroform** while assuming standard state convention of 1atm and 298.15 K (all thermodynamic parameters are given in kcal/mol units)

| Theoretical Method | $Co^{1+}Cbl + H_2O + H_2O \longrightarrow$ | | | $Co^{1+}Cbl$--$H_2O$--$H_2O$ | |
|---|---|---|---|---|---|
| | ΔE | ΔU | ΔH | -TΔS | ΔG |
| HF/6-31++G(d,p) | -4.27 | -3.86 | -4.34 | 13.70 | 9.36 |
| BP86/6-31++G(d,p) | -8.70 | -8.71 | -9.89 | 18.72 | 8.82 |
| ωB97X/6-31++G(d,p) | -12.47 | -11.81 | -12.99 | 16.71 | 3.72 |
| ωB97X-D/6-31++G(d,p) | -13.24 | -12.65 | -13.84 | 16.81 | 2.97 |
| B97-1/6-31++G(d,p) | -9.70 | -9.71 | -10.89 | 17.23 | 6.34 |
| B98/6-31++G(d,p) | -9.40 | -9.31 | -10.23 | 17.80 | 6.78 |
| B97-D/6-31++G(d,p) | -13.36 | -12.98 | -14.16 | 17.82 | 3.66 |

**Table A32:** Computed thermodynamic data for the $Co^{1+}Cbl$--$H_2O$--HOPh complex formation reaction studied in **gas phase** while assuming standard state convention of 1atm and 298.15 K (all thermodynamic parameters are given in kcal/mol units)

| Theoretical Method | $Co^{1+}Cbl + H_2O + PhOH \longrightarrow$ | | | $Co^{1+}Cbl$--$H_2O$--HOPh | |
|---|---|---|---|---|---|
| | ΔE | ΔU | ΔH | -TΔS | ΔG |
| HF/6-31++G(d,p) | -14.14 | -12.29 | -13.47 | 15.98 | 2.51 |
| BP86/6-31++G(d,p) | -14.97 | -13.62 | -14.80 | 17.82 | 3.02 |
| ωB97X/6-31++G(d,p) | -22.84 | -21.69 | -22.88 | 19.82 | -3.06 |
| ωB97X-D/6-31++G(d,p) | -29.62 | -28.31 | -29.50 | 20.19 | -9.30 |
| B97-1/6-31++G(d,p) | -17.12 | -15.88 | -17.06 | 19.14 | 2.07 |
| B98/6-31++G(d,p) | -17.26 | -16.01 | -17.19 | 19.00 | 1.80 |
| B97-D/6-31++G(d,p) | -24.91 | -23.94 | -25.12 | 21.05 | -4.07 |

**Table A33:** Computed thermodynamic data for the $Co^{1+}Cbl$--$H_2O$--HOPh complex formation reaction studied in **chloroform** while assuming standard state convention of 1atm and 298.15 K (all thermodynamic parameters are given in kcal/mol units)

| Theoretical Method | $Co^{1+}Cbl + H_2O + PhOH \longrightarrow$ | | | $Co^{1+}Cbl$--$H_2O$--HOPh | |
|---|---|---|---|---|---|
| | ΔE | ΔU | ΔH | -TΔS | ΔG |
| HF/6-31++G(d,p) | -6.74 | -5.07 | -6.25 | 15.20 | 8.95 |
| BP86/6-31++G(d,p) | -11.09 | -9.54 | -9.84 | 17.12 | 7.28 |
| ωB97X/6-31++G(d,p) | -16.80 | -15.62 | -16.80 | 19.63 | 2.83 |
| ωB97X-D/6-31++G(d,p) | -21.15 | -20.12 | -21.30 | 21.05 | -0.26 |
| B97-1/6-31++G(d,p) | -12.09 | -11.14 | -12.10 | 17.40 | 5.30 |
| B98/6-31++G(d,p) | -11.79 | -10.96 | -12.02 | 17.25 | 6.23 |
| B97-D/6-31++G(d,p) | -19.91 | -18.99 | -20.18 | 21.19 | 1.01 |

**Table A34**: Key structural features of the optimized $Co^{1+}$Cbl--**H**-O-H complex (bond lengths and bond angle are expressed in Å and degree respectively). The values mentioned in parentheses correspond to those in the isolated $H_2O$ ligand.

| Theoretical Method | Co-H | Co-O | H-O | Co-H-O |
|---|---|---|---|---|
| HF/6-31++G(d,p) | 2.62 | 3.54 | 0.95 (0.94) | 164.61 |
| BP86/6-31++G(d,p) | 2.29 | 3.29 | 1.00 (0.97) | 170.32 |
| ωB97X/6-31++G(d,p) | 2.40 | 3.35 | 0.97 (0.96) | 171.73 |
| ωB97X-D/6-31++G(d,p) | 2.39 | 3.33 | 0.97 (0.96) | 162.98 |
| B97-1/6-31++G(d,p) | 2.45 | 3.44 | 0.96 (0.96) | 165.10 |
| B98/6-31++G(d,p) | 2.46 | 3.45 | 0.96 (0.96) | 165.11 |
| B97-D/6-31++G(d,p) | 2.44 | 3.40 | 0.98 (0.97) | 168.06 |

**Table A35**: Key structural features of the optimized $Co^{1+}$Cbi--**H**-O-H complex (bond lengths and bond angle are expressed in Å and degree respectively). The values mentioned in parentheses correspond to those in the isolated $H_2O$ ligand.

| Theoretical Method | Co-H | Co-O | H-O | Co-H-O |
|---|---|---|---|---|
| HF/6-31G(d) 5d | 2.51 | 3.45 | 0.95 (0.95) | 170.71 |
| BP86/6-31G(d) 5d | 2.41 | 3.38 | 0.99 (0.98) | 167.82 |
| ωB97X/6-31G(d) 5d | 2.45 | 3.41 | 0.97 (0.96) | 172.92 |
| ωB97X-D/6-31G(d) 5d | 2.41 | 3.37 | 0.97 (0.96) | 169.74 |
| B97-1/6-31G(d) 5d | 2.55 | 3.50 | 0.97 (0.97) | 166.10 |
| B98/6-31G(d) 5d | 2.53 | 3.49 | 0.97 (0.97) | 165.23 |
| B97-D/6-31G(d) 5d | 2.51 | 3.48 | 0.98 (0.97) | 168.28 |

**Table A36**: Key Structural Features of the optimized $Co^{1+}$Cbl--**H**-N(Im) Complex (bond lengths and bond angles are expressed in Å and degrees respectively). The values mentioned in parentheses correspond to those in the isolated Im ligand.

| Theoretical Method | Co-H | Co-N | H-N | Co-H-N |
|---|---|---|---|---|
| HF/6-31++G(d,p) | 2.50 | 3.49 | 1.00 (0.99) | 174.40 |
| BP86/6-31++G(d,p) | 2.25 | 3.29 | 1.04 (1.02) | 175.22 |
| ωB97X/6-31++G(d,p) | 2.29 | 3.25 | 1.02 (1.01) | 155.54 |
| ωB97X-D/6-31++G(d,p) | 2.22 | 3.13 | 1.02 (1.01) | 147.03 |
| B97-1/6-31++G(d,p) | 2.29 | 3.31 | 1.03 (1.01) | 171.83 |
| B98/6-31++G(d,p) | 2.28 | 3.31 | 1.03 (1.01) | 174.39 |
| B97-D/6-31++G(d,p) | 2.18 | 3.12 | 1.03 (1.01) | 149.92 |

**Table A37**: Key Structural Features of the optimized $Co^{1+}$Cbi--**H**-C(Im)Complex (bond lengths and bond angles are expressed in Å and degrees respectively). The values mentioned in parentheses correspond to those in the isolated Im ligand.

| Theoretical Method | Co-H | Co-C | H-C(Im) | Co-H-C |
|---|---|---|---|---|
| HF/6-31G(d) 5d | 4.09 | 5.06 | 1.07 (1.07) | 152.61 |
| BP86/6-31G(d) 5d | 3.55 | 4.60 | 1.09 (1.09) | 162.13 |
| ωB97X/6-31G(d) 5d | 3.25 | 4.28 | 1.09 (1.08) | 160.21 |
| ωB97X-D/6-31G(d) 5d | 3.05 | 4.06 | 1.08 (1.08) | 154.75 |
| B97-1/6-31G(d) 5d | 3.54 | 4.58 | 1.08 (1.08) | 161.67 |
| B98/6-31G(d) 5d | 3.58 | 4.62 | 1.08 (1.08) | 161.76 |
| B97-D/6-31G(d) 5d | 2.92 | 3.97 | 1.09 (1.09) | 162.55 |

**Table A38.** Key structural features of the optimized H-O-**H**--$Co^{1+}$Cbl--**H**-O-H complex (bond lengths and bond angle are expressed in Å and degree respectively). The values mentioned in parentheses correspond to those in the isolated $H_2O$ ligand.

| Theoretical Method | α-axial ligand | | | | β-axial ligand | | | |
|---|---|---|---|---|---|---|---|---|
| | Co-H | Co-O | H-O | Co-H-O | Co-H | Co-O | H-O | Co-H-O |
| HF/6-31++G(d,p) | 2.63 | 3.55 | 0.95 (0.94) | 162.98 | 2.63 | 3.55 | 0.95 (0.94) | 162.99 |
| BP86/6-31++G(d,p) | 2.32 | 3.30 | 0.99 (0.97) | 169.15 | 2.32 | 3.30 | 0.99 (0.97) | 169.21 |
| ωB97X/6-31++G(d,p) | 2.41 | 3.37 | 0.97 (0.96) | 169.10 | 2.41 | 3.37 | 0.97 (0.96) | 169.20 |
| ωB97X-D/6-31++G(d,p) | 2.40 | 3.34 | 0.97 (0.96) | 160.69 | 2.40 | 3.32 | 0.97 (0.96) | 157.85 |
| B97-1/6-31++G(d,p) | 2.43 | 3.43 | 0.97 (0.96) | 165.12 | 2.44 | 3.45 | 0.97 (0.96) | 166.21 |
| B98/6-31++G(d,p) | 2.40 | 3.36 | 0.97 (0.96) | 167.46 | 2.40 | 3.36 | 0.97 (0.96) | 167.41 |
| B97-D/6-31++G(d,p) | 2.49 | 3.42 | 0.98 (0.97) | 158.52 | 2.50 | 3.42 | 0.98 (0.97) | 157.29 |

**Table A39.** Key structural features of the optimized H-O-**H**--$Co^{1+}$Cbi--**H**-O-H complex (bond lengths and bond angle are expressed in Å and degree respectively). The values mentioned in parentheses correspond to those in the isolated $H_2O$ ligand.

| Theoretical Method | α-axial ligand | | | | β-axial ligand | | | |
|---|---|---|---|---|---|---|---|---|
| | Co-H | Co-O | H-O | Co-H-O | Co-H | Co-O | H-O | Co-H-O |
| HF/6-31G(d) 5d | 3.37 | 3.99 | 0.95 (0.95) | 124.65 | 2.46 | 3.40 | 0.95 (0.95) | 169.49 |
| BP86/6-31G(d) 5d | 2.44 | 3.41 | 0.99 (0.98) | 164.96 | 2.30 | 3.27 | 0.99 (0.98) | 164.57 |
| ωB97X/6-31G(d) 5d | 2.43 | 3.40 | 0.98 (0.96) | 165.12 | 2.32 | 3.23 | 0.98 (0.96) | 152.11 |
| ωB97X-D/6-31G(d) 5d | 2.40 | 3.36 | 0.98 (0.96) | 166.65 | 2.28 | 3.19 | 0.98 (0.96) | 154.77 |
| B97-1/6-31G(d) 5d | 2.46 | 3.42 | 0.98 (0.97) | 166.37 | 2.62 | 3.57 | 0.98 (0.97) | 163.86 |
| B98/6-31G(d) 5d | 2.50 | 3.45 | 0.98 (0.97) | 164.28 | 2.35 | 3.28 | 0.98 (0.97) | 158.71 |
| B97-D/6-31G(d) 5d | 2.56 | 3.50 | 0.98 (0.97) | 161.05 | 2.32 | 3.29 | 0.98 (0.97) | 166.98 |

**Table A40**: Key Structural Features of the optimized H-O-**H**--$Co^{1+}$Cbl--**H**-N(Im) Complex (bond lengths and bond angles are expressed in Å and degrees respectively). The values mentioned in parentheses correspond to those in the isolated Im and $H_2O$ ligands.

| Theoretical Method | α-axial ligand (Im) | | | | β-axial ligand ($H_2O$) | | | |
|---|---|---|---|---|---|---|---|---|
| | Co-H | Co-C | H-N | Co-H-C | Co-H | Co-O | H-O | Co-H-O |
| HF/6-31G(d) 5d | 2.81 | 3.88 | 1.00 (0.99) | 175.69 | 3.41 | 4.01 | 0.95 (0.94) | 122.80 |
| BP86/6-31G(d) 5d | 2.73 | 3.80 | 1.04 (1.02) | 167.61 | 3.53 | 4.04 | 0.99 (0.97) | 114.86 |
| ωB97X/6-31G(d) 5d | 2.60 | 3.66 | 1.02 (1.01) | 167.37 | 3.57 | 4.00 | 0.97 (0.96) | 110.20 |
| ωB97X-D/6-31G(d) 5d | 2.56 | 3.61 | 1.02 (1.01) | 165.01 | 3.37 | 3.85 | 0.97 (0.96) | 111.93 |
| B97-1/6-31G(d) 5d | 2.77 | 3.85 | 1.02 (1.01) | 173.12 | 3.60 | 4.05 | 0.97 (0.96) | 111.42 |
| B98/6-31G(d) 5d | 2.78 | 3.86 | 1.02 (1.01) | 173.42 | 3.61 | 4.06 | 0.97 (0.96) | 110.72 |
| B97-D/6-31G(d) 5d | 2.61 | 3.67 | 1.03 (1.01) | 163.97 | 3.44 | 3.52 | 0.97 (0.97) | 86.43 |

**Table A41**: Key Structural Features of the optimized H-O-**H**--$Co^{1+}$Cbl--**H**-C(Im) Complex (bond lengths and bond angles are expressed in Å and degrees respectively). The values mentioned in parentheses correspond to those in the isolated Im and $H_2O$ ligands.

| Theoretical Method | α-axial ligand (Im) | | | | β-axial ligand ($H_2O$) | | | |
|---|---|---|---|---|---|---|---|---|
| | Co-H | Co-N | H-N | Co-H-N | Co-H | Co-O | H-O | Co-H-O |
| HF/6-31++G(d,p) | 2.53 | 3.52 | 1.07(1.07) | 174.67 | 2.63 | 3.56 | 0.95(0.95) | 169.46 |
| BP86/6-31++G(d,p) | 2.28 | 3.32 | 1.09 (1.09) | 174.66 | 2.33 | 3.31 | 0.98 (0.98) | 168.48 |
| ωB97X/6-31++G(d,p) | 2.32 | 3.25 | 1.08 (1.08) | 150.40 | 2.40 | 3.32 | 0.98 (0.96) | 157.13 |
| ωB97X-D/6-31++G(d,p) | 2.24 | 3.16 | 1.08 (1.08) | 149.77 | 2.36 | 3.26 | 0.97 (0.96) | 154.42 |
| B97-1/6-31++G(d,p) | 2.28 | 3.30 | 1.08 (1.08) | 173.64 | 2.36 | 3.33 | 0.97 (0.97) | 168.12 |
| B98/6-31++G(d,p) | 2.32 | 3.34 | 1.08 (1.08) | 173.73 | 2.40 | 3.36 | 0.97 (0.97) | 168.30 |
| B97-D/6-31++G(d,p) | 2.21 | 3.13 | 1.09 (1.09) | 147.34 | 2.65 | 3.24 | 0.98 (0.97) | 119.44 |

**Table A42:** Computed thermodynamic data for the $Co^{1+}$Cbl--**H**-O-H complex formation reaction studied in **gas phase** while assuming standard state convention of 1atm and 298.15 K (all thermodynamic parameters are given in kcal/mol units).

| Theoretical Method | $Co^{1+}Cbl + H_2O \longrightarrow Co^{1+}Cbl\text{--}H_2O$ | | | | |
|---|---|---|---|---|---|
| | ΔE | ΔU | ΔH | -TΔS | ΔG |
| HF/6-31++G(d,p) | -4.1 | -3.3 | -3.9 | 6.1 | 2.2 |
| BP86/6-31++G(d,p) | -5.4 | -4.9 | -5.5 | 7.5 | 2.0 |
| ωB97X/6-31++G(d,p) | -8.1 | -7.6 | -7.9 | 7.4 | -0.5 |
| ωB97X-D/6-31++G(d,p) | -8.8 | -8.2 | -8.8 | 7.3 | -1.5 |
| B97-1/6-31++G(d,p) | -7.8 | -7.1 | -7.7 | 7.9 | 0.2 |
| B98/6-31++G(d,p) | -7.2 | -6.7 | -7.1 | 7.7 | 0.6 |
| B97-D/6-31++G(d,p) | -9.1 | -8.4 | -9.0 | 7.1 | -1.9 |

**Table A43:** Computed Thermodynamic Data for the $Co^{1+}$Cbl--**H**-O-H Complex Formation Reaction studied in **chloroform solution** assuming standard state convention of 1atm and 298.15 K (all thermodynamic parameters are given in kcal/mol units).

| Theoretical Method | $Co^{1+}$Cbl + $H_2O$ ⟶ $Co^{1+}$Cbl--$H_2O$ | | | | |
|---|---|---|---|---|---|
| | ΔE | ΔU | ΔH | -TΔS | ΔG |
| HF/6-31++G(d,p) | -2.0 | -1.2 | -1.8 | 6.0 | 4.2 |
| BP86/6-31++G(d,p) | -4.4 | -3.8 | -4.3 | 7.4 | 3.0 |
| ωB97X/6-31++G(d,p) | -5.9 | -5.3 | -5.8 | 7.4 | 1.7 |
| ωB97X-D/6-31++G(d,p) | -6.9 | -6.2 | -6.7 | 7.0 | 0.5 |
| B97-1/6-31++G(d,p) | -5.0 | -4.0 | -4.6 | 6.2 | 1.6 |
| B98/6-31++G(d,p) | -4.3 | -3.6 | -4.2 | 6.8 | 2.6 |
| B97-D/6-31++G(d,p) | -7.4 | -6.7 | -7.3 | 7.1 | -0.1 |

**Table A44:** Computed Thermodynamic Data for the $Co^{1+}$Cbl--**H**-O-H Complex Formation Reaction studied in **acetonitrile solution** assuming standard state convention of 1atm and 298.15 K (all thermodynamic parameters are given in kcal/mol units).

| Theoretical Method | $Co^{1+}$Cbl + $H_2O$ ⟶ $Co^{1+}$Cbl--$H_2O$ | | | | |
|---|---|---|---|---|---|
| | ΔE | ΔU | ΔH | -TΔS | ΔG |
| HF/6-31++G(d,p) | -0.9 | -0.0 | -0.6 | 6.0 | 5.4 |
| BP86/6-31++G(d,p) | -3.8 | -3.1 | -3.7 | 6.8 | 3.1 |
| ωB97X/6-31++G(d,p) | -5.0 | -4.2 | -4.8 | 6.4 | 1.8 |
| ωB97X-D/6-31++G(d,p) | -6.0 | -5.8 | -6.4 | 7.4 | 1.2 |
| B97-1/6-31++G(d,p) | -4.0 | -3.3 | -3.8 | 6.3 | 2.5 |
| B98/6-31++G(d,p) | -3.8 | -3.5 | -4.1 | 7.8 | 3.7 |
| B97-D/6-31++G(d,p) | -6.9 | -6.4 | -7.0 | 7.9 | 1.0 |

**Table A45:** Computed Thermodynamic Data for the $Co^{1+}$Cbl--**H**-O-H Complex Formation Reaction studied in **water solution** assuming standard state convention of 1atm and 298.15 K (all thermodynamic parameters are given in kcal/mol units).

| Theoretical Method | $Co^{1+}$Cbl + $H_2O$ ⟶ $Co^{1+}$Cbl--$H_2O$ | | | | |
|---|---|---|---|---|---|
| | ΔE | ΔU | ΔH | -TΔS | ΔG |
| HF/6-31++G(d,p) | -0.8 | 0.1 | -0.5 | 5.9 | 5.4 |
| BP86/6-31++G(d,p) | -3.7 | -3.6 | -4.2 | 8.4 | 4.2 |
| ωB97X/6-31++G(d,p) | -4.8 | -4.1 | -4.7 | 6.9 | 2.4 |
| ωB97X-D/6-31++G(d,p) | -6.2 | -5.6 | -6.2 | 7.5 | 1.5 |
| B97-1/6-31++G(d,p) | -3.9 | -3.2 | -3.8 | 6.9 | 3.1 |
| B98/6-31++G(d,p) | -3.6 | -2.9 | -3.5 | 6.8 | 3.4 |
| B97-D/6-31++G(d,p) | -6.9 | -6.4 | -7.0 | 7.9 | 1.0 |

**Table A46:** Computed thermodynamic data for the $Co^{1+}$Cbi--**H**-O-H complex formation reaction studied in **gas phase** while assuming standard state convention of 1atm and 298.15 K (all thermodynamic parameters are given in kcal/mol units).

| Theoretical Method | $Co^{1+}Cbi + H_2O \longrightarrow Co^{1+}Cbi\text{--}H_2O$ | | | | |
|---|---|---|---|---|---|
| | ΔE | ΔU | ΔH | -TΔS | ΔG |
| HF/6-31G(d) 5d | -4.6 | -4.3 | -4.9 | 8.7 | 3.8 |
| BP86/6-31G(d) 5d | -7.0 | -6.6 | -7.2 | 8.7 | 1.5 |
| ωB97X/6-31G(d) 5d | -17.0 | -10.1 | -10.7 | 8.9 | -1.8 |
| ωB97X-D/6-31G(d) 5d | -11.1 | -11.0 | -11.6 | 9.8 | -1.8 |
| B97-1/6-31G(d) 5d | -12.1 | -11.8 | -12.3 | 9.4 | -2.9 |
| B98/6-31G(d) 5d | -7.9 | -7.5 | -8.1 | 8.4 | 0.3 |
| B97-D/6-31G(d) 5d | -13.5 | -13.4 | -14.0 | 9.2 | -4.8 |

**Table A47:** Computed Thermodynamic Data for the $Co^{1+}$Cbi--**H**-O-H Complex Formation Reaction studied in **chloroform solution** assuming standard state convention of 1atm and 298.15 K (all thermodynamic parameters are given in kcal/mol units).

| Theoretical Method | $Co^{1+}Cbi + H_2O \longrightarrow Co^{1+}Cbi\text{--}H_2O$ | | | | |
|---|---|---|---|---|---|
| | ΔE | ΔU | ΔH | -TΔS | ΔG |
| HF/6-31G(d) 5d | -2.7 | -2.4 | -3.0 | 9.4 | 6.6 |
| BP86/6-31G(d) 5d | -5.8 | -5.4 | -5.9 | 8.2 | 2.5 |
| ωB97X/6-31G(d) 5d | -8.8 | -8.5 | -9.0 | 8.9 | 0.2 |
| ωB97X-D/6-31G(d) 5d | -10.2 | -10.0 | -10.5 | 9.3 | -1.0 |
| B97-1/6-31G(d) 5d | -10.9 | -10.8 | -11.4 | 9.1 | -2.0 |
| B98/6-31G(d) 5d | -6.3 | -5.9 | -6.5 | 8.1 | 1.9 |
| B97-D/6-31G(d) 5d | -11.7 | -11.6 | -12.2 | 8.7 | -3.4 |

**Table A48:** Computed Thermodynamic Data for the $Co^{1+}$Cbi--**H**-O-H Complex Formation Reaction studied in **acetonitrile solution** assuming standard state convention of 1atm and 298.15 K (all thermodynamic parameters are given in kcal/mol units).

| Theoretical Method | $Co^{1+}Cbi + H_2O \longrightarrow Co^{1+}Cbi\text{--}H_2O$ | | | | |
|---|---|---|---|---|---|
| | ΔE | ΔU | ΔH | -TΔS | ΔG |
| HF/6-31G(d) 5d | -2.4 | -1.7 | -2.3 | 8.2 | 6.1 |
| BP86/6-31G(d) 5d | -5.2 | -4.9 | -5.5 | 9.2 | 3.9 |
| ωB97X/6-31G(d) 5d | -8.3 | -8.5 | -9.1 | 10.8 | 2.0 |
| ωB97X-D/6-31G(d) 5d | -9.9 | -9.6 | -10.2 | 9.1 | -0.7 |
| B97-1/6-31G(d) 5d | -8.8 | -8.9 | -9.5 | 9.4 | 0.1 |
| B98/6-31G(d) 5d | -5.9 | -5.6 | -6.2 | 8.6 | 2.7 |
| B97-D/6-31G(d) 5d | -16.1 | -16.4 | -17.0 | 12.5 | -4.4 |

**Table A49:** Computed Thermodynamic Data for the $Co^{1+}$Cbi--**H**-O-H Complex Formation Reaction studied in **water solution** assuming standard state convention of 1atm and 298.15 K (all thermodynamic parameters are given in kcal/mol units).

| Theoretical Method | $Co^{1+}Cbi + H_2O \longrightarrow Co^{1+}Cbi\text{--}H_2O$ | | | | |
|---|---|---|---|---|---|
| | ΔE | ΔU | ΔH | -TΔS | ΔG |
| HF/6-31G(d) 5d | -2.0 | -1.6 | -2.2 | 8.4 | 6.4 |
| BP86/6-31G(d) 5d | -5.1 | -4.9 | -5.4 | 9.8 | 4.6 |
| ωB97X/6-31G(d) 5d | -8.2 | -7.9 | -8.4 | 9.3 | 1.2 |
| ωB97X-D/6-31G(d) 5d | -9.8 | -9.5 | -10.1 | 9.1 | -0.6 |
| B97-1/6-31G(d) 5d | -6.4 | -6.1 | -6.7 | 9.1 | 2.7 |
| B98/6-31G(d) 5d | -5.9 | -5.6 | -6.2 | 9.3 | 3.3 |
| B97-D/6-31G(d) 5d | -16.1 | -16.5 | -17.0 | 12.8 | -4.1 |

**Table A50:** Computed thermodynamic data for the $Co^{1+}$Cbl--**H**-N(Im) complex formation reaction studied in **gas phase** while assuming standard state convention of 1atm and 298.15 K (all thermodynamic parameters are given in kcal/mol units).

| Theoretical Method | $Co^{1+}Cbl + Im \longrightarrow Co^{1+}Cbl\text{--}Im$ | | | | |
|---|---|---|---|---|---|
| | ΔE | ΔU | ΔH | -TΔS | ΔG |
| HF/6-31++G(d,p) | -6.9 | -5.5 | -6.1 | 7.3 | 1.2 |
| BP86/6-31++G(d,p) | -7.5 | -6.1 | -6.7 | 8.0 | 1.3 |
| ωB97X/6-31++G(d,p) | -11.7 | -10.4 | -11.0 | 8.4 | -2.6 |
| ωB97X-D/6-31++G(d,p) | -15.5 | -14.3 | -14.9 | 10.0 | -4.9 |
| B97-1/6-31++G(d,p) | -8.9 | -8.1 | -8.7 | 10.5 | 1.8 |
| B98/6-31++G(d,p) | -8.5 | -7.2 | -7.8 | 8.1 | 0.3 |
| B97-D/6-31++G(d,p) | -15.1 | -14.0 | -14.6 | 10.4 | -4.3 |

**Table A51:** Computed thermodynamic data for the $Co^{1+}$Cbl--**H**-N(Im) complex formation reaction studied in **chloroform** while assuming standard state convention of 1atm and 298.15 K (all thermodynamic parameters are given in kcal/mol units).

| Theoretical Method | $Co^{1+}Cbl + Im \longrightarrow Co^{1+}Cbl\text{--}Im$ | | | | |
|---|---|---|---|---|---|
| | ΔE | ΔU | ΔH | -TΔS | ΔG |
| HF/6-31++G(d,p) | -3.9 | -2.4 | -3.0 | 6.7 | 3.5 |
| BP86/6-31++G(d,p) | -5.7 | -4.3 | -4.9 | 8.4 | 3.1 |
| ωB97X/6-31++G(d,p) | -8.8 | -7.5 | -8.1 | 8.6 | 0.9 |
| ωB97X-D/6-31++G(d,p) | -12.4 | -11.1 | -11.7 | 9.0 | -2.0 |
| B97-1/6-31++G(d,p) | -6.9 | -6.1 | -6.6 | 9.4 | 2.7 |
| B98/6-31++G(d,p) | -6.4 | -5.0 | -5.6 | 8.1 | 2.4 |
| B97-D/6-31++G(d,p) | -12.9 | -11.7 | -12.3 | 9.1 | -2.5 |

**Table A52:** Computed thermodynamic data for the $Co^{1+}$Cbl--**H**-N(Im) complex formation reaction studied in **acetonitrile solvent** while assuming standard state convention of 1atm and 298.15 K (all thermodynamic parameters are given in kcal/mol units).

| Theoretical Method | $Co^{1+}$Cbl + Im ⟶ $Co^{1+}$Cbl--Im | | | | |
|---|---|---|---|---|---|
| | ΔE | ΔU | ΔH | -TΔS | ΔG |
| HF/6-31++G(d,p) | -2.0 | -0.5 | -1.1 | 7.9 | 6.6 |
| BP86/6-31++G(d,p) | -4.3 | -2.9 | -3.5 | 8.1 | 4.3 |
| ωB97X/6-31++G(d,p) | -7.2 | -5.8 | -6.4 | 7.9 | 1.9 |
| ωB97X-D/6-31++G(d,p) | -10.6 | -9.3 | -9.9 | 9.3 | 0.2 |
| B97-1/6-31++G(d,p) | -5.3 | -4.0 | -4.6 | 7.7 | 3.1 |
| B98/6-31++G(d,p) | -5.3 | 3.9 | -4.5 | 7.7 | 3.1 |
| B97-D/6-31++G(d,p) | -11.5 | -10.3 | -10.9 | 9.6 | -0.6 |

**Table A53:** Computed thermodynamic data for the $Co^{1+}$Cbl--**H**-N(Im) complex formation reaction studied in **water solvent** while assuming standard state convention of 1atm and 298.15 K (all thermodynamic parameters are given in kcal/mol units).

| Theoretical Method | $Co^{1+}$Cbl + Im ⟶ $Co^{1+}$Cbl--Im | | | | |
|---|---|---|---|---|---|
| | ΔE | ΔU | ΔH | -TΔS | ΔG |
| HF/6-31++G(d,p) | -1.9 | -0.3 | -0.9 | 7.8 | 6.7 |
| BP86/6-31++G(d,p) | -4.1 | -2.8 | -3.4 | 8.1 | 4.4 |
| ωB97X/6-31++G(d,p) | -7.0 | -5.6 | -6.2 | 7.8 | 2.1 |
| ωB97X-D/6-31++G(d,p) | -10.4 | -9.1 | -9.7 | 9.3 | 0.4 |
| B97-1/6-31++G(d,p) | -5.2 | -3.8 | -4.4 | 7.6 | 3.1 |
| B98/6-31++G(d,p) | -4.7 | -3.3 | -3.9 | 8.0 | 4.0 |
| B97-D/6-31++G(d,p) | -11.4 | -10.7 | -11.3 | 11.5 | 0.8 |

**Table A54:** Computed thermodynamic data for the $Co^{1+}$Cbi--**H**-C(Im) complex formation reaction studied in **gas phase** while assuming standard state convention of 1atm and 298.15 K (all thermodynamic parameters are given in kcal/mol units).

| Theoretical Method | $Co^{1+}$Cbi + Im ⟶ $Co^{1+}$Cbi--Im | | | | |
|---|---|---|---|---|---|
| | ΔE | ΔU | ΔH | -TΔS | ΔG |
| HF/6-31G(d) 5d | -9.0 | -7.8 | -8.4 | 9.9 | 1.5 |
| BP86/6-31G(d) 5d | -10.6 | -9.7 | -10.3 | 11.4 | 1.1 |
| ωB97X/6-31G(d) 5d | -16.6 | -15.9 | -16.5 | 12.7 | -3.8 |
| ωB97X-D/6-31G(d) 5d | -21.0 | -20.2 | -20.8 | 11.8 | -9.0 |
| B97-1/6-31G(d) 5d | -12.9 | -12.2 | -12.8 | 12.3 | -0.4 |
| B98/6-31G(d) 5d | -12.1 | -11.4 | -12.0 | 12.1 | 0.1 |
| B97-D/6-31G(d) 5d | -20.1 | -19.4 | -20.0 | 12.1 | -7.9 |

**Table A55:** Computed thermodynamic data for the $Co^{1+}$Cbi--**H**-C(Im) complex formation reaction studied in **chloroform solvent** while assuming standard state convention of 1atm and 298.15 K (all thermodynamic parameters are given in kcal/mol units).

| Theoretical Method | $Co^{1+}$Cbi + Im ⟶ $Co^{1+}$Cbi--Im | | | | |
|---|---|---|---|---|---|
| | ΔE | ΔU | ΔH | -TΔS | ΔG |
| HF/6-31G(d) 5d | -4.7 | -3.5 | -4.1 | 9.7 | 6.9 |
| BP86/6-31G(d) 5d | -6.5 | -5.3 | -5.9 | 9.8 | 4.2 |
| ωB97X/6-31G(d) 5d | -11.0 | -10.3 | -10.9 | 12.4 | 2.4 |
| ωB97X-D/6-31G(d) 5d | -15.3 | -14.4 | -15.0 | 12.4 | -1.6 |
| B97-1/6-31G(d) 5d | -8.5 | -7.5 | -8.1 | 10.1 | 2.5 |
| B98/6-31G(d) 5d | -7.7 | -6.7 | -7.2 | 9.9 | 3.0 |
| B97-D/6-31G(d) 5d | -15.3 | -14.6 | -15.2 | 13.1 | -0.9 |

**Table A56:** Computed thermodynamic data for the $Co^{1+}$Cbi--**H**-C(Im) complex formation reaction studied in **acetonitrile solvent** while assuming standard state convention of 1atm and 298.15 K (all thermodynamic parameters are given in kcal/mol units).

| Theoretical Method | $Co^{1+}$Cbi + Im ⟶ $Co^{1+}$Cbi--Im | | | | |
|---|---|---|---|---|---|
| | ΔE | ΔU | ΔH | -TΔS | ΔG |
| HF/6-31G(d) 5d | -3.8 | -2.8 | -3.4 | 10.4 | 9.5 |
| BP86/6-31G(d) 5d | -4.7 | -3.7 | -4.2 | 10.3 | 6.4 |
| ωB97X/6-31G(d) 5d | -8.7 | -8.0 | -8.6 | 12.7 | 4.9 |
| ωB97X-D/6-31G(d) 5d | -14.0 | -12.8 | -13.4 | 10.8 | -1.6 |
| B97-1/6-31G(d) 5d | -6.8 | -5.8 | -6.4 | 10.2 | 4.2 |
| B98/6-31G(d) 5d | -6.0 | -5.0 | -5.5 | 9.9 | 4.7 |
| B97-D/6-31G(d) 5d | -13.7 | -12.9 | -13.5 | 12.6 | 0.3 |

**Table A57:** Computed thermodynamic data for the $Co^{1+}$Cbi--**H**-C(Im) complex formation reaction studied in **water solvent** while assuming standard state convention of 1atm and 298.15 K (all thermodynamic parameters are given in kcal/mol units).

| Theoretical Method | $Co^{1+}$Cbi + Im ⟶ $Co^{1+}$Cbi--Im | | | | |
|---|---|---|---|---|---|
| | ΔE | ΔU | ΔH | -TΔS | ΔG |
| HF/6-31G(d) 5d | -3.8 | -2.6 | -3.2 | 8.5 | 13.8 |
| BP86/6-31G(d) 5d | -4.6 | -3.5 | -4.1 | 10.5 | 6.7 |
| ωB97X/6-31G(d) 5d | -8.6 | -7.9 | -8.5 | 12.8 | 5.2 |
| ωB97X-D/6-31G(d) 5d | -13.9 | -12.7 | -13.3 | 10.5 | -1.7 |
| B97-1/6-31G(d) 5d | -6.4 | -5.5 | -6.1 | 12.1 | 6.4 |
| B98/6-31G(d) 5d | -5.7 | -4.8 | -5.4 | 11.6 | 6.5 |
| B97-D/6-31G(d) 5d | -13.4 | -12.7 | -13.3 | 13.2 | 1.1 |

**Table A58:** Computed thermodynamic data for the H-O-**H**--$Co^{1+}$Cbl--**H**-O-H complex formation reaction studied in **gas phase** while assuming standard state convention of 1atm and 298.15 K (all thermodynamic parameters are given in kcal/mol units).

| Theoretical Method | $Co^{1+}Cbl + H_2O + H_2O \longrightarrow OH_2\text{--}Co^{1+}Cbl\text{--}H_2O$ | | | | |
|---|---|---|---|---|---|
| | ΔE | ΔU | ΔH | -TΔS | ΔG |
| HF/6-31++G(d,p) | -8.0 | -6.4 | -7.6 | 12.5 | 4.9 |
| BP86/6-31++G(d,p) | -10.7 | -9.4 | -10.6 | 14.3 | 3.7 |
| ωB97X/6-31++G(d,p) | -15.8 | -14.5 | -15.7 | 15.0 | -0.7 |
| ωB97X-D/6-31++G(d,p) | -17.3 | -16.0 | -17.2 | 14.4 | -2.8 |
| B97-1/6-31++G(d,p) | -12.1 | -10.7 | -11.9 | 14.2 | 2.3 |
| B98/6-31++G(d,p) | -11.5 | -10.1 | -11.3 | 13.8 | 2.5 |
| B97-D/6-31++G(d,p) | -17.7 | -16.3 | -17.5 | 14.8 | -2.7 |

**Table A59:** Computed thermodynamic data for the H-O-**H**--$Co^{1+}$Cbl--**H**-O-H complex formation reaction studied in **chloroform solvent** while assuming standard state convention of 1atm and 298.15 K (all thermodynamic parameters are given in kcal/mol units).

| Theoretical Method | $Co^{1+}Cbl + H_2O + H_2O \longrightarrow OH_2\text{--}Co^{1+}Cbl\text{--}H_2O$ | | | | |
|---|---|---|---|---|---|
| | ΔE | ΔU | ΔH | -TΔS | ΔG |
| HF/6-31++G(d,p) | -4.0 | -2.3 | -3.5 | 12.3 | 8.8 |
| BP86/6-31++G(d,p) | -8.1 | -7.3 | -8.5 | 16.2 | 7.6 |
| ωB97X/6-31++G(d,p) | -11.5 | -10.2 | -11.4 | 15.0 | 3.9 |
| ωB97X-D/6-31++G(d,p) | -13.6 | -12.1 | -13.3 | 13.9 | 0.9 |
| B97-1/6-31++G(d,p) | -9.2 | -7.7 | -8.9 | 13.8 | 5.0 |
| B98/6-31++G(d,p) | -8.7 | -7.1 | -8.3 | 12.7 | 4.4 |
| B97-D/6-31++G(d,p) | -14.8 | -13.8 | -15.0 | 14.5 | -0.4 |

**Table A60:** Computed thermodynamic data for the H-O-**H**--$Co^{1+}$Cbl--**H**-O-H complex formation reaction studied in **acetonitrile solvent** while assuming standard state convention of 1atm and 298.15 K (all thermodynamic parameters are given in kcal/mol units).

| Theoretical Method | $Co^{1+}Cbl + H_2O + H_2O \longrightarrow OH_2\text{--}Co^{1+}Cbl\text{--}H_2O$ | | | | |
|---|---|---|---|---|---|
| | ΔE | ΔU | ΔH | -TΔS | ΔG |
| HF/6-31++G(d,p) | -2.5 | -0.1 | -1.3 | 11.0 | 9.8 |
| BP86/6-31++G(d,p) | -7.0 | -5.6 | -6.8 | 14.1 | 7.2 |
| ωB97X/6-31++G(d,p) | -9.8 | -8.3 | -9.5 | 13.2 | 4.1 |
| ωB97X-D/6-31++G(d,p) | -11.7 | -10.9 | -12.1 | 16.1 | 4.3 |
| B97-1/6-31++G(d,p) | -8.0 | -7.5 | -8.7 | 15.8 | 7.2 |
| B98/6-31++G(d,p) | -7.3 | -6.3 | -7.5 | 13.9 | 6.4 |
| B97-D/6-31++G(d,p) | -13.4 | -12.2 | -13.3 | 14.7 | 1.5 |

**Table A61:** Computed thermodynamic data for the H-O-**H**--$Co^{1+}$Cbl--**H**-O-H complex formation reaction studied in **water solvent** while assuming standard state convention of 1atm and 298.15 K (all thermodynamic parameters are given in kcal/mol units).

| Theoretical Method | $Co^{1+}Cbl + H_2O + H_2O \longrightarrow OH_2\text{--}Co^{1+}Cbl\text{--}H_2O$ | | | | |
|---|---|---|---|---|---|
| | ΔE | ΔU | ΔH | -TΔS | ΔG |
| HF/6-31++G(d,p) | -1.8 | -1.0 | -2.1 | 13.4 | 11.4 |
| BP86/6-31++G(d,p) | -6.9 | -5.5 | -6.7 | 13.5 | 6.7 |
| ωB97X/6-31++G(d,p) | -9.5 | -8.1 | -9.2 | 13.5 | 4.6 |
| ωB97X-D/6-31++G(d,p) | -11.5 | -10.1 | -11.3 | 13.9 | 2.9 |
| B97-1/6-31++G(d,p) | -7.9 | -6.8 | -8.0 | 13.3 | 5.4 |
| B98/6-31++G(d,p) | -7.2 | -6.1 | -7.3 | 13.8 | 6.5 |
| B97-D/6-31++G(d,p) | -13.3 | -12.7 | -13.9 | 16.5 | 2.8 |

**Table A62:** Computed thermodynamic data for the H-O-**H**--$Co^{1+}$Cbi--**H**-O-H complex formation reaction studied in **gas phase** while assuming standard state convention of 1atm and 298.15 K (all thermodynamic parameters are given in kcal/mol units).

| Theoretical Method | $Co^{1+}Cbi + H_2O + H_2O \longrightarrow OH_2\text{--}Co^{1+}Cbi\text{--}H_2O$ | | | | |
|---|---|---|---|---|---|
| | ΔE | ΔU | ΔH | -TΔS | ΔG |
| HF/6-31G(d) 5d | -14.6 | -14.3 | -15.5 | 18.7 | 3.2 |
| BP86/6-31G(d) 5d | -21.4 | -21.4 | -22.6 | 19.6 | -3.0 |
| ωB97X/6-31G(d) 5d | -29.1 | -30.0 | -31.1 | 23.1 | -8.0 |
| ωB97X-D/6-31G(d) 5d | -33.2 | -33.7 | -34.8 | 22.0 | -12.9 |
| B97-1/6-31G(d) 5d | -30.0 | -31.5 | -32.7 | 27.1 | -5.6 |
| B98/6-31G(d) 5d | -21.8 | -22.4 | -23.6 | 22.7 | -0.8 |
| B97-D/6-31G(d) 5d | -35.3 | -35.8 | -37.0 | 22.5 | -14.5 |

**Table A63:** Computed thermodynamic data for the H-O-**H**--$Co^{1+}$Cbi--**H**-O-H complex formation reaction studied in **chloroform solvent** while assuming standard state convention of 1atm and 298.15 K (all thermodynamic parameters are given in kcal/mol units).

| Theoretical Method | $Co^{1+}Cbi + H_2O + H_2O \longrightarrow OH_2\text{--}Co^{1+}Cbi\text{--}H_2O$ | | | | |
|---|---|---|---|---|---|
| | ΔE | ΔU | ΔH | -TΔS | ΔG |
| HF/6-31G(d) 5d | -7.2 | -6.7 | -7.9 | 18.4 | 11.2 |
| BP86/6-31G(d) 5d | -15.9 | -15.7 | -16.9 | 18.9 | 2.4 |
| ωB97X/6-31G(d) 5d | -20.0 | -20.8 | -22.0 | 23.1 | 1.1 |
| ωB97X-D/6-31G(d) 5d | -23.9 | -24.5 | -25.7 | 23.2 | -2.5 |
| B97-1/6-31G(d) 5d | -14.8 | -15.2 | -16.3 | 21.7 | 5.4 |
| B98/6-31G(d) 5d | -13.1 | -13.5 | -14.7 | 21.7 | 7.1 |
| B97-D/6-31G(d) 5d | -27.9 | -28.7 | -29.9 | 23.2 | -6.5 |

**Table A64:** Computed thermodynamic data for the H-O-**H**--$Co^{1+}$Cbi--**H**-O-H complex formation reaction studied in **acetonitrile solvent** while assuming standard state convention of 1atm and 298.15 K (all thermodynamic parameters are given in kcal/mol units).

| Theoretical Method | $Co^{1+}Cbi + H_2O + H_2O \longrightarrow OH_2\text{--}Co^{1+}Cbi\text{--}H_2O$ | | | | |
|---|---|---|---|---|---|
| | ΔE | ΔU | ΔH | -TΔS | ΔG |
| HF/6-31G(d) 5d | -4.4 | -3.6 | -4.8 | 17.0 | 14.3 |
| BP86/6-31G(d) 5d | -13.5 | -13.6 | -14.7 | 20.6 | 11.5 |
| ωB97X/6-31G(d) 5d | -15.6 | -16.6 | -17.8 | 24.1 | 7.8 |
| ωB97X-D/6-31G(d) 5d | -20.9 | -21.3 | -22.5 | 21.9 | 0.8 |
| B97-1/6-31G(d) 5d | -11.1 | -11.6 | -12.8 | 21.5 | 14.4 |
| B98/6-31G(d) 5d | -9.2 | -9.8 | -11.0 | 22.2 | 12.7 |
| B97-D/6-31G(d) 5d | -29.6 | -30.6 | -31.7 | 25.9 | -3.9 |

**Table A65:** Computed thermodynamic data for the H-O-**H**--$Co^{1+}$Cbi--**H**-O-H complex formation reaction studied in **water solvent** while assuming standard state convention of 1atm and 298.15 K (all thermodynamic parameters are given in kcal/mol units).

| Theoretical Method | $Co^{1+}Cbi + H_2O + H_2O \longrightarrow OH_2\text{--}Co^{1+}Cbi\text{--}H_2O$ | | | | |
|---|---|---|---|---|---|
| | ΔE | ΔU | ΔH | -TΔS | ΔG |
| HF/6-31G(d) 5d | -4.1 | -3.3 | -4.5 | 16.8 | 14.5 |
| BP86/6-31G(d) 5d | -13.3 | -13.4 | -14.6 | 20.9 | 12.0 |
| ωB97X/6-31G(d) 5d | -15.0 | -16.8 | -17.9 | 26.6 | 10.1 |
| ωB97X-D/6-31G(d) 5d | -20.5 | -20.8 | -22.0 | 21.9 | 1.2 |
| B97-1/6-31G(d) 5d | -17.0 | -17.7 | -18.9 | 24.4 | 11.2 |
| B98/6-31G(d) 5d | -8.8 | -9.4 | -10.6 | 22.9 | 13.8 |
| B97-D/6-31G(d) 5d | -29.5 | -30.4 | -31.5 | 25.8 | -3.9 |

**Table A66:** Computed thermodynamic data for the H-O-**H**--$Co^{1+}$Cbl--**H**-N(Im) complex formation reaction studied in **gas phase** while assuming standard state convention of 1atm and 298.15 K (all thermodynamic parameters are given in kcal/mol units).

| Theoretical Method | $Co^{1+}Cbl + Im + H_2O \longrightarrow Im\text{--}Co^{1+}Cbl\text{--}H_2O$ | | | | |
|---|---|---|---|---|---|
| | ΔE | ΔU | ΔH | -TΔS | ΔG |
| HF/6-31++G(d,p) | -10.6 | -8.3 | -9.5 | 13.3 | 3.8 |
| BP86/6-31++G(d,p) | -12.3 | -10.2 | -11.4 | 14.7 | 3.3 |
| ωB97X/6-31++G(d,p) | -18.9 | -17.0 | -18.2 | 16.4 | -1.8 |
| ωB97X-D/6-31++G(d,p) | -23.9 | -22.0 | -23.2 | 16.9 | -6.3 |
| B97-1/6-31++G(d,p) | -11.9 | -10.5 | -11.6 | 13.3 | 1.7 |
| B98/6-31++G(d,p) | -13.7 | -11.7 | -12.9 | 15.0 | 2.1 |
| B97-D/6-31++G(d,p) | -23.5 | -21.8 | -23.0 | 17.8 | -5.1 |

**Table A67:** Computed thermodynamic data for the H-O-**H**--$Co^{1+}$Cbl--**H**-N(Im) complex formation reaction studied in **chloroform** while assuming standard state convention of 1atm and 298.15 K (all thermodynamic parameters are given in kcal/mol units).

| Theoretical Method | $Co^{1+}Cbl + Im + H_2O \longrightarrow Im\text{--}Co^{1+}Cbl\text{--}H_2O$ | | | | |
|---|---|---|---|---|---|
| | ΔE | ΔU | ΔH | -TΔS | ΔG |
| HF/6-31++G(d,p) | -5.8 | -3.5 | -4.6 | 12.5 | 7.7 |
| BP86/6-31++G(d,p) | -9.3 | -7.2 | -8.4 | -15.3 | 6.5 |
| ωB97X/6-31++G(d,p) | -14.5 | -12.5 | -13.7 | 15.5 | 2.5 |
| ωB97X-D/6-31++G(d,p) | -19.0 | -17.2 | -18.4 | 17.2 | 0.0 |
| B97-1/6-31++G(d,p) | -11.1 | -9.5 | -10.7 | -16.6 | 6.1 |
| B98/6-31++G(d,p) | -10.4 | -8.3 | -9.5 | 14.4 | 4.6 |
| B97-D/6-31++G(d,p) | -19.8 | -18.1 | -19.3 | 17.4 | -0.8 |

**Table A68:** Computed thermodynamic data for the H-O-**H**--$Co^{1+}$Cbl--**H**-N(Im) complex formation reaction studied in **chloroform** while assuming standard state convention of 1atm and 298.15 K (all thermodynamic parameters are given in kcal/mol units).

| Theoretical Method | $Co^{1+}Cbl + Im + H_2O \longrightarrow Im\text{--}Co^{1+}Cbl\text{--}H_2O$ | | | | |
|---|---|---|---|---|---|
| | ΔE | ΔU | ΔH | -TΔS | ΔG |
| HF/6-31++G(d,p) | -3.0 | -1.1 | -2.3 | 14.2 | 7.7 |
| BP86/6-31++G(d,p) | -7.3 | -5.4 | -6.6 | 15.8 | 6.5 |
| ωB97X/6-31++G(d,p) | -12.0 | -10.0 | -11.1 | 15.2 | 2.5 |
| ωB97X-D/6-31++G(d,p) | -16.6 | -14.7 | -15.9 | 15.9 | 0.0 |
| B97-1/6-31++G(d,p) | -9.0 | -6.8 | -8.0 | 14.5 | 6.1 |
| B98/6-31++G(d,p) | -8.4 | -6.2 | -7.4 | 14.4 | 4.6 |
| B97-D/6-31++G(d,p) | -17.8 | -16.1 | -17.3 | 17.4 | -0.8 |

**Table A69:** Computed thermodynamic data for the H-O-**H**--$Co^{1+}$Cbl--**H**-N(Im) complex formation reaction studied in **water solvent** while assuming standard state convention of 1atm and 298.15 K (all thermodynamic parameters are given in kcal/mol units).

| Theoretical Method | $Co^{1+}Cbl + Im + H_2O \longrightarrow Im\text{--}Co^{1+}Cbl\text{--}H_2O$ | | | | |
|---|---|---|---|---|---|
| | ΔE | ΔU | ΔH | -TΔS | ΔG |
| HF/6-31++G(d,p) | -2.8 | -0.4 | -1.6 | 13.6 | 11.8 |
| BP86/6-31++G(d,p) | -7.1 | -5.2 | -6.4 | 15.8 | 9.1 |
| ωB97X/6-31++G(d,p) | -11.9 | -9.8 | -10.9 | 14.7 | 4.5 |
| ωB97X-D/6-31++G(d,p) | -16.4 | -15.0 | -16.2 | 18.1 | 3.2 |
| B97-1/6-31++G(d,p) | -8.9 | -7.3 | -8.5 | 16.4 | 8.1 |
| B98/6-31++G(d,p) | -8.1 | -6.0 | -7.2 | 14.4 | 7.0 |
| B97-D/6-31++G(d,p) | -17.7 | -16.0 | -17.2 | 17.6 | 1.5 |

**Table A70:** Computed thermodynamic data for the H-O-**H**--$Co^{1+}$Cbi--**H**-C(Im) complex formation reaction studied in **gas phase** while assuming standard state convention of 1atm and 298.15 K (all thermodynamic parameters are given in kcal/mol units).

| Theoretical Method | $Co^{1+}Cbi + Im + H_2O \longrightarrow Im\text{--}Co^{1+}Cbi\text{--}H_2O$ | | | | |
|---|---|---|---|---|---|
| | ΔE | ΔU | ΔH | -TΔS | ΔG |
| HF/6-31G(d) 5d | -19.3 | -18.4 | -19.6 | 22.0 | 2.4 |
| BP86/6-31G(d) 5d | -24.7 | -24.3 | -25.5 | 23.8 | -1.7 |
| ωB97X/6-31G(d) 5d | -37.6 | -37.0 | -38.2 | 23.1 | -15.1 |
| ωB97X-D/6-31G(d) 5d | -44.6 | -44.0 | -45.2 | 23.2 | -22.0 |
| B97-1/6-31G(d) 5d | -31.3 | -30.8 | -32.0 | 23.8 | -8.2 |
| B98/6-31G(d) 5d | -29.2 | -28.6 | -29.8 | 24.0 | -5.9 |
| B97-D/6-31G(d) 5d | -48.4 | -48.1 | -49.3 | 25.3 | -24.0 |

**Table A71:** Computed thermodynamic data for the H-O-**H**--$Co^{1+}$Cbi--**H**-C(Im) complex formation reaction studied in **chloroform** while assuming standard state convention of 1atm and 298.15 K (all thermodynamic parameters are given in kcal/mol units).

| Theoretical Method | $Co^{1+}Cbi + Im + H_2O \longrightarrow Im\text{--}Co^{1+}Cbi\text{--}H_2O$ | | | | |
|---|---|---|---|---|---|
| | ΔE | ΔU | ΔH | -TΔS | ΔG |
| HF/6-31G(d) 5d | -9.3 | -8.3 | -9.5 | 21.3 | 13.3 |
| BP86/6-31G(d) 5d | -17.8 | -17.1 | -18.3 | 22.6 | 6.1 |
| ωB97X/6-31G(d) 5d | -29.8 | -29.3 | -30.5 | 24.0 | -4.7 |
| ωB97X-D/6-31G(d) 5d | -37.5 | -36.8 | -38.0 | 24.1 | -12.1 |
| B97-1/6-31G(d) 5d | -22.4 | -21.7 | -22.9 | 22.6 | 1.5 |
| B98/6-31G(d) 5d | -20.4 | -19.7 | -20.8 | 22.5 | 3.5 |
| B97-D/6-31G(d) 5d | -40.4 | -39.9 | -41.1 | 25.1 | -13.9 |

**Table A72:** Computed thermodynamic data for the H-O-**H**--$Co^{1+}$Cbi--**H**-C(Im) complex formation reaction studied in **acetonitrile solvent** while assuming standard state convention of 1atm and 298.15 K (all thermodynamic parameters are given in kcal/mol units).

| Theoretical Method | $Co^{1+}Cbi + Im + H_2O \longrightarrow Im\text{--}Co^{1+}Cbi\text{--}H_2O$ | | | | |
|---|---|---|---|---|---|
| | ΔE | ΔU | ΔH | -TΔS | ΔG |
| HF/6-31G(d) 5d | -7.1 | -5.8 | -7.0 | 19.7 | 13.3 |
| BP86/6-31G(d) 5d | -14.9 | -14.4 | -15.6 | 23.7 | 6.1 |
| ωB97X/6-31G(d) 5d | -26.0 | -25.6 | -26.7 | 24.9 | -4.7 |
| ωB97X-D/6-31G(d) 5d | -33.5 | -33.0 | -34.2 | 25.0 | -12.1 |
| B97-1/6-31G(d) 5d | -19.0 | -18.3 | -19.5 | 23.6 | 1.5 |
| B98/6-31G(d) 5d | -16.8 | -16.2 | -17.4 | 24.1 | 3.5 |
| B97-D/6-31G(d) 5d | -38.0 | -37.3 | -38.5 | 24.2 | -13.9 |

**Table A73:** Computed thermodynamic data for the H-O-**H**--$Co^{1+}$Cbi--**H**-C(Im) complex formation reaction studied in **water solvent** while assuming standard state convention of 1atm and 298.15 K (all thermodynamic parameters are given in kcal/mol units).

| Theoretical Method | $Co^{1+}Cbi + Im + H_2O \longrightarrow Im\text{--}Co^{1+}Cbi\text{--}H_2O$ | | | | |
|---|---|---|---|---|---|
| | ΔE | ΔU | ΔH | -TΔS | ΔG |
| HF/6-31G(d) 5d | -7.1 | -5.8 | -7.0 | 19.9 | 14.5 |
| BP86/6-31G(d) 5d | -14.8 | -14.2 | -15.4 | 23.6 | 10.0 |
| ωB97X/6-31G(d) 5d | -25.7 | -25.2 | -26.4 | 24.9 | 0.3 |
| ωB97X-D/6-31G(d) 5d | -33.2 | -32.7 | -33.9 | 25.0 | -7.1 |
| B97-1/6-31G(d) 5d | -18.6 | -18.0 | -19.2 | 24.8 | 7.4 |
| B98/6-31G(d) 5d | -16.8 | -16.1 | -17.3 | 24.1 | 8.6 |
| B97-D/6-31G(d) 5d | -37.8 | -37.1 | -38.3 | 24.5 | -11.8 |

**Table A74.** Computed reduction potentials of the $Co^{2+}/Co^{1+}$ couple for various coordination geometries of $Co^{1+}$Cbl and $Co^{1+}$Cbi. The data in parentheses correspond to the tetracoordinated square planar $Co^{1+}$Cbl and $Co^{1+}$Cbi complexes.

| $Co^{2+}/Co^{1+}$ Redox Couple | Reduction Potential [mV] vs NHE | | |
|---|---|---|---|
| | Chloroform | Acetonitrile | Water |
| $Co^{2+}$Cbl--$OH_2$/$Co^{1+}$Cbl--H-O-H | 98 (-203) | 12 (-255) | -5 (-274) |
| $Co^{2+}$Cbi--$OH_2$/$Co^{1+}$Cbi--H-O-H | 5 (3) | -53 (-43) | -116 (-110) |
| $Co^{2+}$Cbl--N(Im)/$Co^{1+}$Cbl--H-N(Im) | 1 (-449) | -128 (-457) | -212 (-423) |
| $Co^{2+}$Cbi--N(Im)/$Co^{1+}$Cbi--H-C(Im) | -168 (-41) | -345 (158) | -432 (85) |
| $H_2O$--$Co^{2+}$Cbl--$OH_2$/H-O-H--$Co^{1+}$Cbl--H-O-H | 198 (-174) | 53 (-167) | 10 (-137) |
| $H_2O$--$Co^{2+}$Cbi--$OH_2$/H-O-H--$Co^{1+}$Cbi--H-O-H | 194 (-5) | -7 (-4) | -90 (27) |
| $H_2O$--$Co^{2+}$Cbl--N(Im)/H-O-H--$Co^{1+}$Cbl--H-N(Im) | 53 (-274) | -87 (-218) | -294 (-140) |
| $H_2O$--$Co^{2+}$Cbi--N(Im)/H-O-H--$Co^{1+}$Cbl--H-C(Im) | -21 (-275) | -344 (-165) | -449 (-64) |

**Table A75.** Key structural features of the optimized tetracoordinated square planar $Co^{1+}$Cbi complex (bond lengths and bond angle are expressed in Å and degree respectively)

| Theoretical Method | Corrin ring | | | |
|---|---|---|---|---|
| | Co-$N_{21}$ | Co-$N_{22}$ | Co-$N_{23}$ | Co-$N_{24}$ |
| HF/6-31G(d) 5d | 1.91 | 1.95 | 1.94 | 1.93 |
| BP86/6-31G(d) 5d | 1.82 | 1.89 | 1.88 | 1.83 |
| ωB97X/6-31G(d) 5d | 1.82 | 1.88 | 1.87 | 1.83 |
| ωB97X-D/6-31G(d) 5d | 1.83 | 1.89 | 1.87 | 1.84 |

**Table A76.** Key structural features of the optimized $Co^{1+}$Cbi--$H_2O$ complex (bond lengths and bond angle are expressed in Å and degree respectively)

| Theoretical Method | Corrin ring | | | | β-axial ligand | | |
|---|---|---|---|---|---|---|---|
| | Co-$N_{21}$ | Co-$N_{22}$ | Co-$N_{23}$ | Co-$N_{24}$ | Co-H | Co-O | Co-H-O |
| HF/6-31G(d) 5d | 1.92 | 1.95 | 1.94 | 1.93 | 2.35 | 3.29 | 167.0 |
| BP86/6-31G(d) 5d | 1.82 | 1.89 | 1.88 | 1.83 | 2.21 | 3.18 | 163.5 |
| ωB97X/6-31G(d) 5d | 1.83 | 1.89 | 1.87 | 1.85 | 2.25 | 3.20 | 163.6 |
| ωB97X-D/6-31G(d) 5d | 1.82 | 1.89 | 1.87 | 1.84 | 2.23 | 3.18 | 161.7 |

**Table A77.** Key structural features of the optimized $Co^{1+}$Cbi--$H_2O$--$H_2O$ complex (bond lengths and bond angle are expressed in Å and degree respectively)

| Theoretical Method | Corrin ring | | | | β-axial ligand | | |
|---|---|---|---|---|---|---|---|
| | Co-$N_{21}$ | Co-$N_{22}$ | Co-$N_{23}$ | Co-$N_{24}$ | Co-H | Co-O | Co-H-O |
| HF/6-31G(d) 5d | 1.92 | 1.95 | 1.94 | 1.93 | 2.55 | 3.48 | 166.2 |
| BP86/6-31G(d) 5d | 1.82 | 1.89 | 1.88 | 1.83 | 2.45 | 3.42 | 166.1 |
| ωB97X/6-31G(d) 5d | 1.83 | 1.88 | 1.88 | 1.84 | 2.44 | 3.40 | 167.0 |
| ωB97X-D/6-31G(d) 5d | 1.82 | 1.88 | 1.87 | 1.84 | 2.42 | 3.37 | 166.3 |

**Table A78.** Key structural features of the optimized $OH_2$--$Co^{1+}$Cbi--$H_2O$ complex (bond lengths and bond angle are expressed in Å and degree respectively)

| Theoretical Method | Corrin ring | | | | α-axial ligand | | | β-axial ligand | | |
|---|---|---|---|---|---|---|---|---|---|---|
| | Co-$N_{21}$ | Co-$N_{22}$ | Co-$N_{23}$ | Co-$N_{24}$ | Co-H | Co-O | Co-H-O | Co-H | Co-O | Co-H-O |
| HF/6-31G(d) 5d | 1.92 | 1.95 | 1.94 | 1.92 | 3.37 | 3.99 | 124.7 | 2.46 | 3.40 | 169.5 |
| BP86/6-31G(d) 5d | 1.82 | 1.89 | 1.88 | 1.83 | 2.44 | 3.41 | 165.0 | 2.30 | 3.27 | 164.6 |
| ωB97X/6-31G(d) 5d | 1.82 | 1.89 | 1.87 | 1.84 | 2.43 | 3.40 | 165.1 | 2.32 | 3.23 | 152.1 |
| ωB97X-D/6-31G(d) 5d | 1.82 | 1.89 | 1.87 | 1.84 | 2.40 | 3.36 | 166.7 | 2.28 | 3.19 | 154.8 |

**Table A79.** Key structural features of the optimized $OH_2$--$Co^{1+}$Cbi--$H_2O$--$H_2O$ complex (bond lengths and bond angle are expressed in Å and degree respectively)

| Theoretical Method | Corrin ring | | | | α-axial ligand | | | β-axial ligand | | |
|---|---|---|---|---|---|---|---|---|---|---|
| | Co-$N_{21}$ | Co-$N_{22}$ | Co-$N_{23}$ | Co-$N_{24}$ | Co-H | Co-O | Co-H-O | Co-H | Co-O | Co-H-O |
| HF/6-31G(d) 5d | 1.91 | 1.96 | 1.94 | 1.93 | 2.64 | 3.55 | 166.3 | 2.34 | 3.27 | 164.6 |
| BP86/6-31G(d) 5d | 1.82 | 1.90 | 1.88 | 1.83 | 2.48 | 3.39 | 154.1 | 2.20 | 3.17 | 162.0 |
| ωB97X/6-31G(d) 5d | 1.84 | 1.90 | 1.87 | 1.85 | 2.39 | 3.31 | 158.1 | 2.23 | 3.18 | 162.5 |
| ωB97X-D/6-31G(d) 5d | 1.83 | 1.89 | 1.87 | 1.84 | 2.36 | 3.28 | 158.6 | 2.20 | 3.15 | 161.1 |

**Table A80.** Key structural features of the optimized $Co^{1+}$Cbi--HOPh complex (bond lengths and bond angle are expressed in Å and degree respectively)

| Theoretical Method | Corrin ring | | | | β-axial ligand | | |
|---|---|---|---|---|---|---|---|
| | Co-$N_{21}$ | Co-$N_{22}$ | Co-$N_{23}$ | Co-$N_{24}$ | Co-H | Co-O | Co-H-O |
| HF/6-31G(d) 5d | 1.92 | 1.95 | 1.94 | 1.93 | 2.39 | 3.34 | 170.5 |
| BP86/6-31G(d) 5d | 1.82 | 1.89 | 1.88 | 1.83 | 2.25 | 3.25 | 172.6 |
| ωB97X/6-31G(d) 5d | 1.84 | 1.89 | 1.88 | 1.84 | 2.27 | 3.25 | 172.6 |
| ωB97X-D/6-31G(d) 5d | 1.83 | 1.89 | 1.87 | 1.84 | 2.24 | 3.21 | 170.0 |

**Table A81.** Key structural features of the optimized $Co^{1+}$Cbi--HOPh--$H_2O$ complex (bond lengths and bond angle are expressed in Å and degree respectively)

| Theoretical Method | Corrin ring | | | | β-axial ligand | | |
|---|---|---|---|---|---|---|---|
| | Co-$N_{21}$ | Co-$N_{22}$ | Co-$N_{23}$ | Co-$N_{24}$ | Co-H | Co-O | Co-H-O |
| HF/6-31G(d) 5d | 1.92 | 1.95 | 1.94 | 1.93 | 2.39 | 3.34 | 172.6 |
| BP86/6-31G(d) 5d | 1.82 | 1.89 | 1.88 | 1.83 | 2.28 | 3.29 | 174.6 |
| ωB97X/6-31G(d) 5d | 1.84 | 1.89 | 1.88 | 1.85 | 2.26 | 3.24 | 173.7 |
| ωB97X-D/6-31G(d) 5d | 1.83 | 1.88 | 1.87 | 1.84 | 2.22 | 3.20 | 171.8 |

**Table A82.** Key structural features of the optimized $OH_2$--$Co^{1+}$Cbi--HOPh complex (bond lengths and bond angle are expressed in Å and degree respectively)

| Theoretical Method | Corrin ring | | | | α-axial ligand | | | β-axial ligand | | |
|---|---|---|---|---|---|---|---|---|---|---|
| | Co-$N_{21}$ | Co-$N_{22}$ | Co-$N_{23}$ | Co-$N_{24}$ | Co-H | Co-O | Co-H-O | Co-H | Co-O | Co-H-O |
| HF/6-31G(d) 5d | 1.92 | 1.95 | 1.94 | 1.93 | 2.63 | 3.56 | 166.5 | 2.41 | 3.36 | 170.2 |
| BP86/6-31G(d) 5d | 1.82 | 1.90 | 1.88 | 1.84 | 2.41 | 3.33 | 154,1 | 2.26 | 3.26 | 172.0 |
| ωB97X/6-31G(d) 5d | 1.84 | 1.89 | 1.88 | 1.85 | 2.38 | 3.31 | 159.5 | 2.27 | 3.25 | 171.0 |
| ωB97X-D/6-31G(d) 5d | 1.83 | 1.89 | 1.87 | 1.84 | 2.36 | 3.27 | 157.3 | 2.23 | 3.20 | 171.4 |

**Table A83.** Key structural features of the optimized $OH_2$--$Co^{1+}$Cbi--HOPh--$H_2O$ complex (bond lengths and bond angle are expressed in Å and degree respectively)

| Theoretical Method | Corrin ring | | | | α-axial ligand | | | β-axial ligand | | |
|---|---|---|---|---|---|---|---|---|---|---|
| | Co-$N_{21}$ | Co-$N_{22}$ | Co-$N_{23}$ | Co-$N_{24}$ | Co-H | Co-O | Co-H-O | Co-H | Co-O | Co-H-O |
| HF/6-31G(d) 5d | 1.92 | 1.96 | 1.94 | 1.94 | 2.64 | 3.57 | 164.6 | 2.40 | 3.35 | 172.3 |
| BP86/6-31G(d) 5d | 1.83 | 1.89 | 1.88 | 1.83 | 2.48 | 3.39 | 153,5 | 2.09 | 3.11 | 174.5 |
| ωB97X/6-31G(d) 5d | 1.84 | 1.89 | 1.88 | 1.85 | 2.39 | 3.30 | 157.2 | 2.26 | 3.24 | 173.0 |
| ωB97X-D/6-31G(d) 5d | 1.83 | 1.89 | 1.87 | 1.84 | 2.34 | 3.25 | 155.7 | 2.21 | 3.19 | 172.3 |

**Table A84.** Computed thermodynamic data for $Co^{1+}$Cbi--$H_2O$ complex formation reaction studied in **gas phase** while assuming standard state convention of 1atm and 298.15 K (all thermodynamic parameters are given in kcal/mol units).

| Theoretical Method | $Co^{1+}$Cbi + $H_2O$ ⟶ $Co^{1+}$Cbi--$H_2O$ | | | | |
|---|---|---|---|---|---|
| | ΔE | ΔU | ΔH | -TΔS | ΔG |
| HF/6-31G(d) 5d | -9.6 | -9.6 | -10.2 | 9.8 | -0.4 |
| BP86/6-31G(d) 5d | -13.9 | -14.0 | -14.6 | 9.6 | -5.1 |
| ωB97X/6-31G(d) 5d | -17.0 | -17.2 | -17.8 | 10.4 | -7.4 |
| ωB97X-D/6-31G(d) 5d | -18.6 | -18.6 | -19.2 | 10.0 | -9.3 |

**Table A85.** Computed thermodynamic data for $Co^{1+}$Cbi--$H_2O$--$H_2O$ complex formation reaction studied in **gas phase** while assuming standard state convention of 1atm and 298.15 K (all thermodynamic parameters are given in kcal/mol units).

| Theoretical Method | $Co^{1+}$Cbi + $H_2O$ + $H_2O$ ⟶ $Co^{1+}$Cbi--$H_2O$--$H_2O$ | | | | |
|---|---|---|---|---|---|
| | ΔE | ΔU | ΔH | -TΔS | ΔG |
| HF/6-31G(d) 5d | -19.6 | -19.1 | -20.3 | 18.0 | -2.3 |
| BP86/6-31G(d) 5d | -27.6 | -27.8 | -29.0 | 19.0 | -9.9 |
| ωB97X/6-31G(d) 5d | -31.2 | -31.3 | -32.5 | 19.5 | -13.0 |
| ωB97X-D/6-31G(d) 5d | -32.5 | -32.5 | -33.7 | 19.0 | -14.6 |

**Table A86.** Computed thermodynamic data for $OH_2$--$Co^{1+}$Cbi--$H_2O$ complex formation reaction studied in **gas phase** while assuming standard state convention of 1atm and 298.15 K (all thermodynamic parameters are given in kcal/mol units).

| Theoretical Method | $H_2O$ + $Co^{1+}$Cbi + $H_2O$ ⟶ $OH_2$--$Co^{1+}$Cbi--$H_2O$ | | | | |
|---|---|---|---|---|---|
| | ΔE | ΔU | ΔH | -TΔS | ΔG |
| HF/6-31G(d) 5d | -14.6 | -14.3 | -15.5 | 18.7 | 3.2 |
| BP86/6-31G(d) 5d | -21.4 | -21.4 | -22.6 | 19.6 | -3.0 |
| ωB97X/6-31G(d) 5d | -29.1 | -30.0 | -31.1 | 23.1 | -8.0 |
| ωB97X-D/6-31G(d) 5d | -33.2 | -33.7 | -34.8 | 22.0 | -12.9 |

**Table A87.** Computed thermodynamic data for $OH_2$--$Co^{1+}$Cbi--$H_2O$--$H_2O$ complex formation reaction studied in **gas phase** while assuming standard state convention of 1atm and 298.15 K (all thermodynamic parameters are given in kcal/mol units).

| Theoretical Method | $H_2O$ + $Co^{1+}$Cbi + $H_2O$ + $H_2O$ ⟶ $OH_2$--$Co^{1+}$Cbi--$H_2O$--$H_2O$ | | | | |
|---|---|---|---|---|---|
| | ΔE | ΔU | ΔH | -TΔS | ΔG |
| HF/6-31G(d) 5d | -22.9 | -22.7 | -24.5 | 28.5 | 4.0 |
| BP86/6-31G(d) 5d | -34.6 | -35.0 | -36.8 | 30.5 | -6.3 |
| Ωb97X/6-31G(d) 5d | -42.6 | -43.4 | -45.8 | 32.2 | -13.0 |
| ωB97X-D/6-31G(d) 5d | -44.8 | -45.7 | -47.5 | 32.4 | -15.1 |

**Table A88.** Computed thermodynamic data for $Co^{1+}$Cbi--HOPh complex formation reaction studied in **gas phase** while assuming standard state convention of 1atm and 298.15 K (all thermodynamic parameters are given in kcal/mol units).

| Theoretical Method | $Co^{1+}$Cbi + HOPh ⟶ $Co^{1+}$Cbi--HOPh | | | | |
|---|---|---|---|---|---|
| | ΔE | ΔU | ΔH | -TΔS | ΔG |
| HF/6-31G(d) 5d | -10.3 | -9.2 | -9.8 | 10.9 | 1.1 |
| BP86/6-31G(d) 5d | -12.5 | -11.3 | -11.9 | 10.0 | -1.9 |
| ωB97X/6-31G(d) 5d | -19.3 | -18.3 | -18.9 | 12.2 | -6.7 |
| ωB97X-D/6-31G(d) 5d | -25.0 | -24.2 | -24.8 | 12.5 | -12.3 |

**Table A89.** Computed thermodynamic data for $Co^{1+}$Cbi--HOPh--$H_2O$ complex formation reaction studied in **gas phase** while assuming standard state convention of 1atm and 298.15 K (all thermodynamic parameters are given in kcal/mol units).

| Theoretical Method | $Co^{1+}$Cbi + HOPh + $H_2O$ ⟶ $Co^{1+}$Cbi--HOPh--$H_2O$ | | | | |
|---|---|---|---|---|---|
| | ΔE | ΔU | ΔH | -TΔS | ΔG |
| HF/6-31G(d) 5d | -17.7 | -16.5 | -17.7 | 20.7 | 3.1 |
| BP86/6-31G(d) 5d | -21.6 | -20.7 | -21.9 | 21.7 | -0.2 |
| ωB97X/6-31G(d) 5d | -31.7 | -31.1 | -32.3 | 23.1 | -9.2 |
| ωB97X-D/6-31G(d) 5d | -37.9 | -37.6 | -38.8 | 24.1 | -14.7 |

**Table A90.** Computed thermodynamic data for $OH_2$--$Co^{1+}$Cbi--HOPh complex formation reaction studied in **gas phase** while assuming standard state convention of 1atm and 298.15 K (all thermodynamic parameters are given in kcal/mol units).

| Theoretical Method | $H_2O$ + $Co^{1+}$Cbi + HOPh ⟶ $OH_2$--$Co^{1+}$Cbi--HOPh | | | | |
|---|---|---|---|---|---|
| | ΔE | ΔU | ΔH | -TΔS | ΔG |
| HF/6-31G(d) 5d | -13.6 | -12.6 | -13.7 | 21.2 | 7.5 |
| BP86/6-31G(d) 5d | -18.2 | -17.7 | -18.9 | 23.3 | 4.3 |
| ωB97X/6-31G(d) 5d | -30.3 | -30.1 | -31.3 | 24.7 | -6.6 |
| ωB97X-D/6-31G(d) 5d | -38.1 | -38.0 | -39.2 | 25.1 | -14.1 |

**Table A91.** Computed thermodynamic data for $OH_2$--$Co^{1+}$Cbi--HOPh--$H_2O$ complex formation reaction studied in **gas phase** while assuming standard state convention of 1atm and 298.15 K (all thermodynamic parameters are given in kcal/mol units).

| Theoretical Method | $H_2O$ + $Co^{1+}$Cbi + HOPh + $H_2O$ ⟶ $OH_2$--$Co^{1+}$Cbi--HOPh--$H_2O$ | | | | |
|---|---|---|---|---|---|
| | ΔE | ΔU | ΔH | -TΔS | ΔG |
| HF/6-31G(d) 5d | -20.8 | -19.7 | -21.5 | 30.9 | 9.4 |
| BP86/6-31G(d) 5d | -31.5 | -31.1 | -32.9 | 33.2 | 0.2 |
| ωB97X/6-31G(d) 5d | -43.3 | -43.1 | -44.9 | 34.7 | -10.2 |
| ωB97X-D/6-31G(d) 5d | -50.6 | -50.6 | -52.4 | 35.4 | -17.0 |

# CURRICULUM VITAE
# Manoj Kumar

Department of Chemistry
University of Louisville,
2320 South Brook St
Louisville, KY-40292

Email: chem.manoj@gmail.com
Phone: 502-751-0598 (Cell)
Fax: 502-852-8149 (Fax)

## EDUCATION

- **PhD, Computational Bioinorganic Chemistry, University of Louisville, Louisville, KY, USA 2007-2012**
  Thesis title: "Computational Modelling of Cobalamin-Dependent Enzymatic Chemical Reactions: $B_{12}$ Catalysis in Adenosylcobalamin-Dependent Mutases and Cob(II)alamin/Cob(I)alamin Reduction Process in Methyltransferases"
- **MS, Computational Material Chemistry, Panjab University, Chandigarh, India 2004-2006**
  Thesis title: "Theoretical Analysis of Finite-Sized Gold Clusters"
- **BS, Physics, Chemistry & Mathematics, SVSD PG College, Bhatoli, Himachal Pradesh University, Shimla, India 2001-2004**

## RESEARCH INTERESTS

- Computational bioinorganic chemistry: molecular modeling of enzyme catalytic cycles
- Computational exploration of structure-reactivity correlation in complex materials

## RESEARCH EXPERIENCE

**Graduate Research Assistant, Department of Chemistry, University of Louisville, 07/2007- 04/2012**

Advisor : Prof. Pawel M. Kozlowski

- Theoretically validated the existence of an unprecedented **$Co^{1+}$--H** interaction adding an important piece to the emerging viewpoint that the H-bond forming feature is a bona fide signature of low spin $d^8$ transition metal ions
- Computationally proved that **Cob(I)alamin**, a ubiquitous $B_{12}$ intermediate is not a tetracoordinated square planar complex, but is a **H-bonded** pentacoordinated square pyramidal state that solves the thermodynamically challenging reduction (i.e., $Co^{2+}/Co^{1+}$ reduction) which is a vital chemical reaction in a wide body of methyltransferases and ATP:Co(I)rrinoid adenosyltransferases
- Proposed a PCET-based mechanistic design for explaining the catalytic activation of Co-C bond in $B_{12}$-dependent mutases.

**MS Research Project, Panjab University, Chandigarh, India 07/2004-06/2006**

Adviser: Prof. Tapan K. Sau and Prof. Keya Dharamveer

- Optimised small sized (3 to 12 atoms) heavy transition metal clusters (Co, Rh and Ir) using DFT-based computational tools
- Optimised various kinds (octahedron, icosahedron etc.) of finite sized (6 to 55 atoms) gold clusters.
- Used Fortran90 code developed by the research group for optimizing the gold clusters.

**Summer Research Project, Jawahar Lal Nehru Centre for Advanced Scientific Research 05/2005-07/2005 (JNCASR), Bangalore**

Adviser: Prof. Swapan K. Pati

- Optimised finite sized face centred cubic gold clusters and studied their interactions with alkane, alkene and alkyne based thiolates to exploit their optical properties
- Used DFT modelling tools and Fortran90 code developed in the lab to compute the density of states using Green's function.

## FELLOWSHIPS, HONORS AND AWARDS

- University of Louisville, PhD Dissertation Completion Award, Spring-2012.
- NSF Travel Award for attending 4$^{th}$ International Workshop and School "Time-Dependent Density-Functional Theory: Prospects and Applications" Benasque, Spain, 2$^{nd}$ - 15$^{th}$ January, 2010.
- UCSD Travel Award for attending 2009 CTBP Summer School, UCSD, La Jolla, San Diego, 4$^{th}$ - 7$^{th}$ August, 2009.
- University of Louisville Graduate Student Council Travel Award for attending 41$^{st}$ Central Regional Meeting of the ACS, Cleveland, Ohio, 20$^{th}$ - 23$^{rd}$ May, 2009.
- University of Louisville Prestigious Graduate Student Fellowship, fall 2007 - fall 2008.
- Department of Science and Technology (Govt. of India) Award (DST) for attending 18$^{th}$ meeting of "Noble Laureates and Students in Chemistry", Lindau, Germany, 25$^{th}$ - 30$^{th}$ June, 2006.
- Rajiv Gandhi National Talent Research Scholar Award (in the category of Theoretical Sciences), 2005.
- Gold Medalist, BS 2004.
- National Merit Scholarship, 1999-2004.
- State Merit Scholarship, 1994-1999.

## PUBLICATIONS & PRESENTATIONS

### Manuscripts (submitting/ in preparation)

1. **M. Kumar,** L. Randaccio and P. M. Kozlowski, "Axial Bonding in Pentaamine Co(III) Complexes and Cobalamins: A Detailed DFT Analysis of Structural Trans Influence", *J. Phys. Chem. B.* (ready for submission).
2. **M. Kumar,** J. Kuta, W. Galezowski and P. M. Kozlowski, "Implications of the One-Electron Reduced Methylcobalamin in the Context of Catalytic Functioning of Methionine Synthase", *J. Phys. Chem. B* (ready for submission).

### Research Publications

1. **M. Kumar** and P. M. Kozlowski, "Role of Tyrosine Residue in the Activation of Co-C bond in Coenzyme $B_{12}$-Dependent Enzymes: Another Case of Proton-Coupled Electron Transfer?", *J. Phys. Chem. B* **2009**, *113*, 9050-9054.

2. **M. Kumar,** and P. M. Kozlowski, "A Biologically Relevant $Co^{1+}$--H Bond: Possible Implications in the Protein-Induced Redox Tuning of $Co^{2+}/Co^{1+}$ Reduction", *Angew. Chem. Int. Ed.* **2011**, *50*, 8702-8705.
3. **M. Kumar,** and P. M. Kozlowski, "Corrin Ring-Based Structural Frustration Tunes The Redox Character of a $B_{12}$ cofactor: Implications for PCET-Inspired Catalysis" *ChemComm* **2012** (accepted).
4. **M. Kumar,** N. Kumar, H. Hirao and P. M. Kozlowski, "$Co^{2+}/Co^{1+}$ Redox Tuning in Methyltransferases Induced by a Conformational Change at the Axial Ligand", *Inorg. Chem.* **2012** (accepted).
5. **M. Kumar,** W. Galezowski and P. M. Kozlowski, "Computational Modelling of Electrochemistry of $B_{12}$ Cofactors", *Int. J. Quant. Chem.* **2012** (accepted).
6. **M. Kumar,** and P. M. Kozlowski, "Can The Local Enzyme Scaffold Participate in $Co^{1+}$--H Bond Formation?: Structural and Biological Consequences for Methyltransferases" *J. Inorg. BioChem.* **2012** (being reviewed).
7. **M. Kumar,** H. Hirao and P. M. Kozlowski, "$Co^{1+}$--H Interaction Inspired Alternate Coordination Geometries of Biologically Important Cob(I)alamin: Possible Structural and Mechanistic Consequences for Methyltransferases", *J. Biol. Inorg. Chem.* **2012** (being reviewed).
8. **M. Kumar,** and P. M. Kozlowski, "Why Hydroxocobalamin is Photocatalytically Active: Implications for DNA and RNA Probing", *J. Am. Chem. Soc.* **2012** (being reviewed).
9. C. A. Masitas, **M. Kumar**, M. S. Mashuta, P. M. Kozlowski and C. A.Grapperhaus "Controlled Sulfur Oxygenation of the Ruthenium Dithiolate (bmmp-TASN)$RuPPh_3$ under Limiting $O_2$ Conditions Yields Thiolato/Sulfinato, Sulfenato/Sulfinato, and Bis-Sulfinato Derivatives", *Inorg. Chem.* **2010,** *49*, 10875-10881.
10. P. M. Kozlowski, **M. Kumar,** P. Piecuch, W. Li, P. Lodowki, and M. Jaworska, "The Co-C Bond Dissociation in Methylcobalamin: New Benchmark Analysis Based on DFT, CASSCF/CASPT2 and Completely Renormalized Coupled-Cluster Calculations.", *J. Chem. Theory Comput.* **2012** (essentially accepted).
11. P. M. Kozlowski, T. Kamachi, **M. Kumar,** and K. Yoshizawa, "Reductive Elimination Reaction Pathway for Homocysteine to Methionine Conversion in Cobalamin-dependent Methionine Synthase", *J. Biol. Inorg. Chem.* **2012** (accepted).
12. P. M. Kozlowski, T. Kamachi, **M. Kumar,** and K. Yoshizawa, "Intial Step of $B_{12}$-Dependent Enzymatic Catalysis: Energetic Implications Regarding the Involvement of One-Electron Reduced form of Adenosylcobalamin Cofactor", *J. Biol. Inorg. Chem.* **2011,** *17*, 293-300.
13. P. M. Kozlowski, T. Kamachi, **M. Kumar,** T. Nakayama and K. Yoshizawa, "Theoretical Analysis of Diradical Nature of Adenosylcobalamin Cofactor–Tyrosine Complex in $B_{12}$-Dependent Mutases: Inspiring PCET-driven Enzymatic Catalysis", *J. Phys. Chem. B* **2010**, *114*, 5928-5939.
14. M. Alfonso-Prieto, X. Bairnes, **M. Kumar**, C. Rovira and P. M. Kozlowski, "The Co-C bond cleavage mechanism in cobalamin-dependent methionine synthase: a Theoretical Study", *J. Phys. Chem. B* **2010,** *114*, 12965-12971.
15. N. Kumar, M. Jaworska, P. Lodowski, **M. Kumar** and P. M. Kozlowski, "Electronic Structure of Cofactor-Substrate Reactant Complex Involved in the Methyl Transfer Reaction Catalyzed by Cobalamin-Dependent Methionine Synthase" *J. Phys. Chem. B* **2011**, *115*, 6722-6731.
16. P. Lodowki, M. Jaworska, T.Andruniów, **M. Kumar** and P. M. Kozlowski, "Photodissociation of Co-C bond in Methyl- and Ethylcobalamin: An Insight from DFT Calculations", *J. Phys. Chem. B* **2009**, *113*, 6898-6909.

## Conferences, Workshops & Summer Schools:

1. Q-Chem Workshop, University of Louisville, Louisville, 30th March, 2010.
2. 4th International Workshop and School "Time-Dependent Density-Functional Theory: Prospects and Applications", Benasque, Spain, 2nd - 15th January, 2010.
3. 42nd Central Regional Meeting of the ACS, Dayton, Ohio, 16th – 19th June, 2010.
4. CTBP Summer School, UCSD, La Jolla, San Diego, 4th - 7th August, 2009.
5. 41st Central Regional Meeting of the ACS, Cleveland, Ohio, 20th - 23rd May, 2009.
6. Q-Chem Workshop, Pittsburgh Supercomputer Center, Pittsburgh, 19th - 20th March, 2009.
7. 18th meeting of "Noble Laureates and Students in Chemistry", Lindau, Germany, 25th - 30th June, 2006.
8. National Meeting on "Nano and Novel Materials", Department of Physics, Panjab University, Chandigarh, India, February, 2006.
9. National Symposium and 2nd R. C. Paul Symposium, Department of Chemistry, Panjab University, Chandigarh, India, December, 2005.
10. Summer Research School, JNCASR, Bangalore, India, May - July, 2005.

## Selected Conference Oral & Poster Presentations:

1. P. M. Kozlowski, **M. Kumar**, and N. Kumar, "Computational modeling of methyl transfer reactions catalyzed by cobalamin-dependent methionine synthase enzyme", 7th Congress of the International Society for Theoretical Chemical Physics, Waseda University, Tokyo, Japan, 2nd – 8th September, 2011 **(oral)**.
2. **M. Kumar**, and P. M. Kozlowski, "A Biologically Relevant $Co^{1+}$--H Bond: Possible Implications in the Protein-Induced Redox Tuning of $Co^{2+}/Co^{1+}$ Reduction", Graduate Research Symposium, University of Louisville, Louisville, KY, 20th March, 2011 **(oral)**.
3. **M. Kumar**, M. Alfonso-Prieto, X. Biarnés, C. Rovira, and P. M. Kozlowski, "The Reductive Cleavage Mechanism of Co-C Bond in Cobalamin-Dependent Methionine Synthase", 42nd Central Regional Meeting of the ACS, Dayton, Ohio, 16th – 19th June, 2010 **(poster)**.
4. **M. Kumar**, and P. M. Kozlowski, "Role of Tyrosine Residue in the Activation of Co-C bond in Coenzyme $B_{12}$-Dependent Enzymes: Another Case of Proton-Coupled Electron Transfer?", 4th International Workshop and School "Time-Dependent Density-Functional Theory: Prospects and Applications", Benasque, Spain, 2nd - 15th January, 2010 **(poster)**.
5. **M. Kumar**, and P. M. Kozlowski, "Role of Tyrosine Residue in the Activation of Co-C bond in Coenzyme $B_{12}$-Dependent Enzymes: Another Case of Proton-Coupled Electron Transfer?", CTBP Summer School, UCSD, La Jolla, San Diego, 4th - 7th August, 2009 **(poster)**.
6. **M. Kumar**, P. Lodowski, M. Jaworska, T. Andruniow, and P. M. Kozlowski, "Photodissociation of Co-C bond in Methyl- and Ethylcobalamin: An Insight from DFT Calculations" 41st Central Regional Meeting of the ACS, Cleveland, Ohio, 20th - 23rd May, 2009 **(poster)**.
7. **M. Kumar**, P. Lodowski, M. Jaworska, T. Andruniow, and P. M. Kozlowski, "Photodissociation of Co-C bond in Methyl- and Ethylcobalamin: An Insight from DFT Calculations", Q-Chem Workshop, Pittsburgh Supercomputer Center, Pittsburgh, 19th -20th March, 2009 **(poster)**.